9-1-2018

Non-Destructive Characterization of Rotated Uniaxial Anisotropic Materials

Alexander G. Knisely

NON-DESTRUCTIVE CHARACTERIZATION OF ROTATED UNIAXIAL ANISOTROPIC MATERIALS

DISSERTATION

Alexander G. Knisely

AFIT-ENG-PhD-18-S-013

DEPARTMENT OF THE AIR FORCE
AIR UNIVERSITY

AIR FORCE INSTITUTE OF TECHNOLOGY

Wright-Patterson Air Force Base, Ohio

AFIT-ENG-PhD-18-S-013

NON-DESTRUCTIVE CHARACTERIZATION OF ROTATED UNIAXIAL ANISOTROPIC MATERIALS

DISSERTATION

Presented to the Faculty

Graduate School of Engineering and Management

Air Force Institute of Technology

Air University

Air Education and Training Command

in Partial Fulfillment of the Requirements for the

Degree of Doctorate of Philosophy in Electrical Engineering

Alexander G. Knisely, B.S.E.E., M.S.E.E.

September 2018

AFIT-ENG-PhD-18-S-013

NON-DESTRUCTIVE CHARACTERIZATION OF ROTATED UNIAXIAL ANISOTROPIC MATERIALS

DISSERTATION

Alexander G. Knisely, B.S.E.E., M.S.E.E.

Committee Membership:

Dr. Michael J. Havrilla
Chair

Dr. Peter J. Collins
Member

Lt.Col. Milo W. Hyde, PhD
Member

Dr. William P. Baker
Member

Dr. Adedeji B. Badiru
Dean, Graduate School of Engineering and Management

AFIT-ENG-PhD-18-S-013

Abstract

Electromagnetic material characterization of anisotropic media requires measurement diversity, minimal measurement uncertainty and insight into sample symmetry. Additionally, non-destructive characterization techniques are valued over legacy measurement techniques because a destructive approach requires sample preparation to execute a measurement. A Single Port Waveguide Probe (SPWP) non-destructive material characterization technique is proposed to accommodate measuring a metal backed, known thickness, rotated uniaxial anisotropic material. A rotated uniaxial sample possesses unique transverse constitutive components and a longitudinal constitutive component which is the same as one of the transverse values. The SPWP consists of a rectangular waveguide aperture cut in the center of a square flange. The flange is place upon a metal-backed material surface, which forms a parallel plate region. Two orthogonal transverse plane measurements aligned with the sample's transverse constitutive parameter components offers measurement diversity. A rotated uniaxial anisotropic parallel plate Green's function is developed and employed in a moment method forward model and is then used to extract the material constitutive parameters. Measured and simulated results are utilized to demonstrate the analytical approach and uncertainty is evaluated demonstrating system accuracy of the non-destructive rotated uniaxial anisotropic measurement technique.

To my family.

Acknowledgements

I would like to thank Dr. Michael J. Havrilla, Dr. Peter J. Collins, Dr. Milo W. Hyde IV and Dr. William P. Baker. Each one of you aided my progression toward a successful defense. I would especially like to thank Dr. Havrilla and Dr. Hyde for their words of wisdom and helping to develop my technical curriculum. I would also like to thank my wife. Your words of encouragement, patience and support motivated me. We did it!

I am the product of my family and my mentors, each one has made me the son, the engineer, and the husband that I am. Thank you!

Alexander G. Knisely

Table of Contents

Page

Page

Page

List of Figures

NON-DESTRUCTIVE CHARACTERIZATION

OF

ROTATED UNIAXIAL ANISOTROPIC MATERIALS

I. Introduction

1.1 Problem Statement

Non-destructive evaluation (NDE) of anisotropic media requires sufficient measurement diversity to characterize a material. Measurement diversity may involve using unique field applicators, orienting the sample into unique positions, or using multiple sample thicknesses to support characterization. Measurement diversity challenges are increased if the sample has a fixed thickness and is backed by a metal substrate. The advent of additive manufacturing technologies such as 3-D polymer printers offers the ability to rapidly produce intricate, electromagnetically-macroscopic crystal structures that possess symmetries which are potentially anisotropic [1], [2]. These crystal structures offer polarization, amplitude and phase controlling properties to a scattered electromagnetic field, as explored in [3]. Combining anisotropic media, with the measurement-restrictive metal substrate poses the challenge: How to non-destructively characterize the material? The solution varies depending on the material anisotropy and availability of measurement diversity.

1.2 Scope and Research Goals

Previous NDE research has successfully demonstrated isotropic permittivity and permeability characterization as well as dielectric uniaxial anisotropic measurements.

Uniaxial Anisotropic materials have permittivity, $\overleftrightarrow{\epsilon}$ and permeability, $\overleftrightarrow{\mu}$ represented by

$$\overleftrightarrow{\epsilon} = \begin{bmatrix} \epsilon_{tt} & 0 & 0 \\ 0 & \epsilon_{tt} & 0 \\ 0 & 0 & \epsilon_{zz} \end{bmatrix} \quad , \quad \overleftrightarrow{\mu} = \begin{bmatrix} \mu_{tt} & 0 & 0 \\ 0 & \mu_{tt} & 0 \\ 0 & 0 & \mu_{zz} \end{bmatrix} . \tag{1.1}$$

Destructive measurements have successfully measured biaxial anisotropic media as demonstrated in [3]. Making an incremental research step toward non-destructively measuring biaxial anisotropic media requires addressing unique transverse tensor elements, which enhances analytical complexity. Evaluating a rotated uniaxial material using a non-destructive evaluation (NDE) technique offers the opportunity to explore the unique transverse components while not attempting to tackle a biaxial anisotropic Green's function, which has proven difficult to evaluate. Uniaxial anisotropic and Rotated-Uniaxial anisotropic media characterization in conjunction with a non-destructive measurement approach are the focus of this research. A rotated-uniaxial anisotropic material has permittivity, $\overleftrightarrow{\epsilon}$ and permeability, $\overleftrightarrow{\mu}$ represented by:

$$\overleftrightarrow{\epsilon} = \begin{bmatrix} \epsilon_{xx} & 0 & 0 \\ 0 & \epsilon_{yy} & 0 \\ 0 & 0 & \epsilon_{xx} \end{bmatrix} \quad , \quad \overleftrightarrow{\mu} = \begin{bmatrix} \mu_{xx} & 0 & 0 \\ 0 & \mu_{yy} & 0 \\ 0 & 0 & \mu_{xx} \end{bmatrix} . \tag{1.2}$$

Assuming the material is permanently attached to a metal substrate, attention is further focused on how various field applicators are utilized to measure the aforementioned tensor elements (either uniaxial or rotated uniaxial). A parallel plate waveguide structure offers a convenient approach, as a the secondary plate can be provided by a measurement apparatus as shown in Figure 1. Having the parallel plate region, supports implementation of a parallel plate Green's function, which relates a current distribution to fields in the parallel plate region. A Magnetic Field Integral Equa-

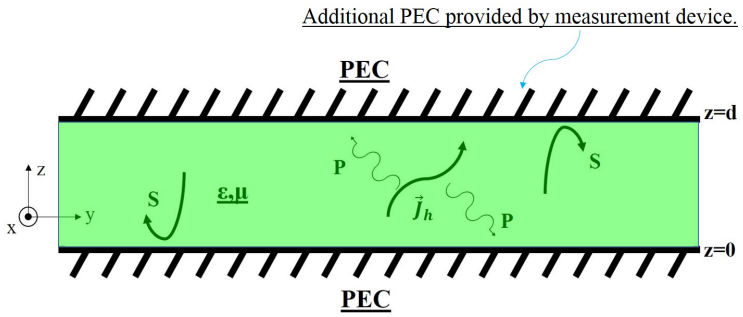

Figure 1. An example measurement scenario demonstrating a parallel plate waveguide exited by a current. This example is used to develop a parallel plate Green's function.

tion (MFIE) and moment method analysis are used to represent a forward model of the field applicator apparatus. The Green's function, MFIE and moment method approach offers physical insight, and direct control over forward model assumptions. Additionally, the approach offers a rigorous solution, over other approaches (such as the finite element method) which offer weak formulations. A single port X-band (8.2-12.4 GHz) rectangular waveguide-flange approach is selected for evaluation. A rectangular waveguide aperture is cut in the center of the flange and allows energy to couple between the rectangular waveguide and parallel plate region. Test samples are produced using 3-D polymer printing technology, which offers control over the material structure and crystal feature size. The goal is to demonstrate two NDE contributions for anisotropic material characterization. Specifically, 1) successful characterization of uniaxial anisotropic media and 2) successful characterization of a rotated uniaxial anisotropic material. The latter of the two cases presents the most novel contribution of this work, as a new parallel-plate Green's function is developed to accommodate the rotated anisotropy. Both uniaxial and rotated uniaxial NDE contributions accommodate critical industry needs as metal backed materials are quite prevalent and measurements currently resort to destructive techniques or assume the material is isotropic.

1.3 Limitations and Challenges

The mathematical developments presented in this research assume both dielectric and magnetic material properties are implicated. However, having both permittivity and permeability present in a material requires sufficient measurement diversity to characterize the material. Additionally, material fabrication challenges are enhanced, as most 3-D printing technologies support only dielectric structures. Relaxing the measurement and sample fabrication challenges, only dielectric samples are considered in measurements and simulations.

1.4 Resource Requirements

The Air Force Institute of Technology (AFIT) material measurements laboratory possesses Vector Network Analyzers, microwave measurement support tooling, the X-band waveguides, flanges, and CST Microwave Studio® licenses to support experimental measurements and computational electromagnetic modeling and simulation. Additionally, AFIT partnership with Air Force Research Laboratory (AFRL), Sensors Directorate, Electromagnetics Research Branch offers ability to fabricate dielectric material samples using their ultraviolet (UV) cured ink-jet type 3-D polymer printer.

1.5 Organization

This research evaluates an X-band single port waveguide probe's ability to measure designed uniaxial and rotated uniaxial materials. Chapter 2 provides background information on various published NDE probe technologies and motivates the research scope. Chapter 3 provides both a fundamental mode only and higher order mode included analytical moment method developments for a Single Port Waveguide Probe

measuring dielectric uniaxial anisotropic media. Chapter 4 provides sample synthesis information, measurement results, uncertainty and system validation. Chapter 5 demonstrates the rotated uniaxial Green's function development using a field-based approach. Both the electric and magnetic fields due to a magnetic aperture current are demonstrated. Chapter 6 implements the rotated uniaxial Green's function in the Single Port Waveguide Probe. Both fundamental mode only and higher order mode included analytical moment method developments are provided. Chapter 7 provides sample synthesis information, measurement results, uncertainty and validation. Chapter 8 provides a conclusion, remarks and suggestions for future work.

II. Background and Motivation

Previous research has addressed isotropic and anisotropic NDE techniques. Each techniques presents its own advantages and disadvantages. The trade-space effects the uncertainty of measurement results or the practicality of implementation. Measurement diversity by using different field configurations or by using multiple sample thicknesses is explored in each technique. Surveying previously devised techniques supports leveraging developed technologies for anisotropic NDE and capitalizes on a measurement systems strengths while minimizing its weaknesses.

2.1 Isotropic NDE techniques

One of the earliest isotropic NDE measurement techniques utilized an MFIE and moment method forward model [4]. The MFIE required an isotropic parallel plate Green's function to relate the uniformly filled parallel plate region to the rectangular waveguide port as shown in Figure 2. The goal of the measurement approach was to

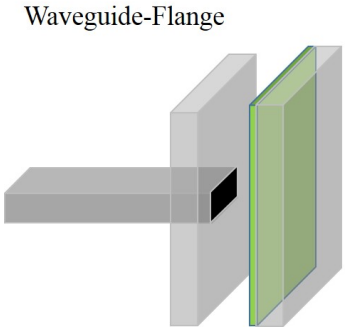

Figure 2. A single port rectangular waveguide probe. The sample is backed by a metal surface. A rectangular waveguide aperture couples into the parallel plate region.

determine a sample's isotropic permittivity and permeability using a 2-sample thickness approach. The rigorous MFIE moment method approach used the fundamental and higher order modes to calculate a propagating reflection coefficient, which was then evaluated against an experimentally obtained value. A Newton's method root

search was employed for the minimization between the calculated and measured values for each sample thickness. Overall the measurement technique demonstrated good performance measuring isotropic permittivity and permeability, however some concern over measurement uncertainty was presented in [5]. Specifically, uniqueness of solutions obtained by measuring 2-thicknesses of the same material is problematic, especially if the sample is quite lossy. Compensating measurement system performance, [6] addressed the issue by measuring a known layer in addition to the material under test (MUT) instead of another MUT thickness. Measurement diversity was somewhat improved.

Taking a significantly different approach to the previous 2-thickness technique, a 2-probe technique was employed in [7]. Using measurements from both a single port rectangular waveguide probe and a coaxial probe, as shown in Figure 3 offers

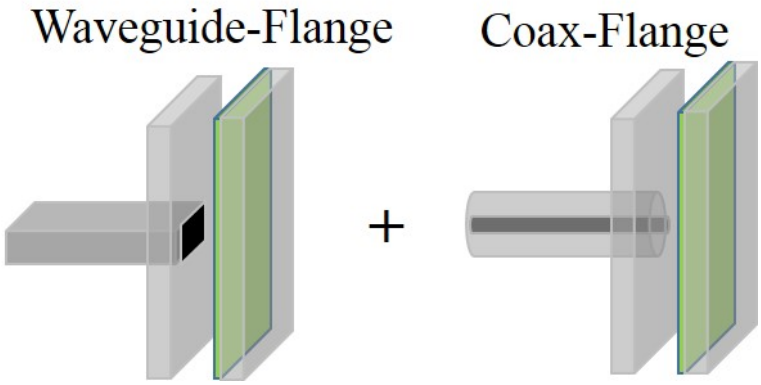

Figure 3. Improved measurement diversity was obtained by using different probes on the same metal-backed material

more measurement diversity by applying different field structures to a single thickness of metal backed isotropic material. Both the coax and rectangular waveguide probes rely on an MFIE which is solved using a moment method approach. This technique provided better measurement diversity and yielded excellent permittivity and permeability measurements of a metal-backed isotropic absorber.

Despite the capabilities offered in the previous two measurement techniques, both

methods present measurement practicality challenges. A 2-thickness method may be difficult to perform if only a single material thickness is present. An example of this might be a uniform sheet of material installed on a metal skin. The 2-probe technique could potentially suffer from measurement uncertainty challenges by requiring two distinct and separate measurements. Ideally, having one measurement system and 1 sample thickness would offer the best compromise from measurement practically and solution uncertainty.

A dual rectangular waveguide probe presented in [8], which accommodates a single sample thickness, and measures isotropic permittivity and permeability as shown in Figure 4. The dual rectangular waveguide ports offer measurement diversity from

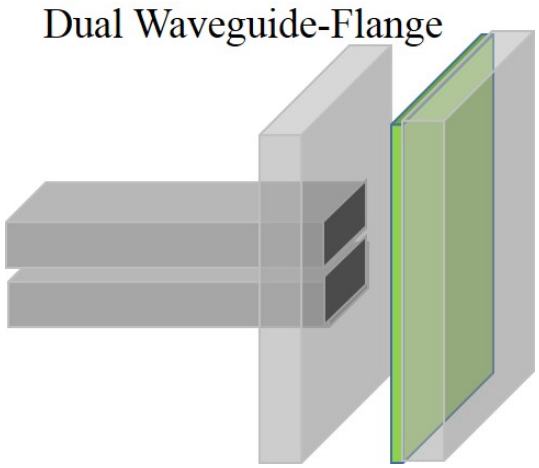

Figure 4. A dual rectangular waveguide flange approach. This technique supports measurement of isotropic permittivity and permeability from a single thickness of a metal backed material.

both the reflected and transmitted measurements. This approach also relied on Green's function based MFIE which was solved using a moment method. A minor disadvantage to this technique is the added hardware needed to perform 2-port network measurements and increased forward model complexity from having both a self-term (relating the reflected fields in the parallel plate region at either port 1 or port 2) and port-coupling term (relating the fields in the parallel plate region at

excited by port 1 and being received at port 2, or visa-versa).

Several isotropic NDE measurement techniques have been presented which demonstrate the measurement diversity trade-space. Each uses different approaches such as, different sample thicknesses, field structures or by added measurement ports. These isotropic NDE techniques satisfy measuring metal backed samples, but do not address measuring anisotropic media.

2.2 Anisotropic NDE techniques

Research in anisotropic NDE techniques offers several measurement approaches, but at the expense of demanding more measurement diversity and additional forward model complexity. Appropriate accommodation of field modal distributions and careful use of numerical methods affects results. Additionally, review of anisotropic media characterization techniques highlights potential sample-field interrogation deficiencies. Measurement uncertainty is also more heavily scrutinized as some anisotropic material have permittivities and/or permeabilities which are close in value. Lacking sufficient measurement sensitivity due to weak interrogating fields, large measurement uncertainty, or an incomplete forward model is detrimental to anisotropic material characterization performance.

Accommodating anisotropic material, a clamped flange waveguide technique demonstrated by [9] explored measuring uniaxial anisotropic media as shown in Figure 5. The clamped flange waveguide approach theoretical development used a uniaxial anisotropic parallel-plate Green's function to relate the equivalent aperture currents provided by the rectangular waveguide ports to the fields in the parallel plate region. A MFIE based forward model was employed to describe the reflected and transmission terms from the waveguide ports, which was then solved using a moment method technique. Only single thickness, dielectric uniaxial anisotropic samples were evalu-

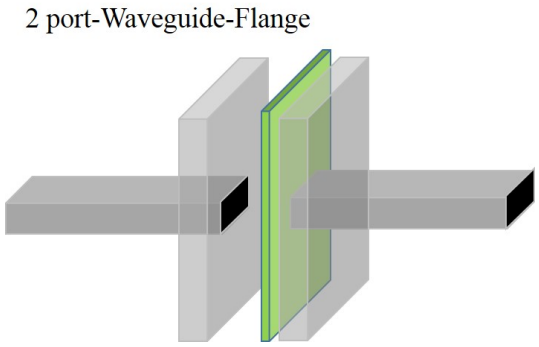

Figure 5. Clamped flange uniaxial anisotropic measurement technique.

ated using the clamped flange technique. Measurement results showed that accurate transverse permittivity results could be successfully extracted while the longitudinal permittivity experiences more uncertainty. Poor longitudinal results were due to rectangular waveguide field distribution offering very little longitudinal field interrogation of the sample region.

An alternative, coaxial clamped flange techniques developed by [10] and shown in Figure 6 also supported uniaxial anisotropic material characterization. This tech-

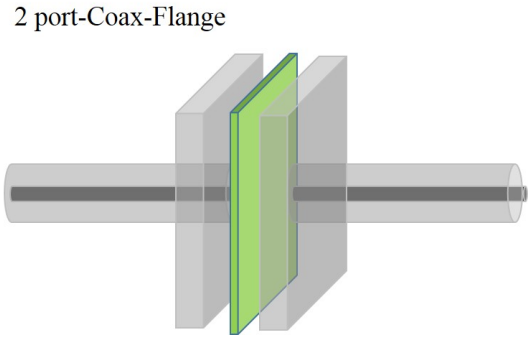

Figure 6. Clamped coaxial flange uniaxial anisotropic measurement technique.

nique also used a uniaxial anisotropic parallel plate Green's function in an MFIE, which was solved using a moment method. Similar to [9] only a dielectric sample is evaluated due to the available measurement diversity. Decent permittivity results are obtained, but it is noted in the research that the measurement apparatus experiences some challenges. In particular, [10], discusses difficulties in coupling from the coaxial

waveguide into the parallel plate region from low-permittivity materials. Poor port to material under test (MUT) coupling also effects the transmission measurements which also negatively impacts measurement performance.

Both of these clamped flanged techniques support measurement of dielectric uniaxial anisotropic material, but do not support measurement of metal backed samples. Measurement diversity is obtained by measuring both transmission and reflection from each of the ports. Additionally, both anisotropic measurement techniques have weaknesses that are inherent to their respective designs, but both offer approaches toward characterizing anisotropic media.

2.3 Motivation

Review of both isotropic and uniaxial anisotropic measurement techniques demonstrates that rectangular waveguide probes generally offer better coupling to a parallel plate sample region as compared to coaxial waveguide probes and that waveguide probes offer a strong transverse field component. The strong transverse field component yields good isotropic and transverse anisotropic permittivity results.

A first incremental step is presented in this research, to explore the single port rectangular waveguide probe's utility measuring anisotropic media. The single port waveguide probe (SPWP) is adapted in Chapter 3 to measure dielectric uniaxial anisotropic media for 2 purposes: 1) a uniaxial anisotropic Green's function exists, which would make a MFIE- moment method implementation relatively simple; and 2) a Single Port waveguide probe which measures anisotropic media offers a new measurement capability. A second step, capitalizing on the strong transverse field component of the SPWP, is to measure anisotropic media, which has unique transverse components. Using the strong transverse field interrogation component a sample would be rotated in the plane of the waveguide flange to offer measurement diversity

as shown in Figure 7.

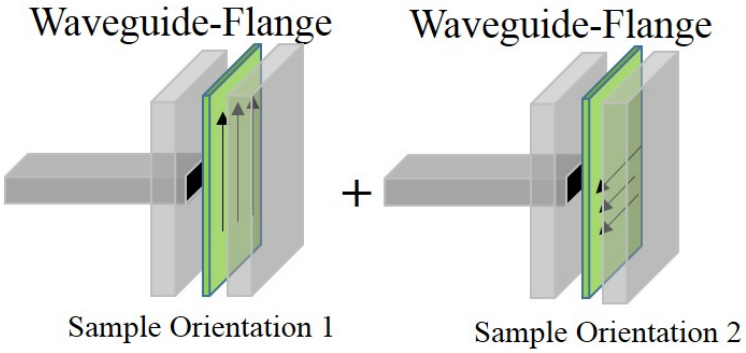

Figure 7. A Single Port Rectangular Waveguide Probe measuring a material with unique transverse material parameter elements.

Overall, previous research has identified biaxial anisotropic media (or higher anisotropy) to be a next logical step in analyzing anisotropic media, however, analysis complexity is quite daunting. An example of the challenge is demonstrated in [11], which provided an electric field integral equation (EFIE) approach which relied on Galerkin's method to compute a forward model. The measurement fixture is similar to the SPWP, but a MUT is not metal-backed, instead, it is free space backed. Measurement diversity is obtained by rotating the probe in the transverse plane to specific angles. While the research presented in [11] is described as successful, it lacks physical insight and rigor. Specifically the absence of a Green's function restricts understanding and appreciation for the phenomenology in the MUT and free space regions. As a result, the research presented in this work takes an incremental step over all of the previous research discussed and focuses on evaluating a rotated uniaxial anisotropic material. Specifically, a rotated uniaxial anisotropic Green's function is used in an MFIE which is solved using a moment method approach, which is rigorous, well understood, and based on previous works. The rotated nature of the the tensor, supports exploiting the strong transverse SPWP field, avoids the poor longitudinal measurement performance and makes a nice intermediate step from a uniaxial anisotropic Green's function toward a

biaxial anisotropic Green's function. The rotated uniaxial research begins in Chapter 5 with the development of the Green's function. It is implemented in Chapter 6 and results are discussed in Chapter 7. Chapter 8 provides conclusions and suggestions for future work.

III. Two Sample Thickness Uniaxial Anisotropic SPWP Technique Methodology

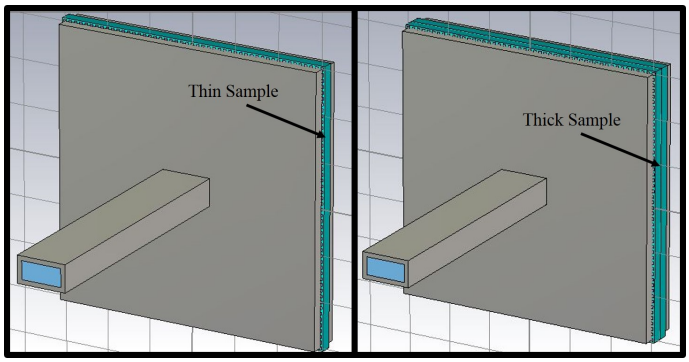

Figure 8. SPWP sample measurement system measuring thin and thick samples.

A non-destructive single port waveguide probe (SPWP), previously used for characterizing isotropic media [4], [6], [7], is enhanced to measure sheets of dielectric uniaxial anisotropic media,

$$\overleftrightarrow{\epsilon} = \begin{bmatrix} \epsilon_t & 0 & 0 \\ 0 & \epsilon_t & 0 \\ 0 & 0 & \epsilon_z \end{bmatrix}. \tag{3.1}$$

A conference paper [12] was presented and published in conjunction with the development of this document. The conference paper contains the same information presented in the fundamental mode-only oriented sections.

3.1 Fundamental Mode-Only Theoretical Development

Material parameter extraction from the SPWP is accomplished by a moment method system model. The SPWP is separated into two regions joined by an equivalent aperture current, as shown in Figure 9. For simplicity of analysis, only the fundamental mode of operation is considered present in the waveguide and at the interface of Regions 1 and 2. Region 1 is rectangular waveguide (major dimension

a, minor dimension b) and Region 2 is a parallel plate waveguide that is infinite in transverse extent and finite in thickness d.

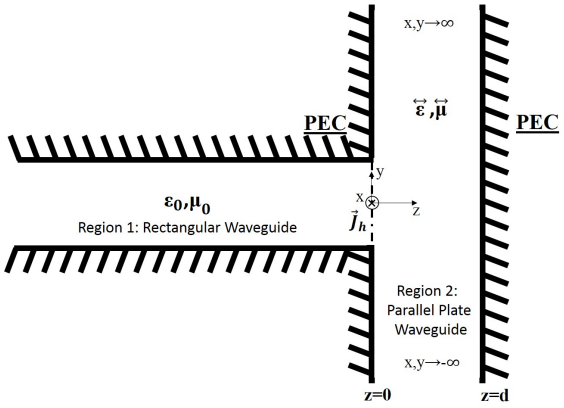

Figure 9. Cross-sectional view of the SPWP. Region 1 and Region 2 are related by a magnetic aperture current supported by Love's equivalence principle.

Moment Method Development.

The fields in Region 1 are the TE_{10}^z mode electric,

$$\vec{e}_{10} = \hat{y}\cos\left(\frac{\pi x}{a}\right) \tag{3.2}$$

and magnetic fields

$$\vec{h}_{10} = -\frac{\hat{z}\times\vec{e}_{10}}{Z_{10}} = -\hat{x}\frac{1}{Z_{10}}\cos\left(\frac{\pi x}{a}\right), \tag{3.3}$$

where $Z_{10} = \frac{j\omega\mu_0}{\gamma}$ and $\gamma = \sqrt{\left(\frac{\pi}{a}\right)^2 - k_0^2}$ with $k_0 = \omega\sqrt{\epsilon_0\mu_0}$. The incident and reflected fields in the waveguide region are

$$\vec{E}_t^{wg} = \vec{e}_{10}e^{-\gamma z} + \Gamma\vec{e}_{10}e^{\gamma z}, \tag{3.4}$$

$$\vec{H}_t^{wg} = \vec{h}_{10}e^{-\gamma z} - \Gamma\vec{h}_{10}e^{\gamma z} \tag{3.5}$$

where Γ is the dominant mode reflection coefficient of the Region 1 and 2 aperture. The aperture between Region 1 and 2 are related by the continuity of tangential electric and magnetic fields. The perfect electric conductor (PEC) flange which surrounds the aperture in Region 2 define the electric fields to be zero everywhere but the aperture; similar to the arbitrary aperture problem described in [13]. Love's equivalence theorem relates the aperture electric field as an equivalent magnetic current,

$$\begin{aligned} \vec{J}_h(\vec{\rho}') = -\hat{z} \times \vec{E}_t^{pp}(z = 0^+) = -\hat{z} \times \vec{E}_t^{wg}(z = 0^-) \\ = \hat{x}(1 + \Gamma) \cos\left(\frac{\pi x'}{a}\right). \end{aligned} \tag{3.6}$$

This allows the parallel plate region to be evaluated separately from the waveguide. The aperture is "closed" by PEC and replaced by the magnetic aperture current. A magnetic field integral equation (MFIE) evaluates the parallel plate region because it relates the equivalent magnetic aperture current, denoted by $\vec{J}_h(\vec{\rho})$ to the magnetic fields in the parallel plate waveguide. The Region 2 magnetic field is described by a scalar potential representation, as discussed in [14],

$$\vec{H}_t^{pp} = \nabla_t \Pi - \hat{z} \times \nabla_t \Psi, \tag{3.7}$$

where

$$\Pi(\vec{r}) = \iint_{S'} \vec{G}_{\pi h,t}(\rho, z|\rho, 0) \cdot \vec{J}_h(\vec{\rho}')dS' \tag{3.8}$$

and

$$\Psi(\vec{r}) = \iint_{S'} \vec{G}_{\psi h,t}(\rho, z|\rho, 0) \cdot \vec{J}_h(\vec{\rho}')dS' \tag{3.9}$$

over the waveguide aperture surface S. The presence of the current in the parallel plate waveguide region requires the use of a uniaxial Green's function $\vec{G}_{h,t}(\rho, z|\rho, 0)$ to relate the current to the parallel plate magnetic fields. These magnetic fields in-turn

are also equivalent to the magnetic fields in the rectangular waveguide at the aperture

$$\vec{H}_t^{wg}(z=0^-) = \vec{H}_t^{pp}(z=0^+) \tag{3.10}$$

and when expanded show

$$\begin{aligned} -\hat{x}\frac{1}{Z_{10}}\cos\left(\frac{\pi x}{a}\right)(1-\Gamma) = \\ \nabla_t \iint\limits_{S'} \vec{G}_{\pi h,t}(\rho,z|\rho,0)\cdot\vec{J}_h(\vec{\rho}')dS' \\ +\nabla_t \times \hat{z} \iint\limits_{S'} \vec{G}_{\psi h,t}(\rho,z|\rho,0)\cdot\vec{J}_h(\vec{\rho}')dS'. \end{aligned} \tag{3.11}$$

Evaluation of the transverse gradient and curl operators on the integrals show $\hat{x}$ and $\hat{y}$ field operators. The parallel plate waveguide has only an x-directed magnetic field at the aperture due to continuity of tangential magnetic fields. This eliminates the y-directed parallel plate field component and leaves

$$\begin{aligned} -\frac{1}{Z_{10}}\cos\left(\frac{\pi x}{a}\right)(1-\Gamma) = \\ (1+\Gamma)\left[\frac{\partial}{\partial x}\iint\limits_{S'} G_{\pi h,x}\cos(\frac{\pi x'}{a})dS' + \right. \\ \left. \frac{\partial}{\partial y}\iint\limits_{S'} G_{\psi h,x}\cos(\frac{\pi x'}{a})dS'\right] \end{aligned} \tag{3.12}$$

which relates the fields between the rectangular waveguide and parallel plate region. A testing operator

$$\iint\limits_{S} \cos(\frac{\pi x}{a})\{\}dS \tag{3.13}$$

is applied to the field expansion relationship (3.12) to capture the fundamental mode component and results in

$$-\frac{1}{Z_{10}}(1-\Gamma)\iint_S \cos^2(\frac{\pi x}{a})dS = \\ (1+\Gamma)\left[\iint_S \cos(\frac{\pi x}{a})\frac{\partial}{\partial x}\iint_{S'} G_{\pi h,x}\cos(\frac{\pi x'}{a})dS'dS + \right. \\ \left. \iint_S \cos(\frac{\pi x}{a})\frac{\partial}{\partial y}\iint_{S'} G_{\psi h,x}\cos(\frac{\pi x'}{a})dS'dS\right]. \tag{3.14}$$

Evaluating the integral on the left side yields a reduced relation

$$-\frac{1}{Z_{10}}b\frac{a}{2}(1-\Gamma) = \\ (1+\Gamma)\left[\iint_S \cos(\frac{\pi x}{a})\frac{\partial}{\partial x}\iint_{S'} G_{\pi h,x}\cos(\frac{\pi x'}{a})dS'dS + \right. \\ \left. \iint_S \cos(\frac{\pi x}{a})\frac{\partial}{\partial y}\iint_{S'} G_{\psi h,x}\cos(\frac{\pi x'}{a})dS'dS\right]. \tag{3.15}$$

The right side requires the evaluation of four integrals, two involving two Green's functions.

Implementation of the Uniaxial Parallel Plate Green's Function.

The Green's functions in (3.15) are spatial domain Green's functions and are represented in terms of a spectral domain Green's function by a 2-D Fourier transform. The spectral domain Green's functions are given by

$$\widetilde{G}_{\pi h,t} = \frac{k_{z\theta}\vec{k}_\rho}{\omega\mu_t 2\vec{k}_\rho^2}\cdot\frac{\cos\left(k_{z\theta}\left(d-|z-z'|\right)\right)+\cos\left(k_{z\theta}\left(d-(z+z')\right)\right)}{\sin(k_{z\theta}d)} \tag{3.16}$$

and

$$\widetilde{G}_{\psi h,t} = -\frac{\hat{z}\times\vec{k}_\rho\omega\epsilon_t}{2k_{z\psi}\vec{k}_\rho^2}\cdot\frac{\cos\left(k_{z\psi}\left(d-|z-z'|\right)\right)+\cos\left(k_{z\psi}\left(d-(z+z')\right)\right)}{\sin(k_{z\psi}d)} \tag{3.17}$$

as provided in [14]. These Green's functions allow for the evaluation of uniaxial dielectric and magnetic media. Integral operations in (3.15) are then rearranged such that the S and S' integrals are evaluated inside the spectral domain integral and the partial differential is applied to each piece. Each part is arranged as

$$C_\pi = \frac{1}{(2\pi)^2} \iint_{-\infty}^{\infty} \widetilde{G}_{\pi m,t}(\vec{k},0,0) j k_x e^{-j\vec{k}\cdot(\vec{\rho}-\vec{\rho}')} \iint_S \cos(\frac{\pi x}{a}) e^{j\vec{k}\cdot\vec{\rho}} dS \iint_{S'} \cos(\frac{\pi x'}{a}) e^{-j\vec{k}\cdot\vec{\rho}'} dS' dk_x dk_y \tag{3.18}$$

and

$$C_\psi = \frac{1}{(2\pi)^2} \iint_{-\infty}^{\infty} \widetilde{G}_{\psi m,t}(\vec{k},0,0) j k_x e^{-j\vec{k}\cdot(\vec{\rho}-\vec{\rho}')} \iint_S \cos(\frac{\pi x}{a}) e^{j\vec{k}\cdot\vec{\rho}} dS \iint_{S'} \cos(\frac{\pi x'}{a}) e^{-j\vec{k}\cdot\vec{\rho}'} dS' dk_x dk_y. \tag{3.19}$$

These integrals are then evaluated separately. The solutions to C_π and C_ψ are added together to complete the simplified relation

$$-\frac{1}{Z_{10}} b \frac{a}{2} (1-\Gamma) = (1+\Gamma)\left[C_\pi + C_\psi\right]. \tag{3.20}$$

Solution to the C_π and C_ψ integrals.

Solving (3.18) and (3.19) is accomplished by complex plane integration (Cauchy's integral theorem and formula) on k_y and numerical integration on k_x. The solution

$$\begin{aligned} C_\pi + C_\psi = \frac{j}{(2\pi)^2}\left(-\left(\frac{\pi}{a}\right)^2\right)\int_{-\infty}^{\infty}\frac{2+2\cos(k_x a)}{(k_x-\frac{\pi}{a})^2(k_x+\frac{\pi}{a})^2} \\ \left[\frac{k_x^2\mu_z j4\pi}{\omega\mu_t^2 d}\sum_{l=0}^{\infty}\left(\frac{l\pi}{d}\right)^2\frac{e^{-jk_{y_\pi l}b}-1}{k_{y_\pi l}^3(k_{y_\pi l}^2+k_x^2)}+\right. \\ \frac{\omega\epsilon_z j4\pi}{d}\sum_{l=0}^{\infty}\frac{e^{-jk_{y_\psi l}b}-1}{k_{y_\psi l}(k_{y_\psi l}^2+k_x^2)(1+\delta_{l=0})}- \\ \left.\frac{2\pi b k_{z\theta}}{\omega\mu_t}\cot(k_{z\theta}d)\right]dk_x \end{aligned} \tag{3.21}$$

combines both the C_π and C_ψ terms for brevity, as parts of the k_x integral are the same. Complex plane analysis on k_y reveals poles which are field propagation constants in the parallel plate structure:

$$k_{z\theta} = k_t\sqrt{1-\left(\frac{k_x}{k_{tz}}\right)^2}, \tag{3.22}$$

$$k_{y_\pi l} = k_{tz}\sqrt{1-\left(\frac{l\pi}{dk_t}\right)^2-\left(\frac{k_x}{k_{tz}}\right)^2}, \tag{3.23}$$

$$k_{y_\psi l} = k_{zt}\sqrt{1-\left(\frac{l\pi}{dk_t}\right)^2-\left(\frac{k_x}{k_{zt}}\right)^2} \tag{3.24}$$

where $k_t = \omega\sqrt{\epsilon_t\mu_t}$, $k_{tz} = \omega\sqrt{\epsilon_t\mu_z}$, $k_{zt} = \omega\sqrt{\epsilon_z\mu_t}$, and l is the parallel plate mode number $l = [0,\infty)$. Confidence in the overall solution is assured as it matches the fundamental TE "self-term" in [9]. Rearranging (3.20) for Γ provides

$$\Gamma = \frac{(1+Z_{10}\frac{2}{ba}[C_\pi+C_\psi])}{(1-Z_{10}\frac{2}{ba}[C_\pi+C_\psi])}. \tag{3.25}$$

This moment method solution provides the reflection coefficient Γ for the fundamental mode given the physical system dimensions, operational frequency, and assumed material parameters.

Moment Method Implementation.

A MATLAB® implementation of the theoretical development solves the numerical integral k_x and iterates the predicted permittivity values until the theoretical reflection coefficient Γ converges with the measured reflection coefficient; the S_{11} S-Parameter. MATLAB®'s `quadgk` function is used to evaluate the k_x integral (3.21). The first 100 parallel plate modes were used in calculations and shown to be sufficient in [9]. MATLAB®'s `lsqcurvefit` function is used to find ϵ_t and ϵ_z. `lsqcurvefit` is operated in "Trusted-Region-Reflective" as it allows specification of a solution search region. The specified search region assumes that the both uniaxial permittivities have a solution that has a real part between 1 and 10 and an imaginary part between 0 and -2.

3.2 Higher Order Mode Introduction

In the previous work, the a two-thickness measurement technique employed by the single port waveguide probe (SPWP), in Figure 8, supports electrically uniaxial anisotropic material characterization and provides excellent transverse permittivity, ϵ_t measurement. Now, both the propagating fundamental and selected evanescent higher order modes are accommodated in a moment method forward model to enhance the measurement of electrically uniaxial anisotropic media. Including the higher order modes provides better physical representation of the SPWP system and improves the longitudinal permittivity component results.

3.3 Higher Order Mode Methodology

A moment method forward model for the theoretical reflection coefficient of the SPWP is developed which assumes a propagating fundamental mode and evanescent higher order modes in the waveguide region. The waveguide has the width of 'a' and the height of 'b' and is assumed to be filled with free space ϵ_0, μ_0. The material under test is conductor backed and is placed adjacent to the waveguide flange, forming the parallel plate region. The MUT in the parallel plate region has a thickness of 'd'. The moment method development supports a set of rectangular waveguide expansion fields (represented by a set of rectangular waveguide modes), which are then tested (using the rectangular waveguide modes) to determine the weight of their contribution to the SPWP's aperture field. This concept is analogous to how moment method computations are performed on other electromagnetic problems in [13]. If infinitely many modes are assumed in both expansion and testing, then an exact representation of the SPWP's propagating reflection coefficient is obtained. However, practical implementation limits the number of modes used.

Rectangular Waveguide Field Expansion.

Formulation of a Magnetic Field Integral Equation (MFIE) begins by relating the incident and reflected fields. The relationship of the incident and scattered fields is described by the reflection coefficient Γ which exists for both the TE and TM modes, however only the Γ_{10}^{TE} is propagating (and measured as an S-parameter), the other terms are evanescent in the operating X-band frequency. The incident and reflected fields in the waveguide region, as shown in Figure 10, are

$$\vec{E}_t^{wg} = \vec{e}_{10}^{TE} e^{-\gamma_{10} z} + \sum_{m=0}^{\infty} \sum_{n=0}^{\infty} \left(\Gamma_{mn}^{TE} \vec{e}_{mn}^{TE} + \Gamma_{mn}^{TM} \vec{e}_{mn}^{TM} \right) e^{\gamma_{mn} z}, \tag{3.26}$$

$$\vec{H}_t^{wg} = \vec{h}_{10}^{TE} e^{-\gamma_{10} z} - \sum_{m=0}^{\infty} \sum_{n=0}^{\infty} \left(\Gamma_{mn}^{TE} \vec{h}_{mn}^{TE} + \Gamma_{mn}^{TM} \vec{h}_{mn}^{TM} \right) e^{\gamma_{mn} z}, \tag{3.27}$$

where

$$\begin{bmatrix} \vec{e}_{mn}^{TE} \\ \vec{e}_{mn}^{TM} \end{bmatrix} = \hat{x} \begin{bmatrix} k_y \\ k_x \end{bmatrix} \cos(k_x x) \sin(k_y y) + \hat{y} \begin{bmatrix} -k_x \\ k_y \end{bmatrix} \sin(k_x x) \cos(k_y y), \tag{3.28}$$

$$\begin{bmatrix} \vec{h}_{mn}^{TE} \\ \vec{h}_{mn}^{TM} \end{bmatrix} = \hat{z} \times \begin{bmatrix} \frac{\vec{e}_{mn}^{TE}}{Z_{mn}^{TE}} \\ \frac{\vec{e}_{mn}^{TM}}{Z_{mn}^{TM}} \end{bmatrix}. \tag{3.29}$$

The waveguide impedances are $Z_{mn}^{TE} = \frac{j\omega\mu_0}{\gamma_{mn}}$, $Z_{mn}^{TM} = \frac{\gamma_{mn}}{j\omega\epsilon_0}$, while the mode wave numbers are: $k_x = \frac{m\pi}{a}$, $k_y = \frac{n\pi}{b}$ and the propagation constraint $\gamma_{mn} = \sqrt{k_x^2 + k_y^2 - k_0^2}$ with $k_0 = \omega\sqrt{\epsilon_0\mu_0}$. Note that based on the symmetry of the waveguide aperture that only a particular set of modes will be excited. Specifically, odd m modes and even n modes will be excited, with the exception that the $n = 0$ modes is are not permitted for the TM field structure. Continuity of the tangential electric and magnetic fields

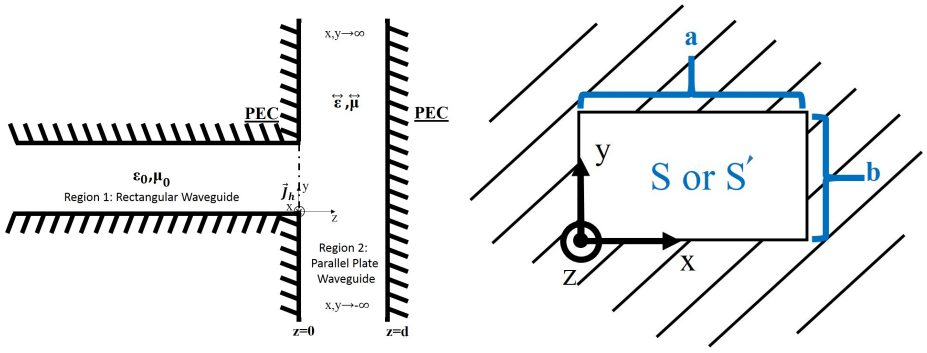

Figure 10. Left: SPWP Cross-Sectional View Right: End-View of Waveguide-Flange Aperture Interface. Note the location of the origin is in the lower left corner of the aperture.

relates the aperture between Region 1 and 2 as shown in Figure 10. Love's equivalence theorem allows the aperture electric field to be represented by an equivalent magnetic

surface current,

$$\vec{J}_h(\hat{x}' + \hat{y}') = \vec{J}_h(\vec{\rho}') = -\hat{z} \times \vec{E}_t^{pp}(z = 0^+) = -\hat{z} \times \vec{E}_t^{wg}(z = 0^-). \tag{3.30}$$

Viewing the aperture current from the waveguide region and applying Love's equivalence theorem,

$$\begin{aligned} -\hat{z} \times \vec{E}_t^{wg}(z = 0^-) &= -Z_{10}^{TE}\vec{h}_{10}^{TE} - \sum_{m=0}^{\infty}\sum_{n=0}^{\infty}\left(\Gamma_{mn}^{TE}Z_{mn}^{TE}\vec{h}_{mn}^{TE} + \Gamma_{mn}^{TM}Z_{mn}^{TM}\vec{h}_{mn}^{TM}\right) \\ = -\sum_{m=0}^{\infty}\sum_{n=0}^{\infty}&\left(\overline{\Gamma}_{mn}^{TE}Z_{mn}^{TE}\vec{h}_{mn}^{TE} + \Gamma_{mn}^{TM}Z_{mn}^{TM}\vec{h}_{mn}^{TM}\right), \text{ where } \overline{\Gamma}_{mn}^{TE} = \left(\delta_{mn10}^{TE} + \Gamma_{mn}^{TE}\right). \end{aligned} \tag{3.31}$$

Note that this changes the above magnetic field equation for the waveguide region to

$$\vec{h}_{10}^{TE} - \sum_{m=0}^{\infty}\sum_{n=0}^{\infty}\left(\Gamma_{mn}^{TE}\vec{h}_{mn}^{TE} + \Gamma_{mn}^{TM}\vec{h}_{mn}^{TM}\right) = 2\vec{h}_{10}^{TE} - \sum_{m=0}^{\infty}\sum_{n=0}^{\infty}\left(\overline{\Gamma}_{mn}^{TE}\vec{h}_{mn}^{TE} + \Gamma_{mn}^{TM}\vec{h}_{mn}^{TM}\right). \tag{3.32}$$

Parallel-Plate Waveguide Field Expansion.

Synthesizing an equivalent magnetic aperture current allows the parallel plate waveguide region (Region 2) to be isolated and evaluated as a magnetic field integral equation (MFIE). The magnetic field in this region is described by a scalar potential representation as discussed in [14]:

$$\vec{H}_t^{pp} = \nabla_t \Pi - \hat{z} \times \nabla_t \Psi, \tag{3.33}$$

where

$$\Pi(\vec{r}) = \iint_{S'} \vec{G}_{\pi h,t}(\rho, z|\rho, 0) \cdot \vec{J}_h(\vec{\rho}')dS', \quad \text{and} \quad \Psi(\vec{r}) = \iint_{S'} \vec{G}_{\psi h,t}(\rho, z|\rho, 0) \cdot \vec{J}_h(\vec{\rho}')dS' \tag{3.34}$$

over the waveguide aperture surface S'. Relating the magnetic aperture current to magnetic fields in the region requires the use of a uniaxial Green's function $\vec{G}_{h,t}(\rho, z|\rho, 0)$. These magnetic fields are also the same as the aperture magnetic fields in the rectangular waveguide,

$$\vec{H}_t^{wg}(z = 0^-) = \vec{H}_t^{pp}(z = 0^+) \tag{3.35}$$

which allows Region 2 to be related back to Region 1. When the field relationship is expanded, it shows

$$\begin{aligned} 2\vec{h}_{10}^{TE} - \lim_{M,N\to\infty} \sum_{m=0}^{M} \sum_{n=0}^{N} \left(\overline{\Gamma}_{mn}^{TE} \vec{h}_{mn}^{TE} + \Gamma_{mn}^{TM} \vec{h}_{mn}^{TM} \right) = \\ \nabla_t \iint_{S'} \vec{G}_{\pi h,t}(\rho, z|\rho, 0) \cdot \left[- \lim_{M,N\to\infty} \sum_{m=0}^{M} \sum_{n=0}^{N} \left(\overline{\Gamma}_{mn}^{TE} Z_{mn}^{TE} \vec{h}_{mn}^{TE} + \Gamma_{mn}^{TM} Z_{mn}^{TM} \vec{h}_{mn}^{TM} \right) \right] dS' \\ + \nabla_t \times \hat{z} \iint_{S'} \vec{G}_{\psi h,t}(\rho, z|\rho, 0) \cdot \left[- \lim_{M,N\to\infty} \sum_{m=0}^{M} \sum_{n=0}^{N} \left(\overline{\Gamma}_{mn}^{TE} Z_{mn}^{TE} \vec{h}_{mn}^{TE} + \Gamma_{mn}^{TM} Z_{mn}^{TM} \vec{h}_{mn}^{TM} \right) \right] dS'. \end{aligned} \tag{3.36}$$

Having the field expansion relationship defined, testing is performed. At this point the mode indices m and n are truncated to respective finite values M and N.

Field Testing.

Testing captures the weight of a particular mode's contribution to the expansion set of fields that describe the aperture of the system. Obtaining a unique solution requires that the number of testing modes be at least the same as the number of expansion modes. Regrouping the terms in (3.36) to consolidate reflection coefficients and applying the testing operator,

$$\iint_S \vec{h}_{uv}^{*} \cdot \{ \quad \} dS, \tag{3.37}$$

where u and v are the mode indices of the testing field distribution, results in a scalar relation and supports additional regrouping. Note that the testing operator tests either TE or TM modes. Employing the Fourier transform,

$$G_{\pi h,t}(\vec{\rho}', z', \vec{\rho}, z) = \frac{1}{(2\pi)^2} \iint_{-\infty}^{\infty} \widetilde{G}_{\pi h,t}(\vec{\lambda}_\rho, z', z) e^{j\vec{\lambda}_\rho \cdot (\vec{\rho} - \vec{\rho}')} d^2\lambda, \quad \text{(Note that } z = z' = 0\text{)} \tag{3.38}$$

the spatial Green's functions are transformed to the spectral domain, which simplifies calculations. Applying the derivatives to the spectral domain Green's functions and rearranging the S and S' integrals within the spectral integrals, such that x' and y' are with the S' set of integrals and x and y are with the S results in an expanded relationship which can be seen in Appendix A as equation (A.2).

Evaluating the testing operator S integrals in (A.2) results in both TE and TM solutions for the x and y magnetic field components:

$$\iint_S h^*_{uvx} e^{j\vec{\lambda}_\rho \cdot \vec{\rho}} dS = C_x \left(\frac{(e^{j(a\lambda_x)}(-1)^u - 1)}{((\frac{u\pi}{a})^2 - \lambda_x^2)} \frac{\lambda_y (e^{j(b\lambda_y)}(-1)^v - 1)}{((\frac{v\pi}{b})^2 - \lambda_y^2)} \right), \tag{3.39}$$

$$\text{where} \quad C_x = \begin{cases} \frac{-j(\frac{u\pi}{a})^2}{Z^{TE}_{uv}}^*, h^{*\ TE}_{uvx} \\ \frac{j\frac{u\pi}{a}\frac{v\pi}{b}}{Z^{TM}_{uv}}^*, h^{*\ TM}_{uvx} \end{cases} \tag{3.40}$$

$$\iint_S h^*_{uvy} e^{j\vec{\lambda}_\rho \cdot \vec{\rho}} dS = C_y \left(\frac{(e^{j(b\lambda_y)}(-1)^v - 1)}{((\frac{v\pi}{b})^2 - \lambda_y^2)} \frac{\lambda_x (e^{j(a\lambda_x)}(-1)^u - 1)}{((\frac{u\pi}{a})^2 - \lambda_x^2)} \right), \tag{3.41}$$

$$\text{where} \quad C_y = \begin{cases} \frac{-j(\frac{v\pi}{b})^2}{Z^{TE}_{uv}}^*, h^{*\ TE}_{uvy} \\ \frac{-j\frac{u\pi}{a}\frac{v\pi}{b}}{Z^{TM}_{uv}}^*, h^{*\ TM}_{uvy} \end{cases} \tag{3.42}$$

The S' integrals in (A.2) are evaluated in a similar fashion, but only have solutions which correspond to either TE or TM. Three remaining integrals in (A.2) need to

be evaluated. These integrals are the testing operators acting on the propagating fundamental mode excitation, and the expansion TE and TM modes respectively.

Moment Method Development Consolidation.

Solving the S and S' integrals created by applying the testing operators to the field expansion terms supports additional consolidation. Inserting the uniaxial Green's functions

$$\widetilde{G}_{\pi h,t} = \frac{\lambda_{z\theta}\vec{\lambda}_\rho}{\omega\mu_t 2\vec{\lambda}_\rho^2} \cdot \frac{\cos\left(\lambda_{z\theta}\left(d-|z-z'|\right)\right)+\cos\left(\lambda_{z\theta}\left(d-(z+z')\right)\right)}{\sin(\lambda_{z\theta}d)} \tag{3.43}$$

and

$$\widetilde{G}_{\psi h,t} = -\frac{\hat{z}\times\vec{\lambda}_\rho\omega\epsilon_t}{2\lambda_{z\psi}\vec{\lambda}_\rho^2} \cdot \frac{\cos\left(\lambda_{z\psi}\left(d-|z-z'|\right)\right)+\cos\left(\lambda_{z\psi}\left(d-(z+z')\right)\right)}{\sin(\lambda_{z\psi}d)} \tag{3.44}$$

where

$$\lambda_{z\theta} = \pm\sqrt{k_t^2-\frac{\mu_t}{\mu_z}(\lambda_x^2+\lambda_y^2)}, \qquad \lambda_{z\psi} = \pm\sqrt{k_t^2-\frac{\epsilon_t}{\epsilon_z}(\lambda_x^2+\lambda_y^2)} \tag{3.45}$$

as provided in [14] into the consolidated relationship described in (A.2) and grouping the λ_x and λ_y integrals results in:

$$\begin{aligned}
2\left(\frac{(\frac{\pi}{a})^2}{Z_{10}^{TE*}Z_{10}^{TE}}\right)\frac{ab}{2}\delta_{uv10}^{TE} = \sum_{m=0}^{M}\sum_{n=0}^{N}\overline{\Gamma}_{mn}^{TE}\Bigg[\left(\left(\frac{m\pi}{a}\right)^2+\left(\frac{n\pi}{b}\right)^2\right)\frac{ab(1+\delta_{uvm0}^{TE})}{4Z_{mn}^{TE*}Z_{mn}^{TE}}\delta_{uvmn}^{TE}+ \\
\frac{(C_x+C_y)(k_x^2+k_y^2)}{\omega\mu_t(2\pi)^2}\Omega+\frac{\omega\epsilon_t C_x k_x^2}{(2\pi)^2}\Phi-\frac{\omega\epsilon_t(C_x k_y^2+C_y k_x^2)}{(2\pi)^2}\Upsilon+\frac{\omega\epsilon_t C_y k_y^2}{(2\pi)^2}X\Bigg]+ \\
\sum_{m=0}^{M}\sum_{n=0}^{N}\Gamma_{mn}^{TM}\Bigg[\left(\left(\frac{m\pi}{a}\right)^2+\left(\frac{n\pi}{b}\right)^2\right)\frac{ab(1+\delta_{uvm0}^{TM})}{4Z_{mn}^{TM*}Z_{mn}^{TM}}\delta_{uvmn}^{TM}- \\
\frac{\omega\epsilon_t C_x k_x k_y}{(2\pi)^2}\Phi+\frac{\omega\epsilon_t(-C_x+C_y)k_x k_y}{(2\pi)^2}\Upsilon+\frac{\omega\epsilon_t C_y k_x k_y}{(2\pi)^2}X\Bigg]
\end{aligned} \tag{3.46}$$

where:

$$\Omega = \int_{-\infty}^{\infty} \frac{(e^{j(a\lambda_x)}(-1)^u - 1)}{((\frac{u\pi}{a})^2 - \lambda_x^2)} \frac{\lambda_x^2 (e^{-j(a\lambda_x)}(-1)^m - 1)}{(k_x^2 - \lambda_x^2)} \int_{-\infty}^{\infty} \frac{\lambda_{z\theta}}{(\lambda_x^2 + \lambda_y^2)} \frac{\cos(\lambda_{z\theta} d)}{\sin(\lambda_{z\theta} d)} \frac{(e^{j(b\lambda_y)}(-1)^v - 1)}{((\frac{v\pi}{b})^2 - \lambda_y^2)} \frac{\lambda_y^2 (e^{-j(b\lambda_y)}(-1)^n - 1)}{(k_y^2 - \lambda_y^2)} d\lambda_y d\lambda_x \tag{3.47}$$

$$\Phi = \int_{-\infty}^{\infty} \frac{(e^{j(a\lambda_x)}(-1)^u - 1)}{((\frac{u\pi}{a})^2 - \lambda_x^2)} \frac{(e^{-j(a\lambda_x)}(-1)^m - 1)}{(k_x^2 - \lambda_x^2)} \int_{-\infty}^{\infty} \frac{1}{\lambda_{z\psi}(\lambda_x^2 + \lambda_y^2)} \frac{\cos(\lambda_{z\psi} d)}{\sin(\lambda_{z\psi} d)} \frac{(e^{j(b\lambda_y)}(-1)^v - 1)}{((\frac{v\pi}{b})^2 - \lambda_y^2)} \frac{\lambda_y^4 (e^{-j(b\lambda_y)}(-1)^n - 1)}{(k_y^2 - \lambda_y^2)} d\lambda_y d\lambda_x \tag{3.48}$$

$$\Upsilon = \int_{-\infty}^{\infty} \frac{(e^{j(a\lambda_x)}(-1)^u - 1)}{((\frac{u\pi}{a})^2 - \lambda_x^2)} \frac{\lambda_x^2 (e^{-j(a\lambda_x)}(-1)^m - 1)}{(k_x^2 - \lambda_x^2)} \int_{-\infty}^{\infty} \frac{1}{\lambda_{z\psi}(\lambda_x^2 + \lambda_y^2)} \frac{\cos(\lambda_{z\psi} d)}{\sin(\lambda_{z\psi} d)} \frac{(e^{j(b\lambda_y)}(-1)^v - 1)}{((\frac{v\pi}{b})^2 - \lambda_y^2)} \frac{\lambda_y^2 (e^{-j(b\lambda_y)}(-1)^n - 1)}{(k_y^2 - \lambda_y^2)} d\lambda_y d\lambda_x \tag{3.49}$$

$$X = \int_{-\infty}^{\infty} \frac{(e^{j(a\lambda_x)}(-1)^u - 1)}{((\frac{u\pi}{a})^2 - \lambda_x^2)} \frac{\lambda_x^4 (e^{-j(a\lambda_x)}(-1)^m - 1)}{(k_x^2 - \lambda_x^2)} \int_{-\infty}^{\infty} \frac{1}{\lambda_{z\psi}(\lambda_x^2 + \lambda_y^2)} \frac{\cos(\lambda_{z\psi} d)}{\sin(\lambda_{z\psi} d)} \frac{(e^{j(b\lambda_y)}(-1)^v - 1)}{((\frac{v\pi}{b})^2 - \lambda_y^2)} \frac{(e^{-j(b\lambda_y)}(-1)^n - 1)}{(k_y^2 - \lambda_y^2)} d\lambda_y d\lambda_x \tag{3.50}$$

At this point the λ_x and λ_y integrals could be evaluated numerically, but at the risk of increasing computational time and potential numerical integration convergence issues. It is also observed in (3.47-3.50) that there are several singularities in each integral. Analyzing the λ_y integrals by complex plane analysis, supports further simplification, and offers physical insight.

Solutions to the λ_y integrals by Complex Plane Integration.

Complex plane analysis as described in [15] is used to evaluate the λ_y integrals. Cauchy's integral theorem is used to evaluate the contributions of each pole. Depending on the selected test and expansion modes employed, different poles may overlap. Five unique analysis cases occur for each λ_y integral. An example of the most general case, $n \neq v \neq 0$ is shown in Figure 11 for the λ_y part of the Ω integral. Physical insight is gained by reviewing the poles in the complex plane. As an example, the series of poles implicated by the $\sin(\lambda_{z\theta} d)$ term occur due to the modes exhibited in the parallel plate waveguide structure. Simplifying the four integrals (3.47-3.50) for each of the five test and expansion case results in 20 independent complex plane integral calculations, however only 16 integrals need to be evaluated as (3.46) mul-

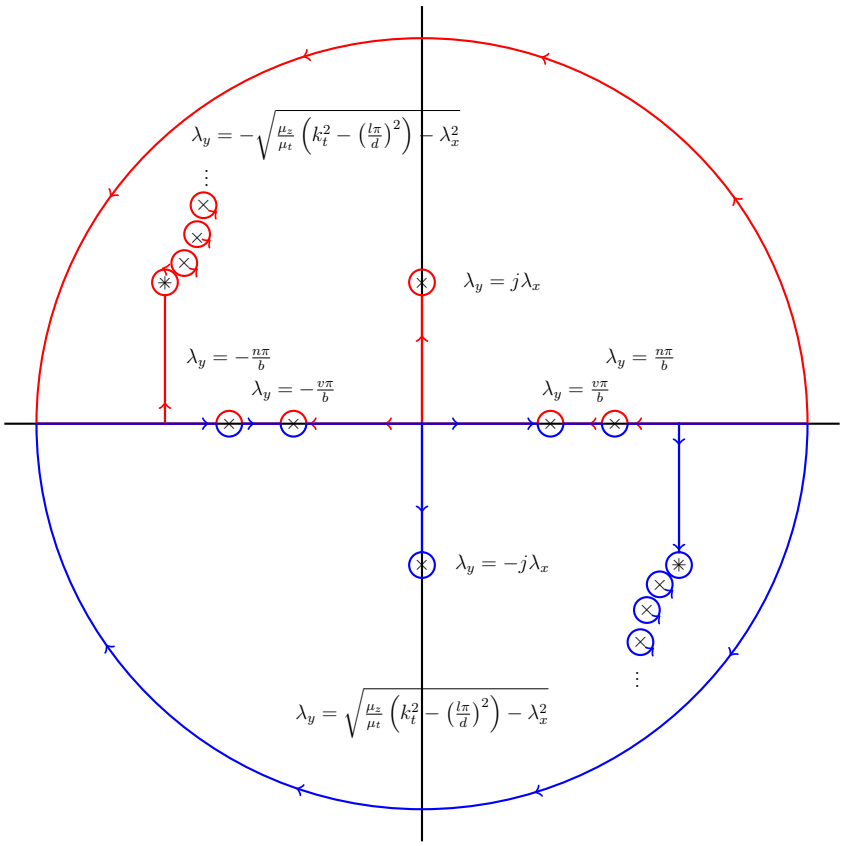

Figure 11. The complex plane showing the poles for the λ_y part of the λ_y part of the Ω integral. Note the series of poles induced by the $\sin(\lambda d)$ part. These represent the parallel plate modes exhibited in the parallel plate waveguide structure. Individual poles are denoted by a $\times$ symbol, while a double pole is denoted by $*$ symbol.

tiplies certain integral cases by zero and thus do not need evaluation. The analysis also shows that the physical symmetry of the SPWP allows for only certain mode distribution values to exist. Specifically, testing v and expansion n values must be even due to x axis symmetry of the fields. It is also inferred by symmetry about the y axis of the aperture that the testing u and expansion m values must be odd. The 16 λ_y integrals, are inserted back into (3.46) for each case, which supports additional

simplification. Rewriting the simplified results leaves

$$2\left(\frac{(\frac{\pi}{a})^2}{Z_{10}^{TE*}Z_{10}^{TE}}\right)\frac{ab}{2}\delta_{uv10}^{TE} = \sum_{m=0}^{M}\sum_{n=0}^{N}\overline{\Gamma}_{mn}^{TE}\left[\left(\left(\frac{m\pi}{a}\right)^2+\left(\frac{n\pi}{b}\right)^2\right)\frac{ab(1+\delta_{uvm0}^{TE})}{4Z_{mn}^{TE*}Z_{mn}^{TE}}\delta_{uvmn}^{TE}+TOT\right]+ \sum_{m=0}^{M}\sum_{n=0}^{N}\Gamma_{mn}^{TM}\left[\left(\left(\frac{m\pi}{a}\right)^2+\left(\frac{n\pi}{b}\right)^2\right)\frac{ab(1+\delta_{uvm0}^{TM})}{4Z_{mn}^{TM*}Z_{mn}^{TM}}\delta_{uvmn}^{TM}+TOT_{TM}\right]. \tag{3.51}$$

TOT and TOT_{TM} change depending on which case is evaluated in (3.51). The cases are identified below. If TOT_{TM} is not explicitly stated for a case, then it is zero.

Case 5 where $n = 0$ and $v = 0$ is the same as the previously developed fundamental mode only solution and is shown to be:

$$TOT = \int_{-\infty}^{\infty}\frac{(e^{j(a\lambda_x)}(-1)^u-1)}{((\frac{u\pi}{a})^2-\lambda_x^2)}\frac{(e^{-j(a\lambda_x)}(-1)^m-1)}{(k_x^2-\lambda_x^2)} \left(\frac{C_xk_x^2}{\omega\mu_t(2\pi)^2}j4\pi\frac{\mu_z}{\mu_t d}\sum_{l=0}^{\infty}\frac{\lambda_x^2(\frac{l\pi}{d})^2}{((\lambda_{y\theta}^B)^2+\lambda_x^2)}\frac{(1-e^{-jb\lambda_{y\theta}^B})}{(\lambda_{y\theta}^B)^3}+ \frac{C_xk_x^2}{\omega\mu_t(2\pi)^2}2\pi b\frac{\lambda_{z\theta}^v\cos(\lambda_{z\theta}^v d)}{\sin(\lambda_{z\theta}^v d)}+\frac{\omega\epsilon_tC_xk_x^2}{(2\pi)^2}j4\pi\frac{\epsilon_z}{\epsilon_t d}\sum_{l=0}^{\infty}\frac{(1-e^{-jb\lambda_{y\psi}^B})}{\lambda_{y\psi}^B((\lambda_{y\psi}^B)^2+\lambda_x^2)(1+\delta_{l,0})}\right)d\lambda_x \tag{3.52}$$

where the parallel plate and waveguide modes describe propagation constraints in the parallel plate region:

$$\lambda_{z\theta}^n = k_t\sqrt{1-\left(\frac{\lambda_x}{k_{tz}}\right)^2-\left(\frac{\frac{\pm n\pi}{b}}{k_{tz}}\right)^2}\quad \lambda_{z\theta}^v = k_t\sqrt{1-\left(\frac{\lambda_x}{k_{tz}}\right)^2-\left(\frac{\frac{\pm v\pi}{b}}{k_{tz}}\right)^2} \tag{3.53}$$

$$\lambda_{y\theta}^B = k_{tz}\sqrt{1-\left(\frac{\frac{l\pi}{d}}{k_t}\right)^2-\left(\frac{\lambda_x}{k_{tz}}\right)^2} \tag{3.54}$$

$$\lambda_{z\psi}^{n} = k_t\sqrt{1-\left(\frac{\lambda_x}{k_{zt}}\right)^2-\left(\frac{\frac{\pm n\pi}{b}}{k_{zt}}\right)^2} \quad \lambda_{z\psi}^{v} = k_t\sqrt{1-\left(\frac{\lambda_x}{k_{zt}}\right)^2-\left(\frac{\frac{\pm v\pi}{b}}{k_{zt}}\right)^2} \tag{3.55}$$

$$\lambda_{y\psi}^{B} = k_{zt}\sqrt{1-\left(\frac{\frac{l\pi}{d}}{k_t}\right)^2-\left(\frac{\lambda_x}{k_{zt}}\right)^2} \tag{3.56}$$

where

$$k_t^2 = \omega^2\epsilon_t\mu_t \quad k_{zt}^2 = \omega^2\epsilon_z\mu_t \quad k_{tz}^2 = \omega^2\epsilon_t\mu_z \tag{3.57}$$

and l is the parallel plate mode number, $l = [0, \infty)$. In computational practice, the number of parallel plate modes are truncated to $l = [0, 100]$ and is shown to be sufficient based on a convergence study performed in [9]. The λ_x integrals are evaluated by numerical integration along the real axis.

A complete summary of the development including the remaining cases is provided in Appendix A.

3.4 Computational Formulation of the Forward Problem

Employing the theoretical development described in the previous section requires casting the summations in (A.3) as a matrix

$$\left[\begin{array}{ccc|ccc} CASE_{TE_{uv},TE_{mn}} & \cdots & & CASE_{TE_{uv},TM_{mn}} & \cdots & \\ \vdots & \ddots & & \vdots & \ddots & \\ \hline CASE_{TM_{uv},TE_{mn}} & \cdots & & CASE_{TM_{uv},TM_{mn}} & \cdots & \\ \vdots & \ddots & & \vdots & \ddots & \end{array}\right] \cdot \begin{bmatrix} \overline{\Gamma}_{mn}^{TE} \\ \vdots \\ \Gamma_{mn}^{TM} \\ \vdots \end{bmatrix} = \begin{bmatrix} 2\left(\frac{(\frac{\pi}{a})^2}{Z_{10}^{TE*}Z_{10}^{TE}}\right)\frac{ab}{2} \\ 0 \\ 0 \\ \vdots \end{bmatrix}. \tag{3.58}$$

This system of equations accommodates the expansion of an arbitrary number of TE or TM modes which are then tested, and also maintains a square matrix for inversion. The square matrix with element terms denoted by $CASE_{test\ mode,expand\ mode}$ are

calculated and populated depending on the five integral solution cases. Calculation of the $\overline{\Gamma}$ and Γ elements is done by inverting the impedance matrix and multiplying it by the right hand side. MATLAB®'s `inv()`, inversion function and `quadgk()` numerical integration function are used for the forward model analysis. MATLAB®'s `lsqcurvefit()`, operated in the "Trusted-Region-Reflective" is used to curve fit the forward model Γ_{10}^{TE} data to measured S_{11} S-parameter data at each frequency point.

IV. Two Sample Thickness Uniaxial Anisotropic SPWP Technique Results

A conference paper [12] was presented and published in conjunction with the development of this document. The conference paper contains the same information presented in the fundamental mode-only oriented results sections.

The SPWP in this analysis consists of a 6" length of X-band (8.2-12.4 GHz) waveguide attached to a 6" square 0.25" thick flange. The flange has a rectangular waveguide aperture cut into the center. A sample is placed in front of the flange aperture and is backed by 6" square metal slab. Measurement diversity is obtained by measuring two different thicknesses of the same metal-backed sample, as shown in Figure 8. Calibrated sample reflection coefficients from the rectangular waveguide-flange aperture are measured with a vector network analyzer (VNA). Obtaining the constitutive parameters requires an inverse solution which compares the measured sample reflection coefficient against a moment method based SPWP sample reflection coefficient forward model given an initial guess of ϵ_t and ϵ_z. The parameters ϵ_t and ϵ_z are refined until the measured and predicted reflection coefficients converge to a specified tolerance.

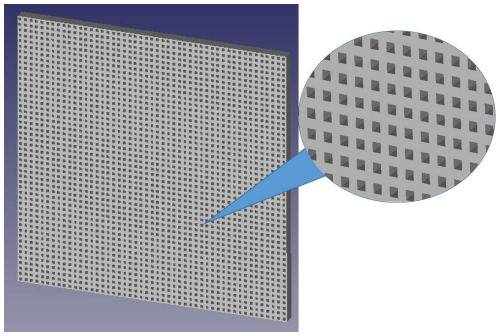

Figure 12. Example of a uniaxial material with tetragonal occlusions.

Aiding SPWP system evaluation, a uniaxial sample is designed via crystallographic symmetry as shown in Figure 12 and simulated in CST Microwave Studio®.

Laboratory measurements of a commercial honeycomb absorber are also made, demonstrating SPWP system performance. Uncertainty in sample thickness is accounted in both simulation and measurement. SPWP simulated results are compared with a lumped element equivalent circuit prediction of permittivity and simulated Nicolson-Ross-Weir rectangular waveguide material measurement technique [16],[17], results.

4.1 Simulated SPWP Evaluation

Simulation of the SPWP provides a controlled means to evaluate system performance. A model of the physical system and Thru-Reflect-Line (TRL) calibration waveguide standards were modeled and simulated in CST Microwave Studio®'s frequency domain solver. Low and high contrast dielectric uniaxial samples were designed to evaluate the SPWP. A 2-port TRL system calibration was performed on the simulated data using the simulated SPWP and standards to remove systematic errors in the models as demonstrated in [18].

Uniaxial Sample Design and Lumped Element Prediction.

The uniaxial sample in Figure 12 is designed using crystallographic symmetry [1] and has uniformly spaced tetragonal cells. These cells are divided into 49 columns and rows $(x,\ y)$ and are embedded in a 6.125" $(w,\ h)$ square slab that is 0.25" thick (l). Each cell is 0.0625" square $(h_c,\ w_c)$ and is 0.25" deep (l_c). A notional slab material with a permittivity (ϵ_m) of $2.5 - j0.2$ and a cell material with a permittivity of (ϵ_a) of $1 - j0$ for the low contrast sample, and $9.9 - j0$ for the high contrast sample are used. The high loss slab material is employed to give the appearance that the 6" square parallel flange and metal plate are infinite in extent, as the energy from the fields will dissipate rapidly as they travel toward the edge of the parallel plate region. Using a less lossy material would require time gating to remove the edge effect discontinuities

[19]. A lumped element equivalent circuit model adapted from [20] provides predicted values for uniaxial permittivity. The transverse uniaxial permittivity component has a solution that is dependent on the slab-cell permittivity contrast. When $\epsilon_a < \epsilon_m$

$$\epsilon_t = \frac{\epsilon_m\ (w - w_c\, x)}{w} + \frac{\epsilon_a\, \epsilon_m\, l_c\, w_c\, x\, h}{l\, w\ (\epsilon_a\, h - \epsilon_a\, h_c\, y + \epsilon_m\, h_c\, y)} \tag{4.1}$$

and for $\epsilon_a > \epsilon_m$

$$\epsilon_t = \frac{h}{l\, w\ \left(\frac{h - h_c\, y}{\epsilon_m w l} + \frac{h_c\, y}{l_c\, (\epsilon_m w + \epsilon_a\, w_c\, x - \epsilon_m w_c\, x)}\right)}. \tag{4.2}$$

The longitudinal permittivity component is

$$\epsilon_z = \frac{\epsilon_m\, l}{l_c} + \frac{h_c\, w_c\, x\, l\, y\ (\epsilon_a - \epsilon_m)}{l_c\, h\, w}. \tag{4.3}$$

These lumped equivalent circuit equations aid design and prediction of a uniaxial material.

Comparison to Rectangular Waveguide.

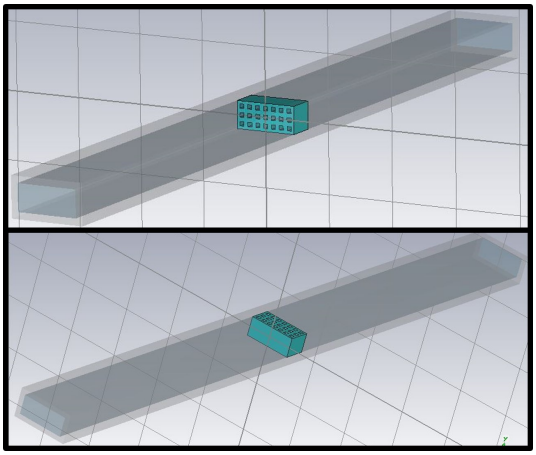

Figure 13. Rectangular waveguide measurement of a uniaxial sample. Top: transverse permittivity measurement, Bottom: normal permittivity measurement.

The lumped element results for the uniaxial low and high contrast samples are also

compared against CST Microwave Studio® simulated rectangular waveguide measurements. These results are compared against the SPWP simulations. Evaluating the uniaxial sample in a legacy measurement system, such a rectangular waveguide demonstrates that the sample is macroscopically homogeneous and verifies agreement with lumped element predicted values. A uniaxial sample from the slab in Figure 12 was "cut" and inserted into the rectangular waveguide. Two measurement orientations are required to measure the transverse ϵ_t and normal ϵ_z permittivites as shown in Figure 13. TRL calibrated waveguide measurement simulations were performed for the low and high contrast uniaxial samples. Due to the sample thickness (0.4") permittivites were extracted using a Newton 1-D root search [21].

SPWP Sample Thickness Uncertainty Analysis.

Two different thickness samples are needed to extract the uniaxial material parameters. Sample thickness is evaluated in a Monte Carlo uncertainty analysis for both samples simulated in CST Microwave Studio®. Each thickness is evaluated as a uniform random variable with the actual thickness (thin sample 0.25" and thick sample 0.5" for low contrast sample and thin sample 0.125" and thick sample 0.25" for high contrast sample) as the mean and the upper and lower limits of the distribution being ±0.004". 1000 MATLAB® trials were run on the simulated reflection coefficients to calculate the mean and 2 standard deviations of uncertainty in uniaxial permittivity.

Fundamental Mode Low and High Contrast Simulated Uniaxial Results.

The low contrast uniaxial sample results shown in Figure 14 demonstrate that the lumped element predicted, rectangular waveguide, and transverse SPWP permittivity results agree, while the longitudinal SPWP permittivity results have large uncertainty

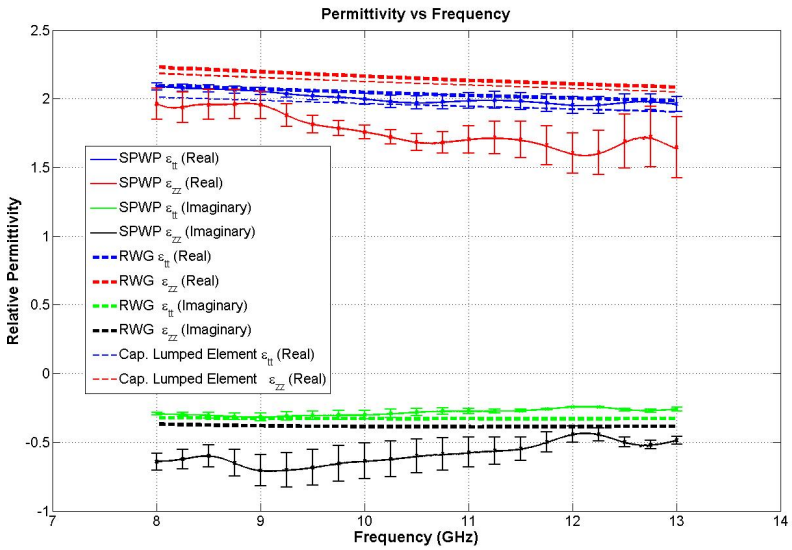

Figure 14. Low contrast uniaxial sample comparison: lumped element, rectangular waveguide, and SPWP.

and are different from the lumped element predicted and rectangular waveguide results. The same performance is observed for the high contrast uniaxial sample case in Figure 15 where the SPWP longitudinal results are different from the lumped element predicted or rectangular waveguide. The poor longitudinal measurement is due to the absence of a strong longitudinal electric field component in the vicinity of the waveguide aperture because the waveguide only produces a transverse electric field. Any significant coupling into the longitudinal field component is not observed by the aperture, as it propagates outward from the aperture area. Potential remedies to these issues include:

1. Accommodating for higher order modes being propagated back into the waveguide region from the parallel plate region, which would require extensive modification to the existing moment method development.

2. Removing the metal backing from the sample for one of the measurements, which would require a new moment method code for the radiation condition.

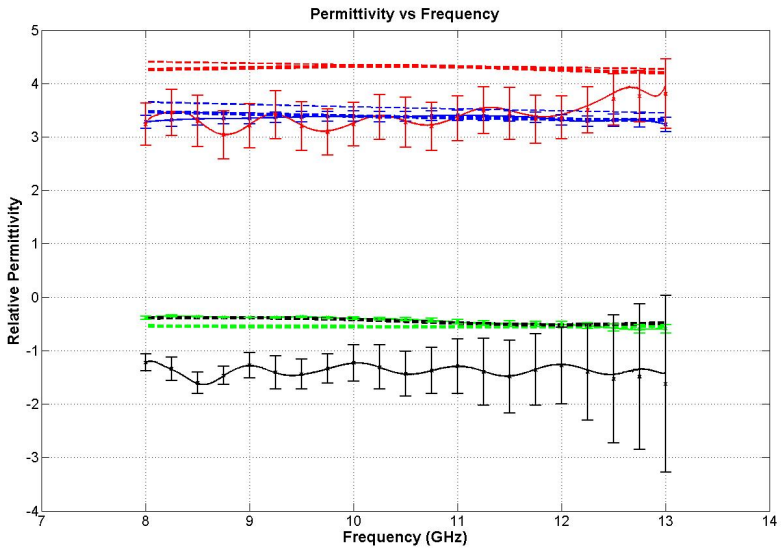

Figure 15. High contrast uniaxial sample comparison: lumped element, rectangular waveguide, and SPWP. Legend is the same as Figure 14.

4.2 Fundamental Mode Experimental SPWP Evaluation

Laboratory measurement of a honeycomb absorber was conducted to see if similar performance was obtained as observed in simulation. Cuming Microwave® "C-RAM

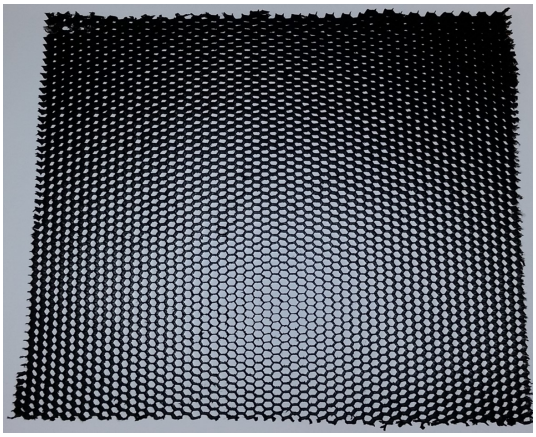

Figure 16. Cuming Microwave® "C-RAM HCUI" broadbanded honeycomb radar absorber.

HCUI" broadbanded honeycomb radar absorber, with 0.125" cells and 0.25" thick, Figure 16, [22] was measured using the SPWP system shown in Figure 17. An Agi-

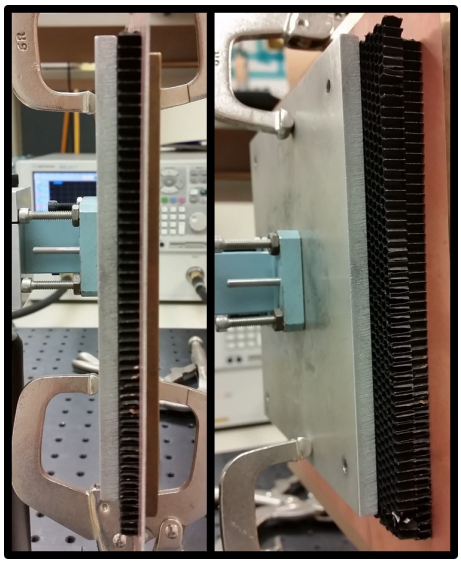

Figure 17. Measurement of the honeycomb absorber. Left: Single thickness, Right: Double Thickness

lent E8362B VNA calibrated using a 2-port TRL calibration, 10 kHz IF bandwidth, and RF bandwidth from 8.2-12.4 GHz collected 1601 sample reflection coefficients. Reflection coefficient results generally show good agreement between the predicted

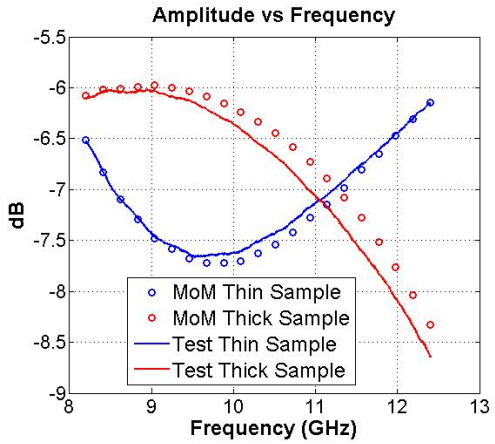

Figure 18. Calibrated magnitude reflection coefficient data.

and measured values as shown in Figure 18. Differences in the magnitude could be explained by not accounting for higher order modes or error in the measured sample thickness. The sample exhibited more variation in thickness, so the tolerance on the sample thickness was increased to ±0.008" in the 1000-trial Monte Carlo sample

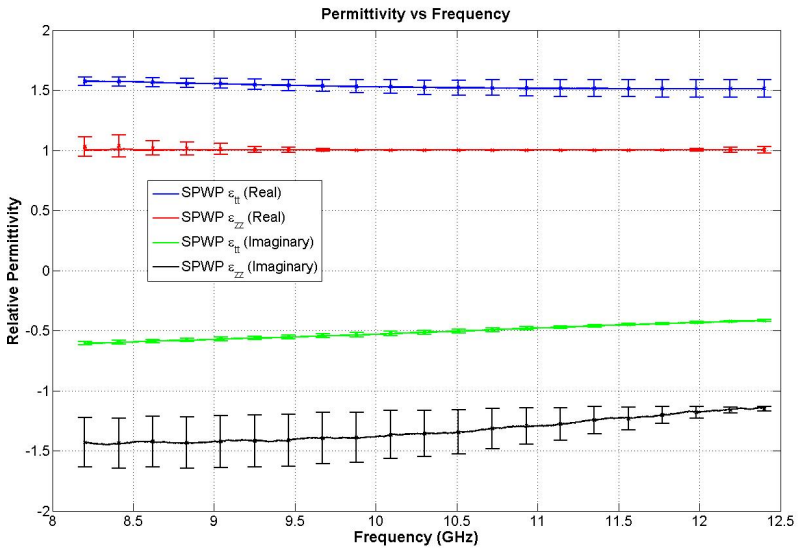

Figure 19. SPWP permittivity data from the Cuming Microwave® "C-RAM HCUI" broadbanded honeycomb radar absorber.

thickness uncertainty analysis. The permittivity results in Figure 19 show a plausible transverse permittivity component, while the longitudinal component is suspect due to the very low permittivity. Insufficient longitudinal electric field sample interrogation makes the longitudinal permittivity results independent of the measurement.

4.3 Fundamental Mode Conclusion

A single port waveguide probe measurement system has been developed. Simulations and a measurement of dielectric uniaxial samples provide system performance information. The results show that the SPWP provides good transverse permittivity,ϵ_t measurement. Measurement results for a uniaxial sample's longitudinal permittivity, ϵ_z component, however, are subject to significant measurement uncertainty due to two challenges: 1) Weak longitudinal electric field (E_z) sample interrogation, as shown in Figure 20; and 2) The moment method forward model only considers the fundamental TE_{10} mode to be present and does not account for higher order rectangular waveguide modes.

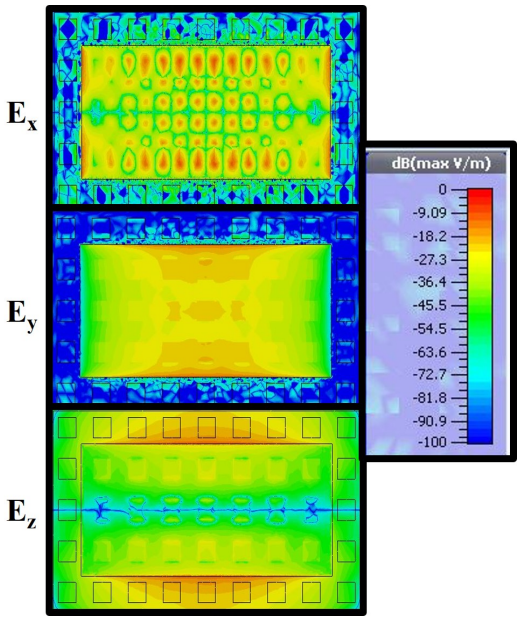

Figure 20. A field plot of the rectangular waveguide, parallel plate interface showing strong transverse (E_y) and weak normal (E_z) electric field components, generated in CST Microwave Studio®.

4.4 Higher Order Mode Results Comparison Introduction

Here, both the propagating fundamental and selected evanescent higher order modes are accommodated in a moment method forward model to enhance the measurement of electrically uniaxial anisotropic media. Including the higher order modes provides better physical representation of the SPWP system and improves the longitudinal component results. Improvement is demonstrated by comparing the fundamental mode and validation results with the higher order mode solutions. Sample measurement was simulated in CST Microwave Studio® at X-band (8.2-12.4 GHz) frequencies using both SPWP and validated with legacy rectangular waveguide material measurement techniques [16], [17], [23] ,[21]. Least squares curve fitting is used to minimize the error between simulated SPWP S_{11} S-parameter data and corresponding S_{11} data generated by the SPWP higher order mode forward model. The forward model and inverse solution process are employed in MATLAB® to obtain uniaxial permittivity results. A root-sum-square (RSS) uncertainty analysis is performed to

address the uncertainty of potential sample thickness error in an actual measurement. Additionally, a plot of the higher order mode reflection coefficient contributions is presented and solution convergence is demonstrated by plotting the error of the SPWP higher order mode solutions against the rectangular waveguide solution versus the number of modes. Results show that as more modes are used, a higher accuracy solution is obtained, and that the longitudinal permittivity agrees more closely with the legacy rectangular waveguide solution.

4.5 Fundamental Mode Comparison to Higher Order Mode Results

The higher order mode SPWP development operating in only the fundamental mode is compared to the development in [12] to demonstrate that results agree as shown in Figure 21. Validation of the designed uniaxial sample was performed by evaluating sections of the sample in a measurement representative rectangular waveguide fixture, as discussed in [12]. The error bars included on the higher order mode results are $\pm 2\sigma$ derived from a RSS uncertainty in sample thickness. The sample thickness standard deviation is ± 0.004" and assumes a uniform distribution. There is good agreement in the uncertainty in the transverse results, while the longitudinal results show more uncertainty variation between the data sets. This is due to the difference in uncertainty calculation techniques. The uncertainty analysis performed in [12] used a 1000-trial Monte Carlo technique, which better captures longitudinal permittivity insensitivity due to the weak longitudinal fields present in the SPWP system. In contrast, the 2 sample RSS calculations relies on only expected and worst case values to derive uncertainty. RSS is used in this paper, because a Monte-Carlo approach would require extensive time to iterate trials for the higher-order mode calculations at each frequency value.

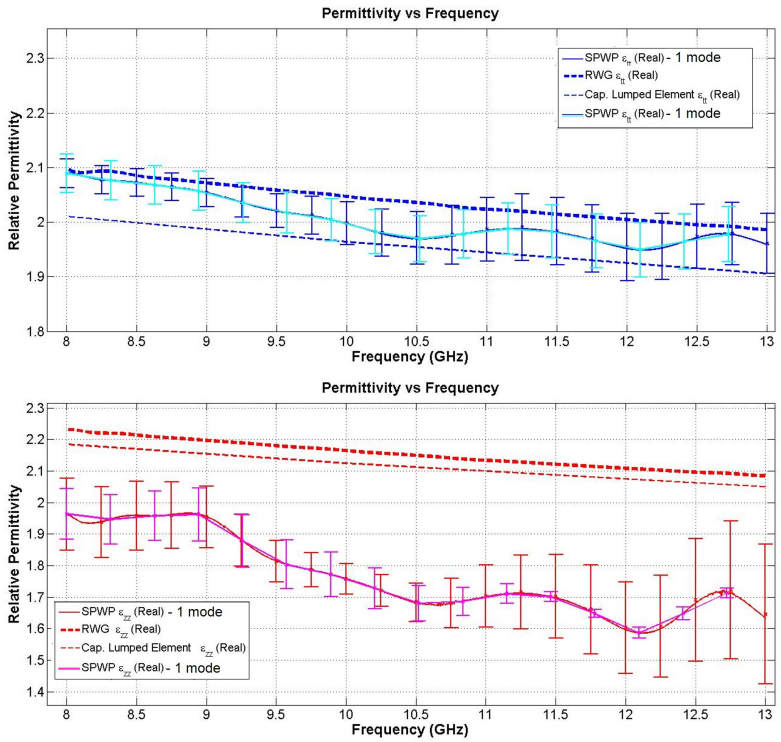

Figure 21. Comparison of the previously published fundamental mode results (blue & red) with only 1 mode being evaluated in the higher order mode approach (cyan & magenta). Simulated rectangular waveguide results (RWG) are considered to be truth. Capacitive Lumped Element Prediction is also provided for comparison. Top is transverse permittivity. Bottom is longitudinal permittivity.

4.6 Higher Order Mode Comparison Results

Evaluating the first 20 rectangular waveguide modes as shown in Figure 22 demonstrates improvement of the longitudinal permittivity component. Accommodating the higher order modes more accurately represented the field structure in the SPWP. Additionally, by including TM^z modes more interrogation of the longitudinal permittivity is captured in the moment method analysis. Once again, the same values for RSS uncertainty are applied to the 20-mode results. Figure 23 shows several plots of the rectangular waveguide aperture at the interface of the parallel plate waveguide region. These plots share similarity to the field plots generated in CST Microwave Studio® as shown in Figure 20. A strong y-directed electric field component is observed.

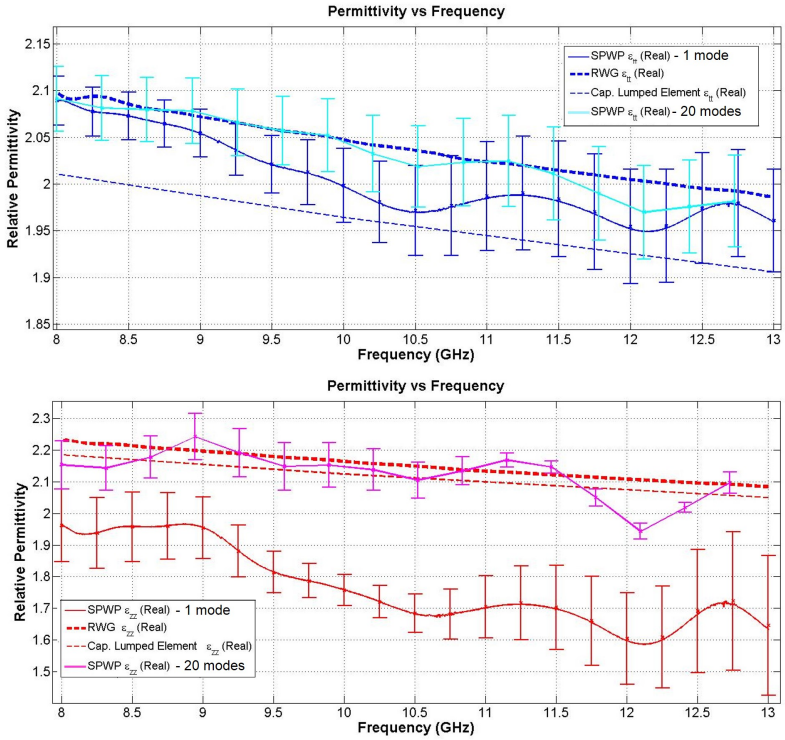

Figure 22. The real part of the complex permittivity results comparing the fundamental mode (1 mode) solution to the higher order mode solution (20 modes). Simulated rectangular waveguide results (RWG) are considered to be truth. Capacitive Lumped Element Prediction is also provided for comparison as it was used to design the sample. Top is transverse permittivity. Bottom is longitudinal permittivity.

4.7 Mode Comparison and Measurement Performance Results

Evaluating how the results change as modes are added by cut-off frequency shows that an efficiency may be obtained in calculating solutions from a subset of higher order modes. Plotting the magnitude of the individual mode contributions shows that certain modes offer more impact on the results, as shown in Figure 24. Reviewing Figure 25, it is observed that generally as more modes are added the accuracy is enhanced. However looking more closely at Figure 25, certain modes may not be needed in computation, as they do not contribute significantly to the results and may decrease accuracy due to potential round off or machine precision errors induced by including them. Judicious selection of the TE and TM rectangular waveguide modes included

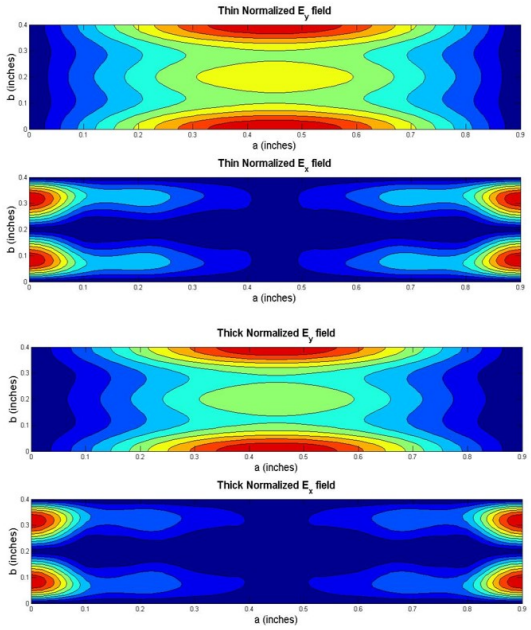

Figure 23. Field Plots of the tangential electric fields of a simulated low contrast uniaxial sample. The top two plots are the y and x electric field components for the single thickness low contrast uniaxial material. The bottom two plots are the fields components for the double thickness sample. The field plots are generated from the first 20 higher order modes moment method approach.

in the higher order mode computations would enable quicker and potentially more accurate solutions. Capitalizing on using only the first 8 most contributing modes, as discussed in [24], the Cuming Microwave® "C-RAM HCUI" Radar absorbing honeycomb data is reevaluated using the $TE_{10,30,12,14,16}$ and the $TM_{12,14,16}$ as shown in Figure 26. Result show some improvement by incorporating the higher order modes.

4.8 Conclusion

A higher order mode moment method technique is developed and employed on the Single Port Waveguide Probe. Comparisons are made on a measurement representative simulated uniaxial material SPWP results. The results show that including higher order modes enhance accuracy and help correct longitudinal permittivity re-

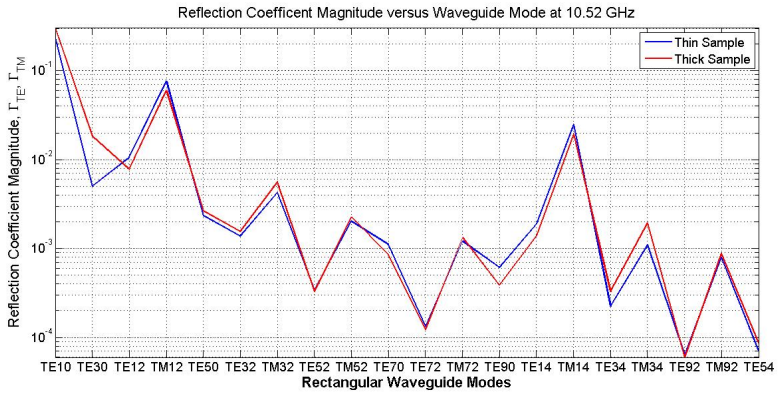

Figure 24. Comparison of the TE_{10} reflection coefficients with the evanescent higher order mode reflection coefficients. Note that certain higher order modes such as the TM_{12} or TM_{14} provide large contributions. Modes are arranged by cut-off frequency.

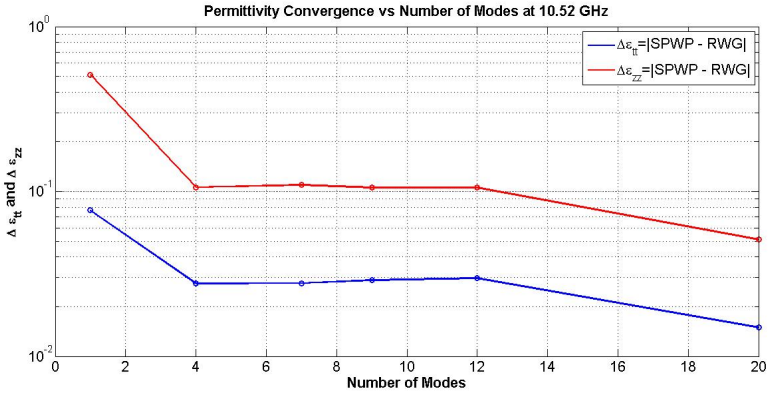

Figure 25. As the number of modes is increased both the transverse and longitudinal permittivity error improves. Error is the difference between the SPWP higher order mode solution and the rectangular waveguide solution for permittivity at the same frequency.

sults which are shown to be deficient using only a fundamental mode moment method development. The higher order moment method approach offers better accuracy for the SPWP non-destructive material measurement technique.

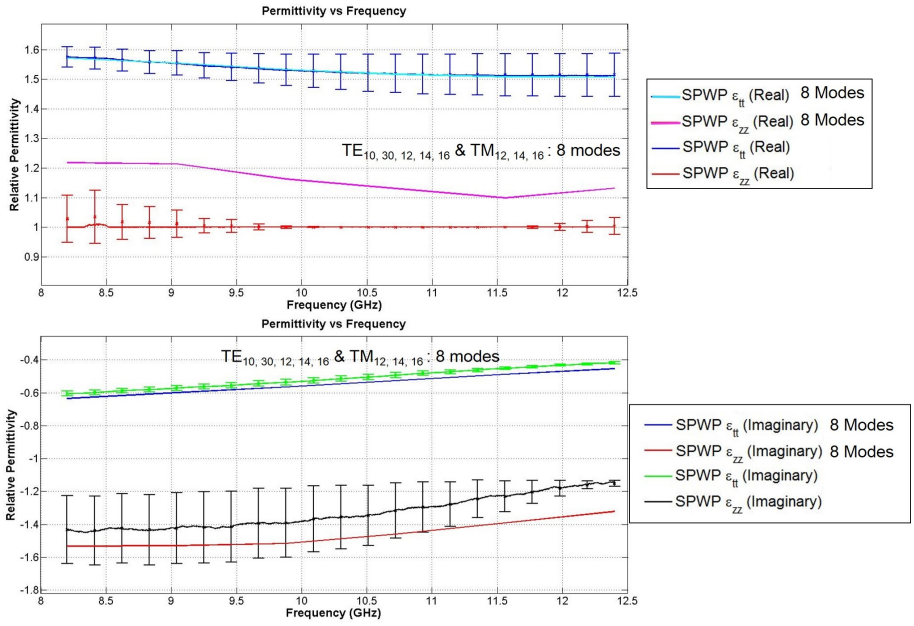

Figure 26. Cuming Microwave® "C-RAM HCUI" Radar absorbing honeycomb reevaluated using 8 higher order modes.

V. Rotated Uniaxial Green's Function Development

A conference paper [25] was presented and published in conjunction with document. The conference paper contains the same information presented in this document.

In this chapter, a field-based approach is used to derive both the principle scattered and total solutions to the rotated uniaxial anisotropic parallel-plate Green's function as shown in Figure 27. Field structure inside a uniformly filled rotated uniaxial parallel-plate region is also explored as part of the derivation. Recall, rotated uniaxial anisotropic media possesses permittivity and permeability tensors appear as

$$\overleftrightarrow{\epsilon} = \begin{bmatrix} \epsilon_{xx} & 0 & 0 \\ 0 & \epsilon_{yy} & 0 \\ 0 & 0 & \epsilon_{xx} \end{bmatrix} \quad , \quad \overleftrightarrow{\mu} = \begin{bmatrix} \mu_{xx} & 0 & 0 \\ 0 & \mu_{yy} & 0 \\ 0 & 0 & \mu_{xx} \end{bmatrix} . \tag{5.1}$$

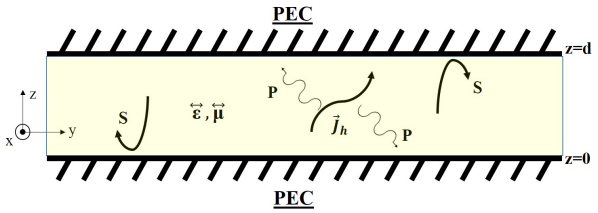

Figure 27. The parallel-plate Green's function scenario shows an equivalent magnetic aperture current inducing field in the parallel-plate structure. The total Green's functions is decomposed into a principle part denoted by 'P' and the scattered part denoted by 'S'.

5.1 Rotated Green's function approach

A field based approach, based on the spectral domain form of Maxwell's Equations is chosen to derive the magnetic field parallel-plate Green's function uniformly filled

with rotated uniaxial anisotropic media. A plane-wave basis is used to describe the field propagation structure. Rather than immediately attempt to obtain a magnetic field parallel-plate Green's function from a magnetic aperture current; the electric field Green's functions are first obtained, because it is easier to enforce the boundary conditions on the PEC parallel-plate structure with tangential electric fields than magnetic fields. The magnetic field Green's functions are then derived from the electric field Green's functions. This is done by using Maxwell's Equations to relate the electric fields to the magnetic fields.

Principle Solution Development.

A magnetic current is used as it is related by Love's Equivalence Principle to the aperture electric fields in a rectangular waveguide from Figure 2. Beginning by obtaining the principle solution, a relationship for the electric fields is obtained for the magnetic current in unbounded space.

Analysis begins with transforming Maxwell's Equations

$$\nabla \times \vec{E} = -\vec{J}_h - j\omega \overleftrightarrow{\mu} \cdot \vec{H}, \quad \nabla \times \vec{H} = \vec{J}_e + j\omega \overleftrightarrow{\epsilon} \cdot \vec{E} \tag{5.2}$$

which posses the material tensors in (5.1) to the spectral domain (as shown in full detail in Appendix B)

$$-j \overleftrightarrow{k} \cdot \vec{\vec{E}} = -\vec{\vec{J}}_h - j\omega \overleftrightarrow{\mu} \cdot \vec{\vec{H}}, \quad -j \overleftrightarrow{k} \cdot \vec{\vec{H}} = \vec{\vec{J}}_e + j\omega \overleftrightarrow{\epsilon} \cdot \vec{\vec{E}}. \tag{5.3}$$

The wave equation is then obtained as

$$\left[\overleftrightarrow{k} \cdot \overleftrightarrow{\mu}^{-1} \cdot \overleftrightarrow{k} + \omega^2 \overleftrightarrow{\epsilon} \right] \cdot \vec{\vec{E}} = j \overleftrightarrow{k} \cdot \overleftrightarrow{\mu}^{-1} \cdot \vec{\vec{J}}_h + j\omega \vec{\vec{J}}_e. \tag{5.4}$$

It is rewritten as

$$\overleftrightarrow{W}_e \cdot \vec{\vec{E}} = j\overleftrightarrow{k} \cdot \overleftrightarrow{\mu}^{-1} \cdot \vec{\vec{J}}_h + j\omega\vec{\vec{J}}_e \tag{5.5}$$

where

$$\overleftrightarrow{W}_e = \begin{bmatrix} -\frac{k_y^2}{\mu_x} - \frac{k_z^2}{\mu_y} + \omega^2\epsilon_x & \frac{k_x k_y}{\mu_x} & \frac{k_x k_z}{\mu_y} \\ \frac{k_x k_y}{\mu_x} & -\frac{k_x^2}{\mu_x} - \frac{k_z^2}{\mu_x} + \omega^2\epsilon_y & \frac{k_y k_z}{\mu_x} \\ \frac{k_x k_z}{\mu_y} & \frac{k_y k_z}{\mu_x} & -\frac{k_x^2}{\mu_y} - \frac{k_y^2}{\mu_x} + \omega^2\epsilon_x \end{bmatrix}. \tag{5.6}$$

Solving for the electric field

$$\vec{\vec{E}} = j\overleftrightarrow{W}_e^{-1} \cdot \overleftrightarrow{k} \cdot \overleftrightarrow{\mu}^{-1} \cdot \vec{\vec{J}}_h + j\omega\overleftrightarrow{W}_e^{-1} \cdot \vec{\vec{J}}_e \tag{5.7}$$

where

$$\overleftrightarrow{W}_e^{-1} = \frac{adj\left(\overleftrightarrow{W}_e\right)}{\left|\overleftrightarrow{W}_e\right|}. \tag{5.8}$$

Finding the determinate $\left|\overleftrightarrow{W}_e\right|$ first,

$$\left|\overleftrightarrow{W}_e\right| = \frac{\omega^2\epsilon_x}{\mu_x\mu_y}\left(k_z^2 - k_{ZTE}^2\right)\left(k_z^2 - k_{ZTM}^2\right) \tag{5.9}$$

where

$$k_{ZTE} = \pm\sqrt{\omega^2\epsilon_x\mu_y - k_x^2 - \frac{\mu_y}{\mu_x}k_y^2} \tag{5.10}$$

$$k_{ZTM} = \pm\sqrt{\omega^2\epsilon_y\mu_x - k_x^2 - \frac{\epsilon_y}{\epsilon_x}k_y^2}. \tag{5.11}$$

These are the propagation constraints for TE and TM polarized fields. The adjoint calculation is omitted for brevity. By superposition we can evaluate each current independently. Looking at the magnetic current and turning off the electric current,

as it is not present in the SPWP

$$\vec{\approx}{E} = j\overleftrightarrow{W}_e^{-1} \cdot \overleftrightarrow{k} \cdot \overleftrightarrow{\mu}^{-1} \cdot \vec{\approx}{J}_h = \overleftrightarrow{\approx}{G}_{eh}^{P} \cdot \vec{\approx}{J}_h. \tag{5.12}$$

The term $\overleftrightarrow{\approx}{G}_{eh}^{P}$ which has the elements

$$\overleftrightarrow{\approx}{G}_{eh}^{P} = \begin{bmatrix} \approx{G}_{eh,xx}^{P} & \approx{G}_{eh,xy}^{P} & \approx{G}_{eh,xz}^{P} \\ \approx{G}_{eh,yx}^{P} & \approx{G}_{eh,yy}^{P} & \approx{G}_{eh,yz}^{P} \\ \approx{G}_{eh,zx}^{P} & \approx{G}_{eh,zy}^{P} & \approx{G}_{eh,zz}^{P} \end{bmatrix} \tag{5.13}$$

is the spectral domain Green's function for the principle part of the solution which relates a magnetic current to an electric field in an unbounded rotated uniaxial anisotropic media. Terms with $\approx$ indicate (k_x, k_y, k_z) domain while terms with $\sim$ indicate (k_x, k_y, z) domain. Looking at each element of $\overleftrightarrow{\approx}{G}_{eh}^{P}$ shows:

$$\begin{bmatrix} \frac{jk_xk_yk_z(\epsilon_y\mu_x-\epsilon_x\mu_y)}{\epsilon_x\mu_x(k_z^2-k_{ZTE}^2)(k_z^2-k_{ZTM}^2)} & \frac{jk_z}{(k_z^2-k_{ZTE}^2)} & \frac{jk_y\epsilon_y(k_{ZTE}^2-\frac{\epsilon_x\mu_y}{\epsilon_y\mu_x}k_z^2)}{\epsilon_x(k_z^2-k_{ZTE}^2)(k_z^2-k_{ZTM}^2)} \\ -\frac{jk_z}{(k_z^2-k_{ZTM}^2)} & 0 & \frac{jk_x}{(k_z^2-k_{ZTM}^2)} \\ -\frac{jk_y\mu_y(k_{ZTM}^2-\frac{\epsilon_x\mu_x}{\epsilon_y\mu_y}k_z^2)}{\mu_x(k_z^2-k_{ZTE}^2)(k_z^2-k_{ZTM}^2)} & -\frac{jk_x}{(k_z^2-k_{ZTE}^2)} & \frac{jk_xk_yk_z(\epsilon_x\mu_y-\epsilon_y\mu_x)}{\epsilon_x\mu_x(k_z^2-k_{ZTE}^2)(k_z^2-k_{ZTM}^2)} \end{bmatrix} \tag{5.14}$$

It is important to note that the currents and fields are in the spectral and not the spatial domain. Establishing the principle Green's function requires transforming back to the (k_x, k_y, z) domain, because the spatial 'z' domain is needed for the enforcement of boundary conditions when calculating the scattered solution. Relating (k_x, k_y, k_z) to (k_x, k_y, z), the inverse Fourier transform

$$\vec{\sim}{E}^{P}(\vec{k}_\rho, z) = \frac{1}{2\pi}\int_{-\infty}^{\infty} \overleftrightarrow{\approx}{G}_{eh}^{P} \cdot \vec{\approx}{J}_h(\vec{k}_\rho, k_z)e^{jk_z(z)}dk_z \tag{5.15}$$

is used. The current is rewritten as

$$\overset{\rightarrow}{\underset{\sim}{E}}^{P}(\vec{k}_\rho, z) = \frac{1}{2\pi}\int_{-\infty}^{\infty} \overset{\leftrightarrow}{\underset{\approx}{G}}^{P}_{eh}(\vec{k}_\rho, k_z) \cdot \int_{z'} \overset{\rightarrow}{\underset{\sim}{J}}_h e^{-jk_z z'} dz' e^{jk_z(z)} dk_z. \tag{5.16}$$

Rearranging the integrals

$$\overset{\rightarrow}{\underset{\sim}{E}}^{P}(\vec{k}_\rho, z) = \int_{z'} \frac{1}{2\pi}\int_{-\infty}^{\infty} \overset{\leftrightarrow}{\underset{\approx}{G}}^{P}_{eh}(\vec{k}_\rho, k_z) e^{jk_z(z-z')} dk_z \cdot \overset{\rightarrow}{\underset{\sim}{J}}_h dz'. \tag{5.17}$$

The inverse Fourier transform integral

$$\overset{\leftrightarrow}{\underset{\sim}{G}}^{P}_{eh}(\vec{k}_\rho, z) = \frac{1}{2\pi}\int_{-\infty}^{\infty} \overset{\leftrightarrow}{\underset{\approx}{G}}^{P}_{eh}(\vec{k}_\rho, k_z) e^{jk_z(z-z')} dk_z \tag{5.18}$$

is evaluated using Complex Plane Integration due to the singularities in the denominator of $\overset{\leftrightarrow}{\underset{\approx}{G}}^{P}_{eh}$. The poles for the spectral domain principle part Green's function in (5.14) are simple poles. The location of the poles are identified by the assumption of positive real and negative imaginary permittivity and permeability components of k_{ZTE} and k_{ZTM}. The poles are plotted on the complex plane as shown in Figure 28. Since these are simple poles Cauchy's Integral Theorem is used, where

$$\oint_{k_{ZTE}|k_{ZTM}} \frac{f(z)}{z - z_0} dz = 2\pi j f(z_0) \tag{5.19}$$

as described in [15]. Notice that $e^{jk_z(z-z')} \rightarrow 0;\ z - z' > 0$ and $Real(k_z) < 0$, $Imaginary(k_z) > 0$ is the upper half plane and the $e^{jk_z(z-z')} \rightarrow 0;\ z - z' < 0$ and $Real(k_z) > 0$, $Imaginary(k_z) < 0$ is the lower half plane. Also note that k_z is either k_{ZTE} or k_{ZTM}. Performing the integration yields the principle solution summary:

$$\overset{\leftrightarrow}{\underset{\sim}{G}}^{P}_{eh} = \overset{\leftrightarrow}{\underset{\sim}{G}}^{P\ TE}_{eh} + \overset{\leftrightarrow}{\underset{\sim}{G}}^{P\ TM}_{eh} \tag{5.20}$$

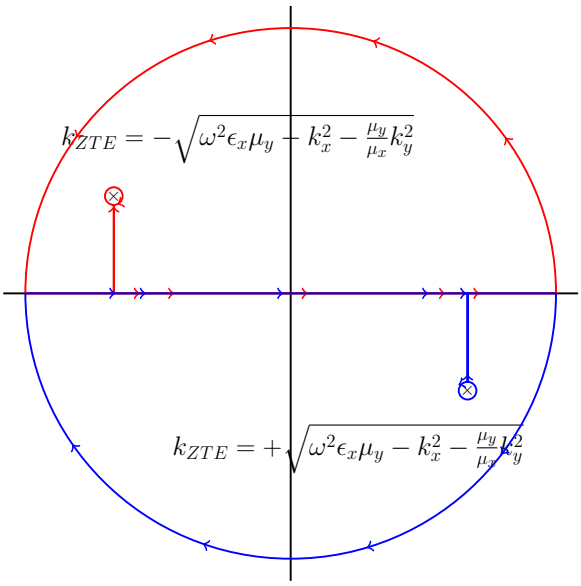

Figure 28. The complex k_z plane showing the k_{ZTE} poles. Red Upper Half Plane, Blue Lower Half Plane

$$\overset{\leftrightarrow}{\underset{\sim}{G}}{}^{TE}_{eh} = \begin{bmatrix} -\frac{sgn(z-z')k_xk_y}{(k_y^2-\omega^2\epsilon_x\mu_x)} & -sgn(z-z') & \frac{k_yk_{ZTE}}{(k_y^2-\omega^2\epsilon_x\mu_x)} \\ 0 & 0 & 0 \\ -\frac{k_x^2k_y}{k_{ZTE}(k_y^2-\omega^2\epsilon_x\mu_x)} & -\frac{k_x}{k_{ZTE}} & \frac{sgn(z-z')k_xk_y}{(k_y^2-\omega^2\epsilon_x\mu_x)} \end{bmatrix} \tilde{g}{}^{P}_{TE} \tag{5.21}$$

$$\overset{\leftrightarrow}{\underset{\sim}{G}}{}^{TM}_{eh} = \begin{bmatrix} \frac{sgn(z-z')k_xk_y}{(k_y^2-\omega^2\epsilon_x\mu_x)} & 0 & \frac{k_x^2k_y}{k_{ZTM}(k_y^2-\omega^2\epsilon_x\mu_x)} \\ sgn(z-z') & 0 & \frac{k_x}{k_{ZTM}} \\ -\frac{k_yk_{ZTM}}{(k_y^2-\omega^2\epsilon_x\mu_x)} & 0 & -\frac{sgn(z-z')k_xk_y}{(k_y^2-\omega^2\epsilon_x\mu_x)} \end{bmatrix} \tilde{g}{}^{P}_{TM} \tag{5.22}$$

$$\tilde{g}{}^{P}_{TE} = \frac{1}{2}e^{-jk_{ZTE}|z-z'|} \qquad \tilde{g}{}^{P}_{TM} = \frac{1}{2}e^{-jk_{ZTM}|z-z'|} \tag{5.23}$$

5.2 Scattered Solution Development

A scattered solution describing the field structure in the parallel-plate region requires solving a homogeneous system of equations

$$\overset{\leftrightarrow}{W}_e \cdot \overset{\rightarrow}{\underset{\sim}{E}}_0 = 0 \tag{5.24}$$

Applying the two eigenvalues (5.10) and (5.11) independently, two sets of eigenvector solutions: TE and TM exist and are a described in terms of the plane wave basis

$$\vec{\tilde{E}} = \left(\hat{x}\tilde{E}_{0x} + \hat{y}\tilde{E}_{0y} + \hat{z}\tilde{E}_{0z}\right) e^{-jk_z z}. \tag{5.25}$$

The TE summary for the scattered solution is:

$$\begin{aligned}\vec{\tilde{E}}_S = &\left(\hat{x} + \hat{z}\frac{k_x}{k_{ZTE}}\right) \tilde{E}_{0x}^{+TE} e^{-jk_{ZTE}z} + \\ &\left(\hat{x} - \hat{z}\frac{k_x}{k_{ZTE}}\right) \tilde{E}_{0x}^{-TE} e^{+jk_{ZTE}z}\end{aligned} \tag{5.26}$$

and is shows that the field distributions are TE_y. The TM summary for the scattered solution is:

$$\begin{aligned}\vec{\tilde{E}}_S = &\left(\hat{x} + \hat{y}\frac{k_y^2 - \omega^2\epsilon_x\mu_x}{k_x k_y} - \hat{z}\frac{k_{ZTM}}{k_x}\right) \tilde{E}_{0x}^{+TM} e^{-jk_{ZTM}z} \\ + &\left(\hat{x} + \hat{y}\frac{k_y^2 - \omega^2\epsilon_x\mu_x}{k_x k_y} + \hat{z}\frac{k_{ZTM}}{k_x}\right) \tilde{E}_{0x}^{-TM} e^{+jk_{ZTM}z}\end{aligned} \tag{5.27}$$

Having the principle and scattered solutions obtained separately, they are combined and yield the total solution. The total solution for the rotated Green's function is described by the sum of the field components,

$$\vec{\tilde{E}}^{TOT} = \vec{\tilde{E}}_P + \vec{\tilde{E}}_S \tag{5.28}$$

and are further separated into

$$\vec{\tilde{E}}^{TOT} = \vec{\tilde{E}}_P^{TE} + \vec{\tilde{E}}_P^{TM} + \vec{\tilde{E}}_S^{TE} + \vec{\tilde{E}}_S^{TM} \tag{5.29}$$

and shows that four unknowns, $\underset{\sim}{E}_{0x}^{+TE}$, $\underset{\sim}{E}_{0x}^{-TE}$, $\underset{\sim}{E}_{0x}^{+TM}$, $\underset{\sim}{E}_{0x}^{-TM}$ must be solved. Boundary condition enforcement at each of the parallel-plates provide four relationships which are $\widetilde{E}_x(z=0)=0$, $\widetilde{E}_x(z=d)=0$, $\widetilde{E}_y(z=0)=0$, and $\widetilde{E}_y(z=d)=0$. Solving for the four unknowns yields:

$$\begin{aligned}\underset{\sim}{E}_{0x}^{+TE} &= \frac{R\ \underset{\sim}{V}_{eh}^{-TE} + R\bar{R}\ \underset{\sim}{V}_{eh}^{+TE} e^{-2jk_{ZTE}d}}{\left(1-R\bar{R}e^{-2jk_{ZTE}d}\right)} \\ &+\frac{R\ \underset{\sim}{V}_{eh}^{-TM} + R\bar{R}\ \underset{\sim}{V}_{eh}^{+TM} e^{-jk_{ZTE}d}e^{-jk_{ZTM}d}}{\left(1-R\bar{R}e^{-2jk_{ZTE}d}\right)}\end{aligned} \tag{5.30}$$

$$\begin{aligned}\underset{\sim}{E}_{0x}^{-TE} &= \frac{\bar{R}\ \underset{\sim}{V}_{eh}^{+TE} e^{-2jk_{ZTE}d} + \bar{R}R\ \underset{\sim}{V}_{eh}^{-TE} e^{-2jk_{ZTE}d}}{\left(1-\bar{R}Re^{-2jk_{ZTE}d}\right)}+ \\ &\frac{\bar{R}\ \underset{\sim}{V}_{eh}^{+TM} e^{-jk_{ZTM}d}e^{-jk_{ZTE}d} + \bar{R}R\ \underset{\sim}{V}_{eh}^{-TM} e^{-2jk_{ZTE}d}}{\left(1-\bar{R}Re^{-2jk_{ZTE}d}\right)}\end{aligned} \tag{5.31}$$

$$\begin{aligned}\underset{\sim}{E}_{0x}^{+TM} &= \left(\frac{R\ \underset{\sim}{V}_{eh,y}^{-TE} + R\bar{R}\ \underset{\sim}{V}_{eh,y}^{+TE} e^{-jk_{ZTE}d}e^{-jk_{ZTM}d}}{\left(1-R\bar{R}e^{-2jk_{ZTM}d}\right)} + \right. \\ &\left.\frac{R\ \underset{\sim}{V}_{eh,y}^{-TM} + R\bar{R}\ \underset{\sim}{V}_{eh,y}^{+TM} e^{-2jk_{ZTM}d}}{\left(1-R\bar{R}e^{-2jk_{ZTM}d}\right)}\right)\left(\frac{k_xk_y}{k_y^2-\omega^2\epsilon_x\mu_x}\right)\end{aligned} \tag{5.32}$$

$$\begin{aligned}\underset{\sim}{E}_{0x}^{-TM} &= \left(\frac{\bar{R}\ \underset{\sim}{V}_{eh,y}^{+TE} e^{-jk_{ZTE}d}e^{-jk_{ZTM}d} + \bar{R}R\ \underset{\sim}{V}_{eh,y}^{-TE} e^{-2jk_{ZTM}d}}{\left(1-\bar{R}Re^{-2jk_{ZTM}d}\right)}+ \right. \\ &\left.\frac{\bar{R}\ \underset{\sim}{V}_{eh,y}^{+TM} e^{-2jk_{ZTM}d} + \bar{R}R\ \underset{\sim}{V}_{eh,y}^{-TM} e^{-2jk_{ZTM}d}}{\left(1-\bar{R}Re^{-2jk_{ZTM}d}\right)}\right)\left(\frac{k_xk_y}{k_y^2-\omega^2\epsilon_x\mu_x}\right).\end{aligned} \tag{5.33}$$

The relationships

$$\underset{\sim}{V}_{eh}^{\pm TE} = \underset{\sim}{V}_{eh,x}^{\pm TE} - \left(\frac{k_xk_y}{k_y^2-\omega^2\epsilon_x\mu_x}\right)\ \underset{\sim}{V}_{eh,y}^{\pm TE} \tag{5.34}$$

and

$$\tilde{V}_{eh}^{\pm TM} = \tilde{V}_{eh,x}^{\pm TM} - \left(\frac{k_x k_y}{k_y^2 - \omega^2 \epsilon_x \mu_x}\right) \tilde{V}_{eh,y}^{\pm TM} \tag{5.35}$$

are a convenient notation adapted from [9]. Furthermore, while the TE and TM scattered vector components are identifiable, the principle Green's function components used in the above solutions are not readily identified. Easing algebraic manipulation the condensed notation:

$$\begin{bmatrix} \tilde{V}_{eh,x}^{-TE} \\ \tilde{V}_{eh,y}^{-TE} \end{bmatrix} = \int_{z'} \left[\hat{x}\ ,\ \hat{y}\right] \cdot \overset{\leftrightarrow}{\tilde{G}}_{P\ eh}^{TE}(z=0) \cdot \overset{\rightarrow}{\tilde{J}}_h dz' \tag{5.36}$$

$$\begin{bmatrix} \tilde{V}_{eh,x}^{-TM} \\ \tilde{V}_{eh,y}^{-TM} \end{bmatrix} = \int_{z'} \left[\hat{x}\ ,\ \hat{y}\right] \cdot \overset{\leftrightarrow}{\tilde{G}}_{P\ eh}^{TM}(z=0) \cdot \overset{\rightarrow}{\tilde{J}}_h dz' \tag{5.37}$$

$$\begin{bmatrix} \tilde{V}_{eh,x}^{+TE}\, e^{-jk_{ZTE}d} \\ \tilde{V}_{eh,y}^{+TE}\, e^{-jk_{ZTE}d} \end{bmatrix} = \int_{z'} \left[\hat{x}\ ,\ \hat{y}\right] \cdot \overset{\leftrightarrow}{\tilde{G}}_{P\ eh}^{TE}(z=d) \cdot \overset{\rightarrow}{\tilde{J}}_h dz' \tag{5.38}$$

$$\begin{bmatrix} \tilde{V}_{eh,x}^{+TM}\, e^{-jk_{ZTM}d} \\ \tilde{V}_{eh,y}^{+TM}\, e^{-jk_{ZTM}d} \end{bmatrix} = \int_{z'} \left[\hat{x}\ ,\ \hat{y}\right] \cdot \overset{\leftrightarrow}{\tilde{G}}_{P\ eh}^{TM}(z=d) \cdot \overset{\rightarrow}{\tilde{J}}_h dz' \tag{5.39}$$

is used for the x and y components of the principle Green's functions employed in the scattered solution development. The terms $R = -1$ and $\bar{R} = -1$ are also used to track the reflections off the boundaries and aides physical insight. The scattered solution is then calculated for each of the vector components in (5.26) and (5.27) using the solutions to the four unknowns. The total scattered solution is represented by the sum of the TE_y and TM_y scattered solution components.

5.3 Combining Principle and Scattered Solution Development

Combining the principle and scattered solution components results in the total parallel-plate Green's function for a rotated uniaxial media. Physical insight is gained by observing the up and down going waves in the parallel-plate structure. As an example,

$$\begin{aligned}\tilde{E}_{xx}^{TE} &= \frac{k_x k_y}{2(k_y^2-\omega^2\epsilon_x\mu_x)}\int_{z'} -sgn(z-z')e^{-jk_{ZTE}|z-z'|}\cdot\tilde{J}_{h,x}dz' \\ &+\frac{k_x k_y}{2(k_y^2-\omega^2\epsilon_x\mu_x)}\int_{z'}\left[\frac{Re^{-jk_{ZTE}(z'+z)}-R\bar{R}e^{-jk_{ZTE}(2d-z'+z)}}{\left(1-\bar{R}Re^{-2jk_{ZTE}d}\right)}\right. \\ &\left.+\frac{-\bar{R}e^{-jk_{ZTE}(2d-z'-z)}+\bar{R}Re^{-jk_{ZTE}(2d+z'-z)}}{\left(1-\bar{R}Re^{-2jk_{ZTE}d}\right)}\right]\cdot\tilde{J}_{h,x}dz'\end{aligned} \tag{5.40}$$

mathematically describes different standing wave cases represented in Figure 29. These standing wave configurations are imposed by the boundary conditions formed by the parallel-plates.

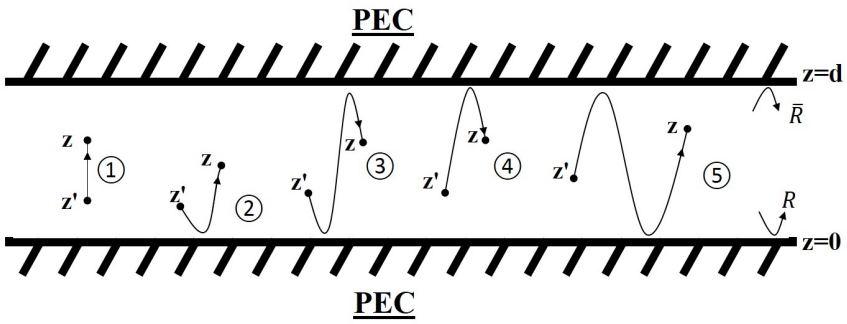

Figure 29. Parallel Plate waveguide showing the different combinations of scattering. 1) $e^{-jk_z|z-z'|}$**, 2)** $Re^{-jk_z(z+z')}$**, 3)** $R\overline{R}e^{-jk_z(2d+z-z')}$**, 4)** $\overline{R}e^{-jk_z(2d-z-z')}$**, 5)** $\overline{R}Re^{-jk_z(2d-z+z')}$

5.4 Solution Summary for the electric field Green's Function

Using Euler's identities further simplifications are made to consolidate the exponential functions. Separating TE and TM solutions

$$\overset{\leftrightarrow}{\sim} G_{eh} = \begin{bmatrix} \tilde{G}^{TE}_{eh,xx} & \tilde{G}^{TE}_{eh,xy} & \tilde{G}^{TE}_{eh,xz} \\ \tilde{G}^{TE}_{eh,yx} & \tilde{G}^{TE}_{eh,yy} & \tilde{G}^{TE}_{eh,yz} \\ \tilde{G}^{TE}_{eh,zx} & \tilde{G}^{TE}_{eh,zy} & \tilde{G}^{TE}_{eh,zz} \end{bmatrix} + \begin{bmatrix} \tilde{G}^{TM}_{eh,xx} & \tilde{G}^{TM}_{eh,xy} & \tilde{G}^{TM}_{eh,xz} \\ \tilde{G}^{TM}_{eh,yx} & \tilde{G}^{TM}_{eh,yy} & \tilde{G}^{TM}_{eh,yz} \\ \tilde{G}^{TM}_{eh,zx} & \tilde{G}^{TM}_{eh,zy} & \tilde{G}^{TM}_{eh,zz} \end{bmatrix} \tag{5.41}$$

where the total electric field in the parallel-plate region is related to a magnetic current by

$$\overset{\rightarrow}{\sim} E(\vec{k}_\rho, z) = \int_{z'} \overset{\leftrightarrow}{\sim} G_{eh} \cdot \overset{\rightarrow}{\sim} J_h dz'. \tag{5.42}$$

The TE solutions spectral domain Green's Functions, $\overset{\leftrightarrow}{\sim}{}^{TE}_{eh}(\vec{k}_\rho, z)$ are consolidated into:

$$\begin{bmatrix} -\frac{k_x k_y}{(k_y^2 - \omega^2 \epsilon_x \mu_x)} \tilde{g}^{+}_{TE_s} & -\tilde{g}^{+}_{TE_s} & \frac{k_y k_{ZTE}}{j(k_y^2 - \omega^2 \epsilon_x \mu_x)} \tilde{g}^{-}_{TE_c} \\ 0 & 0 & 0 \\ -\frac{k_x^2 k_y}{j k_{ZTE}(k_y^2 - \omega^2 \epsilon_x \mu_x)} \tilde{g}^{+}_{TE_c} & -\frac{k_x}{j k_{ZTE}} \tilde{g}^{+}_{TE_c} & \frac{k_x k_y}{(k_y^2 - \omega^2 \epsilon_x \mu_x)} \tilde{g}^{-}_{TE_s} \end{bmatrix} = \overset{\leftrightarrow}{\sim} G^{TE}_{eh} \tag{5.43}$$

where

$$\tilde{g}^{\pm}_{TE_c} = \frac{\cos(k_{ZTE}(d - |z - z'|)) \pm \cos(k_{ZTE}(d - (z + z')))}{2\sin(k_{ZTE} d)} \tag{5.44}$$

and

$$\tilde{g}^{\pm}_{TE_s} = \frac{sgn(z - z')\sin(k_{ZTE}(d - |z - z'|)) \pm \sin(k_{ZTE}(d - (z + z')))}{2\sin(k_{ZTE} d)} \tag{5.45}$$

physically represent the up and down going wave behavior in the z-direction.

Similarly, the TM solutions spectral domain Green's Functions are $\overset{\leftrightarrow}{\sim}{}^{TM}_{G_{eh}}(\vec{k}_\rho, z)$ are consolidated into:

$$\begin{bmatrix} \frac{k_x k_y}{(k_y^2-\omega^2\epsilon_x\mu_x)}\tilde{g}{}^{+}_{TM_s} & 0 & \frac{k_x^2 k_y}{jk_{ZTM}(k_y^2-\omega^2\epsilon_x\mu_x)}\tilde{g}{}^{-}_{TM_c} \\ \tilde{g}{}^{-}_{TM_s} & 0 & \frac{k_x}{jk_{ZTM}}\tilde{g}{}^{-}_{TM_c} \\ -\frac{k_y k_{ZTM}}{j(k_y^2-\omega^2\epsilon_x\mu_x)}\tilde{g}{}^{+}_{TM_c} & 0 & -\frac{k_x k_y}{(k_y^2-\omega^2\epsilon_x\mu_x)}\tilde{g}{}^{-}_{TM_s} \end{bmatrix} = \overset{\leftrightarrow}{\sim}{}^{TM}_{G_{eh}} \tag{5.46}$$

where,

$$\tilde{g}{}^{\pm}_{TM_c} = \frac{\cos(k_{ZTM}(d-|z-z'|))\pm\cos(k_{ZTM}(d-(z+z')))}{2\sin(k_{ZTM}d)} \tag{5.47}$$

and

$$\tilde{g}{}^{\pm}_{TM_s} = \frac{sgn(z-z')\sin(k_{ZTM}(d-|z-z'|))\pm\sin(k_{ZTM}(d-(z+z')))}{2\sin(k_{ZTM}d)} \tag{5.48}$$

also represent up and down going wave behavior in the z-direction. The TE and TM parts of the $\overset{\leftrightarrow}{\sim}{}_{G_{eh}}$ have elements which are zero. These terms demonstrate that the field structure is TE_y and TM_y.

5.5 Calculate the spectral domain magnetic field Green's function .

The magnetic field Green's functions due to a magnetic aperture current is obtained using Faraday's Law to equate the electric to the magnetic field components. Transforming the x and y spatial components to the spectral domain, the Faraday's

Law is rewritten as

$$\begin{bmatrix} \frac{j}{\mu_x\omega} & 0 & 0 \\ 0 & \frac{j}{\mu_y\omega} & 0 \\ 0 & 0 & \frac{j}{\mu_x\omega} \end{bmatrix} \cdot \overset{\rightarrow}{\sim} J_h + \begin{bmatrix} 0 & -j\frac{d}{dz}\frac{1}{\mu_x\omega} & -\frac{k_y}{\mu_x\omega} \\ j\frac{d}{dz}\frac{1}{\mu_y\omega} & 0 & \frac{k_x}{\mu_y\omega} \\ \frac{k_y}{\mu_x\omega} & -\frac{k_x}{\mu_x\omega} & 0 \end{bmatrix} \cdot \overset{\rightarrow}{\sim} E = \overset{\rightarrow}{\sim} H. \tag{5.49}$$

Applying the parallel-plate electric fields, which are related to the magnetic current by the electric field Green's functions,

$$\begin{aligned} \int_{z'} \begin{bmatrix} \frac{j}{\mu_x\omega}\delta(z-z') & 0 & 0 \\ 0 & \frac{j}{\mu_y\omega}\delta(z-z') & 0 \\ 0 & 0 & \frac{j}{\mu_x\omega}\delta(z-z') \end{bmatrix} \cdot \overset{\rightarrow}{\sim} J_h + \\ \begin{bmatrix} 0 & -j\frac{d}{dz}\frac{1}{\mu_x\omega} & -\frac{k_y}{\mu_x\omega} \\ j\frac{d}{dz}\frac{1}{\mu_y\omega} & 0 & \frac{k_x}{\mu_y\omega} \\ \frac{k_y}{\mu_x\omega} & -\frac{k_x}{\mu_x\omega} & 0 \end{bmatrix} \overset{\leftrightarrow}{\sim} G_{eh} \cdot \overset{\rightarrow}{\sim} J_h dz' = \overset{\rightarrow}{\sim} H. \end{aligned} \tag{5.50}$$

Rearrangement of the terms in the integral and evaluating is permitted in the distributional sense as discussed in [26]. Thus the magnetic field Green's function is written as

$$\int_{z'} \overset{\leftrightarrow}{\sim} G_{hh} \cdot \overset{\rightarrow}{\sim} J_h dz' = \overset{\rightarrow}{\sim} H \tag{5.51}$$

where the individual elements are also separated into TE and TM:

$$\begin{bmatrix} \tilde{G}^{TE}_{hh,xx} & \tilde{G}^{TE}_{hh,xy} & \tilde{G}^{TE}_{hh,xz} \\ \tilde{G}^{TE}_{hh,yx} & \tilde{G}^{TE}_{hh,yy} & \tilde{G}^{TE}_{hh,yz} \\ \tilde{G}^{TE}_{hh,zx} & \tilde{G}^{TE}_{hh,zy} & \tilde{G}^{TE}_{hh,zz} \end{bmatrix} + \begin{bmatrix} \tilde{G}^{TM}_{hh,xx} & \tilde{G}^{TM}_{hh,xy} & \tilde{G}^{TM}_{hh,xz} \\ \tilde{G}^{TM}_{hh,yx} & \tilde{G}^{TM}_{hh,yy} & \tilde{G}^{TM}_{hh,yz} \\ \tilde{G}^{TM}_{hh,zx} & \tilde{G}^{TM}_{hh,zy} & \tilde{G}^{TM}_{hh,zz} \end{bmatrix} = \overset{\leftrightarrow}{\sim} G_{hh}. \tag{5.52}$$

Carefully evaluating the distributional derivative $\frac{\partial}{\partial z}$ yields the magnetic field Green's function elements for both the TE and TM pieces. The TE component is

$$\begin{bmatrix} \frac{k_x^2 k_y^2}{\mu_x \omega j k_{ZTE}(k_y^2-\omega^2\epsilon_x\mu_x)}\tilde{g}^{+}_{TE_c} & \frac{k_x k_y}{\mu_x \omega j k_{ZTE}}\tilde{g}^{+}_{TE_c} & -\frac{k_x k_y^2}{\mu_x \omega(k_y^2-\omega^2\epsilon_x\mu_x)}\tilde{g}^{-}_{TE_s} \\ \frac{k_x k_y}{\mu_x \omega j k_{ZTE}}\tilde{g}^{+}_{TE_c} & \frac{(k_y^2-\omega^2\epsilon_x\mu_x)}{\mu_x \omega j k_{ZTE}}\tilde{g}^{+}_{TE_c} & -\frac{k_y}{\mu_x\omega}\tilde{g}^{-}_{TE_s} \\ -\frac{k_x k_y^2}{\mu_x \omega(k_y^2-\omega^2\epsilon_x\mu_x)}\tilde{g}^{+}_{TE_s} & -\frac{k_y}{\mu_x\omega}\tilde{g}^{+}_{TE_s} & \tilde{G}^{TE}_{hh,zz} \end{bmatrix} = \overset{\leftrightarrow}{\tilde{G}}^{TE}_{hh} \tag{5.53}$$

where

$$\tilde{G}^{TE}_{hh,zz} = \frac{j}{\mu_x\omega}\delta(z-z') + \frac{k_y^2 k_{ZTE}}{\mu_x\omega j(k_y^2-\omega^2\epsilon_x\mu_x)}\tilde{g}^{-}_{TE_c} \tag{5.54}$$

contains the depolarizing dyad term, similar to [27]. The TM components are

$$\begin{bmatrix} \frac{\omega\epsilon_x k_{ZTM}}{j(k_y^2-\omega^2\epsilon_x\mu_x)}\tilde{g}^{+}_{TM_c} & 0 & \frac{\omega\epsilon_x k_x}{(k_y^2-\omega^2\epsilon_x\mu_x)}\tilde{g}^{-}_{TM_s} \\ 0 & 0 & 0 \\ \frac{k_x\omega\epsilon_x}{(k_y^2-\omega^2\epsilon_x\mu_x)}\tilde{g}^{+}_{TM_s} & 0 & \frac{\omega\epsilon_x k_x^2}{jk_{ZTM}(k_y^2-\omega^2\epsilon_x\mu_x)}\tilde{g}^{-}_{TM_c} \end{bmatrix} = \overset{\leftrightarrow}{\tilde{G}}^{TM}_{hh} \tag{5.55}$$

Looking at the TM components of the magnetic field Green's function shows that the structure is TM_y.

The TE_y and TM_y modes are supported in the parallel plate structure, which is uniformly filled with a rotated uniaxial anisotropic material as illustrated in the Green's function development. A term that is present for both the TE and TM parts for the electric and magnetic components is $(k_y^2-\omega^2\epsilon_x\mu_x)$. This term's physical explanation is that it permits the existence of the TEM mode in the parallel plate waveguide. This is important because, as an example, a parallel plate waveguide uniformly filled isotropic evaluation of the parallel plate structure permits TE, TM as well as the TEM mode. The structure of the source excitation will determine whether these modes (TE, TM, TEM) are coupled into (i.e. excited) or not. In this case, the excitation is an equivalent rectangular waveguide aperture surface current.

Due to the finite extent of this current, coupling into the TEM mode should not occur. Thus the pole contribution $k_y = \omega^2 \epsilon_x \mu_x$ is expected to be removable, which is observed in the subsequent SPWP moment method development.

5.6 Conclusion

A field based approach for a rotated uniaxial anisotropic parallel-plate Green's functions supported by a magnetic current is presented. Solutions for the electric and magnetic fields are obtained. A subset of these Green's functions is implemented in a moment method code for non-destructive material measurement. The Green's function development presented shows that the parallel plate boundary conditions impact the field configuration in the anisotropic media. This field structure is different than the uniaxial media development presented in [14]. Because the field structure is dictated by both the boundary conditions and material anisotropy it is important to utilize the appropriate Green's function for the corresponding measurement technique.

VI. Rotated Uniaxial Anisotropic SPWP Technique Methodology

A conference paper [28] was presented and published in conjunction with document development. The conference paper contains the same information presented in this section of the document.

Leveraging the strong transverse TE_{10} rectangular waveguide mode, an anisotropic sample with unique transverse permittivity components is measured. A Single Port Waveguide Probe (SPWP) non-destructive material characterization technique is proposed to accommodate measuring a metal backed, single known thickness, rotated uniaxial anisotropic material. These unique transverse permittivity components are parallel to the plane of the waveguide flange. The longitudinal component is chosen to be equivalent to the x-directed permittivity component, thus the material tensor is represented by

$$\overleftrightarrow{\epsilon} = \begin{bmatrix} \epsilon_{xx} & 0 & 0 \\ 0 & \epsilon_{yy} & 0 \\ 0 & 0 & \epsilon_{xx} \end{bmatrix}. \tag{6.1}$$

A rotated uniaxial material is shown in Figure 30 and is designed using crystallographic symmetry, [1] using tetragonal occlusions. Figure 31 shows a comparison of a Uniaxial and Rotated Uniaxial crystal structure as well as the sample design approach.

The SPWP as shown in Figure 32 consists of an X-band (8.2-12.4 GHz) rectangular waveguide aperture cut in the center of a square flange measuring 6" $\times$ 6". The flange is placed upon a metal-backed material surface, which forms a parallel-plate region. Two orthogonal transverse plane measurements aligned with the sample's transverse constitutive parameter components provides measurement diversity. Calibrated reflection coefficients measured at the rectangular waveguide aperture are

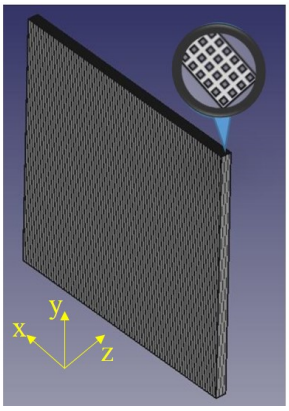

Figure 30. A rotated uniaxial anisotropic sample designed via crystallographic symmetry.

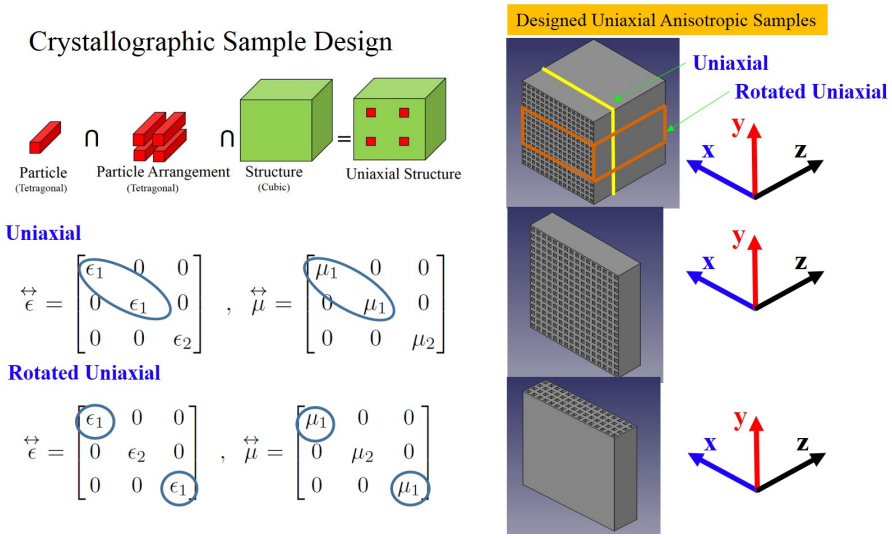

Figure 31. Uniaxial and Rotated Uniaxial Samples designed using crystallographic symmetry. Symmetry impacts the sample's anisotropy.

evaluated against a moment method forward model. Constitutive parameter results are generated by minimizing error between the forward model and the experimental S-parameter reflection coefficients, using a least squares minimization algorithm. In this paper, measurement representative simulations of two different rotated uniaxial samples are made, assessing SPWP measurement performance using a fundamental mode moment method technique.

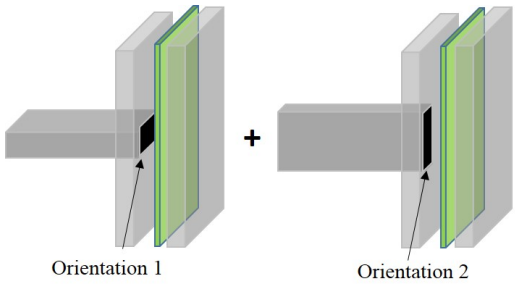

Figure 32. SPWP non-destructive measurement technique. Orientation 2 has a rectangular waveguide aperture that is rotated 90^o from Orientation 1.

6.1 Forward Model Development

The SPWP evaluates rotated uniaxial media by measuring reflections coefficients from two unique transverse orientations which are aligned to ϵ_x and ϵ_y. Two separate moment method techniques are derived to account for each equivalent current distribution posed by both orientations. Each orientation's forward model is employed in the material extraction process. It is assumed that only the TE_{10} mode-only is present at the aperture in each development.

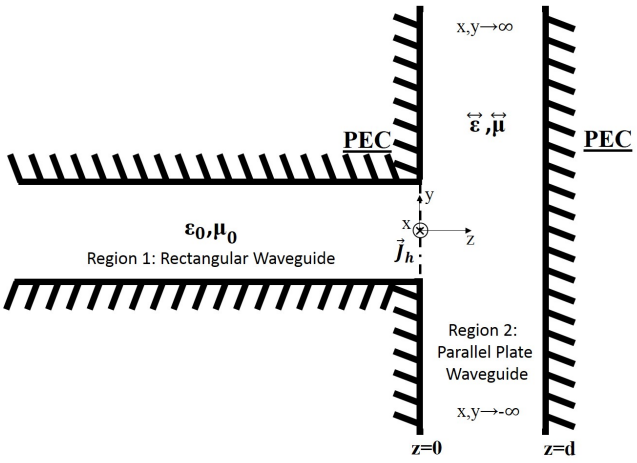

Figure 33. A cross-section of the SPWP showing the rectangular waveguide and parallel-plate regions which are related by an equivalent magnetic aperture current $\vec{J}_h$.

Moment Method Development for $\hat{y}$ aligned electric field.

Evaluation of the fields in the waveguide region begins in the same way as [12]. The fields in Region 1, as shown in Figure 33 for Orientation 1 as illustrated in Figure 32 are the TE_{10}^{z} rectangular waveguide mode electric,

$$\vec{e}_{10} = \hat{y}\cos\left(\frac{\pi x}{a}\right) \tag{6.2}$$

and magnetic fields

$$\vec{h}_{10} = \frac{\hat{z}\times\vec{e}_{10}}{Z_{10}} = -\hat{x}\frac{1}{Z_{10}}\cos\left(\frac{\pi x}{a}\right), \tag{6.3}$$

where $Z_{10} = \frac{j\omega\mu_0}{\gamma}$ and $\gamma = \sqrt{\left(\frac{\pi}{a}\right)^2 - k_0^2}$ with $k_0 = \omega\sqrt{\epsilon_0\mu_0}$. The incident and reflected fields in the waveguide region are

$$\vec{E}_t^{wg} = \vec{e}_{10}e^{-\gamma z} + \Gamma\vec{e}_{10}e^{\gamma z}, \tag{6.4}$$

$$\vec{H}_t^{wg} = \vec{h}_{10}e^{-\gamma z} - \Gamma\vec{h}_{10}e^{\gamma z} \tag{6.5}$$

where Γ is the dominant mode reflection coefficient of the Region 1 and 2 aperture. Love's equivalence theorem relates the aperture electric field as an equivalent magnetic current,

$$\begin{aligned}\vec{J}_h(\vec{\rho}') = -\hat{z}\times\vec{E}_t^{wg}(z=0^-) = -\hat{z}\times\vec{E}_t^{pp}(z=0^+)\\ = \hat{x}(1+\Gamma)\cos\left(\frac{\pi x'}{a}\right).\end{aligned} \tag{6.6}$$

A magnetic field integral equation (MFIE) relates the equivalent magnetic aperture current, $\vec{J}_h(\vec{\rho})$, (where $\vec{\rho} = \hat{x}+\hat{y}$) to the magnetic fields in the parallel-plate waveguide as

$$\vec{H}_t^{pp} = \vec{H}_{TE\,t}^{pp} + \vec{H}_{TM\,t}^{pp} \tag{6.7}$$

where

$$\vec{H}^{pp}_{TE\,t} = \iint\limits_{S'} \overleftrightarrow{G}_{TEh,t}(\rho, z|\rho, 0) \cdot \vec{J}_h(\vec{\rho}')dS' \tag{6.8}$$

and

$$\vec{H}^{pp}_{TM\,t} = \iint\limits_{S'} \overleftrightarrow{G}_{TMh,t}(\rho, z|\rho, 0) \cdot \vec{J}_h(\vec{\rho}')dS' \tag{6.9}$$

over the waveguide aperture surface S'. The rotated uniaxial Green's function $\vec{G}_{h,t}(\rho, z|\rho, 0)$ relates the aperture current to the parallel-plate magnetic fields. Because the tangential fields in the aperture region must be continuous between the waveguide and parallel-plate regions, they are related as

$$\vec{H}^{wg}_t(z = 0^-) = \vec{H}^{pp}_t(z = 0^+). \tag{6.10}$$

Expanding the previous relationship, applying the equivalent current in (6.6) and equating the vector components leads to the scalar integral equation

$$\begin{aligned} -\frac{1}{Z_{10}} \cos\left(\frac{\pi x}{a}\right)(1 - \Gamma) = (1 + \Gamma) \Bigg[&\iint\limits_{S'} G_{TEh,x}(\rho, z|\rho, 0) \cdot \cos\left(\frac{\pi x'}{a}\right) dS' \\ &+ \iint\limits_{S'} G_{TMh,x}(\rho, z|\rho, 0) \cdot \cos\left(\frac{\pi x'}{a}\right) dS' \Bigg]. \end{aligned} \tag{6.11}$$

A testing operator

$$\iint\limits_{S} \cos(\frac{\pi x}{a})\{\}dS \tag{6.12}$$

is applied to the field expansion relationship (6.11) to capture the fundamental mode component over the rectangular waveguide aperture S and results in

$$-\frac{1}{Z_{10}}(1-\Gamma)\iint_S \cos^2(\frac{\pi x}{a})dS = \\ (1+\Gamma)\left[\iint_S \cos(\frac{\pi x}{a})\iint_{S'} G_{TEh,x}\cdot\cos\left(\frac{\pi x'}{a}\right)dS'dS + \right. \\ \left.\iint_S \cos(\frac{\pi x}{a})\iint_{S'} G_{TMh,x}\cdot\cos\left(\frac{\pi x'}{a}\right)dS'dS\right]. \tag{6.13}$$

Note that the $(\rho, z|\rho, 0)$ is suppressed on the spatial Green's function terms for notational convenience. Evaluating the integral on the left side and employing the Fourier transform (Note that the TE, TM notation is intend to consolidate the separate TE and TM relationships for brevity.)

$$G_{TE,TMh,x}(\rho, z|\rho, 0) = \frac{1}{(2\pi)^2}\iint_{-\infty}^{\infty} \tilde{G}^{TE,TM}_{hh,xx}(\vec{k}_\rho, z)e^{j\vec{k}_\rho(\vec{\rho}-\vec{\rho'})}d^2k_\rho \tag{6.14}$$

(where $d^2k_\rho = dk_x dk_y$) on the right side supports simplification

$$-\frac{1}{Z_{10}}b\frac{a}{2}(1-\Gamma) = \\ (1+\Gamma)\left[\frac{1}{(2\pi)^2}\iint_{-\infty}^{\infty}\tilde{G}^{TE}_{hh,xx}(\vec{k}_\rho, z)\iint_S \cos(\frac{\pi x}{a})e^{j\vec{k}_\rho(\vec{\rho})}dS \right. \\ \iint_{S'}\cos\left(\frac{\pi x'}{a}\right)e^{-j\vec{k}_\rho(\vec{\rho'})}dS'd^2k_\rho + \\ \frac{1}{(2\pi)^2}\iint_{-\infty}^{\infty}\tilde{G}^{TM}_{hh,xx}(\vec{k}_\rho, z)\iint_S \cos(\frac{\pi x}{a})e^{j\vec{k}_\rho(\vec{\rho})}dS \\ \left.\iint_{S'}\cos\left(\frac{\pi x'}{a}\right)e^{-j\vec{k}_\rho(\vec{\rho'})}dS'd^2k_\rho\right]. \tag{6.15}$$

The magnetic field parallel-plate Green's functions for the TE component

$$\tilde{G}^{TE}_{hh,xx} = \frac{k_x^2k_y^2}{\mu_x\omega jk_{ZTE}(k_y^2-\omega^2\epsilon_x\mu_x)}\tilde{g}^{+}_{TE_c} \tag{6.16}$$

and TM component

$$\tilde{G}^{TM}_{hh,xx} = \frac{\omega\epsilon_x k_{ZTM}}{j(k_y^2-\omega^2\epsilon_x\mu_x)}\tilde{g}^{+}_{TM_c} \tag{6.17}$$

where

$$\tilde{g}^{+}_{TE_c,TM_c} = \frac{[\cos(k_{ZTE,TM}(d-|z-z'|))+\cos(k_{ZTE,TM}(d-(z+z')))]}{2\sin(k_{ZTE,TM}d)} \tag{6.18}$$

represents the standing wave interaction between the parallel-plate structure for either the TE or TM field structure are inserted into (6.15). The Green's function components are obtained from the development in Chapter 5. Equation (6.15) is then simplified into the following relationship

$$\begin{aligned} -\frac{1}{Z_{10}}b\frac{a}{2}(1-\Gamma) = \\ (1+\Gamma)\frac{-(\frac{\pi}{a})^2}{(2\pi)^2}\left[\frac{1}{\mu_x\omega j}\int_{-\infty}^{\infty}k_x^2\frac{(2+2\cos(k_xa))}{(k_x-(\frac{\pi}{a}))^2(k_x+(\frac{\pi}{a}))^2}C_{TE}dk_x + \right. \\ \left.\frac{\omega\epsilon_x}{j}\int_{-\infty}^{\infty}\frac{(2+2\cos(k_xa))}{(k_x-(\frac{\pi}{a}))^2(k_x+(\frac{\pi}{a}))^2}C_{TM}dk_x\right] \end{aligned} \tag{6.19}$$

where

$$\begin{aligned} C_{TE} = \int_{-\infty}^{\infty}\frac{\cos(k_{ZTE}(d))}{k_{ZTE}\sin(k_{ZTE}d)}\frac{(e^{jk_yb}-1)}{(k_y^2-\omega^2\epsilon_x\mu_x)}dk_y + \\ \int_{-\infty}^{\infty}\frac{\cos(k_{ZTE}(d))}{k_{ZTE}\sin(k_{ZTE}d)}\frac{(e^{-jk_yb}-1)}{(k_y^2-\omega^2\epsilon_x\mu_x)}dk_y. \end{aligned} \tag{6.20}$$

Using complex plane analysis and applying Cauchy's Integral Theorem as described in [15] and illustrated in Figure 34 yields the solution for the TE part of the k_y

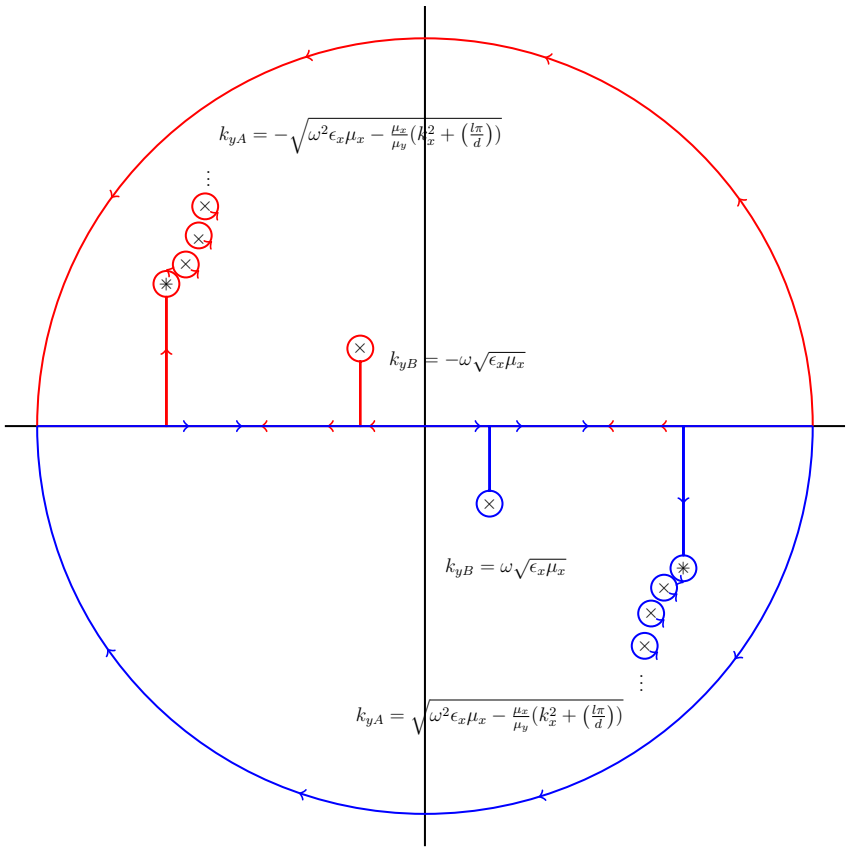

Figure 34. The complex plane showing the poles for the k_y part of the integral. Note the series of poles induced by the $\sin(k_{ZTE}d)$ part, which represent the modes exhibited in the parallel-plate waveguide structure. A double pole occurs due to $k_{ZTE}\sin(k_{ZTE}d)$ at the $l = 0$ parallel-plate mode. Individual poles are denoted by a $\times$ symbol, while a double pole is denoted by $*$ symbol.

integral,

$$C_{TE} = -2\pi\frac{\cos(jk_xd)}{k_x\sin(jk_xd)}\frac{(e^{-j\omega k_{ylTE}b}-1)}{\omega\sqrt{\epsilon_x\mu_x}} \\ -j4\pi\sum_{l=0}^{\infty}\frac{(e^{-jk_{ylTE}b}-1)}{(k_x^2+\left(\frac{l\pi}{d}\right)^2)k_{ylTE}d(1+\delta_{l=0})}. \tag{6.21}$$

The TM k_y integral is

$$C_{TM} = \int_{-\infty}^{\infty}\frac{k_{ZTM}\cos(k_{ZTM}(d))}{(k_y^2-\omega^2\epsilon_x\mu_x)\sin(k_{ZTM}d)}\frac{(e^{jk_yb}-1)}{k_y^2}dk_y + \\ \int_{-\infty}^{\infty}\frac{k_{ZTM}\cos(k_{ZTM}(d))}{(k_y^2-\omega^2\epsilon_x\mu_x)\sin(k_{ZTM}d)}\frac{(e^{-jk_yb}-1)}{k_y^2}dk_y. \tag{6.22}$$

and once again is solved by identifying the poles in the complex plane as shown in Figure 65. Using Cauchy's Integral Theorem yields the following solution

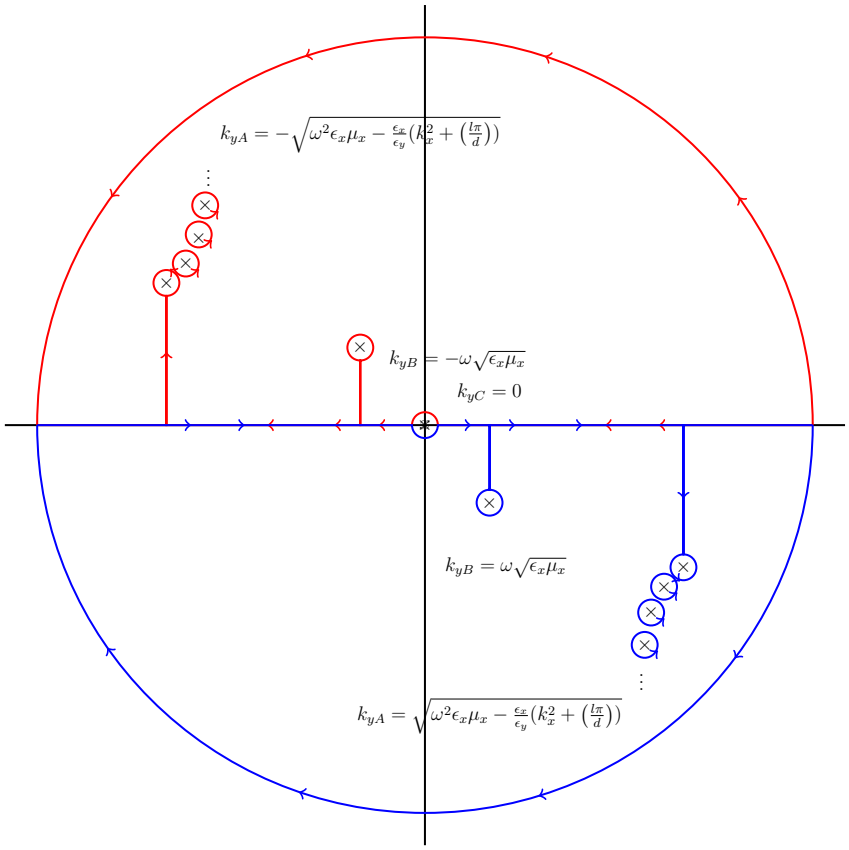

Figure 35. The complex plane showing the poles for the k_y part of the integral. Note the series of poles induced by the $\sin(k_{ZTM}d)$ part, which represent the modes exhibited in the parallel-plate waveguide structure. The double pole at the origin is physically described by the rectangular waveguide mode response on the parallel-plate region. Individual poles are denoted by a $\times$ symbol, while a double pole is denoted by $*$ symbol.

$$\begin{aligned} C_{TM} = 2\pi \frac{k_x \cos(jk_x(d))}{(\omega\sqrt{\epsilon_x\mu_x})\sin(jk_x d)} \frac{(e^{-j\omega\sqrt{\epsilon_x\mu_x}b} - 1)}{(\omega^2\epsilon_x\mu_x)} \\ +2\pi \frac{k_w \cos(k_w(d))b}{(\omega^2\epsilon_x\mu_x)(\sin(k_w d))} \\ -j4\pi \sum_{l=0}^{\infty} \frac{\left(\frac{l\pi}{d}\right)^2}{(k_x^2 + \left(\frac{l\pi}{d}\right)^2)} \frac{(e^{-jk_{ylTM}b} - 1)}{k_{ylTM}^3 d}. \end{aligned} \tag{6.23}$$

Moment Method summary for $\hat{y}$ aligned electric field.

Simplification supports cancellation of a term originating from the k_{yB} pole in both the TE and TM components and results in the following relationship

$$\frac{1}{Z_{10}} b \frac{a}{2} (1 - \Gamma) = (1 + \Gamma)\Omega \tag{6.24}$$

$$\begin{aligned} \Omega = \frac{(\frac{1}{a})^2}{\mu_x \omega j} \int_{-\infty}^{\infty} \frac{(1 + \cos(k_x a))}{(k_x - (\frac{\pi}{a}))^2 (k_x + (\frac{\pi}{a}))^2} \left[C_{TE} \right. \\ \left. + C_{TM} \right] dk_x. \end{aligned} \tag{6.25}$$

where

$$\begin{aligned} C_{TE} + C_{TM} = \\ -j2\pi \sum_{l=0}^{\infty} \frac{k_x^2 (e^{-jk_{ylTE}b} - 1)}{(k_x^2 + \left(\frac{l\pi}{d}\right)^2) k_{ylTE} d (1 + \delta_{l=0})} \\ + \pi \frac{k_w \cos(k_w(d)) b}{(\sin(k_w d))} \\ -j2\pi \sum_{l=0}^{\infty} \frac{(\omega^2 \epsilon_x \mu_x) \left(\frac{l\pi}{d}\right)^2}{(k_x^2 + \left(\frac{l\pi}{d}\right)^2)} \frac{(e^{-jk_{ylTM}b} - 1)}{k_{ylTM}^3 d} \end{aligned} \tag{6.26}$$

and

$$k_{ylTE} = \sqrt{\omega^2 \epsilon_x \mu_x - \frac{\mu_x}{\mu_y} k_x^2 - \frac{\mu_x}{\mu_y} \left(\frac{l\pi}{d}\right)^2}, \tag{6.27}$$

$$k_{ylTM} = \sqrt{\omega^2 \epsilon_x \mu_x - \frac{\epsilon_x}{\epsilon_y} k_x^2 - \frac{\epsilon_x}{\epsilon_y} \left(\frac{l\pi}{d}\right)^2}, \tag{6.28}$$

$$k_w = \sqrt{\omega^2 \epsilon_y \mu_x - k_x^2}. \tag{6.29}$$

Rewriting in terms of the reflection coefficient,

$$\Gamma = \frac{1 - \frac{2Z_{10}}{ab}\Omega}{1 + \frac{2Z_{10}}{ab}\Omega}. \tag{6.30}$$

supports obtaining a reflection coefficient at a given frequency and sample thickness d for a particular set constitutive parameters (ϵ_x, ϵ_y).

Moment Method Development for $\hat{x}$ aligned electric field.

Repeating the previous development, but now for an $\hat{x}$ directed TE_{10} mode induced by rotating the aperture current in the transverse plane as illustrated in Orientation 2 of Figure 32, yields a familiar scalar integral equation

$$\begin{aligned} \frac{1}{Z_{10}} \cos\left(\frac{\pi y}{a}\right)(1-\Gamma) = \\ -(1+\Gamma)\left[\iint\limits_{S'} G_{TEh,y}(\rho, z|\rho, 0) \cdot \cos\left(\frac{\pi y'}{a}\right) dS' \right. \\ \left. + \iint\limits_{S'} G_{TMh,y}(\rho, z|\rho, 0) \cdot \cos\left(\frac{\pi y'}{a}\right) dS' \right]. \end{aligned} \tag{6.31}$$

The rotated current distribution now invokes the y-components of the rotated uniaxial Green's function. Applying the testing operator for the rotated TE_{10} distribution, utilizing the Fourier transform to aid analysis as was done in the previous section and applying the spectral domain Green's function,

$$\tilde{G}{}^{TE}_{hh,yy} = \frac{(k_y^2 - \omega^2 \epsilon_x \mu_x)}{\mu_x \omega j k_{ZTE}} \tilde{g}{}^{+}_{TE_c}, \qquad \tilde{G}{}^{TM}_{hh,yy} = 0 \tag{6.32}$$

yields

$$\begin{aligned} \frac{1}{Z_{10}} b \frac{a}{2}(1-\Gamma) = \\ -(1+\Gamma)\left[\frac{1}{(2\pi)^2} \frac{-(\frac{\pi}{a})^2}{\mu_x \omega j} \int\limits_{-\infty}^{\infty} \frac{(2\cos(k_x b) - 2)}{k_x^2} C_{TE} dk_x \right]. \end{aligned} \tag{6.33}$$

where

$$C_{TE} = \int_{-\infty}^{\infty} \frac{(k_y^2 - \omega^2\epsilon_x\mu_x)\cos(k_{ZTE}(d))}{k_{ZTE}\sin(k_{ZTE}d)} \frac{(1+e^{jk_ya})}{(k_y-(\frac{\pi}{a}))^2(k_y+(\frac{\pi}{a}))^2} dk_y$$
$$+ \int_{-\infty}^{\infty} \frac{(k_y^2 - \omega^2\epsilon_x\mu_x)\cos(k_{ZTE}(d))}{k_{ZTE}\sin(k_{ZTE}d)} \frac{(1+e^{-jk_ya})}{(k_y-(\frac{\pi}{a}))^2(k_y+(\frac{\pi}{a}))^2} dk_y. \tag{6.34}$$

Notice however, in the $\hat{x}$ aligned orientation, that there is only a C_{TE} component present as opposed to having both the C_{TE} and C_{TM} in the previous case. The existence of the C_{TE} and C_{TM} terms is due to the uniformly filled rotated uniaxial parallel-plate region having either TE_y or TM_y parallel-plate field structure as identified in the paper [25] and is also discussed in Chapter 5. Applying the rectangular waveguides fields in Orientation 1 supports both a TE_y and TM_y modes, while Orientation 2 supports only TE_y as shown in Figure 36.

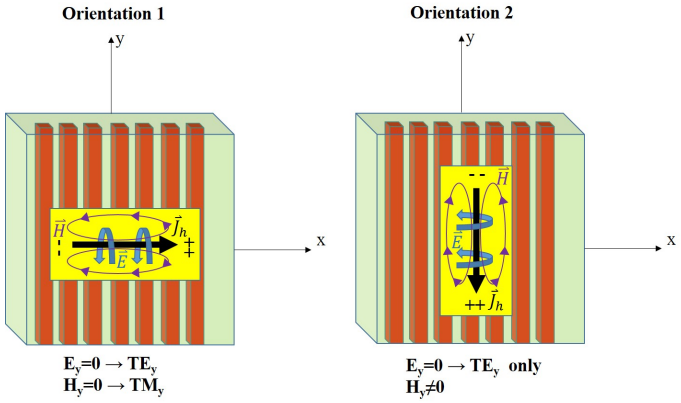

Figure 36. A simplified representation of the SPWP aperture current distribution in the presence of the rotated uniaxial material. The flange and backing structure are omitted for clarity. Orientation 1 has both TE_y and TM_y parallel-plate modes, while orientation 2 has only TE_y. Note which vector components cancel in each case.

Moment Method summary for $\hat{x}$ aligned electric field.

Locating the poles and applying Cauchy's Integral Theorem as shown in Figure 64 result in the simplified expression

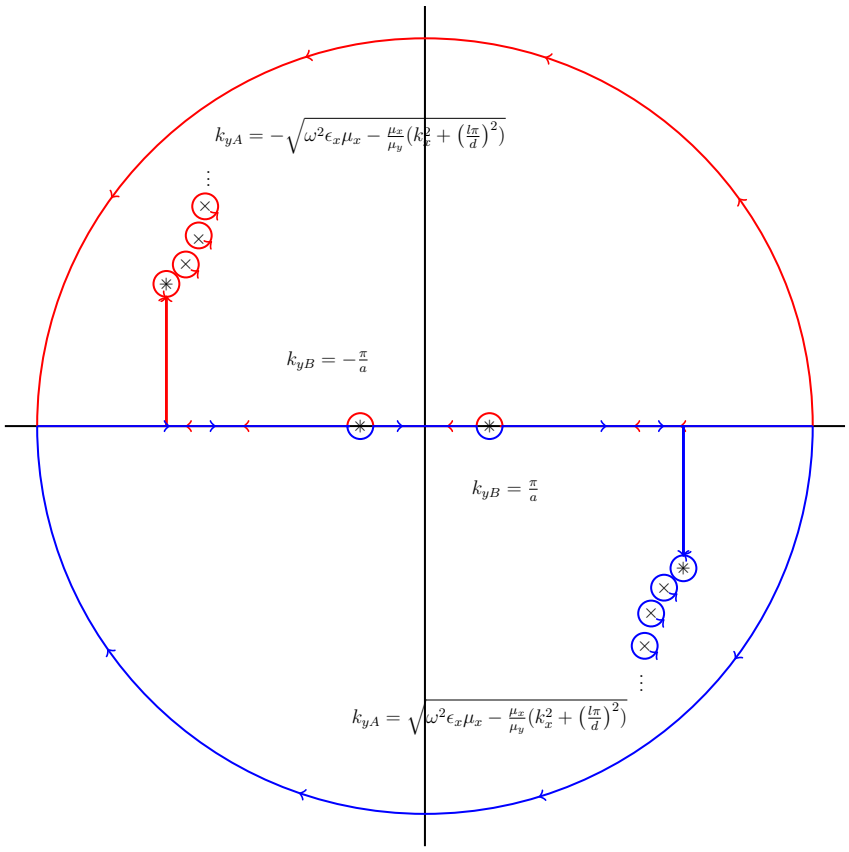

Figure 37. The complex plane showing the poles for the k_y part of the integral. Note the series of poles induced by the $k_{ZTE}\sin(k_{ZTE}d)$ part as before and the rectangular waveguide response poles at $k_y = \pm\frac{\pi}{a}$. Individual poles are denoted by a $\times$ symbol, while a double pole is denoted by $*$ symbol.

$$\frac{1}{Z_{10}}b\frac{a}{2}(1-\Gamma) = (1+\Gamma)\Omega. \tag{6.35}$$

where

$$\Omega = \left[\frac{(\frac{1}{a})^2}{\mu_x\omega j}\int_{-\infty}^{\infty}\frac{(\cos(k_x b)-1)}{k_x^2}C_{TE}dk_x\right]. \tag{6.36}$$

The term

$$\begin{aligned} C_{TE} &= \pi\frac{(\left(\frac{\pi}{a}\right)^2 - \omega^2\epsilon_x\mu_x)\cos(k_a(d))}{k_a(\sin(k_a d))}\frac{a}{(2\left(\frac{\pi}{a}\right)^2)} \\ -j2\pi\sum_{l=0}^{\infty}&\left(\frac{(1+e^{-jk_{ylTE}a})}{(k_{ylTE}^2 - (\frac{\pi}{a})^2)^2}\cdot\frac{(\frac{\mu_x}{\mu_y}k_x^2 + \frac{\mu_x}{\mu_y}\left(\frac{l\pi}{d}\right)^2)}{\left(\frac{\mu_y}{\mu_x}k_{ylTE}d(1+\delta_{l=0})\right)}\right) \end{aligned} \tag{6.37}$$

where

$$k_a = \sqrt{\omega^2 \epsilon_x \mu_y - k_x^2 - \frac{\mu_y}{\mu_x}\left(\frac{\pi}{a}\right)^2}. \tag{6.38}$$

Rewriting in terms of the reflection coefficient

$$\Gamma = \frac{1 - \frac{2Z_{10}}{ab}\Omega}{1 + \frac{2Z_{10}}{ab}\Omega} \tag{6.39}$$

supports obtaining a reflection coefficient at a given frequency for a particular set constitutive parameters (ϵ_x, ϵ_y).

Moment Method Implementation.

A MATLAB® implementation of each orientation's forward model is developed to predict the permittivity values ϵ_x and ϵ_y. The theoretical reflection coefficients Γ are iterated using MATLAB®'s `lsqcurvefit` function to update ϵ_x and ϵ_y. Iterations continue until the theoretical values converges with the measured reflection coefficients (S_{11} S-Parameters) for each orientation . The `lsqcurvefit` function is operated in "Trusted-Region-Reflective" because it constrains the solution search region. MATLAB®'s `quadgk` function evaluates the k_x integrals (6.25 and 6.36). The first 100 parallel-plate modes were used in calculations and are shown to be sufficient in [9]. Prior to evaluating rotated uniaxial media, a verification of the the moment method solutions was performed by using both forward models and the forward model in [12] to generate reflection coefficients for an isotropic material. The accuracy check of the forward models is demonstrated by calculating exactly the same reflection coefficients for all three approaches for isotropic media.

6.2 Higher Order Mode Introduction

In the previous sections of this chapter, the fundamental mode-only rotated uniaxial anisotropic single port waveguide probe (SPWP), in Figure 32, supports rotated uniaxial anisotropic material characterization due to the strong transverse field components of the TE_{10} mode. Now, both the propagating fundamental TE_{10} and selected evanescent higher order modes are accommodated in a moment method forward model to enhance the measurement of rotated uniaxial anisotropic media. Including the higher order modes provides a more physically accurate representation of the SPWP system. The moment method development presented consists of two distinct forward models, one for each orientation, just as discussed in the fundamental mode section of this chapter. Despite the initial appearance that the work to develop the forward model is double, it is shown that derivations from one orientation can be reused to suit calculations for the other orientation. Given the significant number of calculations required, the reader is encouraged to review the appropriate appendices as they are referenced in the chapter.

6.3 Higher Order Mode Methodology

A moment method forward model for the theoretical reflection coefficient of the SPWP is developed which assumes a propagating fundamental mode and evanescent higher order modes in the waveguide region. The waveguide has the width of 'a' and the height of 'b' and is assumed to be filled with free space ϵ_0, μ_0. The material under test is conductor backed and is placed adjacent to the waveguide flange, forming the parallel plate region. The MUT in the parallel plate region has a thickness of 'd'. Both moment method development orientations support a set of rectangular waveguide expansion fields (represented by a set of rectangular waveguide modes), which are then tested (using the rectangular waveguide modes) to determine the

weight of their contribution to the SPWP's aperture field. Once again, if infinitely many modes are assumed in both expansion and testing, then an exact representation of the SPWP's propagating reflection coefficient is obtained. However, practical implementation limits the number of modes used.

Rectangular Waveguide Region Field Expansion of both Orientations.

The incident and reflected fields in the waveguide region are

$$\vec{E}_t^{wg} = \vec{e}_{10}^{TE} e^{-\gamma_{10} z} + \sum_{m=0}^{\infty}\sum_{n=0}^{\infty} \left(\Gamma_{mn}^{TE}\vec{e}_{mn}^{TE} + \Gamma_{mn}^{TM}\vec{e}_{mn}^{TM}\right) e^{\gamma_{mn} z}, \tag{6.40}$$

$$\vec{H}_t^{wg} = \vec{h}_{10}^{TE} e^{-\gamma_{10} z} - \sum_{m=0}^{\infty}\sum_{n=0}^{\infty} \left(\Gamma_{mn}^{TE}\vec{h}_{mn}^{TE} + \Gamma_{mn}^{TM}\vec{h}_{mn}^{TM}\right) e^{\gamma_{mn} z}. \tag{6.41}$$

The electric field components consist of TE^z and TM^z parts

$$\begin{bmatrix} \vec{e}_{mn}^{TE} \\ \\ \vec{e}_{mn}^{TM} \end{bmatrix} = \hat{x} \begin{bmatrix} k_y \\ \\ k_x \end{bmatrix} \cos(k_x x)\sin(k_y y) + \hat{y} \begin{bmatrix} -k_x \\ \\ k_y \end{bmatrix} \sin(k_x x)\cos(k_y y). \tag{6.42}$$

The magnetic field components are described as

$$\begin{bmatrix} \vec{h}_{mn}^{TE} \\ \\ \vec{h}_{mn}^{TM} \end{bmatrix} = \hat{z} \times \begin{bmatrix} \frac{\vec{e}_{mn}^{TE}}{Z_{mn}^{TE}} \\ \\ \frac{\vec{e}_{mn}^{TM}}{Z_{mn}^{TM}} \end{bmatrix}. \tag{6.43}$$

Because a second orientation is needed to characterize rotated uniaxial media, a rotation transformation is applied to the fields present in the waveguide. The coordinate system remains aligned to the first orientation. Figure 38 shows the relationship between both measurement orientations. Aiding readability, and helping to distinguish between orientations, analysis for the second orientation is in blue font, while the first remains in black font. For notation convenience Orientation 1 is also referred to as

$O1$ and Orientation 2, as $O2$.

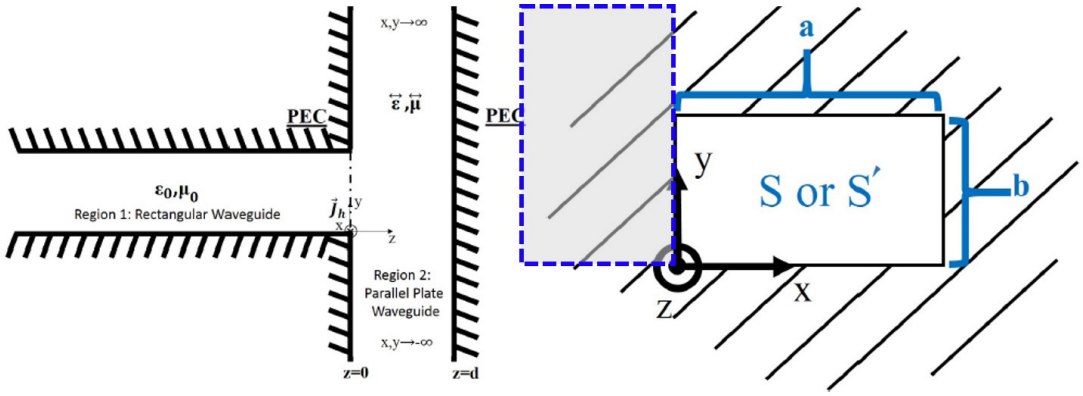

Figure 38. Two measurement orientations are needed to characterize Rotated Uniaxial Anisotropic media. Note the position and orientation of the coordinate system. Orientation 1 is the black aperture outline, while orientation 2 is the dashed and shaded blue aperture outline.

Development of the rotated fields for O2 relies on a coordinate transformation,

$$\vec{E}_{new}(\vec{r}) = \overset{\leftrightarrow}{R} \cdot \vec{E}\left(\overset{\leftrightarrow}{R}^{-1} \cdot (\vec{r})\right) \tag{6.44}$$

which rotates the fields. The rotation transformation, $\overset{\leftrightarrow}{R}^{-1}$ is initially applied to $\vec{r} = \vec{x} + \vec{y}$, as

$$\begin{bmatrix} y \\ -x \end{bmatrix} = \begin{bmatrix} 0 & 1 \\ -1 & 0 \end{bmatrix} \cdot \begin{bmatrix} x \\ y \end{bmatrix} \tag{6.45}$$

and result in the rotation of the waveguide aperture dimensions on the electric field,

$$\begin{bmatrix} \vec{e}^{TE}_{mn} \\ \vec{e}^{TM}_{mn} \end{bmatrix} = \hat{x} \begin{bmatrix} k_y \\ k_x \end{bmatrix} \cos(k_x y)\sin(k_y(-x)) + \hat{y} \begin{bmatrix} -k_x \\ k_y \end{bmatrix} \sin(k_x y)\cos(k_y(-x)). \tag{6.46}$$

Applying the transformation $\overleftrightarrow{R}$ to the fields,

$$\begin{bmatrix} -\begin{bmatrix} -k_x \\ k_y \end{bmatrix} \sin(k_x y)\cos(k_y(-x)) \\ \begin{bmatrix} k_y \\ k_x \end{bmatrix} \cos(k_x y)\sin(k_y(-x)) \end{bmatrix} = \begin{bmatrix} 0 & -1 \\ 1 & 0 \end{bmatrix} \cdot \begin{bmatrix} \begin{bmatrix} k_y \\ k_x \end{bmatrix} \cos(k_x y)\sin(k_y(-x)) \\ \begin{bmatrix} -k_x \\ k_y \end{bmatrix} \sin(k_x(y)\cos(k_y(-x)) \end{bmatrix} \tag{6.47}$$

and simplifying results in the rotated waveguide aperture electric field

$$\begin{bmatrix} \vec{e}_{mn}^{TE} \\ \vec{e}_{mn}^{TM} \end{bmatrix} = \begin{bmatrix} -\begin{bmatrix} -k_x \\ k_y \end{bmatrix} \sin(k_x y)\cos(k_y x) \\ -\begin{bmatrix} k_y \\ k_x \end{bmatrix} \cos(k_x y)\sin(k_y x) \end{bmatrix} = \begin{bmatrix} -\begin{bmatrix} -k_x \\ k_y \end{bmatrix} \sin(k_x y)\cos(k_y(-x)) \\ \begin{bmatrix} k_y \\ k_x \end{bmatrix} \cos(k_x y)\sin(k_y(-x)) \end{bmatrix}. \tag{6.48}$$

The rotated magnetic fields are directly related to the rotated electric fields as:

$$\begin{bmatrix} \vec{h}_{mn}^{TE} \\ \vec{h}_{mn}^{TM} \end{bmatrix} = \hat{z} \times \begin{bmatrix} \frac{\vec{e}_{mn}^{TE}}{Z_{mn}^{TE}} \\ \frac{\vec{e}_{mn}^{TM}}{Z_{mn}^{TM}} \end{bmatrix} \tag{6.49}$$

and simplify to

$$\begin{bmatrix} \vec{h}_{mn}^{TE} \\ \vec{h}_{mn}^{TM} \end{bmatrix} = \begin{bmatrix} \begin{bmatrix} \frac{k_y}{Z_{mn}^{TE}} \\ \frac{k_x}{Z_{mn}^{TM}} \end{bmatrix} \cos(k_x y)\sin(k_y x) \\ -\begin{bmatrix} -\frac{k_x}{Z_{mn}^{TE}} \\ \frac{k_y}{Z_{mn}^{TM}} \end{bmatrix} \sin(k_x y)\cos(k_y x) \end{bmatrix} = \begin{bmatrix} --\begin{bmatrix} \frac{k_y}{Z_{mn}^{TE}} \\ \frac{k_x}{Z_{mn}^{TM}} \end{bmatrix} \cos(k_x y)\sin(k_y x) \\ -\begin{bmatrix} -\frac{k_x}{Z_{mn}^{TE}} \\ \frac{k_y}{Z_{mn}^{TM}} \end{bmatrix} \sin(k_x y)\cos(k_y x) \end{bmatrix} \tag{6.50}$$

where $Z_{mn}^{TE} = \frac{j\omega\mu_0}{\gamma_{mn}}$, $Z_{mn}^{TM} = \frac{\gamma_{mn}}{j\omega\epsilon_0}$, $k_x = \frac{m\pi}{a}$, $k_y = \frac{n\pi}{a}$ and $\gamma_{mn} = \sqrt{k_x^2 + k_y^2 - k_0^2}$ with $k_0 = \omega\sqrt{\epsilon_0\mu_0}$. Note that these parameters are the same as orientation 1.

Field Expansion and Testing.

The field expansion and testing developed posed in this section is valid for both orientations due to the notation used. Applying either O1 or O2 fields to the development provided will yield the correct relationship for either orientation. For brevity, only O1 is used as the example.

The aperture between Region 1 and 2 are related by the continuity of tangential electric and magnetic fields. The perfect electric conductor (PEC) flange which surrounds the aperture in Region 2 define the electric fields to be zero everywhere but the aperture; similar to work done in previous chapters. Love's equivalence theorem relates the aperture electric field as an equivalent magnetic current,

$$\begin{aligned}
\vec{J}_h(\vec{\rho}') &= -\hat{z} \times \vec{E}_t^{pp}(z=0^+) = -\hat{z} \times \vec{E}_t^{wg}(z=0^-) \\
&= -Z_{10}^{TE}\vec{h}_{10}^{TE} - \sum_{m=0}^{\infty}\sum_{n=0}^{\infty}\left(\Gamma_{mn}^{TE}Z_{mn}^{TE}\vec{h}_{mn}^{TE} + \Gamma_{mn}^{TM}Z_{mn}^{TM}\vec{h}_{mn}^{TM}\right) \\
&= -\sum_{m=0}^{\infty}\sum_{n=0}^{\infty}\left(Z_{mn}^{TE}\vec{h}_{mn}^{TE}\delta_{mn10}^{TE} + \Gamma_{mn}^{TE}Z_{mn}^{TE}\vec{h}_{mn}^{TE} + \Gamma_{mn}^{TM}Z_{mn}^{TM}\vec{h}_{mn}^{TM}\right) \\
&= -\sum_{m=0}^{\infty}\sum_{n=0}^{\infty}\left(Z_{mn}^{TE}\vec{h}_{mn}^{TE}\left(\delta_{mn10}^{TE} + \Gamma_{mn}^{TE}\right) + \Gamma_{mn}^{TM}Z_{mn}^{TM}\vec{h}_{mn}^{TM}\right) \\
&= -\sum_{m=0}^{\infty}\sum_{n=0}^{\infty}\left(\overline{\Gamma}_{mn}^{TE}Z_{mn}^{TE}\vec{h}_{mn}^{TE} + \Gamma_{mn}^{TM}Z_{mn}^{TM}\vec{h}_{mn}^{TM}\right)
\end{aligned} \tag{6.51}$$

$$\boxed{\overline{\Gamma}_{mn}^{TE} = \left(\delta_{mn10}^{TE} + \Gamma_{mn}^{TE}\right)} \tag{6.52}$$

By re-writing the reflection coefficient as $\overline{\Gamma}_{mn}^{TE}$, the waveguide tangential magnetic

fields at $z = 0^-$ relationship are revised and shown as:

$$\begin{aligned}
\vec{H}_t^{wg}(z=0^-) = \vec{h}_{10}^{TE} - \sum_{m=0}^{\infty}\sum_{n=0}^{\infty}\left(\Gamma_{mn}^{TE}\vec{h}_{mn}^{TE} + \Gamma_{mn}^{TM}\vec{h}_{mn}^{TM}\right) = \\
\vec{h}_{10}^{TE} - \sum_{m=0}^{\infty}\sum_{n=0}^{\infty}\left(\left(\overline{\Gamma}_{mn}^{TE} - \delta_{mn10}^{TE}\right)\vec{h}_{mn}^{TE} + \Gamma_{mn}^{TM}\vec{h}_{mn}^{TM}\right) = \\
\vec{h}_{10}^{TE} - \sum_{m=0}^{\infty}\sum_{n=0}^{\infty}\left(\overline{\Gamma}_{mn}^{TE}\vec{h}_{mn}^{TE} - \delta_{mn10}^{TE}\vec{h}_{mn}^{TE} + \Gamma_{mn}^{TM}\vec{h}_{mn}^{TM}\right) = \\
\vec{h}_{10}^{TE} + \vec{h}_{10}^{TE} - \sum_{m=0}^{\infty}\sum_{n=0}^{\infty}\left(\overline{\Gamma}_{mn}^{TE}\vec{h}_{mn}^{TE} + \Gamma_{mn}^{TM}\vec{h}_{mn}^{TM}\right) = \\
2\vec{h}_{10}^{TE} - \sum_{m=0}^{\infty}\sum_{n=0}^{\infty}\left(\overline{\Gamma}_{mn}^{TE}\vec{h}_{mn}^{TE} + \Gamma_{mn}^{TM}\vec{h}_{mn}^{TM}\right)
\end{aligned} \tag{6.53}$$

Having synthesized an equivalent aperture current, and reconstituting the tangential magnetic fields at the waveguide aperture, attention is turned to evaluating the parallel plate region. Decoupling the rectangular waveguide portion of the SPWP from the parallel plate portion, the aperture is "closed" by PEC and replaced by the magnetic aperture current. A magnetic field integral equation (MFIE) evaluates the parallel plate region because it relates the equivalent magnetic aperture current, denoted by $\vec{J}_h(\vec{\rho})$ to the magnetic fields in the parallel plate waveguide. The Region 2 magnetic field is described by

$$\vec{H}_t^{pp} = \iint_{S'} \overleftrightarrow{G}_{hh}(\rho, z|\rho, 0) \cdot \vec{J}_h(\vec{\rho}')dS', \tag{6.54}$$

which can be expanded as

$$\vec{H}_t^{pp} = \iint_{S'} \left(\overleftrightarrow{G}_{hh}^{TE}(\rho, z|\rho, 0) + \overleftrightarrow{G}_{hh}^{TM}(\rho, z|\rho, 0)\right) \cdot \vec{J}_h(\vec{\rho}')dS', \tag{6.55}$$

over the waveguide aperture surface S. The presence of the current in the parallel plate waveguide region requires the use of a rotated uniaxial Green's function to relate the current to the parallel plate magnetic fields. These magnetic fields in-turn are

also equivalent to the magnetic fields in the rectangular waveguide at the aperture and are once again related by,

$$\vec{H}_t^{wg}(z=0^-) = \vec{H}_t^{pp}(z=0^+) \tag{6.56}$$

and when expanded show

$$\begin{aligned} 2\vec{h}_{10}^{TE} - \sum_{m=0}^{\infty}\sum_{n=0}^{\infty}\left(\overline{\Gamma}_{mn}^{TE}\vec{h}_{mn}^{TE} + \Gamma_{mn}^{TM}\vec{h}_{mn}^{TM}\right) = \\ \iint_{S'} \overleftrightarrow{G}_{hh}^{TE}(\rho,z|\rho,0)\cdot\left[-\sum_{m=0}^{\infty}\sum_{n=0}^{\infty}\left(\overline{\Gamma}_{mn}^{TE}Z_{mn}^{TE}\vec{h}_{mn}^{TE} + \Gamma_{mn}^{TM}Z_{mn}^{TM}\vec{h}_{mn}^{TM}\right)\right]dS' \\ + \iint_{S'} \overleftrightarrow{G}_{hh}^{TM}(\rho,z|\rho,0)\cdot\left[-\sum_{m=0}^{\infty}\sum_{n=0}^{\infty}\left(\overline{\Gamma}_{mn}^{TE}Z_{mn}^{TE}\vec{h}_{mn}^{TE} + \Gamma_{mn}^{TM}Z_{mn}^{TM}\vec{h}_{mn}^{TM}\right)\right]dS'. \end{aligned} \tag{6.57}$$

Distributing the Green's function through (and suppressing $(\rho,z|\rho,0)$) shows

$$\begin{aligned} 2\vec{h}_{10}^{TE} - \sum_{m=0}^{\infty}\sum_{n=0}^{\infty}\left(\overline{\Gamma}_{mn}^{TE}\vec{h}_{mn}^{TE} + \Gamma_{mn}^{TM}\vec{h}_{mn}^{TM}\right) = \\ -\iint_{S'}\sum_{m=0}^{\infty}\sum_{n=0}^{\infty}\left(\overleftrightarrow{G}_{hh}^{TE}\overline{\Gamma}_{mn}^{TE}Z_{mn}^{TE}\vec{h}_{mn}^{TE} + \overleftrightarrow{G}_{hh}^{TE}\Gamma_{mn}^{TM}Z_{mn}^{TM}\vec{h}_{mn}^{TM}\right)dS' \\ -\iint_{S'}\sum_{m=0}^{\infty}\sum_{n=0}^{\infty}\left(\overleftrightarrow{G}_{hh}^{TM}\overline{\Gamma}_{mn}^{TE}Z_{mn}^{TE}\vec{h}_{mn}^{TE} + \overleftrightarrow{G}_{hh}^{TM}\Gamma_{mn}^{TM}Z_{mn}^{TM}\vec{h}_{mn}^{TM}\right)dS'. \end{aligned} \tag{6.58}$$

Regrouping the terms yields the Field Expansion at the aperture,

$$\begin{aligned} 2\vec{h}_{10}^{TE} = \sum_{m=0}^{\infty}\sum_{n=0}^{\infty}\left[\overline{\Gamma}_{mn}^{TE}\left(\vec{h}_{mn}^{TE} - Z_{mn}^{TE}\left(\iint_{S'}\overleftrightarrow{G}_{hh}^{TE}\cdot\vec{h}_{mn}^{TE}dS' + \iint_{S'}\overleftrightarrow{G}_{hh}^{TM}\cdot\vec{h}_{mn}^{TE}dS'\right)\right)\right] \\ + \sum_{m=0}^{\infty}\sum_{n=0}^{\infty}\left[\Gamma_{mn}^{TM}\left(\vec{h}_{mn}^{TM} - Z_{mn}^{TM}\left(\iint_{S'}\overleftrightarrow{G}_{hh}^{TE}\cdot\vec{h}_{mn}^{TM}dS' + \iint_{S'}\overleftrightarrow{G}_{hh}^{TM}\cdot\vec{h}_{mn}^{TM}dS'\right)\right)\right]. \end{aligned} \tag{6.59}$$

Applying the testing operator

$$\iint_S \vec{h}^*_{uv} \cdot \{ \quad \} dS \tag{6.60}$$

where u and v are the mode indices of the testing field distribution result in the following relationship which is solved using the moment method:

$$\begin{aligned} 2 \iint_S \vec{h}^*_{uv} \cdot \vec{h}^{TE}_{10} dS = \\ \sum_{m=0}^{\infty} \sum_{n=0}^{\infty} \left[\overline{\Gamma}^{TE}_{mn} \left(\iint_S \vec{h}^*_{uv} \cdot \vec{h}^{TE}_{mn} dS - Z^{TE}_{mn} \left(\iint_S \vec{h}^*_{uv} \cdot \iint_{S'} \overleftrightarrow{G}^{TE}_{hh} \cdot \vec{h}^{TE}_{mn} dS' dS \; + \right. \right. \right. \\ \left. \left. \left. \iint_S \vec{h}^*_{uv} \cdot \iint_{S'} \overleftrightarrow{G}^{TM}_{hh} \cdot \vec{h}^{TE}_{mn} dS' dS \right) \right) \right] \\ + \sum_{m=0}^{\infty} \sum_{n=0}^{\infty} \left[\Gamma^{TM}_{mn} \left(\iint_S \vec{h}^*_{uv} \cdot \vec{h}^{TM}_{mn} dS - Z^{TM}_{mn} \left(\iint_S \vec{h}^*_{uv} \cdot \iint_{S'} \overleftrightarrow{G}^{TE}_{hh} \cdot \vec{h}^{TM}_{mn} dS' dS \; + \right. \right. \right. \\ \left. \left. \left. \iint_S \vec{h}^*_{uv} \cdot \iint_{S'} \overleftrightarrow{G}^{TM}_{hh} \cdot \vec{h}^{TM}_{mn} dS' dS \right) \right) \right]. \end{aligned} \tag{6.61}$$

Aiding manipulation of the relation, a Fourier transform is applied to the spatial Green's functions transforms them to the spectral domain,

$$\overleftrightarrow{G}_{hh}(\vec{\rho}', z', \vec{\rho}, z) = \frac{1}{(2\pi)^2} \iint_{-\infty}^{\infty} \overleftrightarrow{\tilde{G}}_{hh}(\vec{\lambda}_\rho, z', z) e^{j\vec{\lambda}_\rho \cdot (\vec{\rho} - \vec{\rho}')} d^2\lambda \tag{6.62}$$

where $z = z' = 0$, because of the sheet aperture current. This transformation supports rearranging the integrals such that x' and y' are with the S' set of integral and x and y are with the S. Both S and S' integrals are within the Spectral Green's function integral.

Attention is turned to evaluating the various integrals associated with the expan-

sion, S' and test S terms. A total of nine integrals are evaluated. It is important to note that depending on the Orientation being evaluated, the form of the integrals will change slightly, due to the orientation of the rectangular waveguide fields from O1 to O2. Examples and solutions are provided for O1 and O2 in Appendix C. Following solving each of the integrals and installing their respective solutions, the spectral domain Green's functions are incorporated. Because the aperture geometry is a sheet in the $x-y$ plane only the transverse Green's function component are implicated. The TE components are:

$$\begin{bmatrix} \frac{\lambda_x^2\lambda_y^2}{\mu_x\omega j k_{ZTE}(k_y^2-\omega^2\epsilon_x\mu_x)}\frac{\cos(k_{ZTE}d)}{\sin(k_{ZTE}d)} & \frac{\lambda_x\lambda_y}{\mu_x\omega j k_{ZTE}}\frac{\cos(k_{ZTE}d)}{\sin(k_{ZTE}d)} \\ \frac{\lambda_x\lambda_y}{\mu_x\omega j k_{ZTE}}\frac{\cos(k_{ZTE}d)}{\sin(k_{ZTE}d)} & \frac{(\lambda_y^2-\omega^2\epsilon_x\mu_x)}{\mu_x\omega j k_{ZTE}}\frac{\cos(k_{ZTE}d)}{\sin(k_{ZTE}d)} \end{bmatrix} = \overset{\leftrightarrow}{\sim}{}^{TE}_{G_{hh}} \tag{6.63}$$

and TM components are

$$\begin{bmatrix} \frac{\omega\epsilon_x k_{ZTM}}{j(\lambda_y^2-\omega^2\epsilon_x\mu_x)}\frac{\cos(k_{ZTM}d)}{\sin(k_{ZTM}d)} & 0 \\ 0 & 0 \end{bmatrix} = \overset{\leftrightarrow}{\sim}{}^{TM}_{G_{hh}} \tag{6.64}$$

Note that these spectral Green's functions have been simplifying due to z=z'=0. Additionally, recall that

$$k_{ZTE} = \pm\sqrt{\omega^2\epsilon_x\mu_y - \lambda_x^2 - \frac{\mu_y}{\mu_x}\lambda_y^2} \qquad k_{ZTM} = \pm\sqrt{\omega^2\epsilon_y\mu_x - \lambda_x^2 - \frac{\epsilon_y}{\epsilon_x}\lambda_y^2} \tag{6.65}$$

because remember k_{ZTE} and k_{ZTM} are associated with the TE and TM modes of the Parallel Plate Green's function. Taking advantage of the '0' terms in the TM part of

the Green's function an updated relationship is presented as:

$$
\begin{aligned}
2\iint_S \vec{h}^{\,*}_{uv}\cdot\vec{h}^{\,TE}_{10}dS = \sum_{m=0}^{\infty}\sum_{n=0}^{\infty}\Bigg[\overline{\Gamma}^{TE}_{mn}\Bigg(\iint_S \vec{h}^{\,*}_{uv}\cdot\vec{h}^{\,TE}_{mn}dS \\
-\frac{Z^{TE}_{mn}}{(2\pi)^2}\Bigg(\iint_{-\infty}^{\infty}\tilde{G}^{TE}_{hh,xx}\iint_S h^{*}_{uv,x}e^{j\vec{\lambda}_\rho\cdot(\vec{\rho})}dS\cdot\iint_{S'} h^{TE}_{mn,x}e^{-j\vec{\lambda}_\rho\cdot(\vec{\rho}')}dS'd^2\lambda \\
+\iint_{-\infty}^{\infty}\tilde{G}^{TE}_{hh,xy}\iint_S h^{*}_{uv,y}e^{j\vec{\lambda}_\rho\cdot(\vec{\rho})}dS\cdot\iint_{S'} h^{TE}_{mn,x}e^{-j\vec{\lambda}_\rho\cdot(\vec{\rho}')}dS'd^2\lambda \\
+\iint_{-\infty}^{\infty}\tilde{G}^{TE}_{hh,yx}\iint_S h^{*}_{uv,x}e^{j\vec{\lambda}_\rho\cdot(\vec{\rho})}dS\cdot\iint_{S'} h^{TE}_{mn,y}e^{-j\vec{\lambda}_\rho\cdot(\vec{\rho}')}dS'd^2\lambda \\
+\iint_{-\infty}^{\infty}\tilde{G}^{TE}_{hh,yy}\iint_S h^{*}_{uv,y}e^{j\vec{\lambda}_\rho\cdot(\vec{\rho})}dS\cdot\iint_{S'} h^{TE}_{mn,y}e^{-j\vec{\lambda}_\rho\cdot(\vec{\rho}')}dS'd^2\lambda \\
+\iint_{-\infty}^{\infty}\tilde{G}^{TM}_{hh,xx}\iint_S h^{*}_{uv,x}e^{j\vec{\lambda}_\rho\cdot(\vec{\rho})}dS\cdot\iint_{S'} h^{TE}_{mn,x}e^{-j\vec{\lambda}_\rho\cdot(\vec{\rho}')}dS'd^2\lambda\Bigg)\Bigg)\Bigg] \\
+\sum_{m=0}^{\infty}\sum_{n=0}^{\infty}\Bigg[\Gamma^{TM}_{mn}\Bigg(\iint_S \vec{h}^{\,*}_{uv}\cdot\vec{h}^{\,TM}_{mn}dS \\
-\frac{Z^{TM}_{mn}}{(2\pi)^2}\Bigg(\iint_{-\infty}^{\infty}\tilde{G}^{TE}_{hh,xx}\iint_S h^{*}_{uv,x}e^{j\vec{\lambda}_\rho\cdot(\vec{\rho})}dS\cdot\iint_{S'} h^{TM}_{mn,x}e^{-j\vec{\lambda}_\rho\cdot(\vec{\rho}')}dS'd^2\lambda \\
+\iint_{-\infty}^{\infty}\tilde{G}^{TE}_{hh,xy}\iint_S h^{*}_{uv,y}e^{j\vec{\lambda}_\rho\cdot(\vec{\rho})}dS\cdot\iint_{S'} h^{TM}_{mn,x}e^{-j\vec{\lambda}_\rho\cdot(\vec{\rho}')}dS'd^2\lambda \\
+\iint_{-\infty}^{\infty}\tilde{G}^{TE}_{hh,yx}\iint_S h^{*}_{uv,x}e^{j\vec{\lambda}_\rho\cdot(\vec{\rho})}dS\cdot\iint_{S'} h^{TM}_{mn,y}e^{-j\vec{\lambda}_\rho\cdot(\vec{\rho}')}dS'd^2\lambda \\
+\iint_{-\infty}^{\infty}\tilde{G}^{TE}_{hh,yy}\iint_S h^{*}_{uv,y}e^{j\vec{\lambda}_\rho\cdot(\vec{\rho})}dS\cdot\iint_{S'} h^{TM}_{mn,y}e^{-j\vec{\lambda}_\rho\cdot(\vec{\rho}')}dS'd^2\lambda \\
+\iint_{-\infty}^{\infty}\tilde{G}^{TM}_{hh,xx}\iint_S h^{*}_{uv,x}e^{j\vec{\lambda}_\rho\cdot(\vec{\rho})}dS\cdot\iint_{S'} h^{TM}_{mn,x}e^{-j\vec{\lambda}_\rho\cdot(\vec{\rho}')}dS'd^2\lambda\Bigg)\Bigg)\Bigg].
\end{aligned}
\tag{6.66}
$$

Upon including the remaining Green's function terms and the various integral so-

lutions (described in Appendix C) a simplified equation relating the fields in the rectangular waveguide to the parallel plate structure is obtained:

$$
\begin{aligned}
2\left(\frac{(\frac{\pi}{a})^2}{Z_{10}^{TE*}Z_{10}^{TE}}\right)\frac{ab}{2}\delta_{uv10}^{TE} = \sum_{m=0}^{\infty}\sum_{n=0}^{\infty}\Bigg[\overline{\Gamma}_{mn}^{TE}\Bigg(\left(\left(\frac{m\pi}{a}\right)^2+\left(\frac{n\pi}{b}\right)^2\right)\frac{ab(1+\delta_{uvm0}^{TE})}{4Z_{mn}^{TE*}Z_{mn}^{TE}}\delta_{uvmn}^{TE} \\
-\frac{1}{(2\pi)^2}\left(\frac{C_xk_x^2}{\mu_x\omega}\Omega+\frac{(C_xk_y^2+C_yk_x^2)}{\mu_x\omega}\Phi+\frac{C_yk_y^2}{\mu_x\omega}\Upsilon+C_xk_x^2\omega\epsilon_xX\right)\Bigg)\Bigg] \\
+\sum_{m=0}^{\infty}\sum_{n=0}^{\infty}\Bigg[\Gamma_{mn}^{TM}\Bigg(\left(\left(\frac{m\pi}{a}\right)^2+\left(\frac{n\pi}{b}\right)^2\right)\frac{ab(1+\delta_{uvm0}^{TM})}{4Z_{mn}^{TM*}Z_{mn}^{TM}}\delta_{uvmn}^{TM} \\
-\frac{k_xk_y}{(2\pi)^2}\left(-\frac{C_x}{\mu_x\omega}\Omega+\frac{(C_x-C_y)}{\mu_x\omega}\Phi+\frac{C_y}{\mu_x\omega}\Upsilon-C_x\omega\epsilon_xX\right)\Bigg)\Bigg].
\end{aligned}
\tag{6.67}
$$

where

$$
C_x = \begin{cases} \frac{-j(\frac{u\pi}{a})^2}{Z_{uv}^{TE}}^*, & h_{uvx}^* \implies h_{uvx}^{*\ TE} \\ \frac{j\frac{u\pi}{a}\frac{v\pi}{b}}{Z_{uv}^{TM}}^*, & h_{uvx}^* \implies h_{uvx}^{*\ TM} \end{cases}
\tag{6.68}
$$

$$
C_y = \begin{cases} \frac{-j(\frac{v\pi}{b})^2}{Z_{uv}^{TE}}^*, & h_{uvy}^* \implies h_{uvy}^{*\ TE} \\ \frac{-j\frac{u\pi}{a}\frac{v\pi}{b}}{Z_{uv}^{TM}}^*, & h_{uvy}^* \implies h_{uvy}^{*\ TM} \end{cases}
\tag{6.69}
$$

corresponds to the test terms used. Further discussion of these terms is found in Appendix C. Four distinct combinations of expansion and testing can occur in the application of the moment method. They are testing with TE rectangular waveguide modes, while expanding with TE rectangular waveguide modes; TE test, TM expand; TM test, TE expand and TM test, TM expand.

The terms Ω, Φ, Υ and X correspond to the integrals below:

$$
\begin{aligned}
\Omega = \iint_{-\infty}^{\infty}\frac{\lambda_x^2\lambda_y^4}{k_{ZTE}(\lambda_y^2-\omega^2\epsilon_x\mu_x)}\frac{\cos(k_{ZTE}d)}{\sin(k_{ZTE}d)}\left(\frac{(e^{j(a\lambda_x)}(-1)^u-1)}{((\frac{u\pi}{a})^2-\lambda_x^2)}\frac{(e^{j(b\lambda_y)}(-1)^v-1)}{((\frac{v\pi}{b})^2-\lambda_y^2)}\right) \\
\left(\frac{(e^{-j(a\lambda_x)}(-1)^m-1)}{(k_x^2-\lambda_x^2)}\frac{(e^{-j(b\lambda_y)}(-1)^n-1)}{(k_y^2-\lambda_y^2)}\right)d^2\lambda
\end{aligned}
\tag{6.70}
$$

$$\Phi = \iint_{-\infty}^{\infty} \frac{\lambda_x^2 \lambda_y^2}{k_{ZTE}} \frac{\cos(k_{ZTE}d)}{\sin(k_{ZTE}d)} \left(\frac{(e^{j(b\lambda_y)}(-1)^v - 1)}{((\frac{v\pi}{b})^2 - \lambda_y^2)} \frac{(e^{j(a\lambda_x)}(-1)^u - 1)}{((\frac{u\pi}{a})^2 - \lambda_x^2)} \right) \left(\frac{(e^{-j(a\lambda_x)}(-1)^m - 1)}{(k_x^2 - \lambda_x^2)} \frac{(e^{-j(b\lambda_y)}(-1)^n - 1)}{(k_y^2 - \lambda_y^2)} \right) d^2\lambda \tag{6.71}$$

$$\Upsilon = \iint_{-\infty}^{\infty} \frac{\lambda_x^2 (\lambda_y^2 - \omega^2 \epsilon_x \mu_x)}{k_{ZTE}} \frac{\cos(k_{ZTE}d)}{\sin(k_{ZTE}d)} \left(\frac{(e^{j(b\lambda_y)}(-1)^v - 1)}{((\frac{v\pi}{b})^2 - \lambda_y^2)} \frac{(e^{j(a\lambda_x)}(-1)^u - 1)}{((\frac{u\pi}{a})^2 - \lambda_x^2)} \right) \left(\frac{(e^{-j(b\lambda_y)}(-1)^n - 1)}{(k_y^2 - \lambda_y^2)} \frac{(e^{-j(a\lambda_x)}(-1)^m - 1)}{(k_x^2 - \lambda_x^2)} \right) d^2\lambda \tag{6.72}$$

$$X = \iint_{-\infty}^{\infty} \frac{\lambda_y^2 k_{ZTM}}{(\lambda_y^2 - \omega^2 \epsilon_x \mu_x)} \frac{\cos(k_{ZTM}d)}{\sin(k_{ZTM}d)} \left(\frac{(e^{j(a\lambda_x)}(-1)^u - 1)}{((\frac{u\pi}{a})^2 - \lambda_x^2)} \frac{(e^{j(b\lambda_y)}(-1)^v - 1)}{((\frac{v\pi}{b})^2 - \lambda_y^2)} \right) \left(\frac{(e^{-j(a\lambda_x)}(-1)^m - 1)}{(k_x^2 - \lambda_x^2)} \frac{(e^{-j(b\lambda_y)}(-1)^n - 1)}{(k_y^2 - \lambda_y^2)} \right) d^2\lambda \tag{6.73}$$

The λ_y portion of the above integrals are solved using Complex Plane Analysis while the λ_x are solved numerically. The λ_x integrals are solved numerically to avoid evaluating the branch cuts and branch points. It is easier to evaluate these integrals using real axis integration in a numerical solver. An example of solving the Ω λ_y integrals is provided in Appendix D. All of these integrals posses singularities, which may change position in the complex plane depending on which expansion and testing mode combination are used. Five cases are identified for Orientation 1 and are: $n = v = 0$, $n = 0 \quad v \neq 0$, $n \neq 0 \quad v = 0$, $n = v \neq 0$ and $n \neq v \neq 0$. Additionally, only even values of n and v are permitted due to the symmetry imposed by the SPWP.

Analysis and Discussion of Orientation 2.

The field expansion and testing development for Orientation 2 is the same a Orientation 1. However, subtle differences in the integral solutions are due to the fields

in rotated waveguide aperture. The O2 solution appears as:

$$
\begin{aligned}
2\left(\frac{(\frac{\pi}{a})^2}{Z_{10}^{TE*}Z_{10}^{TE}}\right)\frac{ab}{2}\delta_{uv10}^{TE} = \sum_{m=0}^{\infty}\sum_{n=0}^{\infty}\Bigg[\overline{\Gamma}_{mn}^{TE}\left(\left(\left(\frac{m\pi}{a}\right)^2+\left(\frac{n\pi}{b}\right)^2\right)\frac{ab(1+\delta_{uvm0}^{TE})}{4Z_{mn}^{TE*}Z_{mn}^{TE}}\delta_{uvmn}^{TE}\right. \\
\left.-\frac{1}{(2\pi)^2}\left(\frac{C_xk_y^2}{\mu_x\omega}\Omega+\frac{(C_yk_y^2+C_xk_x^2)}{\mu_x\omega}\Phi+\frac{C_yk_x^2}{\mu_x\omega}\Upsilon+\frac{C_xk_y^2\omega\epsilon_x}{1}X\right)\right)\Bigg] \\
+\sum_{m=0}^{\infty}\sum_{n=0}^{\infty}\Bigg[\Gamma_{mn}^{TM}\left(\left(\left(\frac{m\pi}{a}\right)^2+\left(\frac{n\pi}{b}\right)^2\right)\frac{ab(1+\delta_{uvm0}^{TM})}{4Z_{mn}^{TM*}Z_{mn}^{TM}}\delta_{uvmn}^{TM}\right. \\
\left.-\frac{k_xk_y}{(2\pi)^2}\left(\frac{C_x}{\mu_x\omega}\Omega+\frac{(C_y-C_x)}{\mu_x\omega}\Phi-\frac{C_y}{\mu_x\omega}\Upsilon+\frac{C_x\omega\epsilon_x}{1}X\right)\right)\Bigg].
\end{aligned}
\tag{6.74}
$$

where

$$
C_x = \begin{cases} \frac{-j(\frac{v\pi}{b})^{2\,*}}{Z_{uv}^{TE}}, & h_{uvx}^* \implies h_{uvx}^{*\ TE} \\ -\frac{j\frac{u\pi}{a}\frac{v\pi}{b}^*}{Z_{uv}^{TM}}, & h_{uvx}^* \implies h_{uvx}^{*\ TM} \end{cases}
\tag{6.75}
$$

and

$$
C_y = \begin{cases} \frac{-j(\frac{u\pi}{b})^{2\,*}}{Z_{uv}^{TE}}, & h_{uvy}^* \implies h_{uvy}^{*\ TE} \\ \frac{j\frac{u\pi}{a}\frac{v\pi}{b}^*}{Z_{uv}^{TM}}, & h_{uvy}^* \implies h_{uvy}^{*\ TM} \end{cases}
\tag{6.76}
$$

serve in the same function as before and are dependent on which testing mode is used. The terms Ω, Φ, Υ and X correspond to the integrals below:

$$
\begin{aligned}
\Omega = \iint_{-\infty}^{\infty}\frac{\lambda_x^2\lambda_y^4}{k_{ZTE}(\lambda_y^2-\omega^2\epsilon_x\mu_x)}\frac{\cos(k_{ZTE}d)}{\sin(k_{ZTE}d)}\left(\frac{(e^{j(b\lambda_x)}(-1)^v-1)}{((\frac{v\pi}{b})^2-\lambda_x^2)}\frac{(e^{j(a\lambda_y)}(-1)^u-1)}{((\frac{u\pi}{a})^2-\lambda_y^2)}\right) \\
\left(\frac{(e^{-j(b\lambda_x)}(-1)^n-1)}{(k_y^2-\lambda_x^2)}\frac{(e^{-j(a\lambda_y)}(-1)^m-1)}{(k_x^2-\lambda_y^2)}\right)d^2\lambda
\end{aligned}
\tag{6.77}
$$

$$
\begin{aligned}
\Phi = \iint_{-\infty}^{\infty}\frac{\lambda_x^2\lambda_y^2}{k_{ZTE}}\frac{\cos(k_{ZTE}d)}{\sin(k_{ZTE}d)}\left(\frac{(e^{j(a\lambda_y)}(-1)^u-1)}{((\frac{u\pi}{a})^2-\lambda_y^2)}\frac{(e^{j(b\lambda_x)}(-1)^v-1)}{((\frac{v\pi}{b})^2-\lambda_x^2)}\right) \\
\left(\frac{(e^{-j(b\lambda_x)}(-1)^n-1)}{(k_y^2-\lambda_x^2)}\frac{(e^{-j(a\lambda_y)}(-1)^m-1)}{(k_x^2-\lambda_y^2)}\right)d^2\lambda
\end{aligned}
\tag{6.78}
$$

$$\Upsilon = \iint_{-\infty}^{\infty} \frac{\lambda_x^2(\lambda_y^2 - \omega^2\epsilon_x\mu_x)}{k_{ZTE}} \frac{\cos(k_{ZTE}d)}{\sin(k_{ZTE}d)} \left(\frac{(e^{j(a\lambda_y)}(-1)^u - 1)}{((\frac{u\pi}{a})^2 - \lambda_y^2)} \frac{(e^{j(b\lambda_x)}(-1)^v - 1)}{((\frac{v\pi}{b})^2 - \lambda_x^2)} \right) \left(\frac{(e^{-j(a\lambda_y)}(-1)^m - 1)}{(k_x^2 - \lambda_y^2)} \frac{(e^{-j(b\lambda_x)}(-1)^n - 1)}{(k_y^2 - \lambda_x^2)} \right) d^2\lambda \tag{6.79}$$

$$X = \iint_{-\infty}^{\infty} \frac{\lambda_y^2 k_{ZTM}}{(\lambda_y^2 - \omega^2\epsilon_x\mu_x)} \frac{\cos(k_{ZTM}d)}{\sin(k_{ZTM}d)} \left(\frac{(e^{j(b\lambda_x)}(-1)^v - 1)}{((\frac{v\pi}{b})^2 - \lambda_x^2)} \frac{(e^{j(a\lambda_y)}(-1)^u - 1)}{((\frac{u\pi}{a})^2 - \lambda_y^2)} \right) \left(\frac{(e^{-j(b\lambda_x)}(-1)^n - 1)}{(k_y^2 - \lambda_x^2)} \frac{(e^{-j(a\lambda_y)}(-1)^m - 1)}{(k_x^2 - \lambda_y^2)} \right) d^2\lambda \tag{6.80}$$

Evaluation of the above integrals, once again, requires complex plane analysis on the λ_y part and numerical integration on the λ_x piece, however, the rotation of the waveguide aperture changes which singularity combinations are permitted. This is due to the 'a' dimension being aligned with the y axis, instead of the 'b' dimension, as before. As a result, a different set of combinations is imposed. They are $m = u \neq 0$ and $m \neq u \neq 0$, where m and u are only odd values as dictated by the SPWP symmetry. These two singularity combinations can be reused from the Orientation 1 development, with the care in correctly applying the m and u are odd constraint as opposed to the n and v are even constraint.

6.4 Solution Summary

The entire solution summary for both Orientations 1 and 2 are provided in Appendix E. For comparison to the fundamental mode development (derived at the beginning of this chapter), case 5 of O1 and case 2 of O2 can be shown to reduce to a form equivalent to the result provided in the fundamental mode-only development. In demonstrating these equivalences, confidence in the a higher order mode approach is validated.

6.5 Computational Formulation of the Forward Problem

Employing the theoretical developments for Orientations 1 and 2 described in the previous sections requires casting the summations for each orientation as a matrix system of equations,

$$\left[\begin{array}{ccc|ccc} CASE_{TE_{uv},TE_{mn}} & \cdots & & CASE_{TE_{uv},TM_{mn}} & \cdots & \\ \vdots & \ddots & & \vdots & \ddots & \\ \hline CASE_{TM_{uv},TE_{mn}} & \cdots & & CASE_{TM_{uv},TM_{mn}} & \cdots & \\ \vdots & \ddots & & \vdots & \ddots & \end{array}\right] \cdot \begin{bmatrix} \overline{\Gamma}_{mn}^{TE} \\ \vdots \\ \Gamma_{mn}^{TM} \\ \vdots \end{bmatrix} = \begin{bmatrix} 2\left(\frac{(\frac{\pi}{a})^2}{Z_{10}^{TE*}Z_{10}^{TE}}\right)\frac{ab}{2} \\ 0 \\ 0 \\ \vdots \end{bmatrix} \tag{6.81}$$

as previously employed in the uniaxial higher order modal development. The excitation is provided by an launched TE_{10} rectangular waveguide mode, which results in a reflected TE_{10} waveguide mode and a set of TE and TM waveguide modes, a described by the reflection coefficients Γ. The relationship between these parameters is governed by the 'CASES' developed in the theoretical development. The cases used to populate the matrix depends on the modes selected. A system of equations is defined for each orientation and constitutes a forward model. The forward model accepts inputs of the material parameters, waveguide dimensions, sample thickness and which modes are used. Reflection coefficients for the corresponding modes are generated. Each orientation's forward model operates independently, but both are needed to provide sufficient measurement diversity to characterize rotated uniaxial media. MATLAB®'s `lsqcurvefit()`, operated in the "Trusted-Region-Reflective" is used to curve fit both forward models Γ_{10}^{TE} data to the measured S_{11} S-parameter data at each frequency point for each orientation.

VII. Rotated Uniaxial Anisotropic SPWP Technique Results

7.1 Sample Design and Simulated SPWP Evaluation

Designing a rotated uniaxial anisotropic sample allows the developed forward models to be tested and demonstrates performance. The dielectric uniaxial sample in Figure 30 is designed using crystallographic symmetry [1] and has uniformly spaced tetragonal cells. These cells are divided into 96 columns and 4 rows and are embedded in a 6" square slab that is 0.25" thick. Each cell is 0.03125" square and runs the full length of the material. A notional slab material with a permittivity of $2.5 - j0.2$ and a cell material with a permittivity of $1 - j0$ for the low contrast sample, and $9.9 - j0$ for the high contrast sample are used. A lumped element equivalent circuit model adapted from [12] and [20] provides predicted values for uniaxial permittivity. The lumped element results for the uniaxial low and high contrast samples are also compared against simulated rectangular waveguide measurements to verify that the samples are macroscopically homogeneous and agree with the lumped element predicted values. Two uniaxial samples from the slab in Figure 30 were "cut" and inserted into the rectangular waveguide for measurement. Two measurement orientations are required to measure both transverse ϵ_x and ϵ_y permittivites and results were extracted using a Newton 1-D root search [21]. Simulation of the rectangular waveguide and SPWP for each orientation was performed in CST Microwave Studio®'s frequency domain solver and are similar to the simulations performed in [12].

SPWP Sample Thickness Uncertainty Analysis.

Sample thickness is evaluated in a Monte Carlo uncertainty analysis for both sample orientations simulated in CST Microwave Studio®. Each orientation thickness

is evaluated as a uniform random variable with the actual sample thickness (0.25)" as the mean. The upper and lower limits of the distribution are ±0.004". The limits are chosen based on the largest permissible error without discarding and replacing the sample for one with tighter tolerances. 1000 MATLAB® trials were run on the simulated reflection coefficient data to calculate the mean and 2 standard deviations of uncertainty in rotated uniaxial permittivity.

Low and High Contrast Simulated Uniaxial Results.

The results show that both of the designed rotated uniaxial low and high contrast material samples yield consistent results between lumped element prediction, rectangular waveguide and the rotated SPWP technique. The uncertainty analysis shows that SPWP maintains consistent measurement performance for both orientations. Results may be further improved by incorporating higher order modes in both moment method developments.

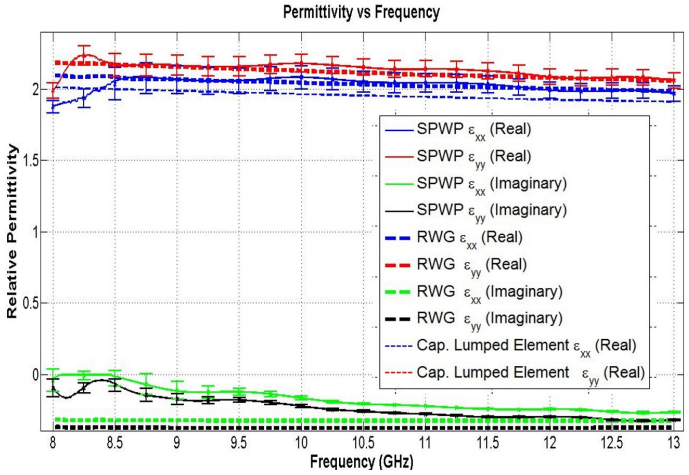

Figure 39. Low contrast rotated uniaxial sample results.

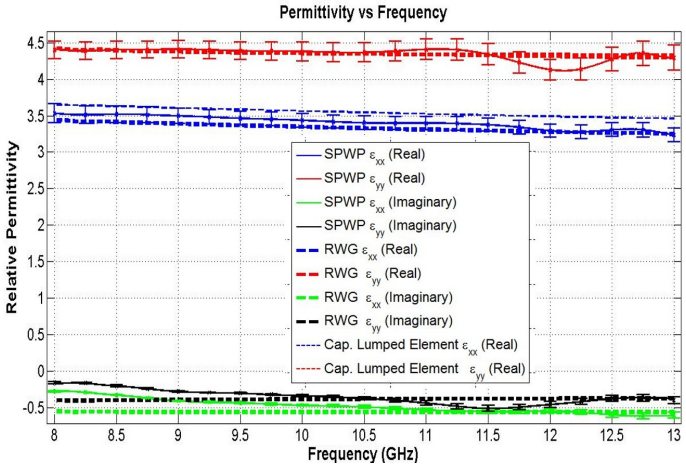

Figure 40. High contrast rotated uniaxial sample results.

7.2 Conclusion

The SPWP is enhanced to accommodate rotated uniaxial anisotropic media. Measurement diversity is obtained by measuring a single sample in two aligned orientations. Each measurement is evaluated against its respective moment method forward model. Results for both low and high contrast samples demonstrate good agreement with the lumped equivalent circuit predictions and the rectangular waveguide results.

7.3 Higher Order Mode Results Introduction

In this section comparisons are made between the fundamental mode-only and fundamental with selected higher order mode results. The comparisons serves two purposes: 1) to verify and validate that the higher order mode development is correct, and 2) to explore measurement improvement is gained by including higher order modes. The results are based on the fundamental mode-only CST Microwave Studio® simulations. Later in this chapter, exploration into laboratory measurements is discussed and features a 3-D printed ABS plastic sample. Lastly, the same 3-D plastic sample loaded with copper wires. Measurement system conclusions are provided with implementation recommendations.

7.4 Comparison to CST-based fundamental mode-only results

A comparison is made between the fundamental mode-only and higher order mode results for the low contrast rotated uniaxial sample previously discussed. Figure 41 shows that good agreement is obtained between the two approaches and is within the uncertainty of the fundamental mode measurement. As an aside, the incorporation of the first 20 modes significantly increased the material parameter run time from mere minutes (for approximately 100 frequency samples using the fundamental mode-only) to days (for 5 frequency samples using the first 20 modes), using the same laptop computer. Figure 42 shows that certain rectangular waveguide mode provide more

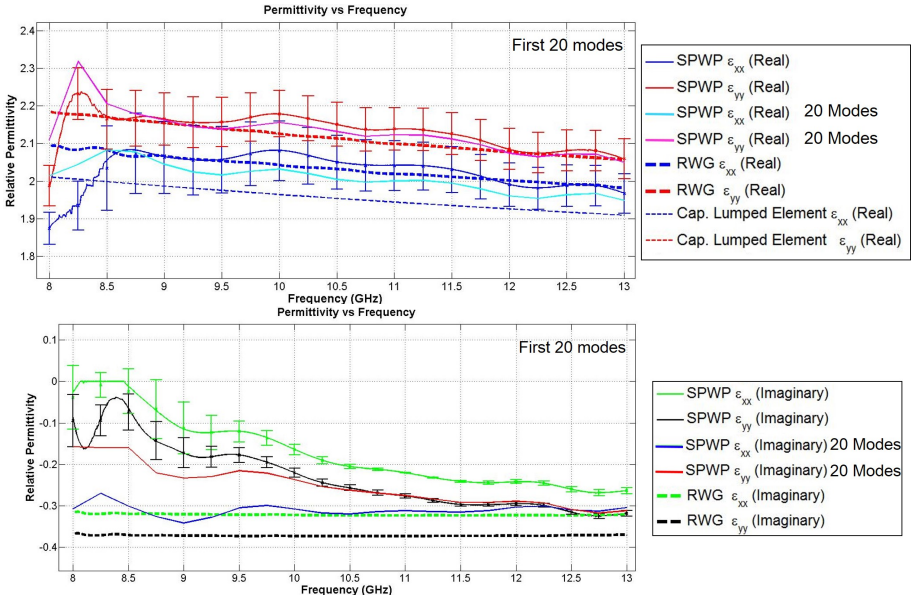

Figure 41. Low Contrast rotated uniaxial media fundamental mode only results being compared against the first 20 modes.

significant contributions to the results as compared to other modes.

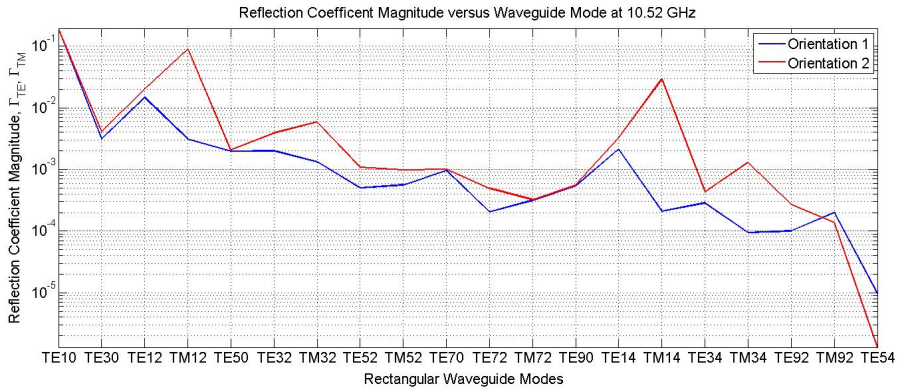

Figure 42. A plot of the waveguide modes showing the weight of their respective contribution to a solution at a given Frequency for the low contrast simulated media.

Capitalizing on this observation and referencing [24], which discussed using the most contributing rectangular waveguide modes, a select 8 modes were employed to improve the run time, while maintaining comparable material parameter extraction performance with the first 20 modes. Figure 43 shows that similar performance is attained, while the run time was approximately a day. An initial assessment of the

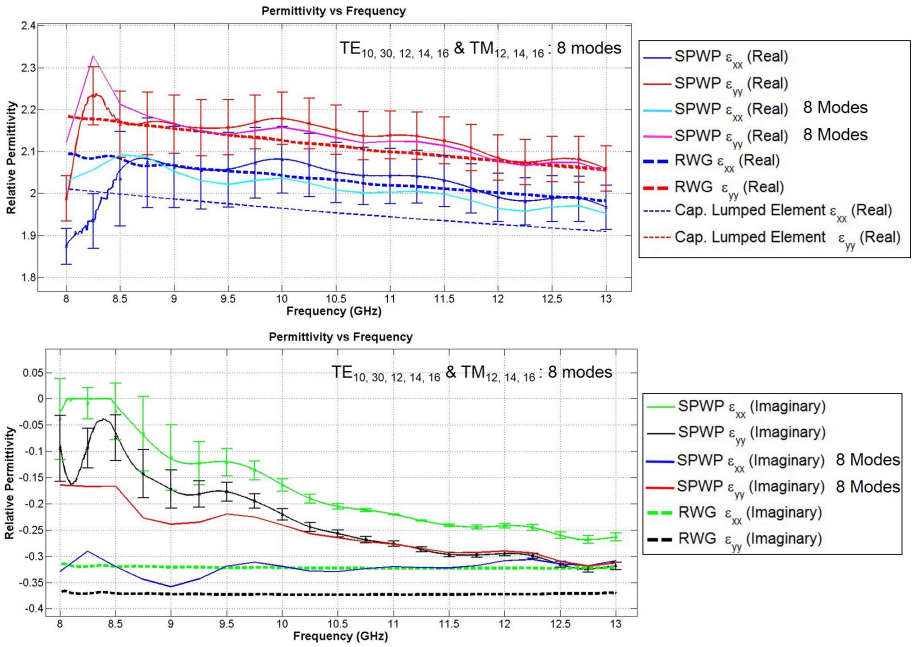

Figure 43. Low Contrast rotated uniaxial media fundamental mode only results being compared against 8 select modes.

higher order mode approach shows that for the low contrast media, comparable results

are obtained. Attention is then turned to the high contrast rotated uniaxial media to further support validation and verification of the higher order mode approach. Repeating the previous analysis for the high contrast media, yield comparable performance. Figure 44 shows good agreement with the fundamental mode-only results, at the cost of taking more time to compute than the fundamental mode-only results, but is comparable to the first 20 modes computation for low contrast media. Looking

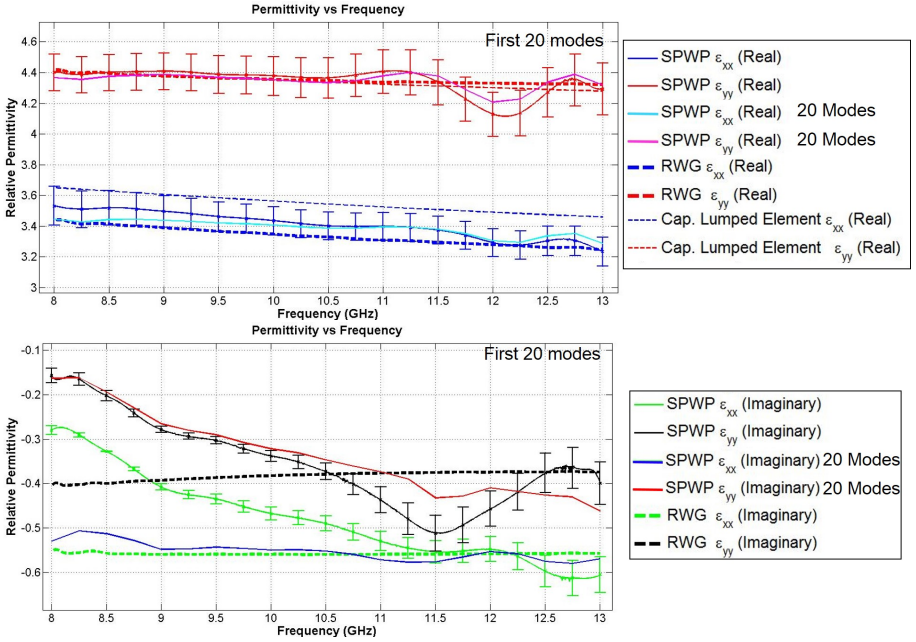

Figure 44. High Contrast rotated uniaxial media fundamental mode only results being compared against the first 20 modes.

at Figure 45, once again, the same modes are observed as the significant contributors as the low contrast media. Evaluating any possible changes in measurement results, while reducing material parameter extraction run time, the same 8 selected modes are used to extract the permittivity from the high contrast media. Result show comparable performance for both time and measurement accuracy as the first 20 modes as shown in Figure 46. Figure 47 shows the transverse electric field at the SPWP aperture. A strong transverse electric fields in both measurement orientations supports successful interrogation of the media.

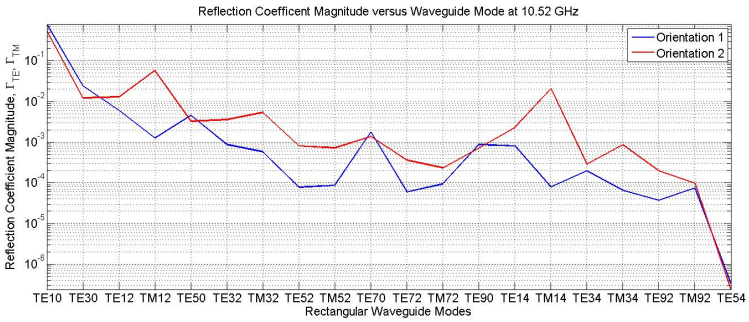

Figure 45. A plot of the waveguide modes showing the weight of their respective contribution to a solution at a given frequency for the high contrast simulated media.

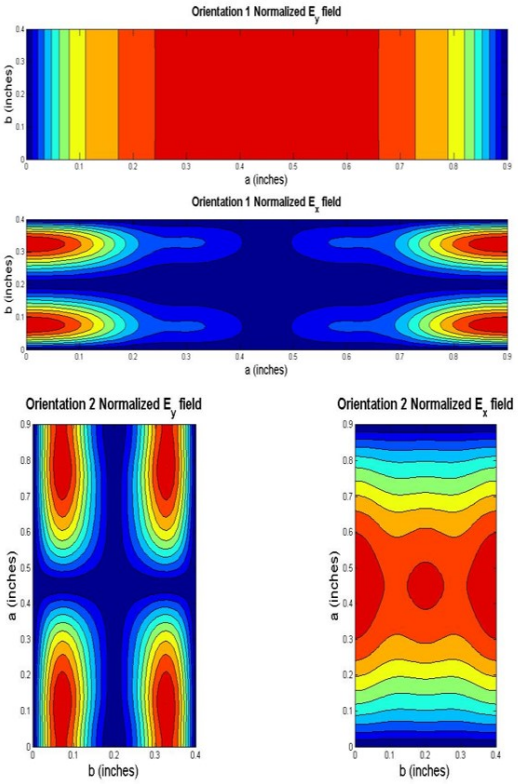

Figure 47. Field Plots of the tangential electric fields of a simulated high contrast rotated uniaxial sample. The top two plots are the y and x electric field components for Orientation 1. The bottom two plots are the fields components for the Orientation 2. The field plots are generated from first 20 higher order modes moment method approach.

The overall conclusion based strictly on simulation results indicates that both the fundamental mode-only and higher order mode results yield comparable accuracy

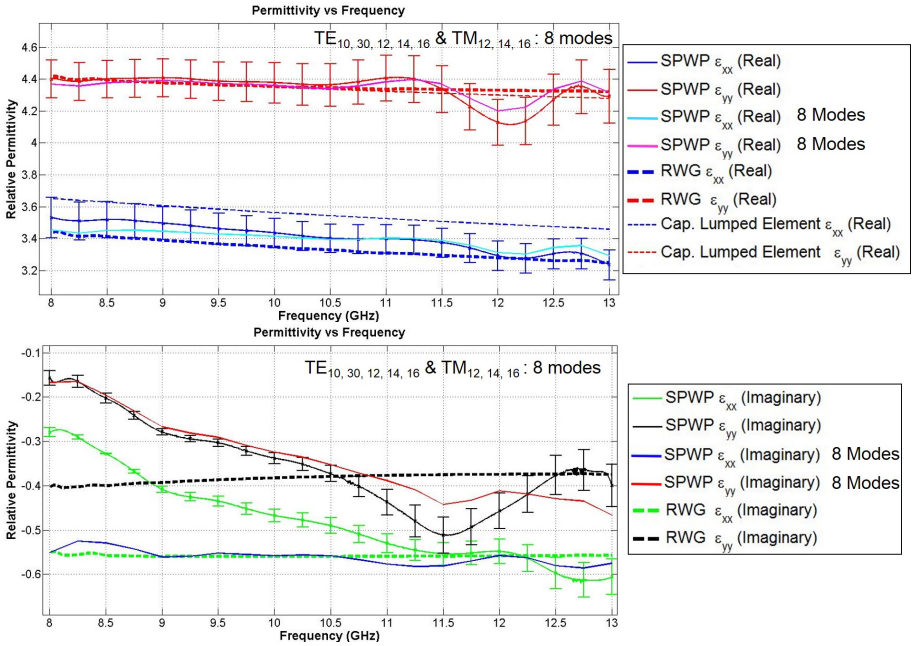

Figure 46. High Contrast rotated uniaxial media fundamental mode only results being compared against 8 select modes.

with more modes increasing the time taken to successfully extract material parameters. Thus using more modes may not yield as significant measurement improvement, as was observed when extracting material parameters on uniaxial media. Recall that the longitudinal permittivity ϵ_{zz} was improved by including higher order modes. The rotated uniaxial simulated results make physical sense as leveraging the strong transverse field components from the rectangular waveguide adequately capture the rotated uniaxial permittivity tenor elements. Hence the lack of significant changes when adding modes is understood.

7.5 SPWP Rotation error uncertainty

Previous evaluations of uncertainty with respect to the SPWP consist of measurement uncertainty in the sample thickness. Given that two measurement orientations are needed form measurement diversity, attention is turned to the effects of error in rotational position uncertainty with respect to the measurement results. Figure 48

shows sample misalignment for a given measurement orientation. While the error is readily noticeable in the image, in-situ measurement may make an egregious error such as this unnoticeable because one may not have edge feature to align the fixture. Quantifying the rotation error requires establishing a limitation on what rotation is

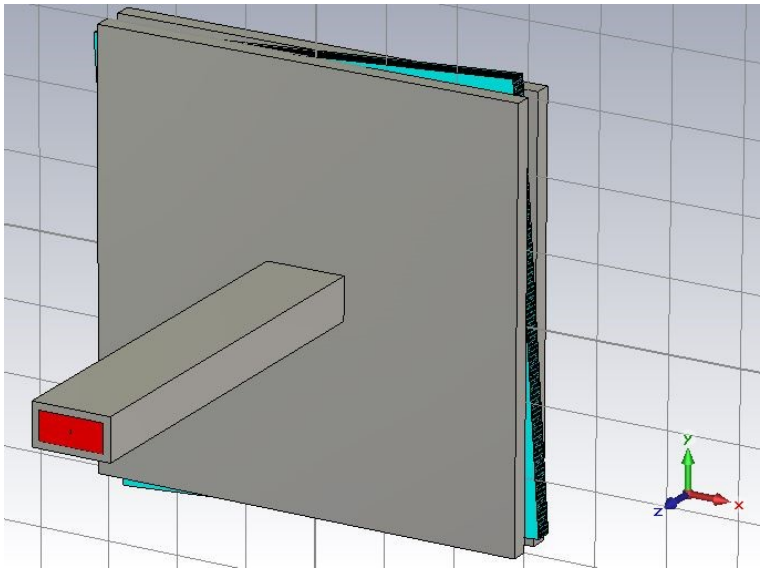

Figure 48. A CST Microwave Studio model showing the SPWP and an installed sample with only 4^o rotation error.

tolerable. Figure 49 describes the approach used in quantifying the maximum tolerable rotation error. Using the high contrast simulated results previously evaluated in this chapter, which have a well understood permittivity, S-parameter data is evaluated using a Monte Carlo approach. Normally distributed random variables are applied to the CST Microwave Studio® data. The random variables are based on the mean and standard deviation data obtained from the Agilent E8362B uncertainty calculator [29]. Uniform random variable are used on physical measurements (i.e. measurements accomplished with a micrometer or calipers) where the nominal value is the average and standard deviations assumed to be ±0.003". 1000 trials were run to support the Monte Carlo. Because it is guaranteed that the sample is aligned in the simulation space, the extracted permittivities are used to support the material

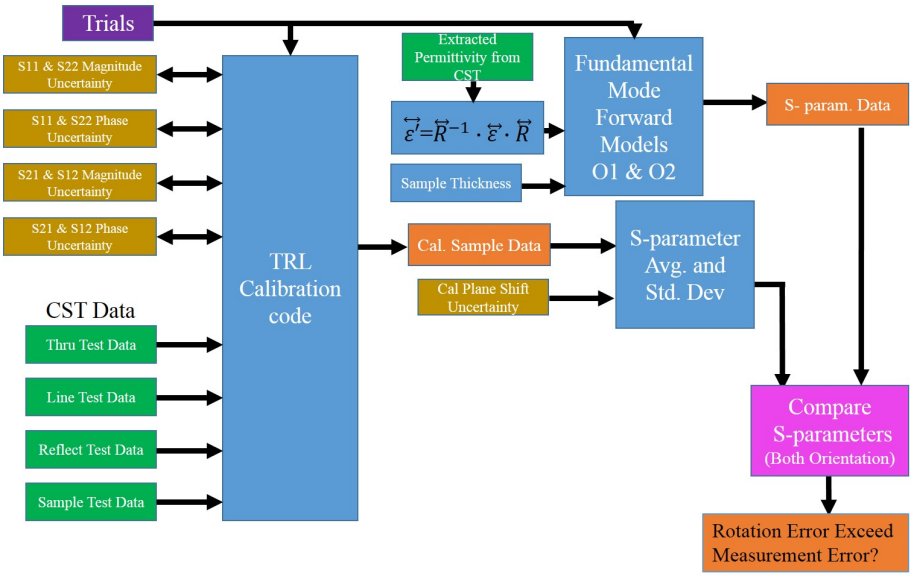

Figure 49. A flow diagram of the rotation error calculation and comparison process. The green blocks indicate data input; the gold blocks are random variables and the blue blocks indicate simulation processes.

rotation aspect of the analysis. A rotation transformation is applied to the material tensor elements for a specific angle value. The output material tensor elements for ϵ_{xx} and ϵ_{yy} are then input into the fundamental mode forward models to generate S-parameter data for each orientation. This first-order approximation does not take into account the off diagonal terms (i.e. ϵ_{xy} and ϵ_{yx}) that may be generated when mis-aligning the measurement system with the rotated uniaxial media. A comparison is made of the nominal CST S-parameter data and 2 standard deviations of error versus the different S-parameter data generated by the first-order rotation error as shown in Figure 50 evaluating the magnitude part of S-parameter data and Figure 51 evaluating the phase part. Validating the use of this approach to characterize rotation error, two CST Microwave studio simulations were run, one for each orientation where an 8^o rotation error was imposed on the high contrast sample. The S-parameter data is also plotted along side the first order approximation data.

Overall, it is observed in both the magnitude and phase figures, that rotation error is not a significant source of measurement error. The first order approach explored

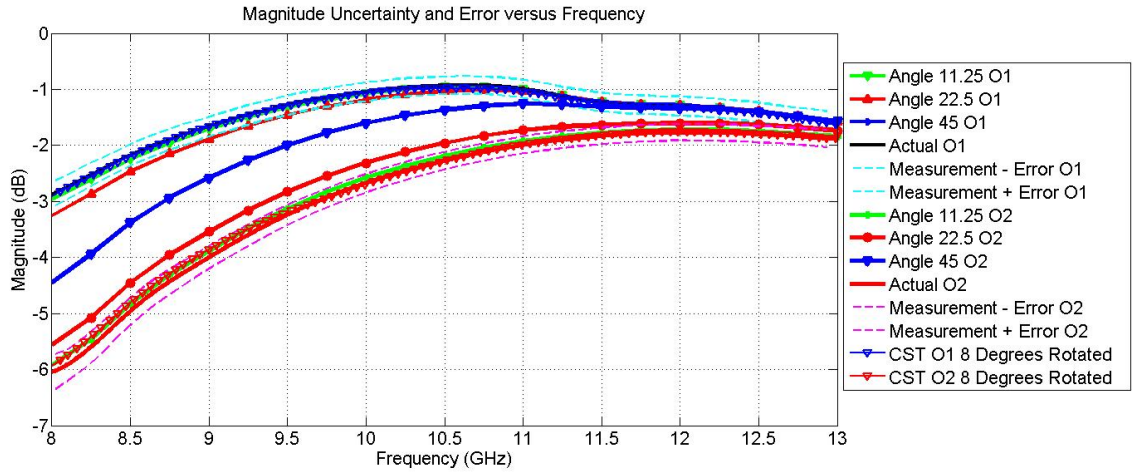

Figure 50. Magnitude data demonstrating SPWP tolerance to rotation error.

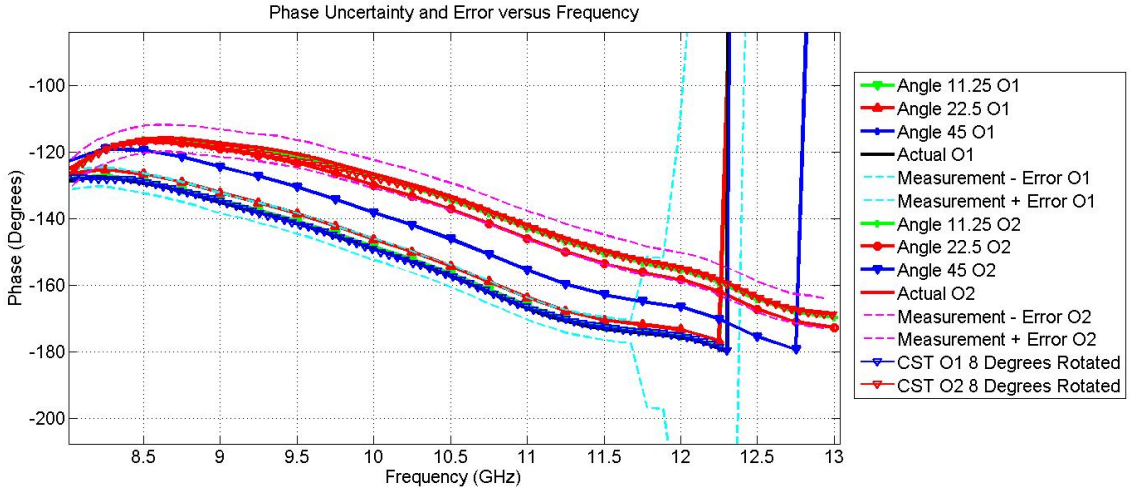

Figure 51. Phase data demonstrating SPWP tolerance to rotation error.

11.25^o, 22.5^o and 45^o rotation error for each orientation. At 11.25^o results are barely distinguishable from nominal and at 22.5^o only begin to exceed the measurement error of S-parameters generated by the network analyzer. At 45^o, the S-parameters become ambiguous with respect to each orientation. In comparing the CST 8^o error data for each orientation, it is show that supports the first order approach and is not a significant contributor to measurement error. Further evaluating this fact, the 8^o error data is used to extract the relative permittivity and is compared with the high contrast perfectly aligned data possessing error bars associated with sample thickness.

Figure 52 show minuscule changes to relative permittivity that are well inside the error bars and helps support that rotation error is not critical for measurement success, though insuring correct alignment does yield more accurate results.

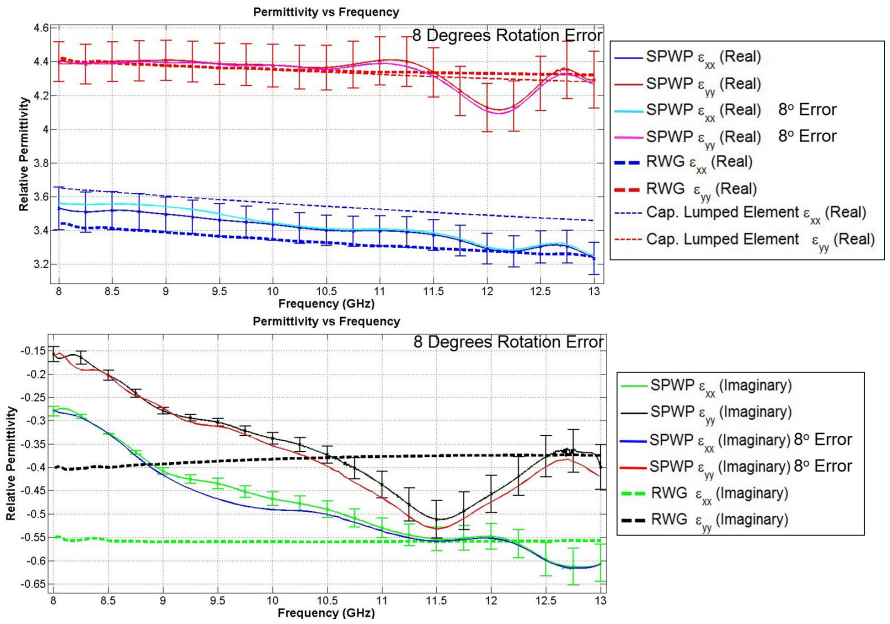

Figure 52. A comparison of the fundamental mode-only high contrast results against an 8^o rotation error induced on the sample in the CST simulation. The fundamental mode permittivity results were extracted using the fundamental mode-only developed and overlaid on the perfectly aligned results.

7.6 Laboratory Measurement of a Designed Rotated Uniaxial Sample

Previous evaluations have only considered simulated data for comparison to both fundamental mode and higher order mode extracted results. In this section, a sample is physically realized using a 3-D printer and measured in the laboratory. Sample fabrication, does pose some challenges not realized in the simulation real. Specifically, the long narrow occlusions of the low contrast sample, which are 6" in length and $\frac{1}{32}$" on both edges are not physically printable designs using the current 3-D printer technologies as the $\frac{1}{32}$" dimension is too small to accurately print. Additionally, the high contrast sample poses its own unique challenge as trying to integrate thin, fragile

pieces of alumina, presents its own difficulties. As a result, a more physically realizable rotated uniaxial sample is fabricated and posses $\frac{1}{16}$" edge length tetragonal occlusions which are 6" in length. A 2 by 48 array of these occlusions is embedded in an edge of a 6" $\times$ 6" $\times \frac{1}{4}$" ABS plastic slab. The tetragonal occlusions have a uniform $\frac{1}{16}$" spacing around each of them. Figure 53 shows the sample being fabricated. Additional, both a solid sample and an $\frac{1}{8}$" 1 by 24 array sample were fabricated, but results are not presented for brevity.

7.7 Rotated Uniaxial ABS Media

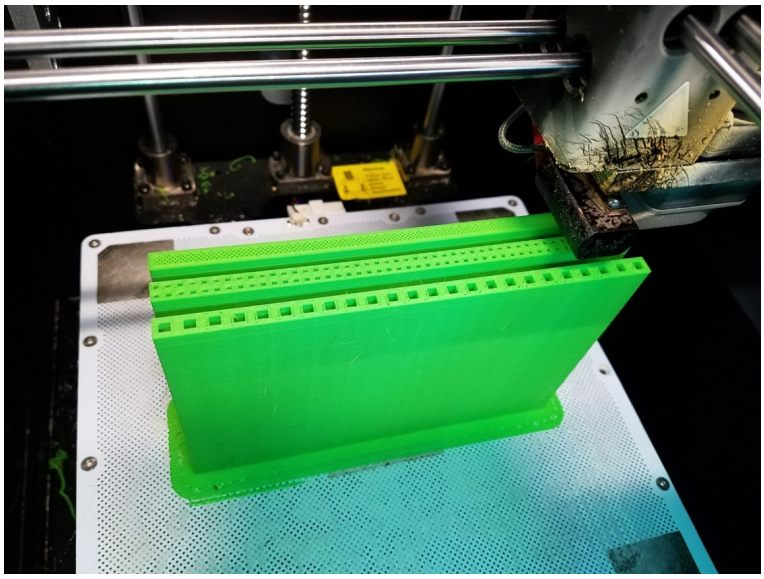

Figure 53. Printing of the ABS samples using a 3-D printer. The center slab, the 2 by 48 array is used in the measurement results presented.

Laboratory measurement of the 3-D printed 2 by 48 slab was conducted using the Agilent E8362B Vector Network Analyzer (VNA) from 7-13 GHz with an intermediate frequency bandwidth (IFBW) of 10kHz. A total of 1601 frequency points was collected. A Thru-Reflect-Line calibration process was employed on-board the VNA and time gating was also employed on the VNA to remove the edge discontinuities of the waveguide flanges and sample. A 1 nanosecond gate was found to be the largest

gate used while still removing the edge discontinuities. Figure 54 shows both orientations and clamps used to hold the sample and the metal backing sheet in place. A

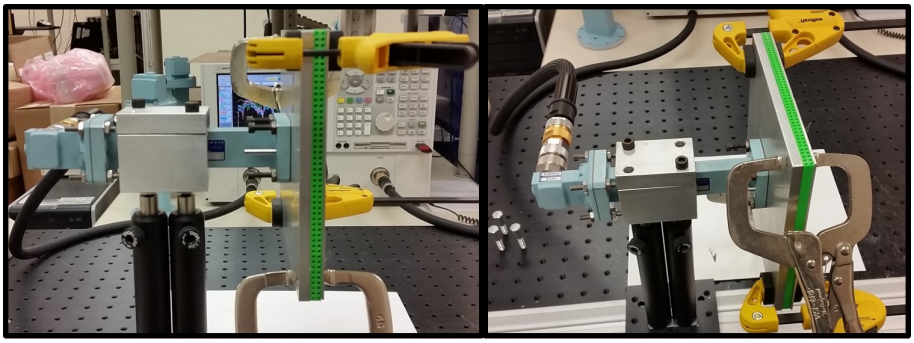

Figure 54. The SPWP measuring a single slab of the 2 by 48 media.

second set of measurements was also conducted using a second ABS sample of equivalent dimensions, as shown in Figure 55. The purpose of the two measurements, with different thicknesses was to explore permittivity result sensitivity to the number of occlusion presented in the parallel plate waveguide. Ideally, permittivity results should be independent of the sample structure assuming it satisfies macroscopic electromagnetics, as discussed in [2]. As the samples are identical, two thicknesses should yield the same permittivites within measurement uncertainty. As it has been previously

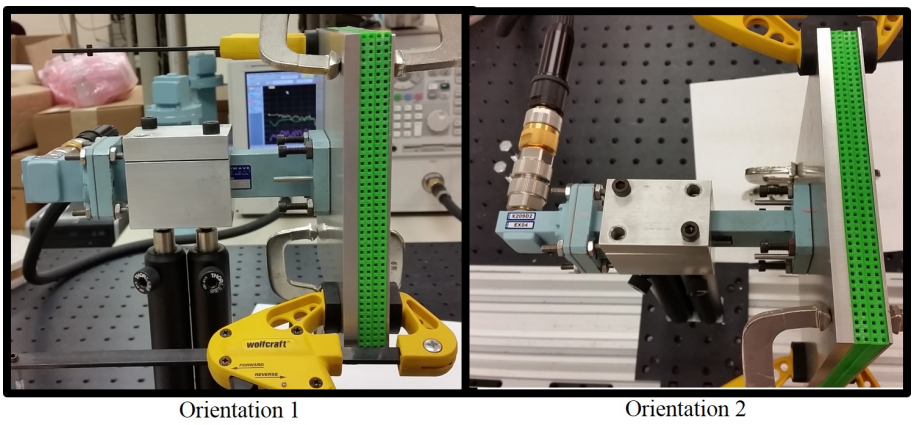

Figure 55. The SPWP measuring two slabs of the 2 by 48 media.

shown that rotation uncertainty is not significant, a Monte Carlo uncertainty anal-

ysis is generated to characterize the measurement data. This uncertainty analysis take into account measurement uncertainty in only the sample data, sample calibration plane uncertainty and sample thickness measurement variationn. Normally distributed random variable are used to characterize the uncertainty of the calibrate sample S_{11} S-parameter data, using [29]. Calibration plane uncertainty and sample thickness uncertainty are accommodate as uniform random variables with the nominal thickness as the average and ± 0.003" as the error in the measurement. The random variables are passed through to a fundamental mode only rotated material parameter extraction routine. Only the fundamental mode was employed, because 1000 trials were run. Including higher order modes would significantly extend the runtime. A block diagram of the Monte Carlo process is show in Figure 56. Measured results of

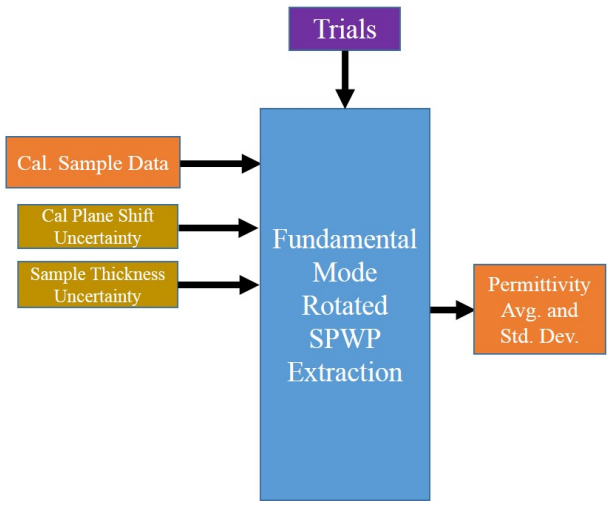

Figure 56. A flow diagram of the Monte Carlo process. The orange blocks are data and the gold blocks are the random variables.

the single thickness sample are shown in Figure 57. These results show 2 standard deviations of error applied to both permittivity components. Extracted permittivity result demonstrate rotated uniaxial anisotropy that is not statistically significant due to the assumed measurement error. The characteristics of the permittivity plot itself are reminiscent of the low contrast uniaxial media evaluated in CST earlier.

Running the same uncertainty analysis and assumng 2 standard deviations for error,

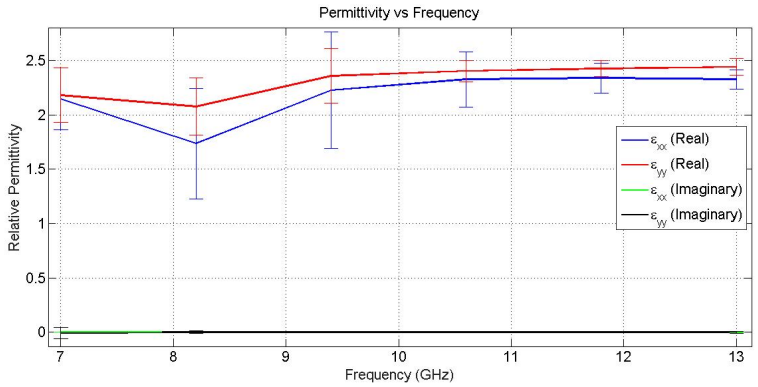

Figure 57. Fundamental mode only extracted material parameters of the thin (single slab) 2 by 48 array sample, featuring 2 standard deviation error bars.

for a double thickness sample, a slightly different set of permittivites are extracted as shown in Figure 58. While also not statistically significant anisotropy with the assumed measurement uncertainty, the results share some agreement with the single thickness.

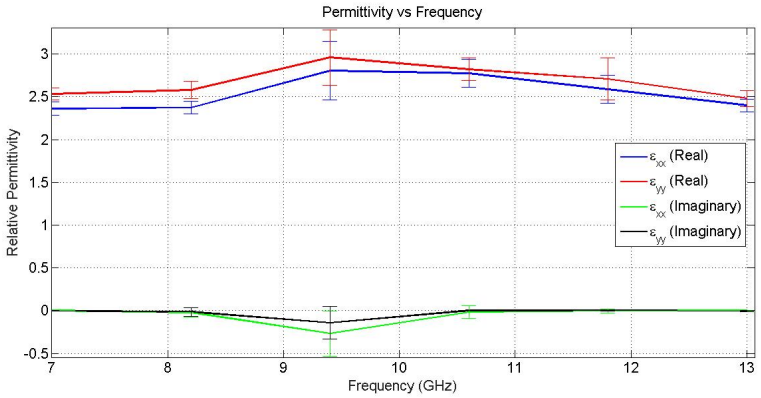

Figure 58. Fundamental mode only extracted material parameters of the thick (double slab) 2 by 48 array sample, featuring 2 standard deviation error bars.

7.8 Rotated Uniaxial Wire Media

In an attempt to generate more statistically significant anisotropy 16 gauge copper wires were inserted into the 2 by 48 array sample. Because the copper wire could

potentially induce a diamagnetic effect on the media, the permeability of the media could no longer be assumed as unity and had to be included in the search space of anisotropic material parameters. As a result two measurement thicknesses and two measurement orientation are needed to characterize the rotated uniaxial anisotropic permittivity and permeability as shown in Figure 59. Characterization of the ABS

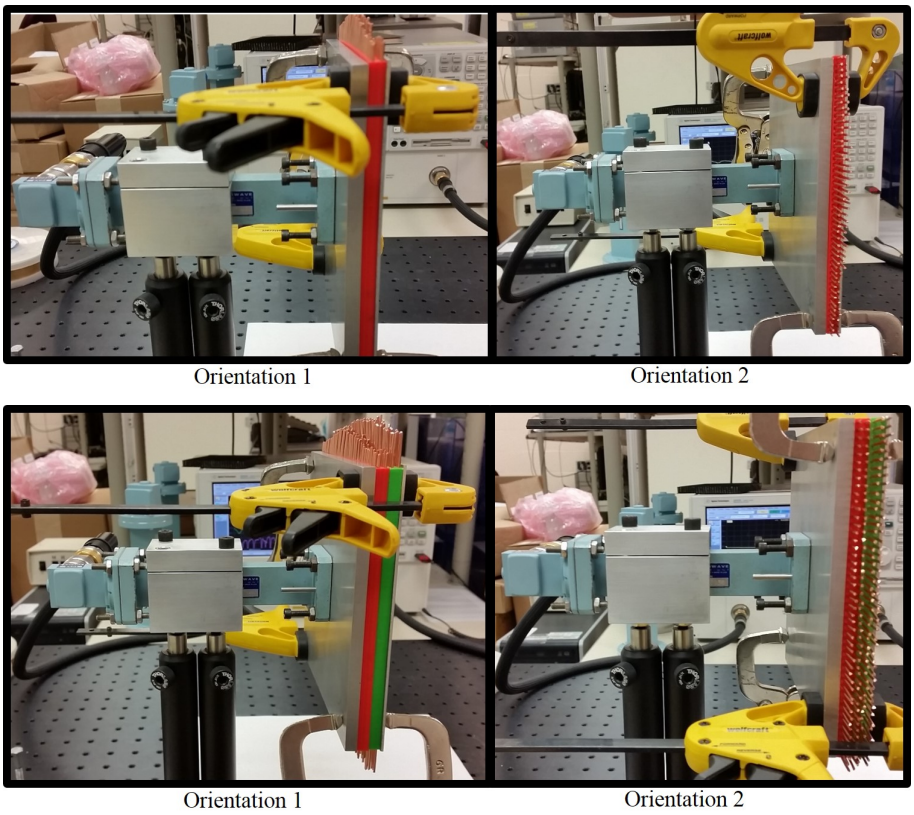

Figure 59. SPWP characterization of the 2 by 48 array media loaded with wires. Two sample thickness as well as the two measurement orientations were employed to provide sufficient measurement diversity.

and wires media used the $TE_{10,12,14}$ and TM_{14} modes. Attempt at characterizing the media using fewer modes resulted in non-physical results, where a proposed solution would automatically jump to the bound of the numerical search space. Additionally, given the increased unknown material parameters, permeability μ_{xx} and μ_{yy} the computational time increased significantly to the order of days using a laptop computer. Hence the use of the number of modes served as a middle ground in attempting to

characterize the media. Figure 60 shows an overall view of the extracted material parameters. The wires media in the y-orientation has an extremely high loss component. Figure 61 is a close up image of the previous plot showing the anisotropic

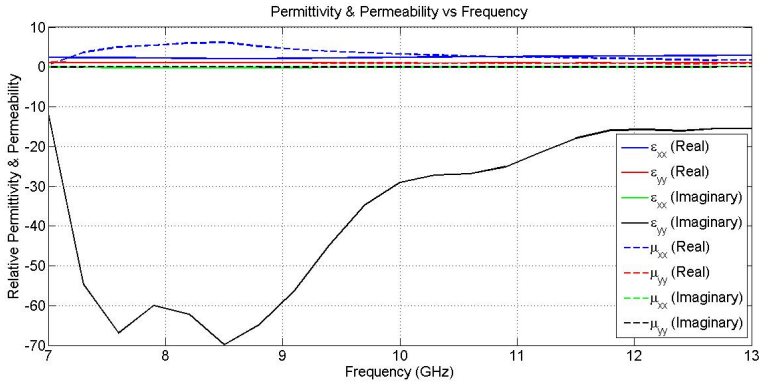

Figure 60. Permittivity and Permeability Results for the 2 by 48 wired media.

permittivity and permeability. Though an uncertainty analysis was not able to be run in time for the development of this document, it is believed that the anisotropy is statistically significant for both the permeability.

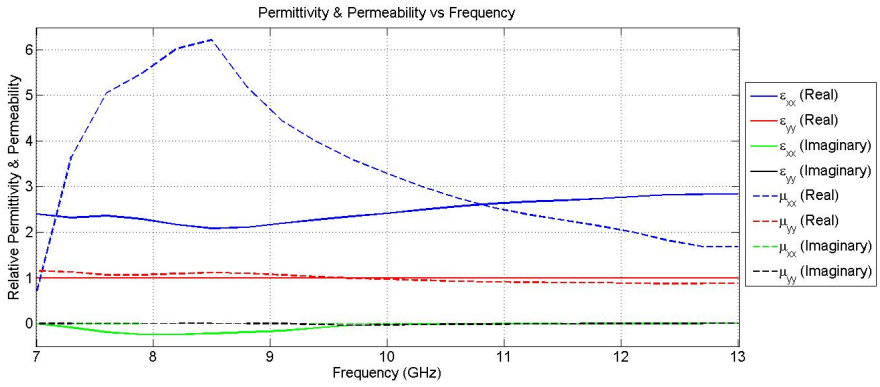

Figure 61. Permittivity and Permeability Results for the 2 by 48 wired media. Note the large loss component for ϵ_{yy}.

7.9 Rotated Uniaxial Results Conclusions

Simulated and experimental results have been presented for characterizing various types of rotated uniaxial anisotropic media. Fundamental mode and higher

order modal results perform consistently well. The measurement system is not significantly effected by rotation uncertainty. Measured data shows successfully usage of the SPWP to characterize rotated uniaxial media, however in the dielectric media case, the anisotropy is not statistically significant. An overall recommendation is to rely on fundamental mode-only extraction, as it provides sufficient accuracy over the range of media evaluated. However, if time is not a concern, more modes should be incorporated to observed any changes in material parameters.

VIII. Conclusions

8.1 Conclusion

A single port waveguide probe (SPWP) has been enhanced to characterize uniaxial and rotated uniaxial anisotropic media. Both the fundamental mode only and the higher order mode developments, accommodate for both sample permittivity and permeability and have been demonstrated in this research. All of the full-wave developments rely on moment method approach that utilize an anisotropic Green's function in its MFIE. Measurement representative simulations and laboratory measurements have demonstrated the utility of the proposed approaches. It has been shown that characterizing uniaxial media is more successful when including higher order modes. Additionally, it is also observed that higher order modes do not significantly enhance measurement performance of rotated uniaxial media using the SPWP approach. Each technique presents a different non-destructive approach at obtaining measurement diversity, with the rotated uniaxial approach being the most novel presented in this document.

8.2 Remarks

The significant analytical work required in the development of each moment method presented in this research poses a question: Why do all of the work, when CST Microwave Studio® could be used instead? The response is based in the physical insight gained in the development and computational efficiency of the moment method code. Specifically, all of the fundamental mode developments present results on the order of seconds at any desired frequency which if replicated in CST would take on the order of hours, depending on the mesh density and sample anisotropy. The trade space being that CST can accommodate a vast array of tasks, while the

tailored moment method code can only solve a very specific type of problem. The accuracy constraints of each approach lie in the basis functions used. CST's mesh must be sufficiently fine to yield solutions of an appropriate accuracy, which drives the duration of a simulation. Accuracy of the moment method development is based in the number of rectangular waveguide modes employed. The rectangular waveguide modes physically describe field propagation and evanescent behavior in the geometry, thus a few modes can offer equivalently accurate results in less time. As for physical insight gained, both the Greens' function and moment method developments give examples. The Green's function approach provides insight into field propagation in the the parallel-plate waveguide structure and what modes are supported. It is important to reiterate that crystallographic symmetry significantly impacts material anisotropy and which impacts the field structure, especially in the presence of boundary conditions. The Green's function also can be reused for other MFIE or EFIE developments, saving future work in analytic developments. The moment method development also gives insight into laboratory measurement sensitivities both in uncertainty and capability to successfully measure anisotropic media. This insight could also be considered an efficiency, as attempting to perform a Monte Carlo error analysis would be drastically time consuming. Examples of this are presented in the thickness and rotation uncertainty developments throughout this research.

The results obtained in the both uniaxial and rotated uniaxial cases have significant contribution to non-destructive anisotropic research, with the rotated uniaxial being most important. Characterization of the uniaxial honeycomb RAM material offers a non-destructive advantage over having to prepare a sample for rectangular waveguide characterization. Characterization of the rotated uniaxial media, offers a new category of materials that can be non-destructively evaluated. Two laboratory measurement examples presented, are the low-contrast ABS plastic and the wire

loaded media. The wire loaded media exhibits an additional element as the wire loaded media presents anisotropy in both the permittivity and permeability, which has not previously been addressed in the aforementioned anisotropic research.

Improvements to this research lie in the need for better rotated uniaxial anisotropic samples. Smaller, higher contrast cells, which satisfy macroscopic EM would greatly aide laboratory assessment of the SPWP measurement approach. The samples presented in this work lack enough contrast to definitively compare to simulated performance results to the current measurement results. Future additive manufacture enhancements would remedy sample development challenges.

8.3 Future Work

Several areas of future work should be explored with respect to non-destructive characterization of anisotropic media. First, a dual port waveguide probe for analyzing metal back rotated uniaxial media could be developed. This approach would offer another measurement port to increase measurement diversity in conjunction with rotating the measurement fixture to two unique orientations. This increased diversity would support characterization of both permittivites and permeabilities from a single metal backed sample. Second, a biaxial anisotropic Green's function could be developed based on the knowledge gained in the rotated uniaxial Green's function presented. Third, more exploration into high contrast anisotropic media design would be most beneficial. This could include various dielectric or magnetic media. Lastly, use of a multi-port square waveguide may support measurement diversity through various waveguide port excitations, and not require the need to index the sample fixture. The multi-port waveguide launch would support both co- and cross-polarized measurement of anisotropic media at the square waveguide aperture.

Appendix A. Higher Order Mode Moment Method Details for Uniaxial Media

A.1 Field Expansion Relationship

The expanded field relationship as discussed in Chapter 3:

$$
\begin{aligned}
&\iint_S \vec{h}^*_{uv} \cdot \{2\vec{h}^{TE}_{10}\} dS = \\
&\sum_{m=0}^{M}\sum_{n=0}^{N} \overline{\Gamma}^{TE}_{mn} \Bigg[\iint_S \vec{h}^*_{uv} \cdot \vec{h}^{TE}_{mn} dS - \\
&Z^{TE}_{mn} \frac{1}{(2\pi)^2} \iint_{-\infty}^{\infty} \widetilde{G}_{\pi h,x}(\vec{\lambda}_\rho) j\lambda_x \iint_S h^*_{uvx} e^{j\vec{\lambda}_\rho\cdot\vec{\rho}} dS \iint_{S'} h^{TE}_{mnx} e^{-j\vec{\lambda}_\rho\cdot\vec{\rho}'} dS' d^2\lambda - \\
&Z^{TE}_{mn} \frac{1}{(2\pi)^2} \iint_{-\infty}^{\infty} \widetilde{G}_{\pi h,y}(\vec{\lambda}_\rho) j\lambda_x \iint_S h^*_{uvx} e^{j\vec{\lambda}_\rho\cdot\vec{\rho}} dS \iint_{S'} h^{TE}_{mny} e^{-j\vec{\lambda}_\rho\cdot\vec{\rho}'} dS' d^2\lambda + \\
&-Z^{TE}_{mn} \frac{1}{(2\pi)^2} \iint_{-\infty}^{\infty} \widetilde{G}_{\psi h,x}(\vec{\lambda}_\rho) j\lambda_y \iint_S h^*_{uvx} e^{j\vec{\lambda}_\rho\cdot\vec{\rho}} dS \iint_{S'} h^{TE}_{mnx} e^{-j\vec{\lambda}_\rho\cdot\vec{\rho}'} dS' d^2\lambda + \\
&-Z^{TE}_{mn} \frac{1}{(2\pi)^2} \iint_{-\infty}^{\infty} \widetilde{G}_{\psi h,y}(\vec{\lambda}_\rho) j\lambda_y \iint_S h^*_{uvx} e^{j\vec{\lambda}_\rho\cdot\vec{\rho}} dS \iint_{S'} h^{TE}_{mny} e^{-j\vec{\lambda}_\rho\cdot\vec{\rho}'} dS' d^2\lambda + \\
&Z^{TE}_{mn} \frac{1}{(2\pi)^2} \iint_{-\infty}^{\infty} \widetilde{G}_{\psi h,x}(\vec{\lambda}_\rho) j\lambda_x \iint_S h^*_{uvy} e^{j\vec{\lambda}_\rho\cdot\vec{\rho}} dS \iint_{S'} h^{TE}_{mnx} e^{-j\vec{\lambda}_\rho\cdot\vec{\rho}'} dS' d^2\lambda + \\
&Z^{TE}_{mn} \frac{1}{(2\pi)^2} \iint_{-\infty}^{\infty} \widetilde{G}_{\psi h,y}(\vec{\lambda}_\rho) j\lambda_x \iint_S h^*_{uvy} e^{j\vec{\lambda}_\rho\cdot\vec{\rho}} dS \iint_{S'} h^{TE}_{mny} e^{-j\vec{\lambda}_\rho\cdot\vec{\rho}'} dS' d^2\lambda - \\
&Z^{TE}_{mn} \frac{1}{(2\pi)^2} \iint_{-\infty}^{\infty} \widetilde{G}_{\pi h,x}(\vec{\lambda}_\rho) j\lambda_y \iint_S h^*_{uvy} e^{j\vec{\lambda}_\rho\cdot\vec{\rho}} dS \iint_{S'} h^{TE}_{mnx} e^{-j\vec{\lambda}_\rho\cdot\vec{\rho}'} dS' d^2\lambda - \\
&Z^{TE}_{mn} \frac{1}{(2\pi)^2} \iint_{-\infty}^{\infty} \widetilde{G}_{\pi h,y}(\vec{\lambda}_\rho) j\lambda_y \iint_S h^*_{uvy} e^{j\vec{\lambda}_\rho\cdot\vec{\rho}} dS \iint_{S'} h^{TE}_{mny} e^{-j\vec{\lambda}_\rho\cdot\vec{\rho}'} dS' d^2\lambda \Bigg] +
\end{aligned}
\tag{A.1}
$$

$$\sum_{m=0}^{M}\sum_{n=0}^{N}\Gamma_{mn}^{TM}\left[\iint\limits_{S}\vec{h}_{uv}^{*}\cdot\vec{h}_{mn}^{TM}dS-\right.$$

$$Z_{mn}^{TM}\frac{1}{(2\pi)^2}\iint\limits_{-\infty}^{\infty}\widetilde{G}_{\pi h,x}(\vec{\lambda}_\rho)j\lambda_x\iint\limits_{S}h_{uvx}^{*}e^{j\vec{\lambda}_\rho\cdot\vec{\rho}}dS\iint\limits_{S'}h_{mn\ x}^{TM}e^{-j\vec{\lambda}_\rho\cdot\vec{\rho}'}dS'd^2\lambda-$$

$$Z_{mn}^{TM}\frac{1}{(2\pi)^2}\iint\limits_{-\infty}^{\infty}\widetilde{G}_{\pi h,y}(\vec{\lambda}_\rho)j\lambda_x\iint\limits_{S}h_{uvx}^{*}e^{j\vec{\lambda}_\rho\cdot\vec{\rho}}dS\iint\limits_{S'}h_{mn\ y}^{TM}e^{-j\vec{\lambda}_\rho\cdot\vec{\rho}'}dS'd^2\lambda+$$

$$-Z_{mn}^{TM}\frac{1}{(2\pi)^2}\iint\limits_{-\infty}^{\infty}\widetilde{G}_{\psi h,x}(\vec{\lambda}_\rho)j\lambda_y\iint\limits_{S}h_{uvx}^{*}e^{j\vec{\lambda}_\rho\cdot\vec{\rho}}dS\iint\limits_{S'}h_{mn\ x}^{TM}e^{-j\vec{\lambda}_\rho\cdot\vec{\rho}'}dS'd^2\lambda+$$

$$-Z_{mn}^{TM}\frac{1}{(2\pi)^2}\iint\limits_{-\infty}^{\infty}\widetilde{G}_{\psi h,y}(\vec{\lambda}_\rho)j\lambda_y\iint\limits_{S}h_{uvx}^{*}e^{j\vec{\lambda}_\rho\cdot\vec{\rho}}dS\iint\limits_{S'}h_{mn\ y}^{TM}e^{-j\vec{\lambda}_\rho\cdot\vec{\rho}'}dS'd^2\lambda+ \qquad \text{(A.2)}$$

$$Z_{mn}^{TM}\frac{1}{(2\pi)^2}\iint\limits_{-\infty}^{\infty}\widetilde{G}_{\psi h,x}(\vec{\lambda}_\rho)j\lambda_x\iint\limits_{S}h_{uvy}^{*}e^{j\vec{\lambda}_\rho\cdot\vec{\rho}}dS\iint\limits_{S'}h_{mn\ x}^{TM}e^{-j\vec{\lambda}_\rho\cdot\vec{\rho}'}dS'd^2\lambda+$$

$$Z_{mn}^{TM}\frac{1}{(2\pi)^2}\iint\limits_{-\infty}^{\infty}\widetilde{G}_{\psi h,y}(\vec{\lambda}_\rho)j\lambda_x\iint\limits_{S}h_{uvy}^{*}e^{j\vec{\lambda}_\rho\cdot\vec{\rho}}dS\iint\limits_{S'}h_{mn\ y}^{TM}e^{-j\vec{\lambda}_\rho\cdot\vec{\rho}'}dS'd^2\lambda-$$

$$Z_{mn}^{TM}\frac{1}{(2\pi)^2}\iint\limits_{-\infty}^{\infty}\widetilde{G}_{\pi h,x}(\vec{\lambda}_\rho)j\lambda_y\iint\limits_{S}h_{uvy}^{*}e^{j\vec{\lambda}_\rho\cdot\vec{\rho}}dS\iint\limits_{S'}h_{mn\ x}^{TM}e^{-j\vec{\lambda}_\rho\cdot\vec{\rho}'}dS'd^2\lambda-$$

$$\left.Z_{mn}^{TM}\frac{1}{(2\pi)^2}\iint\limits_{-\infty}^{\infty}\widetilde{G}_{\pi h,y}(\vec{\lambda}_\rho)j\lambda_y\iint\limits_{S}h_{uvy}^{*}e^{j\vec{\lambda}_\rho\cdot\vec{\rho}}dS\iint\limits_{S'}h_{mn\ y}^{TM}e^{-j\vec{\lambda}_\rho\cdot\vec{\rho}'}dS'd^2\lambda\right]$$

A.2 Solutions to the integrals

After executing the required integration as discussed in as Chapter 3 the solutions are consolidated as:

$$2\left(\frac{(\frac{\pi}{a})^2}{Z_{10}^{TE*}Z_{10}^{TE}}\right)\frac{ab}{2}\delta_{uv10}^{TE} = \sum_{m=0}^{M}\sum_{n=0}^{N}\overline{\Gamma}_{mn}^{TE}\left[\left(\left(\frac{m\pi}{a}\right)^2+\left(\frac{n\pi}{b}\right)^2\right)\frac{ab(1+\delta_{uvm0}^{TE})}{4Z_{mn}^{TE*}Z_{mn}^{TE}}\delta_{uvmn}^{TE}+TOT\right]+ \sum_{m=0}^{M}\sum_{n=0}^{N}\Gamma_{mn}^{TM}\left[\left(\left(\frac{m\pi}{a}\right)^2+\left(\frac{n\pi}{b}\right)^2\right)\frac{ab(1+\delta_{uvm0}^{TM})}{4Z_{mn}^{TM*}Z_{mn}^{TM}}\delta_{uvmn}^{TM}+TOT_{TM}\right]. \tag{A.3}$$

TOT and TOT_{TM} change depending on which case is evaluated in (A.3). The cases are identified below. If TOT_{TM} is not explicitly stated for a case, then it is zero.

Case 5: $n = 0$ and $v = 0$:

$$TOT = \int_{-\infty}^{\infty}\frac{(e^{j(a\lambda_x)}(-1)^u-1)}{((\frac{u\pi}{a})^2-\lambda_x^2)}\frac{(e^{-j(a\lambda_x)}(-1)^m-1)}{(k_x^2-\lambda_x^2)} \left(\frac{C_xk_x^2}{\omega\mu_t(2\pi)^2}j4\pi\frac{\mu_z}{\mu_t d}\sum_{l=0}^{\infty}\frac{\lambda_x^2(\frac{l\pi}{d})^2}{((\lambda_{y\theta}^B)^2+\lambda_x^2)}\frac{(1-e^{-jb\lambda_{y\theta}^B})}{(\lambda_{y\theta}^B)^3}+ \frac{C_xk_x^2}{\omega\mu_t(2\pi)^2}2\pi b\frac{\lambda_{z\theta}^v\cos(\lambda_{z\theta}^v d)}{\sin(\lambda_{z\theta}^v d)}+\frac{\omega\epsilon_tC_xk_x^2}{(2\pi)^2}j4\pi\frac{\epsilon_z}{\epsilon_t d}\sum_{l=0}^{\infty}\frac{(1-e^{-jb\lambda_{y\psi}^B})}{\lambda_{y\psi}^B((\lambda_{y\psi}^B)^2+\lambda_x^2)(1+\delta_{l,0})}\right)d\lambda_x \tag{A.4}$$

Case 4: $n = 0$ and $v \neq 0$:

$$
\begin{aligned}
TOT &= \int_{-\infty}^{\infty} \frac{(e^{j(a\lambda_x)}(-1)^u - 1)}{((\frac{u\pi}{a})^2 - \lambda_x^2)} \frac{(e^{-j(a\lambda_x)}(-1)^m - 1)}{(k_x^2 - \lambda_x^2)} \, (INT) \, d\lambda_x \\
INT &= -\frac{(C_x + C_y)k_x^2}{\omega\mu_t(2\pi)^2} j4\pi \frac{\mu_z}{\mu_t d} \sum_{l=0}^{\infty} \lambda_x^2 \frac{(\frac{l\pi}{d})^2}{((\lambda_{y\theta}^B)^2 + \lambda_x^2)} \frac{(1 - e^{-jb\lambda_{y\theta}^B})}{(\lambda_{y\theta}^B)((\frac{v\pi}{b})^2 - (\lambda_{y\theta}^B)^2)} + \\
&\quad -\frac{\omega\epsilon_t C_x k_x^2}{(2\pi)^2} j4\pi \frac{\epsilon_z}{\epsilon_t d} \sum_{l=0}^{\infty} \frac{\lambda_{y\psi}^B (1 - e^{-jb\lambda_{y\psi}^B})}{((\lambda_{y\psi}^B)^2 + \lambda_x^2)((\frac{v\pi}{b})^2 - (\lambda_{y\psi}^B)^2)(1 + \delta_{l,0})} + \\
&\quad \frac{\omega\epsilon_t (C_y k_x^2)}{(2\pi)^2} j4\pi \frac{\epsilon_z}{\epsilon_t d} \sum_{l=0}^{\infty} \frac{\lambda_x^2 (1 - e^{-jb\lambda_{y\psi}^B})}{\lambda_{y\psi}^B((\lambda_{y\psi}^B)^2 + \lambda_x^2)((\frac{v\pi}{b})^2 - (\lambda_{y\psi}^B)^2)(1 + \delta_{l,0})}
\end{aligned}
\tag{A.5}
$$

Case 3: $n \neq 0$ and $v = 0$:

$$
\begin{aligned}
TOT &= \int_{-\infty}^{\infty} \frac{(e^{j(a\lambda_x)}(-1)^u - 1)}{((\frac{u\pi}{a})^2 - \lambda_x^2)} \frac{(e^{-j(a\lambda_x)}(-1)^m - 1)}{(k_x^2 - \lambda_x^2)} \, (INT) \, d\lambda_x \\
INT &= -\frac{C_x(k_x^2 + k_y^2)}{\omega\mu_t(2\pi)^2} j4\pi \frac{\mu_z}{\mu_t d} \sum_{l=0}^{\infty} \frac{\lambda_x^2 (\frac{l\pi}{d})^2}{(\lambda_{y\theta}^B)((\lambda_{y\theta}^B)^2 + \lambda_x^2)} \frac{(1 - e^{-jb\lambda_{y\theta}^B}(-1)^n)}{((\frac{n\pi}{b})^2 - (\lambda_{y\theta}^B)^2)} \\
&\quad -\frac{\omega\epsilon_t C_x k_x^2}{(2\pi)^2} j4\pi \frac{\epsilon_z}{\epsilon_t d} \sum_{l=0}^{\infty} \frac{\lambda_{y\psi}^B (1 - e^{-jb\lambda_{y\psi}^B}(-1)^n)}{((\lambda_{y\psi}^B)^2 + \lambda_x^2)((\frac{n\pi}{b})^2 - (\lambda_{y\psi}^B)^2)(1 + \delta_{l,0})} \\
&\quad + \frac{\omega\epsilon_t C_x k_y^2}{(2\pi)^2} j4\pi \frac{\epsilon_z}{\epsilon_t d} \sum_{l=0}^{\infty} \frac{\lambda_x^2 (1 - e^{-jb\lambda_{y\psi}^B}(-1)^n)}{\lambda_{y\psi}^B((\lambda_{y\psi}^B)^2 + \lambda_x^2)((\frac{n\pi}{b})^2 - (\lambda_{y\psi}^B)^2)(1 + \delta_{l,0})}
\end{aligned}
\tag{A.6}
$$

$$
\begin{aligned}
TOT_{TM} &= \int_{-\infty}^{\infty} \frac{(e^{j(a\lambda_x)}(-1)^u - 1)}{((\frac{u\pi}{a})^2 - \lambda_x^2)} \frac{(e^{-j(a\lambda_x)}(-1)^m - 1)}{(k_x^2 - \lambda_x^2)} \, (INT_{TM}) \, d\lambda_x \\
INT_{TM} &= \frac{\omega\epsilon_t C_x k_x k_y}{(2\pi)^2} j4\pi \frac{\epsilon_z}{\epsilon_t d} \sum_{l=0}^{\infty} \frac{\lambda_{y\psi}^B (1 - e^{-jb\lambda_{y\psi}^B}(-1)^n)}{((\lambda_{y\psi}^B)^2 + \lambda_x^2)((\frac{n\pi}{b})^2 - (\lambda_{y\psi}^B)^2)(1 + \delta_{l,0})} \\
&\quad + \frac{\omega\epsilon_t C_x k_x k_y}{(2\pi)^2} j4\pi \frac{\epsilon_z}{\epsilon_t d} \sum_{l=0}^{\infty} \frac{\lambda_x^2 (1 - e^{-jb\lambda_{y\psi}^B}(-1)^n)}{\lambda_{y\psi}^B((\lambda_{y\psi}^B)^2 + \lambda_x^2)((\frac{n\pi}{b})^2 - (\lambda_{y\psi}^B)^2)(1 + \delta_{l,0})}
\end{aligned}
\tag{A.7}
$$

Case 2: $n = v \neq 0$:

$$TOT = \int_{-\infty}^{\infty} \frac{(e^{j(a\lambda_x)}(-1)^u - 1)}{((\frac{u\pi}{a})^2 - \lambda_x^2)} \frac{(e^{-j(a\lambda_x)}(-1)^m - 1)}{(k_x^2 - \lambda_x^2)} (INT)\, d\lambda_x$$

$$\begin{aligned} INT = \frac{(C_x + C_y)(k_x^2 + k_y^2)}{\omega\mu_t(2\pi)^2} \Bigg[& j4\pi \frac{\mu_z}{\mu_t d} \sum_{l=0}^{\infty} \frac{\lambda_x^2(\frac{l\pi}{d})^2}{((\lambda_{y\theta}^B)^2 + \lambda_x^2)} \frac{(1 - e^{-jb\lambda_{y\theta}^B}(-1)^n)}{((\frac{n\pi}{b})^2 - (\lambda_{y\theta}^B)^2)} \frac{(\lambda_{y\theta}^B)}{((\frac{n\pi}{b})^2 - (\lambda_{y\theta}^B)^2)} \\ & + \pi b \frac{\lambda_x^2 \lambda_{z\theta}^n}{((\frac{n\pi}{b}) + \lambda_x^2)} \frac{\cos(\lambda_{z\theta}^n d)}{\sin(\lambda_{z\theta}^n d)} \Bigg] \\ & + \frac{\omega\epsilon_t C_x k_x^2}{(2\pi)^2} \Bigg[j4\pi \frac{\epsilon_z}{\epsilon_t d} \sum_{l=0}^{\infty} \frac{(\lambda_{y\psi}^B)^3(1 - e^{-jb\lambda_{y\psi}^B}(-1)^n)}{((\lambda_{y\psi}^B)^2 + \lambda_x^2)((\frac{n\pi}{b})^2 - (\lambda_{y\psi}^B)^2)((\frac{n\pi}{b})^2 - (\lambda_{y\psi}^B)^2)(1 + \delta_{l,0})} \\ & + \frac{\pi^3 n^2}{b} \frac{1}{((\frac{n\pi}{b}) + \lambda_x^2)} \frac{\cos(\lambda_{z\psi}^n d)}{\lambda_{z\psi}^n \sin(\lambda_{z\psi}^n d)} \Bigg] \\ & - \frac{\omega\epsilon_t(C_x k_y^2 + C_y k_x^2)}{(2\pi)^2} \Bigg[j4\pi \frac{\epsilon_z}{\epsilon_t d} \sum_{l=0}^{\infty} \frac{\lambda_x^2 \lambda_{y\psi}^B (1 - e^{-jb\lambda_{y\psi}^B}(-1)^n)}{((\lambda_{y\psi}^B)^2 + \lambda_x^2)((\frac{n\pi}{b})^2 - (\lambda_{y\psi}^B)^2)((\frac{n\pi}{b})^2 - (\lambda_{y\psi}^B)^2)(1 + \delta_{l,0})} \\ & + \pi b \frac{\lambda_x^2}{((\frac{n\pi}{b}) + \lambda_x^2)} \frac{\cos(\lambda_{z\psi}^n d)}{\lambda_{z\psi}^n \sin(\lambda_{z\psi}^n d)} \Bigg] \\ & + \frac{\omega\epsilon_t C_y k_y^2}{(2\pi)^2} \Bigg[j4\pi \frac{\epsilon_z}{\epsilon_t d} \sum_{l=0}^{\infty} \frac{\lambda_x^4 (1 - e^{-jb\lambda_{y\psi}^B}(-1)^n)}{\lambda_{y\psi}^B((\lambda_{y\psi}^B)^2 + \lambda_x^2)((\frac{n\pi}{b})^2 - (\lambda_{y\psi}^B)^2)((\frac{n\pi}{b})^2 - (\lambda_{y\psi}^B)^2)(1 + \delta_{l,0})} \\ & + \frac{b^3}{n^2\pi} \frac{\lambda_x^4}{((\frac{n\pi}{b})^2 + \lambda_x^2)} \frac{\cos(\lambda_{z\psi}^n d)}{\lambda_{z\psi}^n \sin(\lambda_{z\psi}^n d)} \Bigg] \end{aligned} \tag{A.8}$$

$$TOT_{TM} = \int_{-\infty}^{\infty} \frac{(e^{j(a\lambda_x)}(-1)^u - 1)}{((\frac{u\pi}{a})^2 - \lambda_x^2)} \frac{(e^{-j(a\lambda_x)}(-1)^m - 1)}{(k_x^2 - \lambda_x^2)} (INT_{TM})\, d\lambda_x$$

$$\begin{aligned} INT_{TM} = -\frac{\omega\epsilon_t C_x k_x k_y}{(2\pi)^2} \Bigg[& j4\pi \frac{\epsilon_z}{\epsilon_t d} \sum_{l=0}^{\infty} \frac{(\lambda_{y\psi}^B)^3 (1 - e^{-jb\lambda_{y\psi}^B}(-1)^n)}{((\lambda_{y\psi}^B)^2 + \lambda_x^2)((\frac{n\pi}{b})^2 - (\lambda_{y\psi}^B)^2)((\frac{n\pi}{b})^2 - (\lambda_{y\psi}^B)^2)(1 + \delta_{l,0})} \\ & + \frac{\pi^3 n^2}{b} \frac{1}{((\frac{n\pi}{b}) + \lambda_x^2)} \frac{\cos\left(\lambda_{z\psi}^n d\right)}{\lambda_{z\psi}^n \sin(\lambda_{z\psi}^n d)} \Bigg] \\ + \frac{\omega\epsilon_t(-C_x + C_y) k_x k_y}{(2\pi)^2} \Bigg[& j4\pi \frac{\epsilon_z}{\epsilon_t d} \sum_{l=0}^{\infty} \frac{\lambda_x^2 \lambda_{y\psi}^B (1 - e^{-jb\lambda_{y\psi}^B}(-1)^n)}{((\lambda_{y\psi}^B)^2 + \lambda_x^2)((\frac{n\pi}{b})^2 - (\lambda_{y\psi}^B)^2)((\frac{n\pi}{b})^2 - (\lambda_{y\psi}^B)^2)(1 + \delta_{l,0})} \\ & + \pi b \frac{\lambda_x^2}{((\frac{n\pi}{b}) + \lambda_x^2)} \frac{\cos\left(\lambda_{z\psi}^n d\right)}{\lambda_{z\psi}^n \sin(\lambda_{z\psi}^n d)} \Bigg] \\ + \frac{\omega\epsilon_t C_y k_x k_y}{(2\pi)^2} \Bigg[& j4\pi \frac{\epsilon_z}{\epsilon_t d} \sum_{l=0}^{\infty} \frac{\lambda_x^4 (1 - e^{-jb\lambda_{y\psi}^B}(-1)^n)}{\lambda_{y\psi}^B((\lambda_{y\psi}^B)^2 + \lambda_x^2)((\frac{n\pi}{b})^2 - (\lambda_{y\psi}^B)^2)((\frac{n\pi}{b})^2 - (\lambda_{y\psi}^B)^2)(1 + \delta_{l,0})} \\ & + \frac{b^3}{n^2\pi} \frac{\lambda_x^4}{((\frac{n\pi}{b})^2 + \lambda_x^2)} \frac{\cos\left(\lambda_{z\psi}^n d\right)}{\lambda_{z\psi}^n \sin(\lambda_{z\psi}^n d)} \Bigg] \end{aligned} \tag{A.9}$$

Case 1: $n \neq v \neq 0$:

$$TOT = \int_{-\infty}^{\infty} \frac{(e^{j(a\lambda_x)}(-1)^u - 1)}{((\frac{u\pi}{a})^2 - \lambda_x^2)} \frac{(e^{-j(a\lambda_x)}(-1)^m - 1)}{(k_x^2 - \lambda_x^2)} (INT)\, d\lambda_x$$

$$\begin{aligned} INT = & \frac{(C_x + C_y)(k_x^2 + k_y^2)}{\omega\mu_t(2\pi)^2} j4\pi \frac{\mu_z}{\mu_t d} \sum_{l=0}^{\infty} \frac{\lambda_x^2 (\frac{l\pi}{d})^2}{((\lambda_{y\theta}^B)^2 + \lambda_x^2)} \frac{(1 - e^{-jb\lambda_{y\theta}^B}(-1)^n)}{((\frac{v\pi}{b})^2 - (\lambda_{y\theta}^B)^2)} \frac{(\lambda_{y\theta}^B)}{((\frac{n\pi}{b})^2 - (\lambda_{y\theta}^B)^2)} \\ & + \frac{\omega\epsilon_t C_x k_x^2}{(2\pi)^2} j4\pi \frac{\epsilon_z}{\epsilon_t d} \sum_{l=0}^{\infty} \frac{(\lambda_{y\psi}^B)^3 (1 - e^{-jb\lambda_{y\psi}^B}(-1)^n)}{((\lambda_{y\psi}^B)^2 + \lambda_x^2)((\frac{v\pi}{b})^2 - (\lambda_{y\psi}^B)^2)((\frac{n\pi}{b})^2 - (\lambda_{y\psi}^B)^2)(1 + \delta_{l,0})} \\ & - \frac{\omega\epsilon_t(C_x k_y^2 + C_y k_x^2)}{(2\pi)^2} j4\pi \frac{\epsilon_z}{\epsilon_t d} \sum_{l=0}^{\infty} \frac{\lambda_x^2 \lambda_{y\psi}^B (1 - e^{-jb\lambda_{y\psi}^B}(-1)^n)}{((\lambda_{y\psi}^B)^2 + \lambda_x^2)((\frac{v\pi}{b})^2 - (\lambda_{y\psi}^B)^2)((\frac{n\pi}{b})^2 - (\lambda_{y\psi}^B)^2)(1 + \delta_{l,0})} \\ & + \frac{\omega\epsilon_t C_y k_y^2}{(2\pi)^2} j4\pi \frac{\epsilon_z}{\epsilon_t d} \sum_{l=0}^{\infty} \frac{\lambda_x^4 (1 - e^{-jb\lambda_{y\psi}^B}(-1)^n)}{\lambda_{y\psi}^B((\lambda_{y\psi}^B)^2 + \lambda_x^2)((\frac{v\pi}{b})^2 - (\lambda_{y\psi}^B)^2)((\frac{n\pi}{b})^2 - (\lambda_{y\psi}^B)^2)(1 + \delta_{l,0})} \end{aligned} \tag{A.10}$$

$$TOT_{TM} = \int_{-\infty}^{\infty} \frac{(e^{j(a\lambda_x)}(-1)^u - 1)}{((\frac{u\pi}{a})^2 - \lambda_x^2)} \frac{(e^{-j(a\lambda_x)}(-1)^m - 1)}{(k_x^2 - \lambda_x^2)} (INT_{TM})\, d\lambda_x$$

$$INT_{TM} = -\frac{\omega\epsilon_t C_x k_x k_y}{(2\pi)^2} j4\pi \frac{\epsilon_z}{\epsilon_t d} \sum_{l=0}^{\infty} \frac{(\lambda_{y\psi}^B)^3(1 - e^{-jb\lambda_{y\psi}^B}(-1)^n)}{((\lambda_{y\psi}^B)^2 + \lambda_x^2)((\frac{v\pi}{b})^2 - (\lambda_{y\psi}^B)^2)((\frac{n\pi}{b})^2 - (\lambda_{y\psi}^B)^2)(1 + \delta_{l,0})}$$
$$+ \frac{\omega\epsilon_t(-C_x + C_y) k_x k_y}{(2\pi)^2} j4\pi \frac{\epsilon_z}{\epsilon_t d} \sum_{l=0}^{\infty} \frac{\lambda_x^2 \lambda_{y\psi}^B (1 - e^{-jb\lambda_{y\psi}^B}(-1)^n)}{((\lambda_{y\psi}^B)^2 + \lambda_x^2)((\frac{v\pi}{b})^2 - (\lambda_{y\psi}^B)^2)((\frac{n\pi}{b})^2 - (\lambda_{y\psi}^B)^2)(1 + \delta_{l,0})}$$
$$+ \frac{\omega\epsilon_t C_y k_x k_y}{(2\pi)^2} j4\pi \frac{\epsilon_z}{\epsilon_t d} \sum_{l=0}^{\infty} \frac{\lambda_x^4 (1 - e^{-jb\lambda_{y\psi}^B}(-1)^n)}{\lambda_{y\psi}^B((\lambda_{y\psi}^B)^2 + \lambda_x^2)((\frac{v\pi}{b})^2 - (\lambda_{y\psi}^B)^2)((\frac{n\pi}{b})^2 - (\lambda_{y\psi}^B)^2)(1 + \delta_{l,0})} \tag{A.11}$$

For all cases described above, the parallel plate and waveguide modes describe propagation constraints in the parallel plate region:

$$\lambda_{z\theta}^n = k_t \sqrt{1 - \left(\frac{\lambda_x}{k_{tz}}\right)^2 - \left(\frac{\frac{\pm n\pi}{b}}{k_{tz}}\right)^2} \quad \lambda_{z\theta}^v = k_t \sqrt{1 - \left(\frac{\lambda_x}{k_{tz}}\right)^2 - \left(\frac{\frac{\pm v\pi}{b}}{k_{tz}}\right)^2} \tag{A.12}$$

$$\lambda_{y\theta}^B = k_{tz} \sqrt{1 - \left(\frac{\frac{l\pi}{d}}{k_t}\right)^2 - \left(\frac{\lambda_x}{k_{tz}}\right)^2} \tag{A.13}$$

$$\lambda_{z\psi}^n = k_t \sqrt{1 - \left(\frac{\lambda_x}{k_{zt}}\right)^2 - \left(\frac{\frac{\pm n\pi}{b}}{k_{zt}}\right)^2} \quad \lambda_{z\psi}^v = k_t \sqrt{1 - \left(\frac{\lambda_x}{k_{zt}}\right)^2 - \left(\frac{\frac{\pm v\pi}{b}}{k_{zt}}\right)^2} \tag{A.14}$$

$$\lambda_{y\psi}^B = k_{zt} \sqrt{1 - \left(\frac{\frac{l\pi}{d}}{k_t}\right)^2 - \left(\frac{\lambda_x}{k_{zt}}\right)^2} \tag{A.15}$$

where

$$k_t^2 = \omega^2\epsilon_t\mu_t \quad k_{zt}^2 = \omega^2\epsilon_z\mu_t \quad k_{tz}^2 = \omega^2\epsilon_t\mu_z \tag{A.16}$$

Appendix B. Rotated Uniaxial Anisotropic Green's Function Details

Transforming Maxwell's equations for to the spectral domain begins with

$$\nabla \times \vec{E} = -j\omega \overleftrightarrow{\mu} \cdot \vec{H}, \qquad \nabla \times \vec{H} = j\omega \overleftrightarrow{\epsilon} \cdot \vec{E} \tag{B.1}$$

Assuming a plane-wave basis, which is equivalent to a Fourier Transform:

$$\nabla \times \vec{E} e^{-j\vec{k}\cdot\vec{r}} = -j\omega \overleftrightarrow{\mu} \cdot \vec{H} e^{-j\vec{k}\cdot\vec{r}}, \qquad \nabla \times \vec{E} e^{-j\vec{k}\cdot\vec{r}} = j\omega \overleftrightarrow{\epsilon} \cdot \vec{E} e^{-j\vec{k}\cdot\vec{r}} \tag{B.2}$$

$$\nabla e^{j\vec{k}\cdot\vec{r}} \times \vec{E} + e^{-j\vec{k}\cdot\vec{r}} \nabla \times \vec{E}_0 = -j\omega \overleftrightarrow{\mu} \cdot \vec{H} e^{-j\vec{k}\cdot\vec{r}} \tag{B.3}$$

$$\nabla e^{j\vec{k}\cdot\vec{r}} \times \vec{H} + e^{-j\vec{k}\cdot\vec{r}} \nabla \times \vec{H}_0 = -j\omega \overleftrightarrow{\epsilon} \cdot \vec{E} e^{-j\vec{k}\cdot\vec{r}}$$

$$-j\vec{k} e^{-j\vec{k}\cdot\vec{r}} \times \vec{E} e^{-j\vec{k}\cdot\vec{r}} = -j\omega \overleftrightarrow{\mu} \cdot \vec{H} e^{-j\vec{k}\cdot\vec{r}} \tag{B.4}$$

$$-j\vec{k} e^{-j\vec{k}\cdot\vec{r}} \times \vec{H} e^{-j\vec{k}\cdot\vec{r}} = -j\omega \overleftrightarrow{\epsilon} \cdot \vec{E} e^{-j\vec{k}\cdot\vec{r}}$$

$$-j\vec{k} \times \vec{E} = -j\omega \overleftrightarrow{\mu} \cdot \vec{H}, \qquad -j\vec{k} \times \vec{H} = -j\omega \overleftrightarrow{\epsilon} \cdot \vec{E} \tag{B.5}$$

$$-j\vec{k} \times \overleftrightarrow{I} \cdot \vec{E} = -j\omega \overleftrightarrow{\mu} \cdot \vec{H}, \qquad -j\vec{k} \times \overleftrightarrow{I} \cdot \vec{H} = j\omega \overleftrightarrow{\epsilon} \cdot \vec{E} \tag{B.6}$$

$$-j\overleftrightarrow{k} \cdot \vec{E} = -j\omega \overleftrightarrow{\mu} \cdot \vec{H}, \qquad -j\overleftrightarrow{k} \cdot \vec{H} = j\omega \overleftrightarrow{\epsilon} \cdot \vec{E} \tag{B.7}$$

where

$$\vec{k} \times \overleftrightarrow{I} = \begin{bmatrix} 0 & -k_z & k_y \\ k_z & 0 & -k_x \\ -k_y & k_x & 0 \end{bmatrix}. \tag{B.8}$$

Appendix C. Higher Order Mode Moment Method Details for Rotated Uniaxial Media

$$\iint_S h^{*\ TE}_{uvx} e^{j\vec{\lambda}_\rho\cdot\vec{\rho}} dS =$$

$$\iint_S \frac{k_x}{Z^{TE}_{uv}}^{*} \sin(k_x x)\cos(k_y y) e^{j\lambda_x x} e^{j\lambda_y y} dS =$$

$$\frac{k_x}{Z^{TE}_{uv}}^{*} \int_0^b \int_0^a \sin(k_x x)\cos(k_y y) e^{j\lambda_x x} e^{j\lambda_y y} dx dy =$$

$$\frac{k_x}{Z^{TE}_{uv}}^{*} \int_0^a \left[\frac{e^{j(k_x x)} - e^{-j(k_x x)}}{2j}\right] e^{j\lambda_x x} dx \int_0^b \left[\frac{e^{j(k_y y)} + e^{-j(k_y y)}}{2}\right] e^{j\lambda_y y} dy =$$

$$\frac{k_x}{Z^{TE}_{uv}}^{*} \int_0^a \left[\frac{e^{jx(\lambda_x + k_x)} - e^{jx(\lambda_x - k_x)}}{2j}\right] dx \int_0^b \left[\frac{e^{jy(\lambda_y + k_y)} + e^{jy(\lambda_y - k_y)}}{2}\right] dy =$$

$$\frac{k_x}{Z^{TE}_{uv}}^{*} \left(\frac{1}{2j}\left[\frac{e^{aj(\lambda_x+k_x)}-1}{j(k_x+\lambda_x)} + \frac{e^{aj(\lambda_x-k_x)}-1}{j(k_x-\lambda_x)}\right]\frac{1}{2}\left[\frac{e^{bj(\lambda_y+k_y)}-1}{j(k_y+\lambda_y)} - \frac{e^{bj(\lambda_y-k_y)}-1}{j(k_y-\lambda_y)}\right]\right) =$$

$$\frac{k_x}{Z^{TE}_{uv}}^{*} \left(-\frac{1}{2}\left[\frac{e^{aj(\lambda_x+k_x)}-1}{(k_x+\lambda_x)} + \frac{e^{aj(\lambda_x-k_x)}-1}{(k_x-\lambda_x)}\right]\frac{1}{2j}\left[\frac{e^{bj(\lambda_y+k_y)}-1}{(k_y+\lambda_y)} - \frac{e^{bj(\lambda_y-k_y)}-1}{(k_y-\lambda_y)}\right]\right) =$$

$$\frac{k_x}{Z^{TE}_{uv}}^{*} \left(-\frac{1}{2}\left[\frac{e^{j(a\lambda_x+u\pi)}-1}{(k_x+\lambda_x)} + \frac{e^{j(a\lambda_x-u\pi)}-1}{(k_x-\lambda_x)}\right]\frac{1}{2j}\left[\frac{e^{j(b\lambda_y+v\pi)}-1}{(k_y+\lambda_y)} - \frac{e^{j(b\lambda_y-v\pi)}-1}{(k_y-\lambda_y)}\right]\right) =$$

$$\frac{k_x}{Z^{TE}_{uv}}^{*} \left(-\frac{1}{4j}\left[\frac{e^{j(a\lambda_x+u\pi)}-1}{(k_x+\lambda_x)} + \frac{e^{j(a\lambda_x-u\pi)}-1}{(k_x-\lambda_x)}\right]\left[\frac{e^{j(b\lambda_y+v\pi)}-1}{(k_y+\lambda_y)} - \frac{e^{j(b\lambda_y-v\pi)}-1}{(k_y-\lambda_y)}\right]\right) =$$

$$\frac{k_x}{Z^{TE}_{uv}}^{*} \left(-\frac{1}{4j}\frac{2k_x(e^{j(a\lambda_x)}(-1)^u - 1)}{(k_x^2-\lambda_x^2)}\frac{-2\lambda_y(e^{j(b\lambda_y)}(-1)^v - 1)}{(k_y^2-\lambda_y^2)}\right) =$$

$$-\frac{jk_x^2}{Z^{TE}_{uv}}^{*} \left(\frac{(e^{j(a\lambda_x)}(-1)^u - 1)}{(k_x^2-\lambda_x^2)}\frac{\lambda_y(e^{j(b\lambda_y)}(-1)^v - 1)}{(k_y^2-\lambda_y^2)}\right) \tag{C.1}$$

$$\boxed{\iint_S h^{*\ TE}_{uvx} e^{j\vec{\lambda}_\rho\cdot\vec{\rho}} dS = -\frac{jk_x^2}{Z^{TE}_{uv}}^{*} \left(\frac{(e^{j(a\lambda_x)}(-1)^u - 1)}{(k_x^2-\lambda_x^2)}\frac{\lambda_y(e^{j(b\lambda_y)}(-1)^v - 1)}{(k_y^2-\lambda_y^2)}\right)} \tag{C.2}$$

where $Z^{TE}_{uv} = \frac{j\omega\mu_0}{\gamma_{uv}}$, $Z^{TM}_{uv} = \frac{\gamma_{uv}}{j\omega\epsilon_0}$, $k_x = \frac{u\pi}{a}$, $k_y = \frac{v\pi}{b}$ and $\gamma_{uv} = \sqrt{k_x^2 + k_y^2 - k_0^2}$ with $k_0 = \omega\sqrt{\epsilon_0\mu_0}$. Note that the $*$ indicates taking the complex conjugate.

Here is one for the rotated case:

$$\iint_S h^{*\,TE}_{uvy} e^{j\vec{\lambda}_\rho \cdot \vec{\rho}} dS =$$

$$\iint_S \frac{k_x}{Z^{TE}_{uv}}^* \sin(k_x y)\cos(k_y x) e^{j\lambda_x x} e^{j\lambda_y y} dS =$$

$$\frac{k_x}{Z^{TE}_{uv}}^* \int_0^b \int_0^a \sin(k_x y)\cos(k_y x) e^{j\lambda_x x} e^{j\lambda_y y} dx dy =$$

$$\frac{k_x}{Z^{TE}_{uv}}^* \int_0^a \left[\frac{e^{j(k_x y)} - e^{-j(k_x y)}}{2j}\right] e^{j\lambda_y y} dy \int_0^b \left[\frac{e^{j(k_y x)} + e^{-j(k_y x)}}{2}\right] e^{j\lambda_x x} dx =$$

$$\frac{k_x}{Z^{TE}_{uv}}^* \int_0^a \left[\frac{e^{jy(\lambda_y + k_x)} - e^{jy(\lambda_y - k_x)}}{2j}\right] dy \int_0^b \left[\frac{e^{jx(\lambda_x + k_y)} + e^{jx(\lambda_x - k_y)}}{2}\right] dx =$$

$$\frac{k_x}{Z^{TE}_{uv}}^* \left(\frac{1}{2j}\left[\frac{e^{aj(\lambda_y+k_x)}-1}{j(k_x+\lambda_y)} + \frac{e^{aj(\lambda_y-k_x)}-1}{j(k_x-\lambda_y)}\right]\frac{1}{2}\left[\frac{e^{bj(\lambda_x+k_y)}-1}{j(k_y+\lambda_x)} - \frac{e^{bj(\lambda_x-k_y)}-1}{j(k_y-\lambda_x)}\right]\right) =$$

$$\frac{k_x}{Z^{TE}_{uv}}^* \left(-\frac{1}{2}\left[\frac{e^{aj(\lambda_y+k_x)}-1}{(k_x+\lambda_y)} + \frac{e^{aj(\lambda_y-k_x)}-1}{(k_x-\lambda_y)}\right]\frac{1}{2j}\left[\frac{e^{bj(\lambda_x+k_y)}-1}{(k_y+\lambda_x)} - \frac{e^{bj(\lambda_x-k_y)}-1}{(k_y-\lambda_x)}\right]\right) =$$

$$\frac{k_x}{Z^{TE}_{uv}}^* \left(-\frac{1}{2}\left[\frac{e^{j(a\lambda_y+u\pi)}-1}{(k_x+\lambda_y)} + \frac{e^{j(a\lambda_y-u\pi)}-1}{(k_x-\lambda_y)}\right]\frac{1}{2j}\left[\frac{e^{j(b\lambda_x+v\pi)}-1}{(k_y+\lambda_x)} - \frac{e^{j(b\lambda_x-v\pi)}-1}{(k_y-\lambda_x)}\right]\right) =$$

$$\frac{k_x}{Z^{TE}_{uv}}^* \left(-\frac{1}{4j}\left[\frac{e^{j(a\lambda_y+u\pi)}-1}{(k_x+\lambda_y)} + \frac{e^{j(a\lambda_y-u\pi)}-1}{(k_x-\lambda_y)}\right]\left[\frac{e^{j(b\lambda_x+v\pi)}-1}{(k_y+\lambda_x)} - \frac{e^{j(b\lambda_x-v\pi)}-1}{(k_y-\lambda_x)}\right]\right) =$$

$$\frac{k_x}{Z^{TE}_{uv}}^* \left(-\frac{1}{4j}\frac{2k_x(e^{j(a\lambda_y)}(-1)^u - 1)}{(k_x^2-\lambda_y^2)}\frac{-2\lambda_x(e^{j(b\lambda_x)}(-1)^v - 1)}{(k_y^2-\lambda_x^2)}\right) =$$

$$-\frac{jk_x^2}{Z^{TE}_{uv}}^* \left(\frac{(e^{j(a\lambda_y)}(-1)^u - 1)}{(k_x^2-\lambda_y^2)}\frac{\lambda_x(e^{j(b\lambda_x)}(-1)^v - 1)}{(k_y^2-\lambda_x^2)}\right) \tag{C.3}$$

$$\boxed{\iint_S h^{*\,TE}_{uvy} e^{j\vec{\lambda}_\rho \cdot \vec{\rho}} dS = -\frac{jk_x^2}{Z^{TE}_{uv}}^* \left(\frac{(e^{j(a\lambda_y)}(-1)^u - 1)}{(k_x^2-\lambda_y^2)}\frac{\lambda_x(e^{j(b\lambda_x)}(-1)^v - 1)}{(k_y^2-\lambda_x^2)}\right)} \tag{C.4}$$

where $Z^{TE}_{uv} = \frac{j\omega\mu_0}{\gamma_{uv}}$, $Z^{TM}_{uv} = \frac{\gamma_{uv}}{j\omega\epsilon_0}$, $k_x = \frac{u\pi}{a}$, $k_y = \frac{v\pi}{b}$ and $\gamma_{uv} = \sqrt{k_x^2 + k_y^2 - k_0^2}$ with $k_0 = \omega\sqrt{\epsilon_0\mu_0}$. Note that the $*$ indicates taking the complex conjugate.

$$\iint\limits_S h^{*\ TE}_{uvx} e^{j\vec{\lambda}_\rho\cdot\vec{\rho}} dS = -\frac{jk_x^2}{Z^{TE}_{uv}}^* \left(\frac{(e^{j(a\lambda_x)}(-1)^u - 1)}{(k_x^2 - \lambda_x^2)} \frac{\lambda_y (e^{j(b\lambda_y)}(-1)^v - 1)}{(k_y^2 - \lambda_y^2)} \right) \tag{C.5}$$

$$\iint\limits_S h^{*\ TM}_{uvx} e^{j\vec{\lambda}_\rho\cdot\vec{\rho}} dS = \frac{jk_xk_y}{Z^{TM}_{uv}}^* \left(\frac{(e^{j(a\lambda_x)}(-1)^u - 1)}{(k_x^2 - \lambda_x^2)} \frac{\lambda_y (e^{j(b\lambda_y)}(-1)^v - 1)}{(k_y^2 - \lambda_y^2)} \right) \tag{C.6}$$

$$\iint\limits_S h^{*\ TE}_{uvy} e^{j\vec{\lambda}_\rho\cdot\vec{\rho}} dS = -\frac{jk_y^2}{Z^{TE}_{uv}}^* \left(\frac{(e^{j(b\lambda_y)}(-1)^v - 1)}{(k_y^2 - \lambda_y^2)} \frac{\lambda_x (e^{j(a\lambda_x)}(-1)^u - 1)}{(k_x^2 - \lambda_x^2)} \right) \tag{C.7}$$

$$\iint\limits_S h^{*\ TM}_{uvy} e^{j\vec{\lambda}_\rho\cdot\vec{\rho}} dS = -\frac{jk_xk_y}{Z^{TM}_{uv}}^* \left(\frac{(e^{j(b\lambda_y)}(-1)^v - 1)}{(k_y^2 - \lambda_y^2)} \frac{\lambda_x (e^{j(a\lambda_x)}(-1)^u - 1)}{(k_x^2 - \lambda_x^2)} \right) \tag{C.8}$$

$$\iint\limits_{S'} h^{TE}_{mnx} e^{-j\vec{\lambda}_\rho\cdot\vec{\rho}'} dS' = \frac{jk_x^2}{Z^{TE}_{mn}} \left(\frac{(e^{-j(a\lambda_x)}(-1)^m - 1)}{(k_x^2 - \lambda_x^2)} \frac{\lambda_y (e^{-j(b\lambda_y)}(-1)^n - 1)}{(k_y^2 - \lambda_y^2)} \right) \tag{C.9}$$

$$\iint\limits_{S'} h^{TM}_{mn\ x} e^{-j\vec{\lambda}_\rho\cdot\vec{\rho}'} dS' = -\frac{jk_xk_y}{Z^{TM}_{mn}} \left(\frac{(e^{-j(a\lambda_x)}(-1)^m - 1)}{(k_x^2 - \lambda_x^2)} \frac{\lambda_y (e^{-j(b\lambda_y)}(-1)^n - 1)}{(k_y^2 - \lambda_y^2)} \right) \tag{C.10}$$

$$\iint\limits_{S'} h^{TE}_{mny} e^{-j\vec{\lambda}_\rho\cdot\vec{\rho}'} dS' = \frac{jk_y^2}{Z^{TE}_{mn}} \left(\frac{(e^{-j(b\lambda_y)}(-1)^n - 1)}{(k_y^2 - \lambda_y^2)} \frac{\lambda_x (e^{-j(a\lambda_x)}(-1)^m - 1)}{(k_x^2 - \lambda_x^2)} \right) \tag{C.11}$$

$$\iint\limits_{S'} h^{TM}_{mn\ y} e^{-j\vec{\lambda}_\rho\cdot\vec{\rho}'} dS' = \frac{jk_xk_y}{Z^{TM}_{mn}} \left(\frac{(e^{-j(b\lambda_y)}(-1)^n - 1)}{(k_y^2 - \lambda_y^2)} \frac{\lambda_x (e^{-j(a\lambda_x)}(-1)^m - 1)}{(k_x^2 - \lambda_x^2)} \right) \tag{C.12}$$

$$\iint\limits_{S'} h^{TE}_{10} e^{-j\vec{\lambda}_\rho\cdot\vec{\rho}'} dS' = \frac{j\left(\frac{\pi}{a}\right)^2}{Z^{TE}_{10}} \left(\frac{(e^{-j(a\lambda_x)} + 1)}{(\left(\frac{\pi}{a}\right)^2 - \lambda_x^2)} \frac{(e^{-bj(\lambda_y)} - 1)}{(\lambda_y)} \right) \tag{C.13}$$

where $Z^{TE}_{uv,mn} = \frac{j\omega\mu_0}{\gamma_{uv,mn}}$, $Z^{TM}_{uv,mn} = \frac{\gamma_{uv,mn}}{j\omega\epsilon_0}$, $k_x = \frac{u\pi}{a}$ or $k_x = \frac{m\pi}{a}$, $k_y = \frac{v\pi}{b}$ or, $k_y = \frac{n\pi}{b}$ depending on if it is the test or expansion function respectively, and $\gamma_{uv,mn} = \sqrt{k_x^2 + k_y^2 - k_0^2}$ with $k_0 = \omega\sqrt{\epsilon_0\mu_0}$. Note that the $*$ indicates taking the complex conjugate.

$$\iint_{S'} h^{TM}_{mn\ x} e^{-j\vec{\lambda}_\rho\cdot\vec{\rho}'} dS' = \frac{jk_xk_y}{Z^{TM}_{mn}} \left(\frac{(e^{-j(b\lambda_x)}(-1)^n - 1)}{(k_y^2 - \lambda_x^2)} \frac{\lambda_y(e^{-j(a\lambda_y)}(-1)^m - 1)}{(k_x^2 - \lambda_y^2)} \right) \quad \text{(C.14)}$$

$$\iint_{S'} h^{TE}_{mnx} e^{-j\vec{\lambda}_\rho\cdot\vec{\rho}'} dS' = \frac{jk_y^2}{Z^{TE}_{mn}} \left(\frac{(e^{-j(b\lambda_x)}(-1)^n - 1)}{(k_y^2 - \lambda_x^2)} \frac{\lambda_y(e^{-j(a\lambda_y)}(-1)^m - 1)}{(k_x^2 - \lambda_y^2)} \right) \quad \text{(C.15)}$$

$$\iint_{S'} h^{TM}_{mn\ y} e^{-j\vec{\lambda}_\rho\cdot\vec{\rho}'} dS' = -\frac{jk_xk_y}{Z^{TM}_{mn}} \left(\frac{(e^{-j(a\lambda_y)}(-1)^m - 1)}{(k_x^2 - \lambda_y^2)} \frac{\lambda_x(e^{-j(b\lambda_x)}(-1)^n - 1)}{(k_y^2 - \lambda_x^2)} \right) \quad \text{(C.16)}$$

$$\iint_{S'} h^{TE}_{mny} e^{-j\vec{\lambda}_\rho\cdot\vec{\rho}'} dS' = \frac{jk_x^2}{Z^{TE}_{mn}} \left(\frac{(e^{-j(a\lambda_y)}(-1)^m - 1)}{(k_x^2 - \lambda_y^2)} \frac{\lambda_x(e^{-j(b\lambda_x)}(-1)^n - 1)}{(k_y^2 - \lambda_x^2)} \right) \quad \text{(C.17)}$$

$$\iint_{S} h^{*\ TM}_{uvx} e^{j\vec{\lambda}_\rho\cdot\vec{\rho}} dS = -\frac{jk_xk_y}{Z^{TM}_{uv}}^* \left(\frac{(e^{j(b\lambda_x)}(-1)^v - 1)}{(k_y^2 - \lambda_x^2)} \frac{\lambda_y(e^{j(a\lambda_y)}(-1)^u - 1)}{(k_x^2 - \lambda_y^2)} \right) \quad \text{(C.18)}$$

$$\iint_{S} h^{*\ TE}_{uvx} e^{j\vec{\lambda}_\rho\cdot\vec{\rho}} dS = -\frac{jk_y^2}{Z^{TE}_{uv}}^* \left(\frac{(e^{j(b\lambda_x)}(-1)^v - 1)}{(k_y^2 - \lambda_x^2)} \frac{\lambda_y(e^{j(a\lambda_y)}(-1)^u - 1)}{(k_x^2 - \lambda_y^2)} \right) \quad \text{(C.19)}$$

$$\iint_{S} h^{*\ TM}_{uvy} e^{j\vec{\lambda}_\rho\cdot\vec{\rho}} dS = \frac{jk_xk_y}{Z^{TM}_{uv}}^* \left(\frac{(e^{j(a\lambda_y)}(-1)^u - 1)}{(k_x^2 - \lambda_y^2)} \frac{\lambda_x(e^{j(b\lambda_x)}(-1)^v - 1)}{(k_y^2 - \lambda_x^2)} \right) \quad \text{(C.20)}$$

$$\iint_{S} h^{*\ TE}_{uvy} e^{j\vec{\lambda}_\rho\cdot\vec{\rho}} dS = -\frac{jk_x^2}{Z^{TE}_{uv}}^* \left(\frac{(e^{j(a\lambda_y)}(-1)^u - 1)}{(k_x^2 - \lambda_y^2)} \frac{\lambda_x(e^{j(b\lambda_x)}(-1)^v - 1)}{(k_y^2 - \lambda_x^2)} \right) \quad \text{(C.21)}$$

For convenience the above testing integrals can be regrouped:

$$C_x = \begin{cases} \frac{-j(\frac{u\pi}{a})^2}{Z^{TE}_{uv}}^*, & h^*_{uvx} \implies h^{*\ TE}_{uvx} \\ \frac{j\frac{u\pi}{a}\frac{v\pi}{b}}{Z^{TM}_{uv}}^*, & h^*_{uvx} \implies h^{*\ TM}_{uvx} \end{cases} \quad \text{(C.22)}$$

such that

$$\boxed{\iint_S h^*_{uvx} e^{j\vec{\lambda}_\rho \cdot \vec{\rho}} dS = C_x \left(\frac{(e^{j(a\lambda_x)}(-1)^u - 1)}{((\frac{u\pi}{a})^2 - \lambda_x^2)} \frac{\lambda_y (e^{j(b\lambda_y)}(-1)^v - 1)}{((\frac{v\pi}{b})^2 - \lambda_y^2)} \right)} \tag{C.23}$$

$$C_y = \begin{cases} \frac{-j(\frac{v\pi}{b})^2}{Z^{TE}_{uv}}^*, & h^*_{uvy} \implies h^{*\ TE}_{uvy} \\ \frac{-j\frac{u\pi}{a}\frac{v\pi}{b}}{Z^{TM}_{uv}}^*, & h^*_{uvy} \implies h^{*\ TM}_{uvy} \end{cases} \tag{C.24}$$

such that

$$\boxed{\iint_S h^*_{uvy} e^{j\vec{\lambda}_\rho \cdot \vec{\rho}} dS = C_y \left(\frac{(e^{j(b\lambda_y)}(-1)^v - 1)}{((\frac{v\pi}{b})^2 - \lambda_y^2)} \frac{\lambda_x (e^{j(a\lambda_x)}(-1)^u - 1)}{((\frac{u\pi}{a})^2 - \lambda_x^2)} \right)} \tag{C.25}$$

For convenience the above testing integrals can be regrouped:

$$C_x = \begin{cases} \frac{-j(\frac{v\pi}{b})^2}{Z^{TE}_{uv}}^*, & h^*_{uvx} \implies h^{*\ TE}_{uvx} \\ -\frac{j\frac{u\pi}{a}\frac{v\pi}{b}}{Z^{TM}_{uv}}^*, & h^*_{uvx} \implies h^{*\ TM}_{uvx} \end{cases} \tag{C.26}$$

such that

$$\boxed{\iint_S h^*_{uvx} e^{j\vec{\lambda}_\rho \cdot \vec{\rho}} dS = C_x \left(\frac{(e^{j(b\lambda_x)}(-1)^v - 1)}{((\frac{v\pi}{b})^2 - \lambda_x^2)} \frac{\lambda_y (e^{j(a\lambda_y)}(-1)^u - 1)}{((\frac{u\pi}{a})^2 - \lambda_y^2)} \right)} \tag{C.27}$$

$$C_y = \begin{cases} \frac{-j(\frac{u\pi}{b})^2}{Z^{TE}_{uv}}^*, & h^*_{uvy} \implies h^{*\ TE}_{uvy} \\ \frac{j\frac{u\pi}{a}\frac{v\pi}{b}}{Z^{TM}_{uv}}^*, & h^*_{uvy} \implies h^{*\ TM}_{uvy} \end{cases} \tag{C.28}$$

such that

$$\boxed{\iint_S h^*_{uvy} e^{j\vec{\lambda}_\rho \cdot \vec{\rho}} dS = C_y \left(\frac{(e^{j(a\lambda_y)}(-1)^u - 1)}{((\frac{u\pi}{a})^2 - \lambda_y^2)} \frac{\lambda_x (e^{j(b\lambda_x)}(-1)^v - 1)}{((\frac{v\pi}{b})^2 - \lambda_x^2)} \right)} \tag{C.29}$$

Three other integrals need to be evaluated, with the underlying assumption of mode orthogonality. For TE testing on TE expansion modes $u = m$ and $v = n$ yields a solution, while $u \neq m$ and $v \neq n$ results in zero. The same is said for TM modes. Testing TE modes on TM expansion modes or visa versa will yield zero. Recalling

$$\boxed{\vec{h}_{mn}^{TE} = \hat{y}\frac{k_y}{Z_{mn}^{TE}}\cos(k_x x)\sin(k_y y) + \hat{x}\frac{k_x}{Z_{mn}^{TE}}\sin(k_x x)\cos(k_y y)} \tag{C.30}$$

$$\boxed{\vec{h}_{mn}^{TM} = \hat{y}\frac{k_x}{Z_{mn}^{TM}}\cos(k_x x)\sin(k_y y) - \hat{x}\frac{k_y}{Z_{mn}^{TM}}\sin(k_x x)\cos(k_y y)} \tag{C.31}$$

$$\vec{h}_{mn}^{TE} = \hat{x}\frac{k_y}{Z_{mn}^{TE}}\cos(k_x y)\sin(k_y x) + \hat{y}\frac{k_x}{Z_{mn}^{TE}}\sin(k_x y)\cos(k_y x) \tag{C.32}$$

$$\vec{h}_{mn}^{TM} = \hat{x}\frac{k_x}{Z_{mn}^{TM}}\cos(k_x y)\sin(k_y x) - \hat{y}\frac{k_y}{Z_{mn}^{TM}}\sin(k_x y)\cos(k_y x) \tag{C.33}$$

$$\begin{aligned}
\iint_S \vec{h}_{uv}^{*} \cdot \{\vec{h}_{10}^{TE}\} dS = \iint_S h_{uvx}^{*} h_{10\ x}^{TE} + h_{uvy}^{*} h_{10\ y}^{TE} dS = \\
\iint_S h_{uvx}^{*} h_{10\ x}^{TE} dS + \iint_S h_{uvy}^{*} h_{10\ y}^{TE} dS = \\
\int_0^b \int_0^a \frac{\frac{u\pi}{a}}{Z_{uv}^{TE*}} \sin(\frac{u\pi}{a}x)\cos(\frac{v\pi}{b}y)\frac{\frac{\pi}{a}}{Z_{10}^{TE}}\sin(\frac{\pi}{a}x)dxdy + 0 = \\
\frac{\frac{u\pi}{a}}{Z_{uv}^{TE*}}\frac{\frac{\pi}{a}}{Z_{10}^{TE}} \int_0^a \sin(\frac{u\pi}{a}x)\sin(\frac{\pi}{a}x)dx \int_0^b \cos(\frac{v\pi}{b}y)dy = \\
\left(\frac{(\frac{\pi}{a})^2}{Z_{10}^{TE*}Z_{10}^{TE}}\right) \int_0^a \sin^2(\frac{\pi}{a}x)dx \int_0^b dy = \left(\frac{(\frac{\pi}{a})^2}{Z_{10}^{TE*}Z_{10}^{TE}}\right) \int_0^a \sin^2(\frac{\pi}{a}x)dx \cdot b = \left(\frac{(\frac{\pi}{a})^2}{Z_{10}^{TE*}Z_{10}^{TE}}\right)\frac{ab}{2}
\end{aligned} \tag{C.34}$$

$$\iint_S \vec{h}^*_{uv} \cdot \{\vec{h}^{TE}_{10}\} dS = \begin{cases} \left(\frac{(\frac{\pi}{a})^2}{Z^{TE*}_{10} Z^{TE}_{10}}\right) \frac{ab}{2} & u = 1 \quad and \quad v = 0 \\ 0 & u \neq 1 \quad and \quad v \neq 0 \end{cases} \tag{C.35}$$

for only the TE mode. Put it another way:

$$\boxed{\iint_S \vec{h}^*_{uv} \cdot \{\vec{h}^{TE}_{10}\} dS = \left(\frac{(\frac{\pi}{a})^2}{Z^{TE*}_{10} Z^{TE}_{10}}\right) \frac{ab}{2} \delta^{TE}_{uv10}} \tag{C.36}$$

$$\iint_S \vec{h}^*_{uv} \cdot \{\vec{h}^{TE}_{10}\} dS = \iint_S h^*_{uvy} h^{TE}_{10\ y} + h^*_{uvx} h^{TE}_{10\ x} dS =$$

$$\iint_S h^*_{uvy} h^{TE}_{10\ y} dS + \iint_S h^*_{uvx} h^{TE}_{10\ x} dS =$$

$$\int_0^b \int_0^a \frac{\frac{u\pi}{a}}{Z^{TE*}_{uv}} \sin(\frac{u\pi}{a} y) \cos(\frac{v\pi}{b} x) \frac{\frac{\pi}{a}}{Z^{TE}_{10}} \sin(\frac{\pi}{a} y) dy dx + 0 =$$

$$\frac{\frac{u\pi}{a}}{Z^{TE*}_{uv}} \frac{\frac{\pi}{a}}{Z^{TE}_{10}} \int_0^a \sin(\frac{u\pi}{a} y) \sin(\frac{\pi}{a} y) dy \int_0^b \cos(\frac{v\pi}{b} x) dx =$$

$$\left(\frac{(\frac{\pi}{a})^2}{Z^{TE*}_{10} Z^{TE}_{10}}\right) \int_0^a \sin^2(\frac{\pi}{a} y) dy \int_0^b dx = \left(\frac{(\frac{\pi}{a})^2}{Z^{TE*}_{10} Z^{TE}_{10}}\right) \int_0^a \sin^2(\frac{\pi}{a} y) dy \cdot b = \left(\frac{(\frac{\pi}{a})^2}{Z^{TE*}_{10} Z^{TE}_{10}}\right) \frac{ab}{2} \tag{C.37}$$

$$\iint_S \vec{h}^*_{uv} \cdot \{\vec{h}^{TE}_{10}\} dS = \begin{cases} \left(\frac{(\frac{\pi}{a})^2}{Z^{TE*}_{10} Z^{TE}_{10}}\right) \frac{ab}{2} & u = 1 \quad and \quad v = 0 \\ 0 & u \neq 1 \quad and \quad v \neq 0 \end{cases} \tag{C.38}$$

for only the TE mode. Put it another way:

$$\boxed{\iint_S \vec{h}^*_{uv} \cdot \{\vec{h}^{TE}_{10}\} dS = \left(\frac{(\frac{\pi}{a})^2}{Z^{TE*}_{10} Z^{TE}_{10}}\right) \frac{ab}{2} \delta^{TE}_{uv10}} \tag{C.39}$$

$$\iint_S \vec{h}^*_{uv} \cdot \vec{h}^{TE}_{mn} dS = \iint_S h^*_{uvx} h^{TE}_{mnx} + h^*_{uvy} h^{TE}_{mny} dS =$$

$$\iint_S h^*_{uvx} h^{TE}_{mnx} dS + \iint_S h^*_{uvy} h^{TE}_{mny} dS =$$

$$\iint_S \frac{\frac{u\pi}{a}}{Z^{TE*}_{uv}} \sin(\frac{u\pi}{a}x)\cos(\frac{v\pi}{b}y)\frac{\frac{m\pi}{a}}{Z^{TE}_{mn}} \sin(\frac{m\pi}{a}x)\cos(\frac{n\pi}{b}y)dS +$$

$$\iint_S \frac{\frac{v\pi}{b}}{Z^{TE*}_{uv}} \cos(\frac{u\pi}{a}x)\sin(\frac{v\pi}{b}y)\frac{\frac{n\pi}{b}}{Z^{TE}_{mn}} \cos(\frac{m\pi}{a}x)\sin(\frac{n\pi}{b}y)dS =$$

$$\frac{\frac{u\pi}{a}}{Z^{TE*}_{uv}} \frac{\frac{m\pi}{a}}{Z^{TE}_{mn}} \iint_S \sin^2(\frac{m\pi}{a}x)\cos^2(\frac{n\pi}{b}y)dS +$$

$$\frac{\frac{v\pi}{b}}{Z^{TE*}_{uv}} \frac{\frac{n\pi}{b}}{Z^{TE}_{mn}} \iint_S \cos^2(\frac{m\pi}{a}x)\sin^2(\frac{n\pi}{b}y)dS = \tag{C.40}$$

$$\frac{\frac{u\pi}{a}}{Z^{TE*}_{uv}} \frac{\frac{m\pi}{a}}{Z^{TE}_{mn}} \int_0^a \sin^2(\frac{m\pi}{a}x)dx \int_0^b \cos^2(\frac{n\pi}{b}y)dy$$

$$+ \frac{\frac{v\pi}{b}}{Z^{TE*}_{uv}} \frac{\frac{n\pi}{b}}{Z^{TE}_{mn}} \int_0^a \cos^2(\frac{m\pi}{a}x)dx \int_0^b \sin^2(\frac{n\pi}{b}y)dy =$$

$$\frac{(\frac{m\pi}{a})^2}{Z^{TE*}_{mn} Z^{TE}_{mn}} \frac{a}{2}\frac{b}{2} + \frac{(\frac{n\pi}{b})^2}{Z^{TE*}_{mn} Z^{TE}_{mn}} \frac{a}{2}\frac{b}{2}$$

$$= \frac{(\frac{m\pi}{a})^2}{Z^{TE*}_{mn} Z^{TE}_{mn}} \frac{ab}{4} + \frac{(\frac{n\pi}{b})^2}{Z^{TE*}_{mn} Z^{TE}_{mn}} \frac{ab}{4} =$$

$$\left(\left(\frac{m\pi}{a}\right)^2 + \left(\frac{n\pi}{b}\right)^2 \right) \frac{ab}{4 Z^{TE*}_{mn} Z^{TE}_{mn}}$$

$$\iint_S \vec{h}^*_{uv} \cdot \vec{h}^{TE}_{mn} dS = \begin{cases} \left(\left(\frac{m\pi}{a}\right)^2 + \left(\frac{n\pi}{b}\right)^2 \right) \frac{ab}{4 Z^{TE*}_{mn} Z^{TE}_{mn}} & u = m \quad and \quad v = n \\ 0 & u \neq m \quad and \quad v \neq n \end{cases} \tag{C.41}$$

for only the TE mode. Put it another way:

$$\iint_S \vec{h}^*_{uv} \cdot \vec{h}^{TE}_{mn} dS = \left(\left(\frac{m\pi}{a}\right)^2 + \left(\frac{n\pi}{b}\right)^2 \right) \frac{ab}{4 Z^{TE*}_{mn} Z^{TE}_{mn}} \delta^{TE}_{uvmn} \tag{C.42}$$

Notice however this solution does not simplify back to the TE_{10} case therefore the

solution is modified to address the TE_{m0} cases:

$$\boxed{\iint\limits_S \vec{h}^*_{uv}\cdot\vec{h}^{TE}_{mn}dS=\left(\left(\frac{m\pi}{a}\right)^2+\left(\frac{n\pi}{b}\right)^2\right)\frac{ab(1+\delta^{TE}_{uvm0})}{4Z^{TE*}_{mn}Z^{TE}_{mn}}\delta^{TE}_{uvmn}} \tag{C.43}$$

$$\begin{aligned}
\iint\limits_S \vec{h}^*_{uv}\cdot\vec{h}^{TE}_{mn}dS=\iint\limits_S h^*_{uvy}h^{TE}_{mny}+h^*_{uvx}h^{TE}_{mnx}dS=\\
\iint\limits_S h^*_{uvy}h^{TE}_{mny}dS+\iint\limits_S h^*_{uvx}h^{TE}_{mnx}dS=\\
\iint\limits_S \frac{\frac{u\pi}{a}}{Z^{TE*}_{uv}}\sin(\frac{u\pi}{a}y)\cos(\frac{v\pi}{b}x)\frac{\frac{m\pi}{a}}{Z^{TE}_{mn}}\sin(\frac{m\pi}{a}y)\cos(\frac{n\pi}{b}x)dS+\\
\iint\limits_S \frac{\frac{v\pi}{b}}{Z^{TE*}_{uv}}\cos(\frac{u\pi}{a}y)\sin(\frac{v\pi}{b}x)\frac{\frac{n\pi}{b}}{Z^{TE}_{mn}}\cos(\frac{m\pi}{a}y)\sin(\frac{n\pi}{b}x)dS=\\
\frac{\frac{u\pi}{a}}{Z^{TE*}_{uv}}\frac{\frac{m\pi}{a}}{Z^{TE}_{mn}}\iint\limits_S \sin^2(\frac{m\pi}{a}y)\cos^2(\frac{n\pi}{b}x)dS\\
+\frac{\frac{v\pi}{b}}{Z^{TE*}_{uv}}\frac{\frac{n\pi}{b}}{Z^{TE}_{mn}}\iint\limits_S \cos^2(\frac{m\pi}{a}y)\sin^2(\frac{n\pi}{b}x)dS=\\
\frac{\frac{u\pi}{a}}{Z^{TE*}_{uv}}\frac{\frac{m\pi}{a}}{Z^{TE}_{mn}}\int\limits_0^a \sin^2(\frac{m\pi}{a}y)dy\int\limits_0^b \cos^2(\frac{n\pi}{b}x)dx\\
+\frac{\frac{v\pi}{b}}{Z^{TE*}_{uv}}\frac{\frac{n\pi}{b}}{Z^{TE}_{mn}}\int\limits_0^a \cos^2(\frac{m\pi}{a}y)dy\int\limits_0^b \sin^2(\frac{n\pi}{b}x)dx=\\
\frac{(\frac{m\pi}{a})^2}{Z^{TE*}_{mn}Z^{TE}_{mn}}\frac{a}{2}\frac{b}{2}+\frac{(\frac{n\pi}{b})^2}{Z^{TE*}_{mn}Z^{TE}_{mn}}\frac{a}{2}\frac{b}{2}=\frac{(\frac{m\pi}{a})^2}{Z^{TE*}_{mn}Z^{TE}_{mn}}\frac{ab}{4}+\frac{(\frac{n\pi}{b})^2}{Z^{TE*}_{mn}Z^{TE}_{mn}}\frac{ab}{4}=\\
\left(\left(\frac{m\pi}{a}\right)^2+\left(\frac{n\pi}{b}\right)^2\right)\frac{ab}{4Z^{TE*}_{mn}Z^{TE}_{mn}}
\end{aligned} \tag{C.44}$$

$$\iint\limits_S \vec{h}^*_{uv}\cdot\vec{h}^{TE}_{mn}dS=\begin{cases}\left(\left(\frac{m\pi}{a}\right)^2+\left(\frac{n\pi}{b}\right)^2\right)\frac{ab}{4Z^{TE*}_{mn}Z^{TE}_{mn}} & u=m \quad and \quad v=n\\ 0 & u\neq m \quad and \quad v\neq n\end{cases} \tag{C.45}$$

for only the TE mode. Put it another way:

$$\iint_S \vec{h}^*_{uv} \cdot \vec{h}^{TE}_{mn} dS = \left(\left(\frac{m\pi}{a}\right)^2 + \left(\frac{n\pi}{b}\right)^2 \right) \frac{ab}{4 Z^{TE*}_{mn} Z^{TE}_{mn}} \delta^{TE}_{uvmn} \tag{C.46}$$

Notice however this solution does not simplify back to the TE_{10} case therefore the solution is modified to address the TE_{m0} cases:

$$\boxed{\iint_S \vec{h}^*_{uv} \cdot \vec{h}^{TE}_{mn} dS = \left(\left(\frac{m\pi}{a}\right)^2 + \left(\frac{n\pi}{b}\right)^2 \right) \frac{ab(1+\delta^{TE}_{uvm0})}{4 Z^{TE*}_{mn} Z^{TE}_{mn}} \delta^{TE}_{uvmn}} \tag{C.47}$$

$$\begin{aligned}
\iint_S \vec{h}^*_{uv} \cdot \vec{h}^{TM}_{mn} dS &= \iint_S h^*_{uvx} h^{TM}_{mn\,x} + h^*_{uvy} h^{TM}_{mn\,y} dS = \\
&\iint_S h^*_{uvx} h^{TM}_{mn\,x} dS + \iint_S h^*_{uvy} h^{TM}_{mn\,y} dS = \\
\iint_S -\frac{\frac{v\pi}{b}}{Z^{TM*}_{uv}} \sin(\frac{u\pi}{a}x) \cos(\frac{v\pi}{b}y) \frac{-\frac{n\pi}{b}}{Z^{TM}_{mn}} \sin(\frac{m\pi}{a}x) \cos(\frac{n\pi}{b}y) dS \\
+ \iint_S \frac{\frac{u\pi}{a}}{Z^{TM}_{uv}} \cos(\frac{u\pi}{a}x) \sin(\frac{v\pi}{b}y) \frac{\frac{m\pi}{a}}{Z^{TM}_{mn}} \cos(\frac{m\pi}{a}x) \sin(\frac{n\pi}{b}y) dS = \\
-\frac{\frac{v\pi}{b}}{Z^{TM*}_{uv}} \frac{-\frac{n\pi}{b}}{Z^{TM}_{mn}} \iint_S \sin^2(\frac{m\pi}{a}x) \cos^2(\frac{n\pi}{b}y) dS \\
+\frac{\frac{u\pi}{a}}{Z^{TM*}_{uv}} \frac{\frac{m\pi}{a}}{Z^{TM}_{mn}} \iint_S \cos^2(\frac{m\pi}{a}x) \sin^2(\frac{n\pi}{b}y) dS = \\
\frac{\frac{v\pi}{b}}{Z^{TM*}_{uv}} \frac{\frac{n\pi}{b}}{Z^{TM}_{mn}} \int_0^a \sin^2(\frac{m\pi}{a}x) dx \int_0^b \cos^2(\frac{n\pi}{b}y) dy \\
+\frac{\frac{u\pi}{a}}{Z^{TM*}_{uv}} \frac{\frac{m\pi}{a}}{Z^{TM}_{mn}} \int_0^a \cos^2(\frac{m\pi}{a}x) dx \int_0^b \sin^2(\frac{n\pi}{b}y) dy = \\
\frac{(\frac{n\pi}{b})^2}{Z^{TM*}_{mn} Z^{TM}_{mn}} \frac{a}{2} \frac{b}{2} + \frac{(\frac{m\pi}{a})^2}{Z^{TM*}_{mn} Z^{TM}_{mn}} \frac{a}{2} \frac{b}{2} = \frac{(\frac{n\pi}{b})^2}{Z^{TM*}_{mn} Z^{TM}_{mn}} \frac{ab}{4} + \frac{(\frac{m\pi}{a})^2}{Z^{TM*}_{mn} Z^{TM}_{mn}} \frac{ab}{4} = \\
\left(\left(\frac{m\pi}{a}\right)^2 + \left(\frac{n\pi}{b}\right)^2 \right) \frac{ab}{4 Z^{TM*}_{mn} Z^{TM}_{mn}}
\end{aligned} \tag{C.48}$$

$$\iint_S \vec{h}^*_{uv} \cdot \vec{h}^{TM}_{mn} dS = \begin{cases} \left(\left(\frac{m\pi}{a}\right)^2 + \left(\frac{n\pi}{b}\right)^2\right) \frac{ab}{4Z^{TM*}_{mn} Z^{TM}_{mn}} & u = m \quad and \quad v = n \\ 0 & u \neq m \quad and \quad v \neq n \end{cases} \tag{C.49}$$

for only the TE mode. Put it another way:

$$\iint_S \vec{h}^*_{uv} \cdot \vec{h}^{TM}_{mn} dS = \left(\left(\frac{m\pi}{a}\right)^2 + \left(\frac{n\pi}{b}\right)^2\right) \frac{ab}{4Z^{TM*}_{mn} Z^{TM}_{mn}} \delta^{TM}_{uvmn} \tag{C.50}$$

To keep the form consistent with the TE case:

$$\boxed{\iint_S \vec{h}^*_{uv} \cdot \vec{h}^{TM}_{mn} dS = \left(\left(\frac{m\pi}{a}\right)^2 + \left(\frac{n\pi}{b}\right)^2\right) \frac{ab(1+\delta^{TM}_{uvm0})}{4Z^{TM*}_{mn} Z^{TM}_{mn}} \delta^{TM}_{uvmn}} \tag{C.51}$$

$$\iint_S \vec{h}^*_{uv} \cdot \vec{h}^{TM}_{mn} dS = \iint_S h^*_{uvy} h^{TM}_{mn\ y} + h^*_{uvx} h^{TM}_{mn\ x} dS =$$

$$\iint_S h^*_{uvy} h^{TM}_{mn\ y} dS + \iint_S h^*_{uvx} h^{TM}_{mn\ x} dS =$$

$$\iint_S -\frac{\frac{v\pi}{b}}{Z^{TM*}_{uv}} \sin(\frac{u\pi}{a}y)\cos(\frac{v\pi}{b}x) \frac{-\frac{n\pi}{b}}{Z^{TM}_{mn}} \sin(\frac{m\pi}{a}y)\cos(\frac{n\pi}{b}x) dS +$$

$$\iint_S \frac{\frac{u\pi}{a}}{Z^{TM}_{uv}} \cos(\frac{u\pi}{a}y)\sin(\frac{v\pi}{b}x) \frac{\frac{m\pi}{a}}{Z^{TM}_{mn}} \cos(\frac{m\pi}{a}y)\sin(\frac{n\pi}{b}x) dS =$$

$$-\frac{\frac{v\pi}{b}}{Z^{TM*}_{uv}} \frac{-\frac{n\pi}{b}}{Z^{TM}_{mn}} \iint_S \sin^2(\frac{m\pi}{a}y)\cos^2(\frac{n\pi}{b}x) dS + \frac{\frac{u\pi}{a}}{Z^{TM*}_{uv}} \frac{\frac{m\pi}{a}}{Z^{TM}_{mn}} \iint_S \cos^2(\frac{m\pi}{a}y)\sin^2(\frac{n\pi}{b}x) dS =$$

$$\frac{\frac{v\pi}{b}}{Z^{TM*}_{uv}} \frac{\frac{n\pi}{b}}{Z^{TM}_{mn}} \int_0^a \sin^2(\frac{m\pi}{a}y) dy \int_0^b \cos^2(\frac{n\pi}{b}x) dx$$

$$+\frac{\frac{u\pi}{a}}{Z^{TM*}_{uv}} \frac{\frac{m\pi}{a}}{Z^{TM}_{mn}} \int_0^a \cos^2(\frac{m\pi}{a}y) dy \int_0^b \sin^2(\frac{n\pi}{b}x) dx =$$

$$\frac{(\frac{n\pi}{b})^2}{Z^{TM*}_{mn} Z^{TM}_{mn}} \frac{a}{2}\frac{b}{2} + \frac{(\frac{m\pi}{a})^2}{Z^{TM*}_{mn} Z^{TM}_{mn}} \frac{a}{2}\frac{b}{2} = \frac{(\frac{n\pi}{b})^2}{Z^{TM*}_{mn} Z^{TM}_{mn}} \frac{ab}{4} + \frac{(\frac{m\pi}{a})^2}{Z^{TM*}_{mn} Z^{TM}_{mn}} \frac{ab}{4} =$$

$$\left(\left(\frac{m\pi}{a}\right)^2 + \left(\frac{n\pi}{b}\right)^2\right) \frac{ab}{4Z^{TM*}_{mn} Z^{TM}_{mn}} \tag{C.52}$$

$$\iint_S \vec{h}^*_{uv} \cdot \vec{h}^{TM}_{mn} dS = \begin{cases} \left(\left(\frac{m\pi}{a}\right)^2 + \left(\frac{n\pi}{b}\right)^2\right) \frac{ab}{4Z^{TM*}_{mn} Z^{TM}_{mn}} & u = m \quad and \quad v = n \\ 0 & u \neq m \quad and \quad v \neq n \end{cases} \tag{C.53}$$

for only the TE mode. Put it another way:

$$\iint_S \vec{h}^*_{uv} \cdot \vec{h}^{TM}_{mn} dS = \left(\left(\frac{m\pi}{a}\right)^2 + \left(\frac{n\pi}{b}\right)^2\right) \frac{ab}{4Z^{TM*}_{mn} Z^{TM}_{mn}} \delta^{TM}_{uvmn} \tag{C.54}$$

To keep the form consistent with the TE case:

$$\boxed{\iint_S \vec{h}^*_{uv} \cdot \vec{h}^{TM}_{mn} dS = \left(\left(\frac{m\pi}{a}\right)^2 + \left(\frac{n\pi}{b}\right)^2\right) \frac{ab(1+\delta^{TM}_{uvm0})}{4Z^{TM*}_{mn} Z^{TM}_{mn}} \delta^{TM}_{uvmn}} \tag{C.55}$$

Appendix D. Complex Plane Analysis Example

D.1 Complex Plane Integration Example of the Ω Integrals

This example walks through each of the integral cases dictated by the possible pole combinations.

$$\Omega_y = \int_{-\infty}^{\infty} \frac{\lambda_y^4}{k_{ZTE}(\lambda_y^2 - \omega^2\epsilon_x\mu_x)} \frac{\cos(k_{ZTE}d)}{\sin(k_{ZTE}d)} \frac{(e^{j(b\lambda_y)}(-1)^v - 1)}{((\frac{v\pi}{b})^2 - \lambda_y^2)} \frac{(e^{-j(b\lambda_y)}(-1)^n - 1)}{(k_y^2 - \lambda_y^2)} d\lambda_y \tag{D.1}$$

Breaking the integral up into UHP and LHP:

$$\Omega_y = \int_{-\infty}^{\infty} \frac{\lambda_y^4}{k_{ZTE}(\lambda_y^2 - \omega^2\epsilon_x\mu_x)} \frac{\cos(k_{ZTE}d)}{\sin(k_{ZTE}d)} \frac{((-1)^{n+v} - e^{jb\lambda_y}(-1)^v - e^{-jb\lambda_y}(-1)^n + 1)}{((\frac{v\pi}{b})^2 - \lambda_y^2)(k_y^2 - \lambda_y^2)} d\lambda_y \tag{D.2}$$

$$\Omega_y = \int_{-\infty}^{\infty} \frac{\lambda_y^4}{k_{ZTE}(\lambda_y^2 - \omega^2\epsilon_x\mu_x)} \frac{\cos(k_{ZTE}d)}{\sin(k_{ZTE}d)} \frac{((-1)^{n+v} - e^{jb\lambda_y}(-1)^v - e^{-jb\lambda_y}(-1)^n + 1)}{((\frac{v\pi}{b})^2 - \lambda_y^2)(k_y^2 - \lambda_y^2)} d\lambda_y \tag{D.3}$$

$$\Omega_y = \int_{-\infty}^{\infty} \frac{\lambda_y^4}{k_{ZTE}(\lambda_y^2 - \omega^2\epsilon_x\mu_x)} \frac{\cos(k_{ZTE}d)}{\sin(k_{ZTE}d)} \frac{(-1)^{n+v}(1 - e^{jb\lambda_y}(-1)^n) + (1 - e^{-jb\lambda_y}(-1)^n)}{((\frac{v\pi}{b})^2 - \lambda_y^2)(k_y^2 - \lambda_y^2)} d\lambda_y \tag{D.4}$$

UHP:

$$\Omega_y = \int_{-\infty}^{\infty} \frac{\lambda_y^4}{k_{ZTE}(\lambda_y^2 - \omega^2\epsilon_x\mu_x)} \frac{\cos(k_{ZTE}d)}{\sin(k_{ZTE}d)} \frac{(-1)^{n+v}(1 - e^{jb\lambda_y}(-1)^n)}{((\frac{v\pi}{b})^2 - \lambda_y^2)(k_y^2 - \lambda_y^2)} d\lambda_y + \tag{D.5}$$

LHP:

$$\int_{-\infty}^{\infty} \frac{\lambda_y^4}{k_{ZTE}(\lambda_y^2 - \omega^2\epsilon_x\mu_x)} \frac{\cos(k_{ZTE}d)}{\sin(k_{ZTE}d)} \frac{(1 - e^{-jb\lambda_y}(-1)^n)}{((\frac{v\pi}{b})^2 - \lambda_y^2)(k_y^2 - \lambda_y^2)} d\lambda_y \tag{D.6}$$

Case 5 $n = 0$ **and** $v = 0$**.**

$$\Omega_y = \int_{-\infty}^{\infty} \frac{\lambda_y^4}{k_{ZTE}(\lambda_y^2 - \omega^2\epsilon_x\mu_x)} \frac{\cos(k_{ZTE}d)}{\sin(k_{ZTE}d)} \frac{(e^{j(b\lambda_y)}(-1)^v - 1)}{((\frac{v\pi}{b})^2 - \lambda_y^2)} \frac{(e^{-j(b\lambda_y)}(-1)^n - 1)}{(k_y^2 - \lambda_y^2)} d\lambda_y \tag{D.7}$$

Simplifying further:

UHP:

$$\Omega_y = (-1)^{n+v} \int_{-\infty}^{\infty} \frac{\lambda_y^4}{k_{ZTE}(\lambda_y^2 - \omega^2\epsilon_x\mu_x)} \frac{\cos(k_{ZTE}d)}{\sin(k_{ZTE}d)} \frac{(1 - e^{jb\lambda_y}(-1)^n)}{((\frac{v\pi}{b})^2 - \lambda_y^2)(k_y^2 - \lambda_y^2)} d\lambda_y + \tag{D.8}$$

LHP:

$$\int_{-\infty}^{\infty} \frac{\lambda_y^4}{k_{ZTE}(\lambda_y^2 - \omega^2\epsilon_x\mu_x)} \frac{\cos(k_{ZTE}d)}{\sin(k_{ZTE}d)} \frac{(1 - e^{-jb\lambda_y}(-1)^n)}{((\frac{v\pi}{b})^2 - \lambda_y^2)(k_y^2 - \lambda_y^2)} d\lambda_y \tag{D.9}$$

Evaluating each part by inserting the $v = n = 0$:

UHP:

$$\Omega_y = (-1)^{n+v} \int_{-\infty}^{\infty} \frac{\lambda_y^4}{k_{ZTE}(\lambda_y^2 - \omega^2\epsilon_x\mu_x)} \frac{\cos(k_{ZTE}d)}{\sin(k_{ZTE}d)} \frac{(1 - e^{jb\lambda_y}(-1)^n)}{((\frac{v\pi}{b})^2 - \lambda_y^2)(k_y^2 - \lambda_y^2)} d\lambda_y + \tag{D.10}$$

and simplifies to

$$\Omega_y = \int_{-\infty}^{\infty} \frac{\lambda_y^4}{k_{ZTE}(\lambda_y^2 - \omega^2\epsilon_x\mu_x)} \frac{\cos(k_{ZTE}d)}{\sin(k_{ZTE}d)} \frac{(1 - e^{jb\lambda_y})}{(-\lambda_y^2)(-\lambda_y^2)} d\lambda_y + . \tag{D.11}$$

Note that a is removed and results in

$$\Omega_y = \int_{-\infty}^{\infty} \frac{1}{k_{ZTE}(\lambda_y^2 - \omega^2\epsilon_x\mu_x)} \frac{\cos(k_{ZTE}d)}{\sin(k_{ZTE}d)} \frac{(1 - e^{jb\lambda_y})}{1} d\lambda_y + . \tag{D.12}$$

After the simplification the poles are identified.

The k_{ZTE} pole

$$0 = k_{ZTE} = \pm\sqrt{\omega^2\epsilon_x\mu_y - \lambda_x^2 - \frac{\mu_y}{\mu_x}\lambda_y^2} \tag{D.13}$$

results in

$$\lambda_y = \pm\sqrt{\omega^2\epsilon_x\mu_x - \frac{\mu_x}{\mu_y}\lambda_x^2}. \tag{D.14}$$

The $\sin(k_{ZTE}d)$ pole

$$0 = \sin(k_{ZTE}d) \tag{D.15}$$

$$\pm\, l\pi = k_{ZTE}d \tag{D.16}$$

$$\frac{\pm l\pi}{d} = \pm\sqrt{\omega^2\epsilon_x\mu_y - \lambda_x^2 - \frac{\mu_y}{\mu_x}\lambda_y^2} \tag{D.17}$$

$$\left(\frac{l\pi}{d}\right)^2 = \omega^2\epsilon_x\mu_y - \lambda_x^2 - \frac{\mu_y}{\mu_x}\lambda_y^2 \tag{D.18}$$

$$\left(\frac{l\pi}{d}\right)^2 - \omega^2\epsilon_x\mu_y + \lambda_x^2 = -\frac{\mu_y}{\mu_x}\lambda_y^2 \tag{D.19}$$

$$-\frac{\mu_x}{\mu_y}\left(\frac{l\pi}{d}\right)^2 + \frac{\mu_x}{\mu_y}\omega^2\epsilon_x\mu_y - \frac{\mu_x}{\mu_y}\lambda_x^2 = \lambda_y^2 \tag{D.20}$$

becomes

$$\lambda_y = \pm\sqrt{\omega^2\epsilon_x\mu_x - \frac{\mu_x}{\mu_y}\lambda_x^2 - \frac{\mu_x}{\mu_y}\left(\frac{l\pi}{d}\right)^2}. \tag{D.21}$$

The $\lambda_y^2 - \omega^2\epsilon_x\mu_x$ pole, when evaluated

$$0 = \lambda_y^2 - \omega^2\epsilon_x\mu_x \tag{D.22}$$

yields

$$\pm\sqrt{\omega^2\epsilon_x\mu_x} = \lambda_y. \tag{D.23}$$

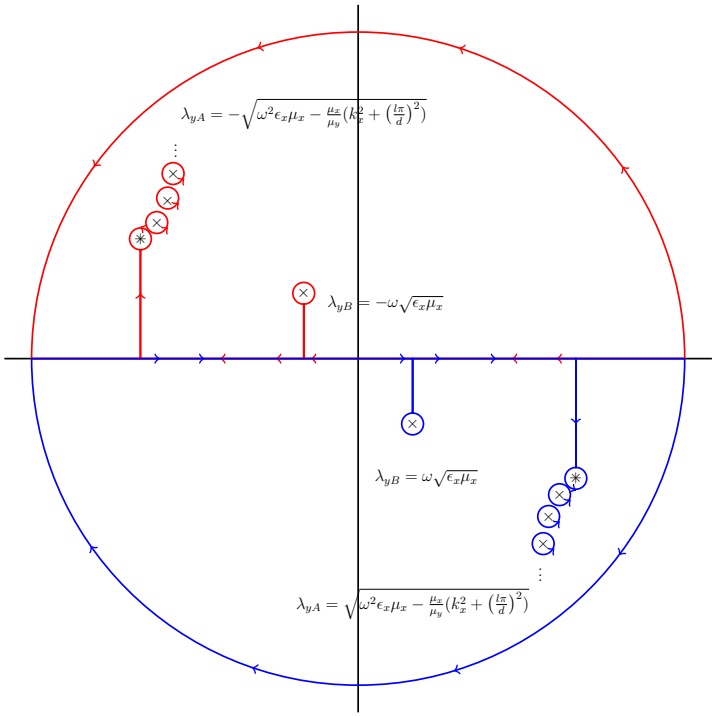

Figure 62. The complex plane showing the poles for the λ_y part of the integral. Note the series of poles induced by the $\sin(k_{ZTE}d)$ part, which represent the modes exhibited in the parallel-plate waveguide structure. A double pole occurs due to $k_{ZTE}\sin(k_{ZTE}d)$ at the $l = 0$ parallel-plate mode. Individual poles are denoted by a $\times$ symbol, while a double pole is denoted by $*$ symbol.

Plotting the poles on the complex plane yields the plot in Figure 62. Applying Jordan's Lemma and evaluating the Upper-Half-Plane (UHP) first,

$$\int_{-\infty}^{\infty} + \oint_{\lambda_{yA}} + \oint_{\lambda_{yB}} + \oint_{C_R} = 0 \tag{D.24}$$

where C_R is the radius at infinity,

$$\int_{-\infty}^{\infty} + \oint_{\lambda_{yA}} + \oint_{\lambda_{yB}} + \cancelto{0}{\oint_{C_R}} = 0 \tag{D.25}$$

and results in

$$\int_{-\infty}^{\infty} = -\oint_{\lambda_{yA}} - \oint_{\lambda_{yB}} \tag{D.26}$$

which is re-written as

$$\int_{-\infty}^{\infty} = \oint_{\lambda_{yA}} + \oint_{\lambda_{yB}} . \tag{D.27}$$

Utilizing Cauchy's Integral Theorem on each pole:

$$\oint_{\lambda_{yA}} \frac{f(z)}{z-z_0} = j2\pi f(z_0) =$$

$$j2\pi \left. \frac{\cos(k_{ZTE}(d))}{k_{ZTE}\sin(k_{ZTE}d)} \frac{(1-e^{j\lambda_y b})}{(\lambda_y - \omega\sqrt{\epsilon_x\mu_x})} \right|_{\lambda_y=-\omega\sqrt{\epsilon_x\mu_x}} =$$

$$j2\pi \left. \frac{\cos(\sqrt{\omega^2\epsilon_x\mu_y - \lambda_x^2 - \frac{\mu_y}{\mu_x}\lambda_y^2}(d))}{\sqrt{\omega^2\epsilon_x\mu_y - \lambda_x^2 - \frac{\mu_y}{\mu_x}\lambda_y^2}\sin(\sqrt{\omega^2\epsilon_x\mu_y - \lambda_x^2 - \frac{\mu_y}{\mu_x}\lambda_y^2}d)} \frac{(1-e^{j\lambda_y b})}{(\lambda_y - \omega\sqrt{\epsilon_x\mu_x})} \right|_{\lambda_y=-\omega\sqrt{\epsilon_x\mu_x}} = \quad \text{(D.28)}$$

$$j2\pi \frac{\cos(\sqrt{-\lambda_x^2}(d))}{\sqrt{-\lambda_x^2}\sin(\sqrt{-\lambda_x^2}d)} \frac{(1-e^{-j\left(\omega\sqrt{\epsilon_x\mu_x}\right)b})}{-2\omega\sqrt{\epsilon_x\mu_x}} =$$

$$j2\pi \frac{\cos(j\lambda_x(d))}{j\lambda_x\sin(j\lambda_x d)} \frac{(1-e^{-j\omega\sqrt{\epsilon_x\mu_x}b})}{-2\omega\sqrt{\epsilon_x\mu_x}} =$$

$$-\pi \frac{\cos(j\lambda_x d)}{\lambda_x\sin(j\lambda_x d)} \frac{(1-e^{-j\omega\sqrt{\epsilon_x\mu_x}b})}{\omega\sqrt{\epsilon_x\mu_x}} =$$

$$\boxed{-\pi \frac{\cos(j\lambda_x d)}{\lambda_x\sin(j\lambda_x d)} \frac{(1-e^{-j\omega\sqrt{\epsilon_x\mu_x}b})}{\omega\sqrt{\epsilon_x\mu_x}}} \quad \text{for UHP Pole } \lambda_{yA}. \quad \text{(D.29)}$$

$\oint_{\lambda_{yB}}$ contains a double pole and is not a simple pole. Additionally it is constituted by a sum of poles, l. When $l = 0$, $\lambda_y = \pm\sqrt{\omega^2\epsilon_x\mu_x - \frac{\mu_x}{\mu_y}\lambda_x^2}$ and when $l \neq 0$, $\lambda_y = \pm\sqrt{\omega^2\epsilon_x\mu_x - \frac{\mu_x}{\mu_y}\lambda_x^2 - \frac{\mu_x}{\mu_y}\left(\frac{l\pi}{d}\right)^2}$.

$$\sum_{l=0}^{\infty} \oint_{\lambda_{yB}} \frac{f(z)}{z - z_0} = j2\pi \sum_{l=0}^{\infty} \frac{f_1(z_0)}{f_2'(z_0)}$$

$$f(\lambda_y) = \frac{\cos(k_{ZTE}(d))}{k_{ZTE}\sin(k_{ZTE}d)} \frac{(1 - e^{j\lambda_y b})}{(\lambda_y - \omega\sqrt{\epsilon_x\mu_x})(\lambda_y + \omega\sqrt{\epsilon_x\mu_x})}$$

Evaluating the l=0 part first:

$$f_1(\lambda_{yl=0}) = \frac{\cos(k_{ZTE}(d))}{1} \frac{(1 - e^{j\lambda_y b})}{(\lambda_y - \omega\sqrt{\epsilon_x\mu_x})(\lambda_y + \omega\sqrt{\epsilon_x\mu_x})} \tag{D.30}$$

$$f_2(\lambda_{yl=0}) = k_{ZTE}\sin(k_{ZTE}d)$$

$$f_2'(\lambda_{yl=0}) = \sin(k_{ZTE}d)\frac{1}{2k_{ZTE}}\left(-2\frac{\mu_y}{\mu_x}\lambda_y d\right) + k_{ZTE}\cos(k_{ZTE}d)\frac{1}{2k_{ZTE}}\left(-2\frac{\mu_y}{\mu_x}k_y d\right)$$

$$f_2'(\lambda_{yl=0}) = -\sin(k_{ZTE}d)\frac{1}{k_{ZTE}}\left(\frac{\mu_y}{\mu_x}\lambda_y d\right) - cos(k_{ZTE}d)\left(\frac{\mu_y}{\mu_x}\lambda_y d\right)$$

$$f_2'(\lambda_{yl=0}) = -\left(\frac{\mu_y}{\mu_x}\lambda_y d\right)\left[\sin(k_{ZTE}d)\frac{1}{k_{ZTE}} + cos(k_{ZTE}d)\right]$$

$$f_2'(\lambda_{yl=0}) = \left(\frac{\mu_y}{\mu_x}\sqrt{\omega^2\epsilon_x\mu_x - \frac{\mu_x}{\mu_y}\lambda_x^2}d\right)[1+1]$$

$$f_2'(\lambda_{yl=0}) = 2\left(\frac{\mu_y}{\mu_x}\sqrt{\omega^2\epsilon_x\mu_x - \frac{\mu_x}{\mu_y}\lambda_x^2}d\right)$$

$$f_1(\lambda_{yl=0}) = \frac{\cos(k_{ZTE}(d))}{1}\frac{(1-e^{j\lambda_y b})}{(\lambda_y - \omega\sqrt{\epsilon_x\mu_x})(\lambda_y + \omega\sqrt{\epsilon_x\mu_x})}$$

$$f_1(\lambda_{yl=0}) = \frac{(1-e^{-j\sqrt{\omega^2\epsilon_x\mu_x - \frac{\mu_x}{\mu_y}\lambda_x^2}b})}{(\sqrt{\omega^2\epsilon_x\mu_x - \frac{\mu_x}{\mu_y}\lambda_x^2} - \omega\sqrt{\epsilon_x\mu_x})(\sqrt{\omega^2\epsilon_x\mu_x - \frac{\mu_x}{\mu_y}\lambda_x^2} + \omega\sqrt{\epsilon_x\mu_x})} \tag{D.31}$$

$$f_1(\lambda_{yl=0}) = \frac{(1-e^{-j\sqrt{\omega^2\epsilon_x\mu_x - \frac{\mu_x}{\mu_y}\lambda_x^2}b})}{(\omega^2\epsilon_x\mu_x - \frac{\mu_x}{\mu_y}\lambda_x^2 - \omega^2\epsilon_x\mu_x)}$$

$$f_1(\lambda_{yl=0}) = \frac{(1-e^{-j\sqrt{\omega^2\epsilon_x\mu_x - \frac{\mu_x}{\mu_y}\lambda_x^2}b})}{-\frac{\mu_x}{\mu_y}\lambda_x^2}$$

$$j2\pi\frac{f_1(\lambda_{yl=0})}{f_2'(\lambda_{yl=0})} = j2\pi\frac{(1-e^{-j\sqrt{\omega^2\epsilon_x\mu_x - \frac{\mu_x}{\mu_y}\lambda_x^2}b})}{-\frac{\mu_x}{\mu_y}\lambda_x^2}\frac{1}{2\frac{\mu_y}{\mu_x}\sqrt{\omega^2\epsilon_x\mu_x - \frac{\mu_x}{\mu_y}\lambda_x^2}d}$$

$$j2\pi\frac{f_1(\lambda_{yl=0})}{f_2'(\lambda_{yl=0})} = j2\pi\frac{(1-e^{-j\sqrt{\omega^2\epsilon_x\mu_x - \frac{\mu_x}{\mu_y}\lambda_x^2}b})}{\frac{\mu_x}{\mu_y}\lambda_x^2}\frac{1}{2\frac{\mu_y}{\mu_x}\sqrt{\omega^2\epsilon_x\mu_x - \frac{\mu_x}{\mu_y}\lambda_x^2}d} \tag{D.32}$$

$$j2\pi\frac{f_1(\lambda_{yl=0})}{f_2'(\lambda_{yl=0})} = j2\pi\frac{(1-e^{-j\sqrt{\omega^2\epsilon_x\mu_x - \frac{\mu_x}{\mu_y}\lambda_x^2}b})}{-\lambda_x^2}\frac{1}{2\sqrt{\omega^2\epsilon_x\mu_x - \frac{\mu_x}{\mu_y}\lambda_x^2}d} \tag{D.33}$$

$$\sum_{l=0}^{\infty} \oint_{\lambda_{yB}} \frac{f(z)}{z-z_0} = j2\pi \sum_{l=0}^{\infty} \frac{f_1(z_0)}{f_2'(z_0)}$$

$$f(\lambda_y) = \frac{\cos(k_{ZTE}(d))}{k_{ZTE}\sin(k_{ZTE}d)} \frac{(1-e^{j\lambda_y b})}{(\lambda_y - \omega\sqrt{\epsilon_x\mu_x})(\lambda_y + \omega\sqrt{\epsilon_x\mu_x})}$$

Evaluating the $l \neq 0$ case second:

$$f_1(\lambda_{yl\neq 0}) = \frac{\cos(k_{ZTE}(d))}{k_{ZTE}} \frac{(1-e^{j\lambda_y b})}{(\lambda_y - \omega\sqrt{\epsilon_x\mu_x})(\lambda_y + \omega\sqrt{\epsilon_x\mu_x})}$$

$$f_2(\lambda_{yl\neq 0}) = \sin(k_{ZTE}d)$$

$$f_2'(\lambda_{yl\neq 0}) = \cos(k_{ZTE}d)\frac{1}{2k_{ZTE}}\left(-2\frac{\mu_y}{\mu_x}\lambda_y d\right) \tag{D.34}$$

$$f_2'(\lambda_{yl\neq 0}) = -\cos(k_{ZTE}d)\frac{1}{k_{ZTE}}\left(\frac{\mu_y}{\mu_x}\lambda_y d\right)$$

$$f_2'(\lambda_{yl\neq 0}) = \frac{(-1)^l}{\pm\frac{l\pi}{d}}\left(\frac{\mu_y}{\mu_x}\sqrt{\omega^2\epsilon_x\mu_x - \frac{\mu_x}{\mu_y}\lambda_x^2 - \frac{\mu_x}{\mu_y}\left(\frac{l\pi}{d}\right)^2}\, d\right)$$

$$f_1(\lambda_{yl\neq 0}) = \frac{\cos(k_{ZTE}(d))}{k_{ZTE}} \frac{(1-e^{j\lambda_y b})}{(\lambda_y - \omega\sqrt{\epsilon_x\mu_x})(\lambda_y + \omega\sqrt{\epsilon_x\mu_x})}$$

$$f_1(\lambda_{yl\neq 0}) = \frac{(-1)^l}{\frac{l\pi}{d}} \frac{(1-e^{-j\sqrt{\omega^2\epsilon_x\mu_x - \frac{\mu_x}{\mu_y}\lambda_x^2 - \frac{\mu_x}{\mu_y}\left(\frac{l\pi}{d}\right)^2}\, b})}{(\omega^2\epsilon_x\mu_x - \frac{\mu_x}{\mu_y}\lambda_x^2 - \frac{\mu_x}{\mu_y}\left(\frac{l\pi}{d}\right)^2 - \omega^2\epsilon_x\mu_x)}$$

$$f_1(\lambda_{yl\neq 0}) = \frac{(-1)^l}{\frac{l\pi}{d}} \frac{(1-e^{-j\sqrt{\omega^2\epsilon_x\mu_x - \frac{\mu_x}{\mu_y}\lambda_x^2 - \frac{\mu_x}{\mu_y}\left(\frac{l\pi}{d}\right)^2}\, b})}{-\frac{\mu_x}{\mu_y}(\lambda_x^2 + \left(\frac{l\pi}{d}\right)^2)} \tag{D.35}$$

$$j2\pi\frac{f_1(\lambda_{yl\neq 0})}{f_2'(\lambda_{yl\neq 0})} = j2\pi\frac{(-1)^l}{\frac{l\pi}{d}}\frac{(1-e^{-j\sqrt{\omega^2\epsilon_x\mu_x-\frac{\mu_x}{\mu_y}\lambda_x^2-\frac{\mu_x}{\mu_y}\left(\frac{l\pi}{d}\right)^2}b})}{-\frac{\mu_x}{\mu_y}(\lambda_x^2+\left(\frac{l\pi}{d}\right)^2)}\cdot \frac{\pm\frac{l\pi}{d}}{(-1)^l}\left(\frac{\mu_x}{\mu_y}\frac{1}{\sqrt{\omega^2\epsilon_x\mu_x-\frac{\mu_x}{\mu_y}\lambda_x^2-\frac{\mu_x}{\mu_y}\left(\frac{l\pi}{d}\right)^2}d}\right) \tag{D.36}$$

$$= j2\pi\frac{f_1(\lambda_{yl\neq 0})}{f_2'(\lambda_{yl\neq 0})} = j2\pi\frac{(1-e^{-j\sqrt{\omega^2\epsilon_x\mu_x-\frac{\mu_x}{\mu_y}\lambda_x^2-\frac{\mu_x}{\mu_y}\left(\frac{l\pi}{d}\right)^2}b})}{-(\lambda_x^2+\left(\frac{l\pi}{d}\right)^2)\sqrt{\omega^2\epsilon_x\mu_x-\frac{\mu_x}{\mu_y}\lambda_x^2-\frac{\mu_x}{\mu_y}\left(\frac{l\pi}{d}\right)^2}d} \tag{D.37}$$

Combining the $l\neq 0$ and $l=0$ parts:

$$j2\pi\frac{f_1(\lambda_{yl=0})}{f_2'(\lambda_{yl=0})} = j2\pi\frac{(1-e^{-j\sqrt{\omega^2\epsilon_x\mu_x-\frac{\mu_x}{\mu_y}\lambda_x^2}b})}{-\lambda_x^2 2\sqrt{\omega^2\epsilon_x\mu_x-\frac{\mu_x}{\mu_y}\lambda_x^2}d} \tag{D.38}$$

$$j2\pi\frac{f_1(\lambda_{yl\neq 0})}{f_2'(\lambda_{yl\neq 0})} = j2\pi\frac{(1-e^{-j\sqrt{\omega^2\epsilon_x\mu_x-\frac{\mu_x}{\mu_y}\lambda_x^2-\frac{\mu_x}{\mu_y}\left(\frac{l\pi}{d}\right)^2}b})}{-(\lambda_x^2+\left(\frac{l\pi}{d}\right)^2)\sqrt{\omega^2\epsilon_x\mu_x-\frac{\mu_x}{\mu_y}\lambda_x^2-\frac{\mu_x}{\mu_y}\left(\frac{l\pi}{d}\right)^2}d} \tag{D.39}$$

$$\boxed{-j2\pi\sum_{l=0}^{\infty}\frac{(1-e^{-j\sqrt{\omega^2\epsilon_x\mu_x-\frac{\mu_x}{\mu_y}\lambda_x^2-\frac{\mu_x}{\mu_y}\left(\frac{l\pi}{d}\right)^2}b})}{(\lambda_x^2+\left(\frac{l\pi}{d}\right)^2)\sqrt{\omega^2\epsilon_x\mu_x-\frac{\mu_x}{\mu_y}\lambda_x^2-\frac{\mu_x}{\mu_y}\left(\frac{l\pi}{d}\right)^2}d(1+\delta_{l=0})}} \quad \text{for UHP Pole } \lambda_{yB}. \tag{D.40}$$

LHP:

$$\int_{-\infty}^{\infty} \frac{\lambda_y^4}{k_{ZTE}(\lambda_y^2 - \omega^2\epsilon_x\mu_x)} \frac{\cos(k_{ZTE}d)}{\sin(k_{ZTE}d)} \frac{(1 - e^{-jb\lambda_y}(-1)^n)}{((\frac{v\pi}{b})^2 - \lambda_y^2)(k_y^2 - \lambda_y^2)} d\lambda_y \tag{D.41}$$

$$\int_{-\infty}^{\infty} \frac{\lambda_y^4}{k_{ZTE}(\lambda_y^2 - \omega^2\epsilon_x\mu_x)} \frac{\cos(k_{ZTE}d)}{\sin(k_{ZTE}d)} \frac{(1 - e^{-jb\lambda_y})}{(-\lambda_y^2)(-\lambda_y^2)} d\lambda_y \tag{D.42}$$

$$\int_{-\infty}^{\infty} \frac{1}{k_{ZTE}(\lambda_y^2 - \omega^2\epsilon_x\mu_x)} \frac{\cos(k_{ZTE}d)}{\sin(k_{ZTE}d)} \frac{(1 - e^{-jb\lambda_y})}{1} d\lambda_y \tag{D.43}$$

Identification of the poles:

$$0 = k_{ZTE} = \pm\sqrt{\omega^2\epsilon_x\mu_y - \lambda_x^2 - \frac{\mu_y}{\mu_x}\lambda_y^2} \tag{D.44}$$

$$\lambda_y = \pm\sqrt{\omega^2\epsilon_x\mu_x - \frac{\mu_x}{\mu_y}\lambda_x^2} \tag{D.45}$$

$$0 = \sin(k_{ZTE}d) \tag{D.46}$$

$$\pm\, l\pi = k_{ZTE}d \tag{D.47}$$

$$\frac{\pm l\pi}{d} = \pm\sqrt{\omega^2\epsilon_x\mu_y - \lambda_x^2 - \frac{\mu_y}{\mu_x}\lambda_y^2} \tag{D.48}$$

$$\left(\frac{l\pi}{d}\right)^2 = \omega^2\epsilon_x\mu_y - \lambda_x^2 - \frac{\mu_y}{\mu_x}\lambda_y^2 \tag{D.49}$$

$$\left(\frac{l\pi}{d}\right)^2 - \omega^2\epsilon_x\mu_y + \lambda_x^2 = -\frac{\mu_y}{\mu_x}\lambda_y^2 \tag{D.50}$$

$$-\frac{\mu_x}{\mu_y}\left(\frac{n\pi}{d}\right)^2 + \frac{\mu_x}{\mu_y}\omega^2\epsilon_x\mu_y - \frac{\mu_x}{\mu_y}\lambda_x^2 = \lambda_y^2 \tag{D.51}$$

$$\lambda_y = \pm\sqrt{\omega^2\epsilon_x\mu_x - \frac{\mu_x}{\mu_y}\lambda_x^2 - \frac{\mu_x}{\mu_y}\left(\frac{l\pi}{d}\right)^2} \tag{D.52}$$

$$0 = \lambda_y^2 - \omega^2\epsilon_x\mu_x \tag{D.53}$$

$$\pm\sqrt{\omega^2\epsilon_x\mu_x} = \lambda_y \tag{D.54}$$

Now evaluating the lower half plane.

$$\int_{-\infty}^{\infty} + \oint_{\lambda_{yA}} + \oint_{\lambda_{yB}} + \oint_{C_R} = 0 \tag{D.55}$$

where C_R is the radius at infinity.

$$\int_{-\infty}^{\infty} + \oint_{\lambda_{yA}} + \oint_{\lambda_{yB}} + \cancelto{0}{\oint_{C_R}} = 0 \tag{D.56}$$

$$\int_{-\infty}^{\infty} = -\oint_{\lambda_{yA}} - \oint_{\lambda_{yB}} \tag{D.57}$$

Evaluating the poles and being careful of the signs:

$$
\begin{aligned}
-\oint_{\lambda_{yA}} \frac{f(z)}{z-z_0} = -j2\pi f(z_0) = \\
-j2\pi \left. \frac{\cos(k_{ZTE}(d))}{k_{ZTE}\sin(k_{ZTE}d)} \frac{(1-e^{-j\lambda_y b})}{(\lambda_y+\omega\sqrt{\epsilon_x\mu_x})} \right|_{\lambda_y=\omega\sqrt{\epsilon_x\mu_x}} = \\
-j2\pi \left. \frac{\cos(\sqrt{\omega^2\epsilon_x\mu_y-\lambda_x^2-\frac{\mu_y}{\mu_x}\lambda_y^2}(d))}{\sqrt{\omega^2\epsilon_x\mu_y-\lambda_x^2-\frac{\mu_y}{\mu_x}\lambda_y^2}\sin(\sqrt{\omega^2\epsilon_x\mu_y-\lambda_x^2-\frac{\mu_y}{\mu_x}\lambda_y^2}d)} \frac{(1-e^{-j\lambda_y b})}{(\lambda_y+\omega\sqrt{\epsilon_x\mu_x})} \right|_{\lambda_y=\omega\sqrt{\epsilon_x\mu_x}} = \\
-j2\pi \frac{\cos(\sqrt{-\lambda_x^2}(d))}{\sqrt{-\lambda_x^2}\sin(\sqrt{-\lambda_x^2}d)} \frac{(1-e^{-j\left(\omega\sqrt{\epsilon_x\mu_x}\right)b})}{2\omega\sqrt{\epsilon_x\mu_x}} = \\
-j2\pi \frac{\cos(j\lambda_x(d))}{j\lambda_x\sin(j\lambda_x d)} \frac{(1-e^{-j\omega\sqrt{\epsilon_x\mu_x}b})}{2\omega\sqrt{\epsilon_x\mu_x}} = \\
-\pi \frac{\cos(j\lambda_x d)}{\lambda_x\sin(j\lambda_x d)} \frac{(1-e^{-j\omega\sqrt{\epsilon_x\mu_x}b})}{\omega\sqrt{\epsilon_x\mu_x}} =
\end{aligned}
\tag{D.58}
$$

$$
\boxed{-\pi \frac{\cos(j\lambda_x d)}{\lambda_x\sin(j\lambda_x d)} \frac{(1-e^{-j\omega\sqrt{\epsilon_x\mu_x}b})}{\omega\sqrt{\epsilon_x\mu_x}}} \qquad \text{for LHP Pole } \lambda_{yA}. \tag{D.59}
$$

$\oint_{\lambda_{yB}}$ contains a double pole and is not a simple pole. Additionally it is constituted by a sum of poles, l. When $l = 0$, $\lambda_y = \pm\sqrt{\omega^2\epsilon_x\mu_x - \frac{\mu_x}{\mu_y}\lambda_x^2}$ and when $l \neq 0$, $\lambda_y = \pm\sqrt{\omega^2\epsilon_x\mu_x - \frac{\mu_x}{\mu_y}\lambda_x^2 - \frac{\mu_x}{\mu_y}\left(\frac{l\pi}{d}\right)^2}$

$$-\sum_{l=0}^{\infty}\oint_{\lambda_{yB}}\frac{f(z)}{z-z_0}=-j2\pi\sum_{l=0}^{\infty}\frac{f_1(z_0)}{f_2'(z_0)}=$$

$$f(\lambda_y)=\frac{\cos(k_{ZTE}(d))}{k_{ZTE}\sin(k_{ZTE}d)}\frac{(1-e^{-j\lambda_y b})}{(\lambda_y-\omega\sqrt{\epsilon_x\mu_x})(\lambda_y+\omega\sqrt{\epsilon_x\mu_x})}$$

Evaluating the l=0 part first:

$$f_1(\lambda_{yl=0})=\frac{\cos(k_{ZTE}(d))}{1}\frac{(1-e^{-j\lambda_y b})}{(\lambda_y-\omega\sqrt{\epsilon_x\mu_x})(\lambda_y+\omega\sqrt{\epsilon_x\mu_x})}$$

$$f_2(\lambda_y)=k_{ZTE}\sin(k_{ZTE}d) \tag{D.60}$$

$$f_2'(\lambda_{yl=0})=\sin(k_{ZTE}d)\frac{1}{2k_{ZTE}}\left(-2\frac{\mu_y}{\mu_x}\lambda_y d\right)+$$

$$k_{ZTE}\cos(k_{ZTE}d)\frac{1}{2k_{ZTE}}\left(-2\frac{\mu_y}{\mu_x}\lambda_y d\right)$$

$$f_2'(\lambda_{yl=0})=-\sin(k_{ZTE}d)\frac{1}{k_{ZTE}}\left(\frac{\mu_y}{\mu_x}\lambda_y d\right)-cos(k_{ZTE}d)\left(\frac{\mu_y}{\mu_x}\lambda_y d\right)$$

$$f_2'(\lambda_{yl=0})=-\left(\frac{\mu_y}{\mu_x}\lambda_y d\right)\left[\sin(k_{ZTE}d)\frac{1}{k_{ZTE}}+cos(k_{ZTE}d)\right]$$

$$f_2'(\lambda_{yl=0}) = -\left(\frac{\mu_y}{\mu_x}\sqrt{\omega^2\epsilon_x\mu_x - \frac{\mu_x}{\mu_y}\lambda_x^2}d\right)[1+1]$$

$$f_2'(\lambda_{yl=0}) = -2\left(\frac{\mu_y}{\mu_x}\sqrt{\omega^2\epsilon_x\mu_x - \frac{\mu_x}{\mu_y}\lambda_x^2}d\right)$$

$$f_1(\lambda_{yl=0}) = \frac{\cos(k_{ZTE}(d))}{1}\frac{(1-e^{-j\lambda_y b})}{(\lambda_y - \omega\sqrt{\epsilon_x\mu_x})(\lambda_y + \omega\sqrt{\epsilon_x\mu_x})}$$

$$f_1(\lambda_{yl=0}) = \frac{(1-e^{-j\sqrt{\omega^2\epsilon_x\mu_x - \frac{\mu_x}{\mu_y}\lambda_x^2}b})}{(\sqrt{\omega^2\epsilon_x\mu_x - \frac{\mu_x}{\mu_y}\lambda_x^2} - \omega\sqrt{\epsilon_x\mu_x})(\sqrt{\omega^2\epsilon_x\mu_x - \frac{\mu_x}{\mu_y}\lambda_x^2} + \omega\sqrt{\epsilon_x\mu_x})} \tag{D.61}$$

$$f_1(\lambda_{yl=0}) = \frac{(1-e^{-j\sqrt{\omega^2\epsilon_x\mu_x - \frac{\mu_x}{\mu_y}\lambda_x^2}b})}{(\omega^2\epsilon_x\mu_x - \frac{\mu_x}{\mu_y}\lambda_x^2 - \omega^2\epsilon_x\mu_x)}$$

$$f_1(\lambda_{yl=0}) = \frac{(1-e^{-j\sqrt{\omega^2\epsilon_x\mu_x - \frac{\mu_x}{\mu_y}\lambda_x^2}b})}{-\frac{\mu_x}{\mu_y}\lambda_x^2}$$

$$-j2\pi\frac{f_1(\lambda_{yl=0})}{f_2'(\lambda_{yl=0})} = -j2\pi\frac{(1-e^{-j\sqrt{\omega^2\epsilon_x\mu_x - \frac{\mu_x}{\mu_y}\lambda_x^2}b})}{-\frac{\mu_x}{\mu_y}\lambda_x^2}\frac{1}{-2\frac{\mu_y}{\mu_x}\sqrt{\omega^2\epsilon_x\mu_x - \frac{\mu_x}{\mu_y}\lambda_x^2}d}$$

$$-j2\pi\frac{f_1(\lambda_{yl=0})}{f_2'(\lambda_{yl=0})} = -j2\pi\frac{(1-e^{-j\sqrt{\omega^2\epsilon_x\mu_x - \frac{\mu_x}{\mu_y}\lambda_x^2}b})}{-\frac{\mu_x}{\mu_y}\lambda_x^2}\frac{1}{-2\frac{\mu_y}{\mu_x}\sqrt{\omega^2\epsilon_x\mu_x - \frac{\mu_x}{\mu_y}\lambda_x^2}d} \tag{D.62}$$

$$-j2\pi\frac{f_1(\lambda_{yl=0})}{f_2'(\lambda_{yl=0})} = -j2\pi\frac{(1-e^{-j\sqrt{\omega^2\epsilon_x\mu_x - \frac{\mu_x}{\mu_y}\lambda_x^2}b})}{-\lambda_x^2}\frac{1}{-2\sqrt{\omega^2\epsilon_x\mu_x - \frac{\mu_x}{\mu_y}\lambda_x^2}d} \tag{D.63}$$

$$-\sum_{l=0}^{\infty}\oint_{\lambda_{yB}}\frac{f(z)}{z-z_0}=-j2\pi\sum_{l=0}^{\infty}\frac{f_1(z_0)}{f_2'(z_0)}=$$

$$f_1(\lambda_y)=\frac{\cos(k_{ZTE}(d))}{k_{ZTE}\sin(k_{ZTE}d)}\frac{(1-e^{-j\lambda_y b})}{(\lambda_y-\omega\sqrt{\epsilon_x\mu_x})(\lambda_y+\omega\sqrt{\epsilon_x\mu_x})}$$

Evaluating the $l\neq 0$ part second:

$$f_1(\lambda_{yl\neq 0})=\frac{\cos(k_{ZTE}(d))}{k_{ZTE}}\frac{(1-e^{-j\lambda_y b})}{(\lambda_y-\omega\sqrt{\epsilon_x\mu_x})(\lambda_y+\omega\sqrt{\epsilon_x\mu_x})}$$

$$f_2(\lambda_{yl\neq 0})=\sin(k_{ZTE}d)$$

$$f_2'(\lambda_{yl\neq 0})=\cos(k_{ZTE}d)\frac{1}{2k_{ZTE}}\left(-2\frac{\mu_y}{\mu_x}\lambda_y d\right) \tag{D.64}$$

$$f_2'(\lambda_{yl\neq 0})=-cos(k_{ZTE}d)\frac{1}{k_{ZTE}}\left(\frac{\mu_y}{\mu_x}\lambda_y d\right)$$

$$f_2'(\lambda_{yl\neq 0})=-\frac{(-1)^l}{\pm\frac{l\pi}{d}}\left(\frac{\mu_y}{\mu_x}\sqrt{\omega^2\epsilon_x\mu_x-\frac{\mu_x}{\mu_y}\lambda_x^2-\frac{\mu_x}{\mu_y}\left(\frac{l\pi}{d}\right)^2}d\right)$$

$$f_1(\lambda_{yl\neq 0})=\frac{\cos(k_{ZTE}(d))}{k_{ZTE}}\frac{(1-e^{-j\lambda_y b})}{(\lambda_y-\omega\sqrt{\epsilon_x\mu_x})(\lambda_y+\omega\sqrt{\epsilon_x\mu_x})}$$

$$f_1(\lambda_{yl\neq 0})=\frac{(-1)^l}{\frac{l\pi}{d}}\frac{(1-e^{-j\sqrt{\omega^2\epsilon_x\mu_x-\frac{\mu_x}{\mu_y}\lambda_x^2-\frac{\mu_x}{\mu_y}\left(\frac{l\pi}{d}\right)^2}b})}{(\omega^2\epsilon_x\mu_x-\frac{\mu_x}{\mu_y}\lambda_x^2-\frac{\mu_x}{\mu_y}\left(\frac{l\pi}{d}\right)^2-\omega^2\epsilon_x\mu_x)}$$

$$f_1(\lambda_{yl\neq 0})=\frac{(-1)^l}{\frac{l\pi}{d}}\frac{(1-e^{-j\sqrt{\omega^2\epsilon_x\mu_x-\frac{\mu_x}{\mu_y}\lambda_x^2-\frac{\mu_x}{\mu_y}\left(\frac{l\pi}{d}\right)^2}b})}{-\frac{\mu_x}{\mu_y}(\lambda_x^2+\left(\frac{l\pi}{d}\right)^2)} \tag{D.65}$$

$$-j2\pi\frac{f_1(\lambda_{yl\neq0})}{f_2'(\lambda_{yl\neq0})}=-j2\pi\frac{(1-e^{-j\sqrt{\omega^2\epsilon_x\mu_x-\frac{\mu_x}{\mu_y}\lambda_x^2-\frac{\mu_x}{\mu_y}\left(\frac{l\pi}{d}\right)^2}b})}{-(\lambda_x^2+\left(\frac{l\pi}{d}\right)^2)(-\sqrt{\omega^2\epsilon_x\mu_x-\frac{\mu_x}{\mu_y}\lambda_x^2-\frac{\mu_x}{\mu_y}\left(\frac{l\pi}{d}\right)^2}d)} \tag{D.66}$$

Combining the $l\neq0$ and $l=0$ cases:

$$j2\pi\frac{f_1(\lambda_{yl\neq0})}{f_2'(\lambda_{yl\neq0})}=j2\pi\frac{(1-e^{-j\sqrt{\omega^2\epsilon_x\mu_x-\frac{\mu_x}{\mu_y}\lambda_x^2}b})}{-\lambda_x^2}\frac{1}{2\sqrt{\omega^2\epsilon_x\mu_x-\frac{\mu_x}{\mu_y}\lambda_x^2}d} \tag{D.67}$$

$$=j2\pi\frac{f_1(\lambda_{yl\neq0})}{f_2'(\lambda_{yl\neq0})}=j2\pi\frac{(1-e^{-j\sqrt{\omega^2\epsilon_x\mu_x-\frac{\mu_x}{\mu_y}\lambda_x^2-\frac{\mu_x}{\mu_y}\left(\frac{l\pi}{d}\right)^2}b})}{-(\lambda_x^2+\left(\frac{l\pi}{d}\right)^2)\sqrt{\omega^2\epsilon_x\mu_x-\frac{\mu_x}{\mu_y}\lambda_x^2-\frac{\mu_x}{\mu_y}\left(\frac{l\pi}{d}\right)^2}d} \tag{D.68}$$

$$\boxed{-j2\pi\sum_{l=0}^{\infty}\frac{(1-e^{-j\sqrt{\omega^2\epsilon_x\mu_x-\frac{\mu_x}{\mu_y}\lambda_x^2-\frac{\mu_x}{\mu_y}\left(\frac{l\pi}{d}\right)^2}b})}{(\lambda_x^2+\left(\frac{l\pi}{d}\right)^2)\sqrt{\omega^2\epsilon_x\mu_x-\frac{\mu_x}{\mu_y}\lambda_x^2-\frac{\mu_x}{\mu_y}\left(\frac{l\pi}{d}\right)^2}d(1+\delta_{l=0})}} \tag{D.69}$$

for LHP Pole λ_{yB}. Adding the upper and lower half plane contributions results in the total solution for Case 5, where

$n = v = 0$:

$$\Omega_y = \int_{-\infty}^{\infty} \frac{\cos(k_{ZTE}(d))}{k_{ZTE}\sin(k_{ZTE}d)} \frac{(1 - e^{j\lambda_y b} + 1 - e^{-j\lambda_y b})}{(\lambda_y^2 - \omega^2\epsilon_x\mu_x)} d\lambda_y =$$

$$-2\pi \frac{\cos(j\lambda_x d)}{\lambda_x \sin(j\lambda_x d)} \frac{(1 - e^{-j\omega\sqrt{\epsilon_x\mu_x}b})}{\omega\sqrt{\epsilon_x\mu_x}} \tag{D.70}$$

$$-j4\pi \sum_{l=0}^{\infty} \frac{(1 - e^{-j\sqrt{\omega^2\epsilon_x\mu_x - \frac{\mu_x}{\mu_y}\lambda_x^2 - \frac{\mu_x}{\mu_y}\left(\frac{l\pi}{d}\right)^2}b})}{(\lambda_x^2 + \left(\frac{l\pi}{d}\right)^2)\sqrt{\omega^2\epsilon_x\mu_x - \frac{\mu_x}{\mu_y}\lambda_x^2 - \frac{\mu_x}{\mu_y}\left(\frac{l\pi}{d}\right)^2} d(1 + \delta_{l=0})}$$

Case 4 $n = 0$ **and** $v \neq 0$**.**

Starting again with the original form

$$\Omega_y = \int_{-\infty}^{\infty} \frac{\lambda_y^4}{k_{ZTE}(\lambda_y^2 - \omega^2\epsilon_x\mu_x)} \frac{\cos(k_{ZTE}d)}{\sin(k_{ZTE}d)} \frac{(e^{j(b\lambda_y)}(-1)^v - 1)}{((\frac{v\pi}{b})^2 - \lambda_y^2)} \frac{(e^{-j(b\lambda_y)}(-1)^n - 1)}{(k_y^2 - \lambda_y^2)} d\lambda_y \tag{D.71}$$

and separating it in the upper and lower half planes:

UHP:

$$\Omega_y = (-1)^{n+v} \int_{-\infty}^{\infty} \frac{\lambda_y^4}{k_{ZTE}(\lambda_y^2 - \omega^2\epsilon_x\mu_x)} \frac{\cos(k_{ZTE}d)}{\sin(k_{ZTE}d)} \frac{(1 - e^{jb\lambda_y}(-1)^n)}{((\frac{v\pi}{b})^2 - \lambda_y^2)(k_y^2 - \lambda_y^2)} d\lambda_y + \tag{D.72}$$

LHP:

$$\int_{-\infty}^{\infty} \frac{\lambda_y^4}{k_{ZTE}(\lambda_y^2 - \omega^2\epsilon_x\mu_x)} \frac{\cos(k_{ZTE}d)}{\sin(k_{ZTE}d)} \frac{(1 - e^{-jb\lambda_y}(-1)^n)}{((\frac{v\pi}{b})^2 - \lambda_y^2)(k_y^2 - \lambda_y^2)} d\lambda_y \tag{D.73}$$

Evaluating the UHP with $n = 0$ and $v \neq 0$:

UHP:

$$\Omega_y = (-1)^{n+v} \int_{-\infty}^{\infty} \frac{\lambda_y^4}{k_{ZTE}(\lambda_y^2 - \omega^2\epsilon_x\mu_x)} \frac{\cos(k_{ZTE}d)}{\sin(k_{ZTE}d)} \frac{(1 - e^{jb\lambda_y}(-1)^n)}{((\frac{v\pi}{b})^2 - \lambda_y^2)(k_y^2 - \lambda_y^2)} d\lambda_y + \tag{D.74}$$

$$\Omega_y = (-1)^{v} \int_{-\infty}^{\infty} \frac{\lambda_y^4}{k_{ZTE}(\lambda_y^2 - \omega^2\epsilon_x\mu_x)} \frac{\cos(k_{ZTE}d)}{\sin(k_{ZTE}d)} \frac{(1 - e^{jb\lambda_y})}{((\frac{v\pi}{b})^2 - \lambda_y^2)(-\lambda_y^2)} d\lambda_y + \tag{D.75}$$

$$\Omega_y = -(-1)^v \int_{-\infty}^{\infty} \frac{\lambda_y^2}{k_{ZTE}(\lambda_y^2 - \omega^2\epsilon_x\mu_x)} \frac{\cos(k_{ZTE}d)}{\sin(k_{ZTE}d)} \frac{(1 - e^{jb\lambda_y})}{((\frac{v\pi}{b})^2 - \lambda_y^2)} d\lambda_y + \tag{D.76}$$

Identification of the poles:

$$\lambda_y = \pm\sqrt{\omega^2\epsilon_x\mu_x - \frac{\mu_x}{\mu_y}\lambda_x^2} \tag{D.77}$$

$$\lambda_y = \pm\sqrt{\omega^2\epsilon_x\mu_x - \frac{\mu_x}{\mu_y}\lambda_x^2 - \frac{\mu_x}{\mu_y}\left(\frac{l\pi}{d}\right)^2} \tag{D.78}$$

$$\pm\sqrt{\omega^2\epsilon_x\mu_x} = \lambda_y \tag{D.79}$$

$$\pm\frac{v\pi}{b} = \lambda_y \tag{D.80}$$

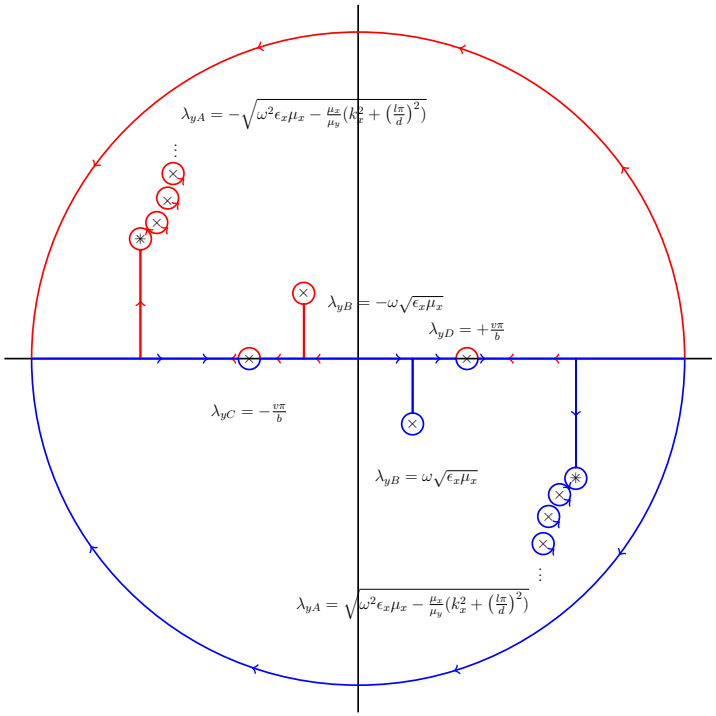

Figure 63. The complex plane showing the poles for the λ_y part of the integral. Note the series of poles induced by the $\sin(k_{ZTE}d)$ part, which represent the modes exhibited in the parallel-plate waveguide structure. A double pole occurs due to $k_{ZTE}\sin(k_{ZTE}d)$ at the $l = 0$ parallel-plate mode. Individual poles are denoted by a $\times$ symbol, while a double pole is denoted by $*$ symbol.

Plotting of all of the poles results in Figure 63. Applying Jordan's Lemma and evaluating the Upper-Half-Plane (UHP) first,

$$\int_{-\infty}^{\infty} + \oint_{\lambda_{yA}} + \oint_{\lambda_{yB}} + \oint_{\lambda_{yC}} + \oint_{\lambda_{yD}} + \oint_{C_R} = 0 \tag{D.81}$$

where C_R is the radius at infinity,

$$\int_{-\infty}^{\infty} + \oint_{\lambda_{yA}} + \oint_{\lambda_{yB}} + \oint_{\lambda_{yC}} + \oint_{\lambda_{yD}} + \cancelto{0}{\oint_{C_R}} = 0 \tag{D.82}$$

and results in

$$\int_{-\infty}^{\infty} = -\oint_{\lambda_{yA}} - \oint_{\lambda_{yB}} - \oint_{\lambda_{yC}} - \oint_{\lambda_{yD}} \tag{D.83}$$

which is re-written as

$$\int_{-\infty}^{\infty} = \oint_{\lambda_{yA}} + \oint_{\lambda_{yB}} + \oint_{\lambda_{yC}} + \oint_{\lambda_{yD}} . \tag{D.84}$$

Utilizing Cauchy's Integral Theorem:

$$\begin{aligned}
\oint_{\lambda_{yB}} \frac{f(z)}{z-z_0} = j2\pi f(z_0) = \\
-(-1)^v j2\pi \left. \frac{\lambda_y^2 \cos(k_{ZTE}(d))}{k_{ZTE}\sin(k_{ZTE}d)} \frac{(1-e^{j\lambda_y b})}{((\frac{v\pi}{b})-\lambda_y)((\frac{v\pi}{b})+\lambda_y)(\lambda_y-\omega\sqrt{\epsilon_x\mu_x})} \right|_{\lambda_y=-\omega\sqrt{\epsilon_x\mu_x}} = \\
j2\pi \frac{\omega\sqrt{\epsilon_x\mu_x}\cos(\sqrt{-\lambda_x^2}(d))}{\sqrt{-\lambda_x^2}\sin(\sqrt{-\lambda_x^2}d)} \frac{(1-e^{-j\left(\omega\sqrt{\epsilon_x\mu_x}\right)b})}{-2((\frac{v\pi}{b})^2-\omega^2\epsilon_x\mu_x)} = \\
j2\pi \frac{\omega\sqrt{\epsilon_x\mu_x}\cos(j\lambda_x(d))}{j\lambda_x\sin(j\lambda_x d)} \frac{(1-e^{-j\omega\sqrt{\epsilon_x\mu_x}b})}{-2((\frac{v\pi}{b})^2-\omega^2\epsilon_x\mu_x)} = \\
-\pi \frac{\omega\sqrt{\epsilon_x\mu_x}\cos(j\lambda_x d)}{\lambda_x\sin(j\lambda_x d)} \frac{(1-e^{-j\omega\sqrt{\epsilon_x\mu_x}b})}{((\frac{v\pi}{b})^2-\omega^2\epsilon_x\mu_x)} =
\end{aligned} \tag{D.85}$$

$$\boxed{(-1)^v \pi\omega\sqrt{\epsilon_x\mu_x}\frac{\cos(j\lambda_x d)}{\lambda_x \sin(j\lambda_x d)}\frac{(1-e^{-j\omega\sqrt{\epsilon_x\mu_x}b})}{((\frac{v\pi}{b})^2-\omega^2\epsilon_x\mu_x)}} \qquad \text{for UHP Pole } \lambda_{yB} \tag{D.86}$$

$\oint_{\lambda_{yA}}$ contains a double pole and is not a simple pole. Additionally it is constituted by a sum of poles, l. When $l = 0$, $\lambda_y = \pm\sqrt{\omega^2\epsilon_x\mu_x - \frac{\mu_x}{\mu_y}\lambda_x^2}$ and when $l \neq 0$, $\lambda_y = \pm\sqrt{\omega^2\epsilon_x\mu_x - \frac{\mu_x}{\mu_y}\lambda_x^2 - \frac{\mu_x}{\mu_y}\left(\frac{l\pi}{d}\right)^2}$. Utilizing Cauchy's Integral Theorem:

$$\sum_{l=0}^{\infty}\oint_{\lambda_{yB}}\frac{f(z)}{z-z_0} = j2\pi\sum_{l=0}^{\infty}\frac{f_1(z_0)}{f_2'(z_0)}$$

$$f(\lambda_y) = \frac{\lambda_y^2}{((\frac{v\pi}{b})-\lambda_y)((\frac{v\pi}{b})+\lambda_y)}\frac{\cos(k_{ZTE}(d))}{k_{ZTE}\sin(k_{ZTE}d)}\frac{(1-e^{j\lambda_y b})}{(\lambda_y-\omega\sqrt{\epsilon_x\mu_x})(\lambda_y+\omega\sqrt{\epsilon_x\mu_x})}$$

Evaluating the l=0 part first:

$$f_1(\lambda_{yl=0}) = \frac{\lambda_y^2}{((\frac{v\pi}{b})-\lambda_y)((\frac{v\pi}{b})+\lambda_y)}\frac{\cos(k_{ZTE}(d))}{1}\frac{(1-e^{j\lambda_y b})}{(\lambda_y-\omega\sqrt{\epsilon_x\mu_x})(\lambda_y+\omega\sqrt{\epsilon_x\mu_x})} \tag{D.87}$$

$$f_2(\lambda_{yl=0}) = k_{ZTE}\sin(k_{ZTE}d)$$

$$f_2'(\lambda_{yl=0}) = \sin(k_{ZTE}d)\frac{1}{2k_{ZTE}}\left(-2\frac{\mu_y}{\mu_x}\lambda_y d\right)$$

$$+k_{ZTE}\cos(k_{ZTE}d)\frac{1}{2k_{ZTE}}\left(-2\frac{\mu_y}{\mu_x}k_y d\right)$$

$$f_2'(\lambda_{yl=0}) = -\sin(k_{ZTE}d)\frac{1}{k_{ZTE}}\left(\frac{\mu_y}{\mu_x}\lambda_y d\right) - cos(k_{ZTE}d)\left(\frac{\mu_y}{\mu_x}\lambda_y d\right)$$

$$f_2'(\lambda_{yl=0}) = -\left(\frac{\mu_y}{\mu_x}\lambda_y d\right)\left[\sin(k_{ZTE}d)\frac{1}{k_{ZTE}} + cos(k_{ZTE}d)\right]$$

$$f_2'(\lambda_{yl=0}) = \left(\frac{\mu_y}{\mu_x}\sqrt{\omega^2\epsilon_x\mu_x - \frac{\mu_x}{\mu_y}\lambda_x^2}d\right)[1+1]$$

$$f_2'(\lambda_{yl=0}) = 2\left(\frac{\mu_y}{\mu_x}\sqrt{\omega^2\epsilon_x\mu_x - \frac{\mu_x}{\mu_y}\lambda_x^2}d\right)$$

$$f_1(\lambda_{yl=0}) = \frac{\lambda_y^2}{((\frac{v\pi}{b}) - \lambda_y)((\frac{v\pi}{b}) + \lambda_y)}\frac{\cos(k_{ZTE}(d))}{1}\frac{(1-e^{j\lambda_y b})}{(\lambda_y - \omega\sqrt{\epsilon_x\mu_x})(\lambda_y + \omega\sqrt{\epsilon_x\mu_x})} \tag{D.88}$$

$$f_1(\lambda_{yl=0}) = \frac{\omega^2\epsilon_x\mu_x - \frac{\mu_x}{\mu_y}\lambda_x^2}{((\frac{v\pi}{b})^2 - \omega^2\epsilon_x\mu_x + \frac{\mu_x}{\mu_y}\lambda_x^2)}\frac{(1-e^{-j\sqrt{\omega^2\epsilon_x\mu_x - \frac{\mu_x}{\mu_y}\lambda_x^2}b})}{(\omega^2\epsilon_x\mu_x - \frac{\mu_x}{\mu_y}\lambda_x^2 - \omega^2\epsilon_x\mu_x)}$$

$$f_1(\lambda_{yl=0}) = \frac{\omega^2\epsilon_x\mu_x - \frac{\mu_x}{\mu_y}\lambda_x^2}{((\frac{v\pi}{b})^2 - \omega^2\epsilon_x\mu_x + \frac{\mu_x}{\mu_y}\lambda_x^2)}\frac{(1-e^{-j\sqrt{\omega^2\epsilon_x\mu_x - \frac{\mu_x}{\mu_y}\lambda_x^2}b})}{-\frac{\mu_x}{\mu_y}\lambda_x^2}$$

$$j2\pi\frac{f_1(\lambda_{yl=0})}{f_2'(\lambda_{yl=0})} = j2\pi\frac{\omega^2\epsilon_x\mu_x - \frac{\mu_x}{\mu_y}\lambda_x^2}{((\frac{v\pi}{b})^2 - \omega^2\epsilon_x\mu_x + \frac{\mu_x}{\mu_y}\lambda_x^2)}\frac{(1-e^{-j\sqrt{\omega^2\epsilon_x\mu_x - \frac{\mu_x}{\mu_y}\lambda_x^2}b})}{-\frac{\mu_x}{\mu_y}\lambda_x^2 2\frac{\mu_y}{\mu_x}\sqrt{\omega^2\epsilon_x\mu_x - \frac{\mu_x}{\mu_y}\lambda_x^2}d}$$

$$j2\pi\frac{f_1(\lambda_{yl=0})}{f_2'(\lambda_{yl=0})} = j2\pi\frac{\omega^2\epsilon_x\mu_x - \frac{\mu_x}{\mu_y}\lambda_x^2}{((\frac{v\pi}{b})^2 - \omega^2\epsilon_x\mu_x + \frac{\mu_x}{\mu_y}\lambda_x^2)}\frac{(1-e^{-j\sqrt{\omega^2\epsilon_x\mu_x - \frac{\mu_x}{\mu_y}\lambda_x^2}b})}{-\frac{\mu_x}{\mu_y}\lambda_x^2 2\frac{\mu_y}{\mu_x}\sqrt{\omega^2\epsilon_x\mu_x - \frac{\mu_x}{\mu_y}\lambda_x^2}d} \tag{D.89}$$

$$j2\pi\frac{f_1(\lambda_{yl=0})}{f_2'(\lambda_{yl=0})} = j2\pi\frac{\sqrt{\omega^2\epsilon_x\mu_x - \frac{\mu_x}{\mu_y}\lambda_x^2}}{((\frac{v\pi}{b})^2 - \omega^2\epsilon_x\mu_x + \frac{\mu_x}{\mu_y}\lambda_x^2)}\frac{(1-e^{-j\sqrt{\omega^2\epsilon_x\mu_x - \frac{\mu_x}{\mu_y}\lambda_x^2}b})}{-\lambda_x^2}\frac{1}{2d} \tag{D.90}$$

$$\sum_{l=0}^{\infty} \oint_{\lambda_{yB}} \frac{f(z)}{z-z_0} = j2\pi \sum_{l=0}^{\infty} \frac{f_1(z_0)}{f_2'(z_0)}$$

$$f(\lambda_y) = j2\pi \frac{\lambda_y^2}{((\frac{v\pi}{b})-\lambda_y)((\frac{v\pi}{b})+\lambda_y)} \frac{\cos(k_{ZTE}(d))}{k_{ZTE}\sin(k_{ZTE}d)} \frac{(1-e^{j\lambda_y b})}{(\lambda_y-\omega\sqrt{\epsilon_x\mu_x})(\lambda_y+\omega\sqrt{\epsilon_x\mu_x})}$$

$l \neq 0$ second

$$f_1(\lambda_{yl\neq 0}) = \frac{\lambda_y^2}{((\frac{v\pi}{b})-\lambda_y)((\frac{v\pi}{b})+\lambda_y)} \frac{\cos(k_{ZTE}(d))}{k_{ZTE}} \frac{(1-e^{j\lambda_y b})}{(\lambda_y-\omega\sqrt{\epsilon_x\mu_x})(\lambda_y+\omega\sqrt{\epsilon_x\mu_x})}$$

$$f_2(\lambda_{yl\neq 0}) = \sin(k_{ZTE}d)$$

$$f_2'(\lambda_{yl\neq 0}) = \cos(k_{ZTE}d)\frac{1}{2k_{ZTE}}\left(-2\frac{\mu_y}{\mu_x}\lambda_y d\right)$$

$$f_2'(\lambda_{yl\neq 0}) = -cos(k_{ZTE}d)\frac{1}{k_{ZTE}}\left(\frac{\mu_y}{\mu_x}\lambda_y d\right) \tag{D.91}$$

$$f_2'(\lambda_{yl\neq 0}) = \frac{(-1)^l}{\pm\frac{l\pi}{d}}\left(\frac{\mu_y}{\mu_x}\sqrt{\omega^2\epsilon_x\mu_x - \frac{\mu_x}{\mu_y}\lambda_x^2 - \frac{\mu_x}{\mu_y}\left(\frac{l\pi}{d}\right)^2}\, d\right)$$

$$f_1(\lambda_{yl\neq 0}) = \frac{\lambda_y^2}{((\frac{v\pi}{b})-\lambda_y)((\frac{v\pi}{b})+\lambda_y)} \frac{\cos(k_{ZTE}(d))}{k_{ZTE}} \frac{(1-e^{j\lambda_y b})}{(\lambda_y-\omega\sqrt{\epsilon_x\mu_x})(\lambda_y+\omega\sqrt{\epsilon_x\mu_x})}$$

$$f_1(\lambda_{yl\neq 0}) = \frac{\omega^2\epsilon_x\mu_x - \frac{\mu_x}{\mu_y}\lambda_x^2 - \frac{\mu_x}{\mu_y}\left(\frac{l\pi}{d}\right)^2}{((\frac{v\pi}{b})^2 - \omega^2\epsilon_x\mu_x + \frac{\mu_x}{\mu_y}\lambda_x^2 + \frac{\mu_x}{\mu_y}\left(\frac{l\pi}{d}\right)^2)} \frac{(-1)^l}{\frac{l\pi}{d}} \cdot \frac{(1-e^{-j\sqrt{\omega^2\epsilon_x\mu_x - \frac{\mu_x}{\mu_y}\lambda_x^2 - \frac{\mu_x}{\mu_y}\left(\frac{l\pi}{d}\right)^2}\, b})}{(\omega^2\epsilon_x\mu_x - \frac{\mu_x}{\mu_y}\lambda_x^2 - \frac{\mu_x}{\mu_y}\left(\frac{l\pi}{d}\right)^2 - \omega^2\epsilon_x\mu_x)}$$

$$f_1(\lambda_{yl\neq 0}) = \frac{\omega^2\epsilon_x\mu_x - \frac{\mu_x}{\mu_y}\lambda_x^2 - \frac{\mu_x}{\mu_y}\left(\frac{l\pi}{d}\right)^2}{((\frac{v\pi}{b})^2 - \omega^2\epsilon_x\mu_x + \frac{\mu_x}{\mu_y}\lambda_x^2 + \frac{\mu_x}{\mu_y}\left(\frac{l\pi}{d}\right)^2)} \frac{(-1)^l}{\frac{l\pi}{d}} \frac{(1 - e^{-j\sqrt{\omega^2\epsilon_x\mu_x - \frac{\mu_x}{\mu_y}\lambda_x^2 - \frac{\mu_x}{\mu_y}\left(\frac{l\pi}{d}\right)^2}b})}{-\frac{\mu_x}{\mu_y}(\lambda_x^2 + \left(\frac{l\pi}{d}\right)^2)} \tag{D.92}$$

$$\begin{aligned} j2\pi\frac{f_1(\lambda_{yl\neq 0})}{f_2'(\lambda_{yl\neq 0})} = j2\pi & \frac{\omega^2\epsilon_x\mu_x - \frac{\mu_x}{\mu_y}\lambda_x^2 - \frac{\mu_x}{\mu_y}\left(\frac{l\pi}{d}\right)^2}{((\frac{v\pi}{b})^2 - \omega^2\epsilon_x\mu_x + \frac{\mu_x}{\mu_y}\lambda_x^2 + \frac{\mu_x}{\mu_y}\left(\frac{l\pi}{d}\right)^2)} \frac{(-1)^l}{\frac{l\pi}{d}} \cdot \\ & \frac{(1 - e^{-j\sqrt{\omega^2\epsilon_x\mu_x - \frac{\mu_x}{\mu_y}\lambda_x^2 - \frac{\mu_x}{\mu_y}\left(\frac{l\pi}{d}\right)^2}b})}{-\frac{\mu_x}{\mu_y}(\lambda_x^2 + \left(\frac{l\pi}{d}\right)^2)} \cdot \\ & \frac{\pm\frac{l\pi}{d}}{(-1)^l}\left(\frac{\mu_x}{\mu_y}\frac{1}{\sqrt{\omega^2\epsilon_x\mu_x - \frac{\mu_x}{\mu_y}\lambda_x^2 - \frac{\mu_x}{\mu_y}\left(\frac{l\pi}{d}\right)^2}d}\right) \end{aligned} \tag{D.93}$$

$$\begin{aligned} j2\pi\frac{f_1(\lambda_{yl\neq 0})}{f_2'(\lambda_{yl\neq 0})} = j2\pi & \frac{\sqrt{\omega^2\epsilon_x\mu_x - \frac{\mu_x}{\mu_y}\lambda_x^2 - \frac{\mu_x}{\mu_y}\left(\frac{l\pi}{d}\right)^2}}{((\frac{v\pi}{b})^2 - \omega^2\epsilon_x\mu_x + \frac{\mu_x}{\mu_y}\lambda_x^2 + \frac{\mu_x}{\mu_y}\left(\frac{l\pi}{d}\right)^2)} \cdot \\ & \frac{(1 - e^{-j\sqrt{\omega^2\epsilon_x\mu_x - \frac{\mu_x}{\mu_y}\lambda_x^2 - \frac{\mu_x}{\mu_y}\left(\frac{l\pi}{d}\right)^2}b})}{-(\lambda_x^2 + \left(\frac{l\pi}{d}\right)^2)} \cdot \left(\frac{1}{d}\right) \end{aligned} \tag{D.94}$$

Combining: $l \neq 0$ and $l = 0$

$$j2\pi\frac{f_1(\lambda_{yl=0})}{f_2'(\lambda_{yl=0})} = j2\pi\frac{\sqrt{\omega^2\epsilon_x\mu_x - \frac{\mu_x}{\mu_y}\lambda_x^2}}{((\frac{v\pi}{b})^2 - \omega^2\epsilon_x\mu_x + \frac{\mu_x}{\mu_y}\lambda_x^2)} \frac{(1 - e^{-j\sqrt{\omega^2\epsilon_x\mu_x - \frac{\mu_x}{\mu_y}\lambda_x^2}b})}{-\lambda_x^2 2d} \tag{D.95}$$

$$j2\pi\frac{f_1(\lambda_{yl\neq 0})}{f_2'(\lambda_{yl\neq 0})} = j2\pi\sum_{l=0}^{\infty}\frac{\sqrt{\omega^2\epsilon_x\mu_x-\frac{\mu_x}{\mu_y}\lambda_x^2-\frac{\mu_x}{\mu_y}\left(\frac{l\pi}{d}\right)^2}}{((\frac{v\pi}{b})^2-\omega^2\epsilon_x\mu_x+\frac{\mu_x}{\mu_y}\lambda_x^2+\frac{\mu_x}{\mu_y}\left(\frac{l\pi}{d}\right)^2)}\frac{(1-e^{-j\sqrt{\omega^2\epsilon_x\mu_x-\frac{\mu_x}{\mu_y}\lambda_x^2-\frac{\mu_x}{\mu_y}\left(\frac{l\pi}{d}\right)^2}b})}{-(\lambda_x^2+\left(\frac{l\pi}{d}\right)^2)d} \tag{D.96}$$

Applying the $(-1)^v$ term to the each part results in:

$$\boxed{= (-1)^v j2\pi\sum_{l=0}^{\infty}\frac{\sqrt{\omega^2\epsilon_x\mu_x-\frac{\mu_x}{\mu_y}\lambda_x^2-\frac{\mu_x}{\mu_y}\left(\frac{l\pi}{d}\right)^2}}{((\frac{v\pi}{b})^2-\omega^2\epsilon_x\mu_x+\frac{\mu_x}{\mu_y}\lambda_x^2+\frac{\mu_x}{\mu_y}\left(\frac{l\pi}{d}\right)^2)}\frac{(1-e^{-j\sqrt{\omega^2\epsilon_x\mu_x-\frac{\mu_x}{\mu_y}\lambda_x^2-\frac{\mu_x}{\mu_y}\left(\frac{l\pi}{d}\right)^2}b})}{(\lambda_x^2+\left(\frac{l\pi}{d}\right)^2)d(1+\delta_{l=0})}} \tag{D.97}$$

which describe the contribution for the λ_{yA} pole.

Evaluating the next pole, λ_{yC}:

$$\begin{aligned}
\oint_{\lambda_{yC}}\frac{f(z)}{z-z_0} = j\pi f(z_0) = \\
-(-1)^v j\pi\ \frac{\lambda_y^2\cos(k_{ZTE}(d))}{k_{ZTE}\sin(k_{ZTE}d)}\frac{(1-e^{j\lambda_y b})}{((\frac{v\pi}{b})-\lambda_y)(\lambda_y-\omega\sqrt{\epsilon_x\mu_x})(\lambda_y+\omega\sqrt{\epsilon_x\mu_x})}\Bigg|_{\lambda_y=-\frac{v\pi}{b}} = \\
-(-1)^v j\pi\frac{(\frac{v\pi}{b})\cos(\sqrt{\omega^2\epsilon_x\mu_y-\lambda_x^2-\frac{\mu_y}{\mu_x}(-\frac{v\pi}{b})^2}(d))}{\sqrt{\omega^2\epsilon_x\mu_y-\lambda_x^2-\frac{\mu_y}{\mu_x}(-\frac{v\pi}{b})^2}\sin(\sqrt{\omega^2\epsilon_x\mu_y-\lambda_x^2-\frac{\mu_y}{\mu_x}(-\frac{v\pi}{b})^2}d)}\frac{(1-e^{-j(\frac{v\pi}{b})b})}{2((\frac{v\pi}{b})^2-\omega^2\epsilon_x\mu_x)} = \\
-j\pi\frac{(\frac{v\pi}{b})\cos(\sqrt{\omega^2\epsilon_x\mu_y-\lambda_x^2-\frac{\mu_y}{\mu_x}(\frac{v\pi}{b})^2}(d))}{\sqrt{\omega^2\epsilon_x\mu_y-\lambda_x^2-\frac{\mu_y}{\mu_x}(\frac{v\pi}{b})^2}\sin(\sqrt{\omega^2\epsilon_x\mu_y-\lambda_x^2-\frac{\mu_y}{\mu_x}(\frac{v\pi}{b})^2}d)}\frac{((-1)^v-1)}{2((\frac{v\pi}{b})^2-\omega^2\epsilon_x\mu_x)} =
\end{aligned} \tag{D.98}$$

$$\boxed{-j\pi\frac{(\frac{v\pi}{b})\cos(\sqrt{\omega^2\epsilon_x\mu_y-\lambda_x^2-\frac{\mu_y}{\mu_x}(\frac{v\pi}{b})^2}(d))}{\sqrt{\omega^2\epsilon_x\mu_y-\lambda_x^2-\frac{\mu_y}{\mu_x}(\frac{v\pi}{b})^2}\sin(\sqrt{\omega^2\epsilon_x\mu_y-\lambda_x^2-\frac{\mu_y}{\mu_x}(\frac{v\pi}{b})^2}d)}\frac{((-1)^v-1)}{2((\frac{v\pi}{b})^2-\omega^2\epsilon_x\mu_x)}} \tag{D.99}$$

Evaluating the next pole, λ_{yD}:

$$\oint_{\lambda_{yD}}\frac{f(z)}{z-z_0}=j\pi f(z_0)=$$

$$-(-1)^v j\pi\left.\frac{\lambda_y^2\cos(k_{ZTE}(d))}{k_{ZTE}\sin(k_{ZTE}d)}\frac{(1-e^{j\lambda_y b})}{((\frac{v\pi}{b})+\lambda_y)(\lambda_y-\omega\sqrt{\epsilon_x\mu_x})(\lambda_y+\omega\sqrt{\epsilon_x\mu_x})}\right|_{\lambda_y=\frac{v\pi}{b}}=$$

$$-(-1)^v j\pi\frac{(\frac{v\pi}{b})\cos(\sqrt{\omega^2\epsilon_x\mu_y-\lambda_x^2-\frac{\mu_y}{\mu_x}(\frac{v\pi}{b})^2}(d))}{\sqrt{\omega^2\epsilon_x\mu_y-\lambda_x^2-\frac{\mu_y}{\mu_x}(\frac{v\pi}{b})^2}\sin(\sqrt{\omega^2\epsilon_x\mu_y-\lambda_x^2-\frac{\mu_y}{\mu_x}(\frac{v\pi}{b})^2}d)}\frac{(1-(-1)^v)}{2((\frac{v\pi}{b})^2-\omega^2\epsilon_x\mu_x)}= \tag{D.100}$$

$$-j\pi\frac{(\frac{v\pi}{b})\cos(\sqrt{\omega^2\epsilon_x\mu_y-\lambda_x^2-\frac{\mu_y}{\mu_x}(\frac{v\pi}{b})^2}(d))}{\sqrt{\omega^2\epsilon_x\mu_y-\lambda_x^2-\frac{\mu_y}{\mu_x}(\frac{v\pi}{b})^2}\sin(\sqrt{\omega^2\epsilon_x\mu_y-\lambda_x^2-\frac{\mu_y}{\mu_x}(\frac{v\pi}{b})^2}d)}\frac{((-1)^v-1)}{2((\frac{v\pi}{b})^2-\omega^2\epsilon_x\mu_x)}=$$

$$\boxed{-j\pi\frac{(\frac{v\pi}{b})\cos(\sqrt{\omega^2\epsilon_x\mu_y-\lambda_x^2-\frac{\mu_y}{\mu_x}(\frac{v\pi}{b})^2}(d))}{\sqrt{\omega^2\epsilon_x\mu_y-\lambda_x^2-\frac{\mu_y}{\mu_x}(\frac{v\pi}{b})^2}\sin(\sqrt{\omega^2\epsilon_x\mu_y-\lambda_x^2-\frac{\mu_y}{\mu_x}(\frac{v\pi}{b})^2}d)}\frac{((-1)^v-1)}{2((\frac{v\pi}{b})^2-\omega^2\epsilon_x\mu_x)}} \tag{D.101}$$

LHP:

$$\int_{-\infty}^{\infty}\frac{\lambda_y^4}{k_{ZTE}(\lambda_y^2-\omega^2\epsilon_x\mu_x)}\frac{\cos(k_{ZTE}d)}{\sin(k_{ZTE}d)}\frac{(1-e^{-jb\lambda_y}(-1)^n)}{((\frac{v\pi}{b})^2-\lambda_y^2)(k_y^2-\lambda_y^2)}d\lambda_y \tag{D.102}$$

$$\int_{-\infty}^{\infty} \frac{\lambda_y^4}{k_{ZTE}(\lambda_y^2 - \omega^2\epsilon_x\mu_x)} \frac{\cos(k_{ZTE}d)}{\sin(k_{ZTE}d)} \frac{(1 - e^{-jb\lambda_y})}{((\frac{v\pi}{b})^2 - \lambda_y^2)(-\lambda_y^2)} d\lambda_y \tag{D.103}$$

$$- \int_{-\infty}^{\infty} \frac{\lambda_y^2}{k_{ZTE}(\lambda_y^2 - \omega^2\epsilon_x\mu_x)} \frac{\cos(k_{ZTE}d)}{\sin(k_{ZTE}d)} \frac{(1 - e^{-jb\lambda_y})}{((\frac{v\pi}{b})^2 - \lambda_y^2)} d\lambda_y \tag{D.104}$$

Identification of the poles:

$$\lambda_y = \pm\sqrt{\omega^2\epsilon_x\mu_x - \frac{\mu_x}{\mu_y}\lambda_x^2} \tag{D.105}$$

$$\lambda_y = \pm\sqrt{\omega^2\epsilon_x\mu_x - \frac{\mu_x}{\mu_y}\lambda_x^2 - \frac{\mu_x}{\mu_y}\left(\frac{l\pi}{d}\right)^2} \tag{D.106}$$

$$\pm\sqrt{\omega^2\epsilon_x\mu_x} = \lambda_y \tag{D.107}$$

$$\pm\frac{v\pi}{b} = \lambda_y \tag{D.108}$$

Now evaluating the lower half plane.

$$\int_{-\infty}^{\infty} + \oint_{\lambda_{yA}} + \oint_{\lambda_{yB}} + \oint_{\lambda_{yC}} + \oint_{\lambda_{yD}} + \oint_{C_R} = 0 \tag{D.109}$$

where C_R is the radius at infinity.

$$\int_{-\infty}^{\infty} + \oint_{\lambda_{yA}} + \oint_{\lambda_{yB}} + \oint_{\lambda_{yC}} + \oint_{\lambda_{yD}} + \cancelto{0}{\oint_{C_R}} = 0 \tag{D.110}$$

$$\int_{-\infty}^{\infty} = -\oint_{\lambda_{yA}} - \oint_{\lambda_{yB}} - \oint_{\lambda_{yC}} - \oint_{\lambda_{yD}} \tag{D.111}$$

The poles in the lower half plane are evaluated:

$$\begin{aligned} -\oint_{\lambda_{yB}} \frac{f(z)}{z - z_0} &= -j2\pi f(z_0) = \\ -j2\pi \left. \frac{\lambda_y^2}{(\frac{\upsilon\pi}{b} - \lambda_y)(\frac{\upsilon\pi}{b} + \lambda_y)} \frac{\cos(k_{ZTE}(d))}{k_{ZTE}\sin(k_{ZTE}d)} \frac{(1 - e^{-j\lambda_y b})}{(\lambda_y + \omega\sqrt{\epsilon_x\mu_x})} \right|_{\lambda_y = \omega\sqrt{\epsilon_x\mu_x}} &= \\ -j2\pi \frac{\omega\sqrt{\epsilon_x\mu_x}}{((\frac{\upsilon\pi}{b})^2 - \omega^2\epsilon_x\mu_x)} \frac{\cos(j\lambda_x(d))}{j\lambda_x\sin(j\lambda_x d)} \frac{(1 - e^{-j\omega\sqrt{\epsilon_x\mu_x}b})}{2} &= \\ -\pi \frac{\omega\sqrt{\epsilon_x\mu_x}}{((\frac{\upsilon\pi}{b})^2 - \omega^2\epsilon_x\mu_x)} \frac{\cos(j\lambda_x d)}{\lambda_x\sin(j\lambda_x d)} \frac{(1 - e^{-j\omega\sqrt{\epsilon_x\mu_x}b})}{1} &= \end{aligned} \tag{D.112}$$

$$\boxed{- - \pi \frac{\omega\sqrt{\epsilon_x\mu_x}}{((\frac{\upsilon\pi}{b})^2 - \omega^2\epsilon_x\mu_x)} \frac{\cos(j\lambda_x d)}{\lambda_x\sin(j\lambda_x d)} \frac{(e^{-j\omega\sqrt{\epsilon_x\mu_x}b} - 1)}{1}} \quad \text{for LHP Pole } \lambda_{yB}. \tag{D.113}$$

$\oint_{\lambda_{yA}}$ contains a double pole and is not a simple pole. Additionally it is constituted by a sum of terms l. When $l = 0$, $\lambda_y = \pm\sqrt{\omega^2\epsilon_x\mu_x - \frac{\mu_x}{\mu_y}\lambda_x^2}$ and when $l \neq 0$, $\lambda_y = \pm\sqrt{\omega^2\epsilon_x\mu_x - \frac{\mu_x}{\mu_y}\lambda_x^2 - \frac{\mu_x}{\mu_y}\left(\frac{l\pi}{d}\right)^2}$

$$-\sum_{l=0}^{\infty}\oint_{\lambda_{yA}}\frac{f(z)}{z-z_0}=-j2\pi\sum_{l=0}^{\infty}\frac{f_1(z_0)}{f_2'(z_0)}$$

$$f(\lambda_y)=\frac{\lambda_y^2}{(\frac{v\pi}{b}-\lambda_y)(\frac{v\pi}{b}+\lambda_y)}\frac{\cos(k_{ZTE}(d))}{k_{ZTE}\sin(k_{ZTE}d)}\frac{(1-e^{-j\lambda_y b})}{(\lambda_y-\omega\sqrt{\epsilon_x\mu_x})(\lambda_y+\omega\sqrt{\epsilon_x\mu_x})}$$

Evaluating the l=0 part first:

$$f_1(\lambda_{yl=0})=\frac{\lambda_y^2}{(\frac{v\pi}{b}-\lambda_y)(\frac{v\pi}{b}+\lambda_y)}\frac{\cos(k_{ZTE}(d))}{1}\frac{(1-e^{-j\lambda_y b})}{(\lambda_y-\omega\sqrt{\epsilon_x\mu_x})(\lambda_y+\omega\sqrt{\epsilon_x\mu_x})} \tag{D.114}$$

$$f_2(\lambda_{yl=0})=k_{ZTE}\sin(k_{ZTE}d)$$

$$f_2'(\lambda_{yl=0})=\sin(k_{ZTE}d)\frac{1}{2k_{ZTE}}\left(-2\frac{\mu_y}{\mu_x}\lambda_y d\right)+$$

$$k_{ZTE}\cos(k_{ZTE}d)\frac{1}{2k_{ZTE}}\left(-2\frac{\mu_y}{\mu_x}\lambda_y d\right)$$

$$f_2'(\lambda_{yl=0})=-\sin(k_{ZTE}d)\frac{1}{k_{ZTE}}\left(\frac{\mu_y}{\mu_x}\lambda_y d\right)-cos(k_{ZTE}d)\left(\frac{\mu_y}{\mu_x}\lambda_y d\right)$$

$$f_2'(\lambda_{yl=0}) = -\left(\frac{\mu_y}{\mu_x}\lambda_y d\right)\left[\sin(k_{ZTE}d)\frac{1}{k_{ZTE}} + cos(k_{ZTE}d)\right]$$

$$f_2'(\lambda_{yl=0}) = -\left(\frac{\mu_y}{\mu_x}\sqrt{\omega^2\epsilon_x\mu_x - \frac{\mu_x}{\mu_y}\lambda_x^2}d\right)[1+1]$$

$$f_2'(\lambda_{yl=0}) = -2\left(\frac{\mu_y}{\mu_x}\sqrt{\omega^2\epsilon_x\mu_x - \frac{\mu_x}{\mu_y}\lambda_x^2}d\right)$$

$$f_1(\lambda_{yl=0}) = \frac{\lambda_y^2}{(\frac{v\pi}{b} - \lambda_y)(\frac{v\pi}{b} + \lambda_y)}\frac{\cos(k_{ZTE}(d))}{1}\frac{(1 - e^{-j\lambda_y b})}{(\lambda_y - \omega\sqrt{\epsilon_x\mu_x})(\lambda_y + \omega\sqrt{\epsilon_x\mu_x})} \tag{D.115}$$

$$f_1(\lambda_{yl=0}) = \frac{\omega^2\epsilon_x\mu_x - \frac{\mu_x}{\mu_y}\lambda_x^2}{((\frac{v\pi}{b})^2 - \omega^2\epsilon_x\mu_x + \frac{\mu_x}{\mu_y}\lambda_x^2)}\frac{(1 - e^{-j\sqrt{\omega^2\epsilon_x\mu_x - \frac{\mu_x}{\mu_y}\lambda_x^2}b})}{-\frac{\mu_x}{\mu_y}\lambda_x^2}$$

$$-j2\pi\frac{f_1(\lambda_{yl=0})}{f_2'(\lambda_{yl=0})} = -j2\pi\frac{\omega^2\epsilon_x\mu_x - \frac{\mu_x}{\mu_y}\lambda_x^2}{((\frac{v\pi}{b})^2 - \omega^2\epsilon_x\mu_x + \frac{\mu_x}{\mu_y}\lambda_x^2)}\frac{(1 - e^{-j\sqrt{\omega^2\epsilon_x\mu_x - \frac{\mu_x}{\mu_y}\lambda_x^2}b})}{-\frac{\mu_x}{\mu_y}\lambda_x^2(-2\frac{\mu_y}{\mu_x}\sqrt{\omega^2\epsilon_x\mu_x - \frac{\mu_x}{\mu_y}\lambda_x^2}d)}$$

$$-j2\pi\frac{f_1(\lambda_{yl=0})}{f_2'(\lambda_{yl=0})} = -j2\pi\frac{\sqrt{\omega^2\epsilon_x\mu_x - \frac{\mu_x}{\mu_y}\lambda_x^2}}{((\frac{v\pi}{b})^2 - \omega^2\epsilon_x\mu_x + \frac{\mu_x}{\mu_y}\lambda_x^2)}\frac{(e^{-j\sqrt{\omega^2\epsilon_x\mu_x - \frac{\mu_x}{\mu_y}\lambda_x^2}b} - 1)}{-\lambda_x^2(-2d)} \tag{D.116}$$

$$-\sum_{l=0}^{\infty}\oint_{\lambda_{yB}}\frac{f(z)}{z-z_0}=-j2\pi\sum_{l=0}^{\infty}\frac{f_1(z_0)}{f_2'(z_0)}=$$

$$f(\lambda_y)=\frac{\lambda_y^2}{(\frac{v\pi}{b}-\lambda_y)(\frac{v\pi}{b}+\lambda_y)}\frac{\cos(k_{ZTE}(d))}{k_{ZTE}\sin(k_{ZTE}d)}\frac{(1-e^{-j\lambda_y b})}{(\lambda_y-\omega\sqrt{\epsilon_x\mu_x})(\lambda_y+\omega\sqrt{\epsilon_x\mu_x})}$$

Evaluating the $l\neq 0$ part second:

$$f_1(\lambda_{yl\neq 0})=\frac{\lambda_y^2}{(\frac{v\pi}{b}-\lambda_y)(\frac{v\pi}{b}+\lambda_y)}\frac{\cos(k_{ZTE}(d))}{k_{ZTE}}\frac{(1-e^{-j\lambda_y b})}{(\lambda_y-\omega\sqrt{\epsilon_x\mu_x})(\lambda_y+\omega\sqrt{\epsilon_x\mu_x})}$$

$$f_2(\lambda_{yl\neq 0})=\sin(k_{ZTE}d) \tag{D.117}$$

$$f_2'(\lambda_{yl\neq 0})=\cos(k_{ZTE}d)\frac{1}{2k_{ZTE}}\left(-2\frac{\mu_y}{\mu_x}\lambda_y d\right)$$

$$f_2'(\lambda_{yl\neq 0})=-cos(k_{ZTE}d)\frac{1}{k_{ZTE}}\left(\frac{\mu_y}{\mu_x}\lambda_y d\right)$$

$$f_2'(\lambda_{yl\neq 0})=-\frac{(-1)^l}{\pm\frac{l\pi}{d}}\left(\frac{\mu_y}{\mu_x}\sqrt{\omega^2\epsilon_x\mu_x-\frac{\mu_x}{\mu_y}\lambda_x^2-\frac{\mu_x}{\mu_y}\left(\frac{l\pi}{d}\right)^2}\,d\right)$$

$$f_1(\lambda_{yl\neq 0})=\frac{\lambda_y^2}{(\frac{v\pi}{b}-\lambda_y)(\frac{v\pi}{b}+\lambda_y)}\frac{\cos(k_{ZTE}(d))}{k_{ZTE}}\frac{(1-e^{-j\lambda_y b})}{(\lambda_y-\omega\sqrt{\epsilon_x\mu_x})(\lambda_y+\omega\sqrt{\epsilon_x\mu_x})}$$

$$f_1(\lambda_{yl\neq 0})=\frac{\omega^2\epsilon_x\mu_x-\frac{\mu_x}{\mu_y}\lambda_x^2-\frac{\mu_x}{\mu_y}\left(\frac{l\pi}{d}\right)^2}{((\frac{v\pi}{b})^2-\omega^2\epsilon_x\mu_x+\frac{\mu_x}{\mu_y}\lambda_x^2+\frac{\mu_x}{\mu_y}\left(\frac{l\pi}{d}\right)^2)}\frac{(-1)^l}{\frac{l\pi}{d}}\frac{(1-e^{-j\sqrt{\omega^2\epsilon_x\mu_x-\frac{\mu_x}{\mu_y}\lambda_x^2-\frac{\mu_x}{\mu_y}\left(\frac{l\pi}{d}\right)^2}b})}{-\frac{\mu_x}{\mu_y}(\lambda_x^2+\left(\frac{l\pi}{d}\right)^2)} \tag{D.118}$$

$$f_1(\lambda_{yl\neq 0})=\frac{\omega^2\epsilon_x\mu_x-\frac{\mu_x}{\mu_y}\left(\lambda_x^2+\left(\frac{l\pi}{d}\right)^2\right)}{((\frac{v\pi}{b})^2-\omega^2\epsilon_x\mu_x+\frac{\mu_x}{\mu_y}\left(\lambda_x^2+\left(\frac{l\pi}{d}\right)^2\right))}\frac{(-1)^l}{\frac{l\pi}{d}}\frac{(e^{-j\sqrt{\omega^2\epsilon_x\mu_x-\frac{\mu_x}{\mu_y}\lambda_x^2-\frac{\mu_x}{\mu_y}\left(\frac{l\pi}{d}\right)^2}b}-1)}{-\frac{\mu_x}{\mu_y}(\lambda_x^2+\left(\frac{l\pi}{d}\right)^2)} \tag{D.119}$$

$$-j2\pi\frac{f_1(\lambda_{yl\neq 0})}{f_2'(\lambda_{yl\neq 0})} = -j2\pi\frac{\omega^2\epsilon_x\mu_x - \frac{\mu_x}{\mu_y}\left(\lambda_x^2 + \left(\frac{l\pi}{d}\right)^2\right)}{((\frac{v\pi}{b})^2 - \omega^2\epsilon_x\mu_x + \frac{\mu_x}{\mu_y}\left(\lambda_x^2 + \left(\frac{l\pi}{d}\right)^2\right))}\cdot$$
$$\frac{(-1)^l}{\frac{l\pi}{d}}\frac{(e^{-j\sqrt{\omega^2\epsilon_x\mu_x - \frac{\mu_x}{\mu_y}\lambda_x^2 - \frac{\mu_x}{\mu_y}\left(\frac{l\pi}{d}\right)^2}b} - 1)}{-\frac{\mu_x}{\mu_y}(\lambda_x^2 + \left(\frac{l\pi}{d}\right)^2)}\cdot -\frac{\pm\frac{l\pi}{d}}{(-1)^l}\left(\frac{\mu_x}{\mu_y}\frac{1}{\sqrt{\omega^2\epsilon_x\mu_x - \frac{\mu_x}{\mu_y}\lambda_x^2 - \frac{\mu_x}{\mu_y}\left(\frac{l\pi}{d}\right)^2 d}}\right) \tag{D.120}$$

$$= -j2\pi\frac{f_1(\lambda_{yl\neq 0})}{f_2'(\lambda_{yl\neq 0})} = -j2\pi\frac{\sqrt{\omega^2\epsilon_x\mu_x - \frac{\mu_x}{\mu_y}\lambda_x^2 - \frac{\mu_x}{\mu_y}\left(\frac{l\pi}{d}\right)^2}}{((\frac{v\pi}{b})^2 - \omega^2\epsilon_x\mu_x + \frac{\mu_x}{\mu_y}\left(\lambda_x^2 + \left(\frac{l\pi}{d}\right)^2\right))}\frac{(e^{-j\sqrt{\omega^2\epsilon_x\mu_x - \frac{\mu_x}{\mu_y}\lambda_x^2 - \frac{\mu_x}{\mu_y}\left(\frac{l\pi}{d}\right)^2}b} - 1)}{(\lambda_x^2 + \left(\frac{l\pi}{d}\right)^2)d} \tag{D.121}$$

Combining: $l \neq 0$ and $l = 0$

$$-j2\pi\frac{f_1(z_0)}{f_2'(z_0)} = -j2\pi\frac{\sqrt{\omega^2\epsilon_x\mu_x - \frac{\mu_x}{\mu_y}\lambda_x^2}}{((\frac{v\pi}{b})^2 - \omega^2\epsilon_x\mu_x + \frac{\mu_x}{\mu_y}\lambda_x^2)}\frac{(e^{-j\sqrt{\omega^2\epsilon_x\mu_x - \frac{\mu_x}{\mu_y}\lambda_x^2}b} - 1)}{-\lambda_x^2}\frac{1}{-2d} \tag{D.122}$$

$$-j2\pi\sum_{l=0}^{\infty}\frac{f_1(\lambda_{yl\neq 0})}{f_2'(\lambda_{yl\neq 0})} =$$
$$-j2\pi\sum_{l=0}^{\infty}\frac{\sqrt{\omega^2\epsilon_x\mu_x - \frac{\mu_x}{\mu_y}\lambda_x^2 - \frac{\mu_x}{\mu_y}\left(\frac{l\pi}{d}\right)^2}}{((\frac{v\pi}{b})^2 - \omega^2\epsilon_x\mu_x + \frac{\mu_x}{\mu_y}\left(\lambda_x^2 + \left(\frac{l\pi}{d}\right)^2\right))}\frac{(e^{-j\sqrt{\omega^2\epsilon_x\mu_x - \frac{\mu_x}{\mu_y}\lambda_x^2 - \frac{\mu_x}{\mu_y}\left(\frac{l\pi}{d}\right)^2}b} - 1)}{(\lambda_x^2 + \left(\frac{l\pi}{d}\right)^2)d} \tag{D.123}$$

$$-j2\pi\sum_{l=0}^{\infty}\frac{f_1(\lambda_{yl\neq 0})}{f_2'(\lambda_{yl\neq 0})}= \tag{D.124}$$

$$-j2\pi\sum_{l=0}^{\infty}\frac{\sqrt{\omega^2\epsilon_x\mu_x-\frac{\mu_x}{\mu_y}\lambda_x^2-\frac{\mu_x}{\mu_y}\left(\frac{l\pi}{d}\right)^2}}{((\frac{v\pi}{b})^2-\omega^2\epsilon_x\mu_x+\frac{\mu_x}{\mu_y}\left(\lambda_x^2+\left(\frac{l\pi}{d}\right)^2\right))}\frac{(e^{-j\sqrt{\omega^2\epsilon_x\mu_x-\frac{\mu_x}{\mu_y}\lambda_x^2-\frac{\mu_x}{\mu_y}\left(\frac{l\pi}{d}\right)^2}b}-1)}{(\lambda_x^2+\left(\frac{l\pi}{d}\right)^2)d(1+\delta_{l=0})}$$

$$\boxed{--j2\pi\sum_{l=0}^{\infty}\frac{\sqrt{\omega^2\epsilon_x\mu_x-\frac{\mu_x}{\mu_y}\lambda_x^2-\frac{\mu_x}{\mu_y}\left(\frac{l\pi}{d}\right)^2}}{((\frac{v\pi}{b})^2-\omega^2\epsilon_x\mu_x+\frac{\mu_x}{\mu_y}\left(\lambda_x^2+\left(\frac{l\pi}{d}\right)^2\right))}\frac{(e^{-j\sqrt{\omega^2\epsilon_x\mu_x-\frac{\mu_x}{\mu_y}\lambda_x^2-\frac{\mu_x}{\mu_y}\left(\frac{l\pi}{d}\right)^2}b}-1)}{(\lambda_x^2+\left(\frac{l\pi}{d}\right)^2)d(1+\delta_{l=0})}} \tag{D.125}$$

for LHP Pole λ_{yA}.

On to the next pole:

$$-\oint_{\lambda_{yC}}\frac{f(z)}{z-z_0}=-j\pi f(z_0)= \tag{D.126}$$

$$-j\pi\left.\frac{\lambda_y^2}{(\frac{v\pi}{b}-\lambda_y)}\frac{\cos(k_{ZTE}(d))}{k_{ZTE}\sin(k_{ZTE}d)}\frac{(1-e^{-j\lambda_y b})}{(\lambda_y+\omega\sqrt{\epsilon_x\mu_x})(\lambda_y-\omega\sqrt{\epsilon_x\mu_x})}\right|_{\lambda_y=-\frac{v\pi}{b}}$$

$$--j\pi\frac{(\frac{v\pi}{b})}{2}\frac{\cos(\sqrt{\omega^2\epsilon_x\mu_y-\lambda_x^2-\frac{\mu_y}{\mu_x}(\frac{v\pi}{b})^2}(d))}{\sqrt{\omega^2\epsilon_x\mu_y-\lambda_x^2-\frac{\mu_y}{\mu_x}(\frac{v\pi}{b})^2}\sin(\sqrt{\omega^2\epsilon_x\mu_y-\lambda_x^2-\frac{\mu_y}{\mu_x}(\frac{v\pi}{b})^2}d)}\frac{(1-(-1)^v)}{((\frac{v\pi}{b})^2-\omega^2\epsilon_x\mu_x)}=$$

$$\boxed{j\pi\frac{(\frac{v\pi}{b})}{2}\frac{\cos(\sqrt{\omega^2\epsilon_x\mu_y-\lambda_x^2-\frac{\mu_y}{\mu_x}(\frac{v\pi}{b})^2}(d))}{\sqrt{\omega^2\epsilon_x\mu_y-\lambda_x^2-\frac{\mu_y}{\mu_x}(\frac{v\pi}{b})^2}\sin(\sqrt{\omega^2\epsilon_x\mu_y-\lambda_x^2-\frac{\mu_y}{\mu_x}(\frac{v\pi}{b})^2}d)}\frac{(1-(-1)^v)}{((\frac{v\pi}{b})^2-\omega^2\epsilon_x\mu_x)}} \tag{D.127}$$

for LHP Pole λ_{yC}.

On to the next pole:

$$-\oint_{\lambda_{yD}} \frac{f(z)}{z-z_0} = -j\pi f(z_0) = \tag{D.128}$$
$$-j\pi \left. \frac{\lambda_y^2}{(\frac{v\pi}{b}+\lambda_y)} \frac{\cos(k_{ZTE}(d))}{k_{ZTE}\sin(k_{ZTE}d)} \frac{(1-e^{-j\lambda_y b})}{(\lambda_y+\omega\sqrt{\epsilon_x\mu_x})(\lambda_y-\omega\sqrt{\epsilon_x\mu_x})} \right|_{\lambda_y=\frac{v\pi}{b}}$$
$$--j\pi\frac{(\frac{v\pi}{b})}{2} \frac{\cos(\sqrt{\omega^2\epsilon_x\mu_y-\lambda_x^2-\frac{\mu_y}{\mu_x}(\frac{v\pi}{b})^2}(d))}{\sqrt{\omega^2\epsilon_x\mu_y-\lambda_x^2-\frac{\mu_y}{\mu_x}(\frac{v\pi}{b})^2}\sin(\sqrt{\omega^2\epsilon_x\mu_y-\lambda_x^2-\frac{\mu_y}{\mu_x}(\frac{v\pi}{b})^2}d)} \frac{(1-(-1)^v)}{((\frac{v\pi}{b})^2-\omega^2\epsilon_x\mu_x)} =$$

$$\boxed{j\pi\frac{(\frac{v\pi}{b})}{2} \frac{\cos(\sqrt{\omega^2\epsilon_x\mu_y-\lambda_x^2-\frac{\mu_y}{\mu_x}(\frac{v\pi}{b})^2}(d))}{\sqrt{\omega^2\epsilon_x\mu_y-\lambda_x^2-\frac{\mu_y}{\mu_x}(\frac{v\pi}{b})^2}\sin(\sqrt{\omega^2\epsilon_x\mu_y-\lambda_x^2-\frac{\mu_y}{\mu_x}(\frac{v\pi}{b})^2}d)} \frac{(1-(-1)^v)}{((\frac{v\pi}{b})^2-\omega^2\epsilon_x\mu_x)}} \tag{D.129}$$

for LHP Pole λ_{yD}.

Combining the upper and lower half plane parts results in the total solution:

$$\Omega_y = \int_{-\infty}^{\infty} \frac{\lambda_y^4}{k_{ZTE}(\lambda_y^2-\omega^2\epsilon_x\mu_x)} \frac{\cos(k_{ZTE}d)}{\sin(k_{ZTE}d)} \frac{(e^{j(b\lambda_y)}(-1)^v-1)}{((\frac{v\pi}{b})^2-\lambda_y^2)} \frac{(e^{-j(b\lambda_y)}(-1)^n-1)}{(k_y^2-\lambda_y^2)} d\lambda_y = \tag{D.130}$$

$$(-1^v+1)\pi\omega\sqrt{\epsilon_x\mu_x}\frac{\cos(j\lambda_x d)}{\lambda_x\sin(j\lambda_x d)}\frac{(1-e^{-j\omega\sqrt{\epsilon_x\mu_x}b})}{((\frac{v\pi}{b})^2-\omega^2\epsilon_x\mu_x)}+$$
$$((-1)^v+1)j2\pi\sum_{l=0}^{\infty}\frac{\sqrt{\omega^2\epsilon_x\mu_x-\frac{\mu_x}{\mu_y}\lambda_x^2-\frac{\mu_x}{\mu_y}\left(\frac{l\pi}{d}\right)^2}}{((\frac{v\pi}{b})^2-\omega^2\epsilon_x\mu_x+\frac{\mu_x}{\mu_y}\lambda_x^2+\frac{\mu_x}{\mu_y}\left(\frac{l\pi}{d}\right)^2)}\frac{(1-e^{-j\sqrt{\omega^2\epsilon_x\mu_x-\frac{\mu_x}{\mu_y}\lambda_x^2-\frac{\mu_x}{\mu_y}\left(\frac{l\pi}{d}\right)^2}b})}{(\lambda_x^2+\left(\frac{l\pi}{d}\right)^2)d(1+\delta_{l=0})}+ \tag{D.131}$$
$$j2\pi\frac{(\frac{v\pi}{b})\cos(\sqrt{\omega^2\epsilon_x\mu_y-\lambda_x^2-\frac{\mu_y}{\mu_x}(\frac{v\pi}{b})^2}(d))}{\sqrt{\omega^2\epsilon_x\mu_y-\lambda_x^2-\frac{\mu_y}{\mu_x}(\frac{v\pi}{b})^2}\sin(\sqrt{\omega^2\epsilon_x\mu_y-\lambda_x^2-\frac{\mu_y}{\mu_x}(\frac{v\pi}{b})^2}d)}\frac{(1-(-1)^v)}{((\frac{v\pi}{b})^2-\omega^2\epsilon_x\mu_x)}$$

Case 3 $n\neq 0$ **and** $v=0$**.**

Starting with the original equation

$$\Omega_y=\int_{-\infty}^{\infty}\frac{\lambda_y^4}{k_{ZTE}(\lambda_y^2-\omega^2\epsilon_x\mu_x)}\frac{\cos(k_{ZTE}d)}{\sin(k_{ZTE}d)}\frac{(e^{j(b\lambda_y)}(-1)^v-1)}{((\frac{v\pi}{b})^2-\lambda_y^2)}\frac{(e^{-j(b\lambda_y)}(-1)^n-1)}{(k_y^2-\lambda_y^2)}d\lambda_y \tag{D.132}$$

and separating the upper and lower half plane parts:

UHP:

$$\Omega_y=(-1)^{n+v}\int_{-\infty}^{\infty}\frac{\lambda_y^4}{k_{ZTE}(\lambda_y^2-\omega^2\epsilon_x\mu_x)}\frac{\cos(k_{ZTE}d)}{\sin(k_{ZTE}d)}\frac{(1-e^{jb\lambda_y}(-1)^n)}{((\frac{v\pi}{b})^2-\lambda_y^2)(k_y^2-\lambda_y^2)}d\lambda_y+ \tag{D.133}$$

LHP:

$$\int_{-\infty}^{\infty}\frac{\lambda_y^4}{k_{ZTE}(\lambda_y^2-\omega^2\epsilon_x\mu_x)}\frac{\cos(k_{ZTE}d)}{\sin(k_{ZTE}d)}\frac{(1-e^{-jb\lambda_y}(-1)^n)}{((\frac{v\pi}{b})^2-\lambda_y^2)(k_y^2-\lambda_y^2)}d\lambda_y \tag{D.134}$$

Evaluating each part:

UHP:

$$\Omega_y = (-1)^{n+v} \int_{-\infty}^{\infty} \frac{\lambda_y^4}{k_{ZTE}(\lambda_y^2 - \omega^2\epsilon_x\mu_x)} \frac{\cos(k_{ZTE}d)}{\sin(k_{ZTE}d)} \frac{(1 - e^{jb\lambda_y}(-1)^n)}{((\frac{v\pi}{b})^2 - \lambda_y^2)(k_y^2 - \lambda_y^2)} d\lambda_y + \tag{D.135}$$

$$\Omega_y = (-1)^{n+v} \int_{-\infty}^{\infty} \frac{\lambda_y^4}{k_{ZTE}(\lambda_y^2 - \omega^2\epsilon_x\mu_x)} \frac{\cos(k_{ZTE}d)}{\sin(k_{ZTE}d)} \frac{(1 - e^{jb\lambda_y}(-1)^n)}{(-\lambda_y^2)(k_y^2 - \lambda_y^2)} d\lambda_y + \tag{D.136}$$

$$\Omega_y = -(-1)^{n} \int_{-\infty}^{\infty} \frac{\lambda_y^2}{k_{ZTE}(\lambda_y^2 - \omega^2\epsilon_x\mu_x)} \frac{\cos(k_{ZTE}d)}{\sin(k_{ZTE}d)} \frac{(1 - e^{jb\lambda_y}(-1)^n)}{(k_y^2 - \lambda_y^2)} d\lambda_y + \tag{D.137}$$

Identification of the poles:

$$\lambda_y = \pm\sqrt{\omega^2\epsilon_x\mu_x - \frac{\mu_x}{\mu_y}\lambda_x^2} \tag{D.138}$$

$$\lambda_y = \pm\sqrt{\omega^2\epsilon_x\mu_x - \frac{\mu_x}{\mu_y}\lambda_x^2 - \frac{\mu_x}{\mu_y}\left(\frac{l\pi}{d}\right)^2} \tag{D.139}$$

$$\pm\sqrt{\omega^2\epsilon_x\mu_x} = \lambda_y \tag{D.140}$$

$$\pm\frac{n\pi}{b} = \lambda_y \tag{D.141}$$

Plotting the poles on the complex plane results in Figure 64.

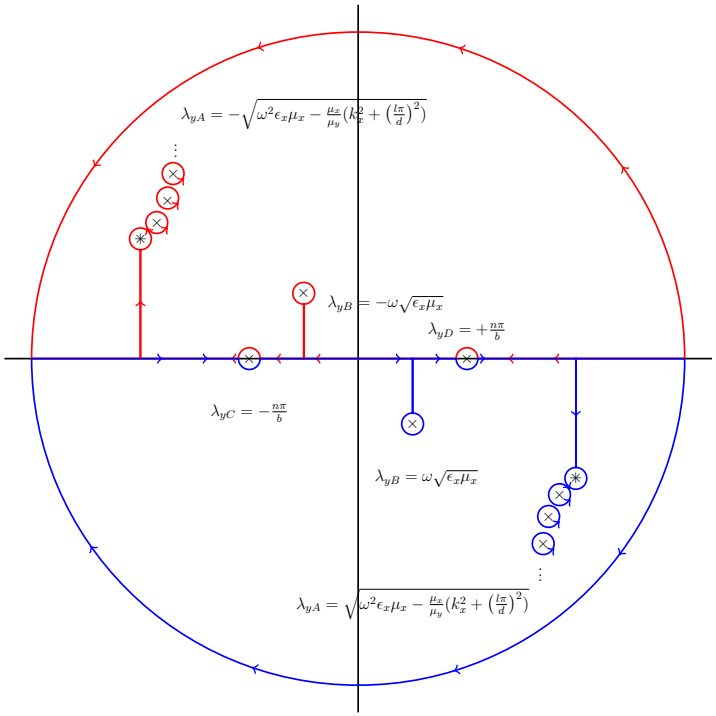

Figure 64. The complex plane showing the poles for the λ_y part of the integral. Note the series of poles induced by the $\sin(k_{ZTE}d)$ part, which represent the modes exhibited in the parallel-plate waveguide structure. A double pole occurs due to $k_{ZTE}\sin(k_{ZTE}d)$ at the $l = 0$ parallel-plate mode. Individual poles are denoted by a $\times$ symbol, while a double pole is denoted by $*$ symbol.

$$\int_{-\infty}^{\infty} + \oint_{\lambda_{yA}} + \oint_{\lambda_{yB}} + \oint_{\lambda_{yC}} + \oint_{\lambda_{yD}} + \oint_{C_R} = 0 \tag{D.142}$$

where C_R is the radius at infinity.

$$\int_{-\infty}^{\infty} + \oint_{\lambda_{yA}} + \oint_{\lambda_{yB}} + \oint_{\lambda_{yC}} + \oint_{\lambda_{yD}} + \cancelto{0}{\oint_{C_R}} = 0 \tag{D.143}$$

$$\int_{-\infty}^{\infty} = -\oint_{\lambda_{yA}} - \oint_{\lambda_{yB}} - \oint_{\lambda_{yC}} - \oint_{\lambda_{yD}} \tag{D.144}$$

$$\int_{-\infty}^{\infty} = \oint_{\lambda_{yA}} + \oint_{\lambda_{yB}} + \oint_{\lambda_{yC}} + \oint_{\lambda_{yD}} \tag{D.145}$$

Utilizing Cauchy's Integral Theorem:

$$\begin{aligned}
\oint_{\lambda_{yB}} \frac{f(z)}{z-z_0} = j2\pi f(z_0) = \\
-(-1)^n j2\pi \left. \frac{\lambda_y^2 \cos(k_{ZTE}(d))}{k_{ZTE}\sin(k_{ZTE}d)} \frac{(1-e^{j\lambda_y b}(-1)^n)}{((\frac{n\pi}{b})-\lambda_y)((\frac{n\pi}{b})+\lambda_y)(\lambda_y-\omega\sqrt{\epsilon_x\mu_x})} \right|_{\lambda_y=-\omega\sqrt{\epsilon_x\mu_x}} = \\
j2\pi \frac{\omega\sqrt{\epsilon_x\mu_x}\cos(\sqrt{-\lambda_x^2}(d))}{\sqrt{-\lambda_x^2}\sin(\sqrt{-\lambda_x^2}d)} \frac{(1-e^{-j\left(\omega\sqrt{\epsilon_x\mu_x}\right)b}(-1)^n)}{-2((\frac{n\pi}{b})^2-\omega^2\epsilon_x\mu_x)} = \\
-\pi \frac{\omega\sqrt{\epsilon_x\mu_x}\cos(j\lambda_x d)}{\lambda_x\sin(j\lambda_x d)} \frac{(1-e^{-j\omega\sqrt{\epsilon_x\mu_x}b}(-1)^n)}{((\frac{n\pi}{b})^2-\omega^2\epsilon_x\mu_x)} =
\end{aligned} \tag{D.146}$$

$$\boxed{+(-1)^n\pi\omega\sqrt{\epsilon_x\mu_x}\frac{\cos(j\lambda_x d)}{\lambda_x\sin(j\lambda_x d)}\frac{(1-e^{-j\omega\sqrt{\epsilon_x\mu_x}b}(-1)^n)}{((\frac{n\pi}{b})^2-\omega^2\epsilon_x\mu_x)}} \quad \text{for UHP Pole } \lambda_{yB} \tag{D.147}$$

$\oint_{\lambda_{yA}}$ contains a double pole and is not a simple pole. Additionally it is constituted by a sum of terms l. When $l = 0$, $\lambda_y = \pm\sqrt{\omega^2\epsilon_x\mu_x - \frac{\mu_x}{\mu_y}\lambda_x^2}$ and when $l \neq 0$, $\lambda_y = \pm\sqrt{\omega^2\epsilon_x\mu_x - \frac{\mu_x}{\mu_y}\lambda_x^2 - \frac{\mu_x}{\mu_y}\left(\frac{l\pi}{d}\right)^2}$

$$\sum_{l=0}^{\infty} \oint_{\lambda_{yA}} \frac{f(z)}{z-z_0} = j2\pi \sum_{l=0}^{\infty} \frac{f_1(z_0)}{f_2'(z_0)}$$

$$f(\lambda_y) = \frac{\lambda_y^2}{((\frac{n\pi}{b})-\lambda_y)((\frac{n\pi}{b})+\lambda_y)} \frac{\cos(k_{ZTE}(d))}{k_{ZTE}\sin(k_{ZTE}d)} \frac{(1-e^{j\lambda_y b}(-1)^n)}{(\lambda_y-\omega\sqrt{\epsilon_x\mu_x})(\lambda_y+\omega\sqrt{\epsilon_x\mu_x})}$$

Evaluating the l=0 part first:

$$f_1(\lambda_{yl=0}) = \frac{\lambda_y^2}{((\frac{n\pi}{b})-\lambda_y)((\frac{n\pi}{b})+\lambda_y)} \frac{\cos(k_{ZTE}(d))}{1} \frac{(1-e^{j\lambda_y b}(-1)^n)}{(\lambda_y-\omega\sqrt{\epsilon_x\mu_x})(\lambda_y+\omega\sqrt{\epsilon_x\mu_x})}$$

$$f_2(\lambda_y) = k_{ZTE}\sin(k_{ZTE}d)$$

$$f_2'(\lambda_{yl=0}) = \sin(k_{ZTE}d)\frac{1}{2k_{ZTE}}\left(-2\frac{\mu_y}{\mu_x}\lambda_y d\right) + k_{ZTE}\cos(k_{ZTE}d)\frac{1}{2k_{ZTE}}\left(-2\frac{\mu_y}{\mu_x}k_y d\right)$$

$$f_2'(\lambda_{yl=0}) = -\sin(k_{ZTE}d)\frac{1}{k_{ZTE}}\left(\frac{\mu_y}{\mu_x}\lambda_y d\right) - cos(k_{ZTE}d)\left(\frac{\mu_y}{\mu_x}\lambda_y d\right) \tag{D.148}$$

$$f_2'(\lambda_{yl=0}) = -\left(\frac{\mu_y}{\mu_x}\lambda_y d\right)\left[\sin(k_{ZTE}d)\frac{1}{k_{ZTE}} + cos(k_{ZTE}d)\right]$$

$$f_2'(\lambda_{yl=0}) = \left(\frac{\mu_y}{\mu_x}\sqrt{\omega^2\epsilon_x\mu_x - \frac{\mu_x}{\mu_y}\lambda_x^2}d\right)[1+1]$$

$$f_2'(\lambda_{yl=0}) = 2\left(\frac{\mu_y}{\mu_x}\sqrt{\omega^2\epsilon_x\mu_x - \frac{\mu_x}{\mu_y}\lambda_x^2}d\right)$$

$$f_1(\lambda_{yl=0}) = \frac{\lambda_y^2}{((\frac{n\pi}{b})-\lambda_y)((\frac{n\pi}{b})+\lambda_y)} \frac{\cos(k_{ZTE}(d))}{1} \frac{(1-e^{j\lambda_y b}(-1)^n)}{(\lambda_y-\omega\sqrt{\epsilon_x\mu_x})(\lambda_y+\omega\sqrt{\epsilon_x\mu_x})}$$

$$f_1(\lambda_{yl=0}) = \frac{\omega^2\epsilon_x\mu_x - \frac{\mu_x}{\mu_y}\lambda_x^2}{((\frac{n\pi}{b})^2 - \omega^2\epsilon_x\mu_x + \frac{\mu_x}{\mu_y}\lambda_x^2)} \frac{(1-e^{-j\sqrt{\omega^2\epsilon_x\mu_x - \frac{\mu_x}{\mu_y}\lambda_x^2}b}(-1)^n)}{(\omega^2\epsilon_x\mu_x - \frac{\mu_x}{\mu_y}\lambda_x^2 - \omega^2\epsilon_x\mu_x)}$$

$$f_1(\lambda_{yl=0}) = \frac{\omega^2\epsilon_x\mu_x - \frac{\mu_x}{\mu_y}\lambda_x^2}{((\frac{n\pi}{b})^2 - \omega^2\epsilon_x\mu_x + \frac{\mu_x}{\mu_y}\lambda_x^2)} \frac{(1-e^{-j\sqrt{\omega^2\epsilon_x\mu_x - \frac{\mu_x}{\mu_y}\lambda_x^2}b}(-1)^n)}{-\frac{\mu_x}{\mu_y}\lambda_x^2}$$

$$j2\pi\frac{f_1(\lambda_{yl=0})}{f_2'(\lambda_{yl=0})} = j2\pi\frac{\omega^2\epsilon_x\mu_x - \frac{\mu_x}{\mu_y}\lambda_x^2}{((\frac{n\pi}{b})^2 - \omega^2\epsilon_x\mu_x + \frac{\mu_x}{\mu_y}\lambda_x^2)}\frac{(1 - e^{-j\sqrt{\omega^2\epsilon_x\mu_x - \frac{\mu_x}{\mu_y}\lambda_x^2}b}(-1)^n)}{-\frac{\mu_x}{\mu_y}\lambda_x^2 2\frac{\mu_y}{\mu_x}\sqrt{\omega^2\epsilon_x\mu_x - \frac{\mu_x}{\mu_y}\lambda_x^2}d} \tag{D.149}$$

$$j2\pi\frac{f_1(\lambda_{yl=0})}{f_2'(\lambda_{yl=0})} = j2\pi\frac{\sqrt{\omega^2\epsilon_x\mu_x - \frac{\mu_x}{\mu_y}\lambda_x^2}}{((\frac{n\pi}{b})^2 - \omega^2\epsilon_x\mu_x + \frac{\mu_x}{\mu_y}\lambda_x^2)}\frac{(1 - e^{-j\sqrt{\omega^2\epsilon_x\mu_x - \frac{\mu_x}{\mu_y}\lambda_x^2}b}(-1)^n)}{-\lambda_x^2}\frac{1}{2d} \tag{D.150}$$

$$\sum_{l=0}^{\infty} \oint_{\lambda_y B} \frac{f(z)}{z - z_0} = j2\pi \sum_{l=0}^{\infty} \frac{f_1(z_0)}{f_2'(z_0)}$$

$$f(\lambda_y) = \frac{\lambda_y^2}{((\frac{n\pi}{b}) - \lambda_y)((\frac{n\pi}{b}) + \lambda_y)} \frac{\cos(k_{ZTE}(d))}{k_{ZTE}\sin(k_{ZTE}d)} \frac{(1 - e^{j\lambda_y b}(-1)^n)}{(\lambda_y - \omega\sqrt{\epsilon_x\mu_x})(\lambda_y + \omega\sqrt{\epsilon_x\mu_x})}$$

Evaluated the $l \neq 0$ part second:

$$f_1(\lambda_{yl\neq 0}) = \frac{\lambda_y^2}{((\frac{n\pi}{b}) - \lambda_y)((\frac{n\pi}{b}) + \lambda_y)} \frac{\cos(k_{ZTE}(d))}{k_{ZTE}} \frac{(1 - e^{j\lambda_y b}(-1)^n)}{(\lambda_y - \omega\sqrt{\epsilon_x\mu_x})(\lambda_y + \omega\sqrt{\epsilon_x\mu_x})}$$

$$f_2(\lambda_{yl\neq 0}) = \sin(k_{ZTE}d)$$

$$f_2'(\lambda_{yl\neq 0}) = \cos(k_{ZTE}d)\frac{1}{2k_{ZTE}}\left(-2\frac{\mu_y}{\mu_x}\lambda_y d\right) \tag{D.151}$$

$$f_2'(\lambda_{yl\neq 0}) = -cos(k_{ZTE}d)\frac{1}{k_{ZTE}}\left(\frac{\mu_y}{\mu_x}\lambda_y d\right)$$

$$f_2'(\lambda_{yl\neq 0}) = \frac{(-1)^l}{\pm\frac{l\pi}{d}}\left(\frac{\mu_y}{\mu_x}\sqrt{\omega^2\epsilon_x\mu_x - \frac{\mu_x}{\mu_y}\lambda_x^2 - \frac{\mu_x}{\mu_y}\left(\frac{l\pi}{d}\right)^2}\, d\right)$$

$$f_1(\lambda_{yl\neq 0}) = \frac{\lambda_y^2}{((\frac{n\pi}{b}) - \lambda_y)((\frac{n\pi}{b}) + \lambda_y)} \frac{\cos(k_{ZTE}(d))}{k_{ZTE}} \frac{(1 - e^{j\lambda_y b}(-1)^n)}{(\lambda_y - \omega\sqrt{\epsilon_x\mu_x})(\lambda_y + \omega\sqrt{\epsilon_x\mu_x})}$$

$$f_1(\lambda_{yl\neq 0}) = \frac{\omega^2\epsilon_x\mu_x - \frac{\mu_x}{\mu_y}\lambda_x^2 - \frac{\mu_x}{\mu_y}\left(\frac{l\pi}{d}\right)^2}{((\frac{n\pi}{b})^2 - \omega^2\epsilon_x\mu_x + \frac{\mu_x}{\mu_y}\lambda_x^2 + \frac{\mu_x}{\mu_y}\left(\frac{l\pi}{d}\right)^2)} \frac{(-1)^l}{\frac{l\pi}{d}} \frac{(1 - e^{-j\sqrt{\omega^2\epsilon_x\mu_x - \frac{\mu_x}{\mu_y}\lambda_x^2 - \frac{\mu_x}{\mu_y}\left(\frac{l\pi}{d}\right)^2}b}(-1)^n)}{(\omega^2\epsilon_x\mu_x - \frac{\mu_x}{\mu_y}\lambda_x^2 - \frac{\mu_x}{\mu_y}\left(\frac{l\pi}{d}\right)^2 - \omega^2\epsilon_x\mu_x)}$$

$$f_1(\lambda_{yl\neq 0}) = \frac{\omega^2\epsilon_x\mu_x - \frac{\mu_x}{\mu_y}\lambda_x^2 - \frac{\mu_x}{\mu_y}\left(\frac{l\pi}{d}\right)^2}{((\frac{n\pi}{b})^2 - \omega^2\epsilon_x\mu_x + \frac{\mu_x}{\mu_y}\lambda_x^2 + \frac{\mu_x}{\mu_y}\left(\frac{l\pi}{d}\right)^2)} \frac{(-1)^l}{\frac{l\pi}{d}} \frac{(1 - e^{-j\sqrt{\omega^2\epsilon_x\mu_x - \frac{\mu_x}{\mu_y}\lambda_x^2 - \frac{\mu_x}{\mu_y}\left(\frac{l\pi}{d}\right)^2}b}(-1)^n)}{-\frac{\mu_x}{\mu_y}(\lambda_x^2 + \left(\frac{l\pi}{d}\right)^2)} \tag{D.152}$$

$$j2\pi\frac{f_1(\lambda_{yl\neq 0})}{f_2'(\lambda_{yl\neq 0})} = j2\pi\frac{\omega^2\epsilon_x\mu_x - \frac{\mu_x}{\mu_y}\lambda_x^2 - \frac{\mu_x}{\mu_y}\left(\frac{l\pi}{d}\right)^2}{((\frac{n\pi}{b})^2 - \omega^2\epsilon_x\mu_x + \frac{\mu_x}{\mu_y}\lambda_x^2 + \frac{\mu_x}{\mu_y}\left(\frac{l\pi}{d}\right)^2)}\cdot \frac{(1-e^{-j\sqrt{\omega^2\epsilon_x\mu_x - \frac{\mu_x}{\mu_y}\lambda_x^2 - \frac{\mu_x}{\mu_y}\left(\frac{l\pi}{d}\right)^2}b}(-1)^n)}{-(\lambda_x^2 + \left(\frac{l\pi}{d}\right)^2)\sqrt{\omega^2\epsilon_x\mu_x - \frac{\mu_x}{\mu_y}\lambda_x^2 - \frac{\mu_x}{\mu_y}\left(\frac{l\pi}{d}\right)^2}d} \tag{D.153}$$

$$= j2\pi\frac{\sqrt{\omega^2\epsilon_x\mu_x - \frac{\mu_x}{\mu_y}\lambda_x^2 - \frac{\mu_x}{\mu_y}\left(\frac{l\pi}{d}\right)^2}}{((\frac{n\pi}{b})^2 - \omega^2\epsilon_x\mu_x + \frac{\mu_x}{\mu_y}\lambda_x^2 + \frac{\mu_x}{\mu_y}\left(\frac{l\pi}{d}\right)^2)}\frac{(1-e^{-j\sqrt{\omega^2\epsilon_x\mu_x - \frac{\mu_x}{\mu_y}\lambda_x^2 - \frac{\mu_x}{\mu_y}\left(\frac{l\pi}{d}\right)^2}b}(-1)^n)}{-(\lambda_x^2 + \left(\frac{l\pi}{d}\right)^2)d} \tag{D.154}$$

Combining $l \neq 0$ and $l = 0$ parts:

$$j2\pi\frac{f_1(z_0)}{f_2'(z_0)} = j2\pi\frac{\sqrt{\omega^2\epsilon_x\mu_x - \frac{\mu_x}{\mu_y}\lambda_x^2}}{((\frac{n\pi}{b})^2 - \omega^2\epsilon_x\mu_x + \frac{\mu_x}{\mu_y}\lambda_x^2)}\frac{(1-e^{-j\sqrt{\omega^2\epsilon_x\mu_x - \frac{\mu_x}{\mu_y}\lambda_x^2}b}(-1)^n)}{-\lambda_x^2}\frac{1}{2d} \tag{D.155}$$

$$j2\pi\frac{f_1(\lambda_{yl\neq 0})}{f_2'(\lambda_{yl\neq 0})} = j2\pi\sum_{l=0}^{\infty}\frac{\sqrt{\omega^2\epsilon_x\mu_x - \frac{\mu_x}{\mu_y}\lambda_x^2 - \frac{\mu_x}{\mu_y}\left(\frac{l\pi}{d}\right)^2}}{((\frac{n\pi}{b})^2 - \omega^2\epsilon_x\mu_x + \frac{\mu_x}{\mu_y}\lambda_x^2 + \frac{\mu_x}{\mu_y}\left(\frac{l\pi}{d}\right)^2)}\frac{(1-e^{-j\sqrt{\omega^2\epsilon_x\mu_x - \frac{\mu_x}{\mu_y}\lambda_x^2 - \frac{\mu_x}{\mu_y}\left(\frac{l\pi}{d}\right)^2}b}(-1)^n)}{-(\lambda_x^2 + \left(\frac{l\pi}{d}\right)^2)d} \tag{D.156}$$

$$- j2\pi\sum_{l=0}^{\infty}\frac{\sqrt{\omega^2\epsilon_x\mu_x - \frac{\mu_x}{\mu_y}\lambda_x^2 - \frac{\mu_x}{\mu_y}\left(\frac{l\pi}{d}\right)^2}}{((\frac{n\pi}{b})^2 - \omega^2\epsilon_x\mu_x + \frac{\mu_x}{\mu_y}\lambda_x^2 + \frac{\mu_x}{\mu_y}\left(\frac{l\pi}{d}\right)^2)}\frac{(1-e^{-j\sqrt{\omega^2\epsilon_x\mu_x - \frac{\mu_x}{\mu_y}\lambda_x^2 - \frac{\mu_x}{\mu_y}\left(\frac{l\pi}{d}\right)^2}b}(-1)^n)}{(\lambda_x^2 + \left(\frac{l\pi}{d}\right)^2)d(1+\delta_{l=0})} \tag{D.157}$$

$$\boxed{(-1)^n j2\pi \sum_{l=0}^{\infty} \frac{\sqrt{\omega^2\epsilon_x\mu_x - \frac{\mu_x}{\mu_y}\lambda_x^2 - \frac{\mu_x}{\mu_y}\left(\frac{l\pi}{d}\right)^2}}{((\frac{n\pi}{b})^2 - \omega^2\epsilon_x\mu_x + \frac{\mu_x}{\mu_y}\lambda_x^2 + \frac{\mu_x}{\mu_y}\left(\frac{l\pi}{d}\right)^2)} \frac{(1 - e^{-j\sqrt{\omega^2\epsilon_x\mu_x - \frac{\mu_x}{\mu_y}\lambda_x^2 - \frac{\mu_x}{\mu_y}\left(\frac{l\pi}{d}\right)^2}b}(-1)^n)}{(\lambda_x^2 + \left(\frac{l\pi}{d}\right)^2)d(1+\delta_{l=0})}} \tag{D.158}$$

for UHP Pole λ_{yA}.

$$\oint_{\lambda_{yC}} \frac{f(z)}{z - z_0} = j\pi f(z_0) =$$

$$-(-1)^n j\pi \left. \frac{\lambda_y^2 \cos(k_{ZTE}(d))}{k_{ZTE}\sin(k_{ZTE}d)} \frac{(1 - e^{j\lambda_y b}(-1)^n)}{((\frac{n\pi}{b}) - \lambda_y)(\lambda_y - \omega\sqrt{\epsilon_x\mu_x})(\lambda_y + \omega\sqrt{\epsilon_x\mu_x})} \right|_{\lambda_y = -\frac{n\pi}{b}} = 0 \tag{D.159}$$

$$(1 - e^{j(-\frac{n\pi}{b})b}(-1)^n) = (1 - (-1)^n(-1)^n) = (1 - (-1)^{2n}) = (1 - 1) = 0$$

$\boxed{0}$ for UHP Pole λ_{yC}.

$$\oint_{\lambda_{yD}} \frac{f(z)}{z - z_0} = j\pi f(z_0) =$$

$$-(-1)^n j\pi \left. \frac{\lambda_y^2 \cos(k_{ZTE}(d))}{k_{ZTE}\sin(k_{ZTE}d)} \frac{(1 - e^{j\lambda_y b}(-1)^n)}{((\frac{n\pi}{b}) + \lambda_y)(\lambda_y - \omega\sqrt{\epsilon_x\mu_x})(\lambda_y + \omega\sqrt{\epsilon_x\mu_x})} \right|_{\lambda_y = \frac{n\pi}{b}} = \tag{D.160}$$

$$(1 - e^{j(\frac{n\pi}{b})b}(-1)^n) = (1 - (-1)^n(-1)^n) = (1 - (-1)^{2n}) = (1 - 1) = 0$$

$\boxed{0}$ for UHP Pole λ_{yD}.

LHP:

$$\int_{-\infty}^{\infty} \frac{\lambda_y^4}{k_{ZTE}(\lambda_y^2 - \omega^2\epsilon_x\mu_x)} \frac{\cos(k_{ZTE}d)}{\sin(k_{ZTE}d)} \frac{(1 - e^{-jb\lambda_y}(-1)^n)}{((\frac{v\pi}{b})^2 - \lambda_y^2)(k_y^2 - \lambda_y^2)} d\lambda_y \tag{D.161}$$

$$\int_{-\infty}^{\infty} \frac{\lambda_y^4}{k_{ZTE}(\lambda_y^2 - \omega^2\epsilon_x\mu_x)} \frac{\cos(k_{ZTE}d)}{\sin(k_{ZTE}d)} \frac{(1 - e^{-jb\lambda_y}(-1)^n)}{(-\lambda_y^2)(k_y^2 - \lambda_y^2)} d\lambda_y \tag{D.162}$$

$$- \int_{-\infty}^{\infty} \frac{\lambda_y^2}{k_{ZTE}(\lambda_y^2 - \omega^2\epsilon_x\mu_x)} \frac{\cos(k_{ZTE}d)}{\sin(k_{ZTE}d)} \frac{(1 - e^{-jb\lambda_y}(-1)^n)}{(k_y^2 - \lambda_y^2)} d\lambda_y \tag{D.163}$$

Identification of the poles:

$$\lambda_y = \pm\sqrt{\omega^2\epsilon_x\mu_x - \frac{\mu_x}{\mu_y}\lambda_x^2} \tag{D.164}$$

$$\lambda_y = \pm\sqrt{\omega^2\epsilon_x\mu_x - \frac{\mu_x}{\mu_y}\lambda_x^2 - \frac{\mu_x}{\mu_y}\left(\frac{l\pi}{d}\right)^2} \tag{D.165}$$

$$\pm\sqrt{\omega^2\epsilon_x\mu_x} = \lambda_y \tag{D.166}$$

$$\pm\frac{n\pi}{b} = \lambda_y \tag{D.167}$$

Now doing the lower half plane.

$$\int_{-\infty}^{\infty} + \oint_{\lambda_{yA}} + \oint_{\lambda_{yB}} + \oint_{\lambda_{yC}} + \oint_{\lambda_{yD}} + \oint_{C_R} = 0 \tag{D.168}$$

where C_R is the radius at infinity.

$$\int_{-\infty}^{\infty} + \oint_{\lambda_{yA}} + \oint_{\lambda_{yB}} + \oint_{\lambda_{yC}} + \oint_{\lambda_{yD}} + \cancelto{0}{\oint_{C_R}} = 0 \tag{D.169}$$

$$\int_{-\infty}^{\infty} = -\oint_{\lambda_{yA}} - \oint_{\lambda_{yB}} - \oint_{\lambda_{yC}} - \oint_{\lambda_{yD}} \tag{D.170}$$

Evaluating λ_{yB} pole:

$$\begin{aligned}
-\oint_{\lambda_{yB}} \frac{f(z)}{z-z_0} = -j2\pi f(z_0) = \\
-j2\pi \left. \frac{\lambda_y^2}{(\frac{n\pi}{b}-\lambda_y)(\frac{n\pi}{b}+\lambda_y)} \frac{\cos(k_{ZTE}(d))}{k_{ZTE}\sin(k_{ZTE}d)} \frac{(1-e^{-j\lambda_y b}(-1)^n)}{(\lambda_y+\omega\sqrt{\epsilon_x\mu_x})} \right|_{\lambda_y=\omega\sqrt{\epsilon_x\mu_x}} = \\
-j2\pi \frac{\omega^2\epsilon_x\mu_x}{((\frac{n\pi}{b})^2-\omega^2\epsilon_x\mu_x)} \frac{\cos(\sqrt{-\lambda_x^2}(d))}{\sqrt{-\lambda_x^2}\sin(\sqrt{-\lambda_x^2}d)} \frac{(e^{-j\left(\omega\sqrt{\epsilon_x\mu_x}\right)b}(-1)^n-1)}{2\omega\sqrt{\epsilon_x\mu_x}} = \\
-\pi \frac{\omega\sqrt{\epsilon_x\mu_x}}{((\frac{n\pi}{b})^2-\omega^2\epsilon_x\mu_x)} \frac{\cos(j\lambda_x d)}{\lambda_x\sin(j\lambda_x d)} \frac{(e^{-j\omega\sqrt{\epsilon_x\mu_x}b}(-1)^n-1)}{1} =
\end{aligned} \tag{D.171}$$

$$\boxed{- - \pi \frac{\omega\sqrt{\epsilon_x\mu_x}}{((\frac{n\pi}{b})^2-\omega^2\epsilon_x\mu_x)} \frac{\cos(j\lambda_x d)}{\lambda_x\sin(j\lambda_x d)} \frac{(e^{-j\omega\sqrt{\epsilon_x\mu_x}b}(-1)^n-1)}{1}} \quad \text{for LHP } \lambda_{yB}. \tag{D.172}$$

$\oint_{\lambda_{yA}}$ contains a double pole and is not a simple pole. Additionally it is constituted by a sum of terms l. When $l=0$, $\lambda_y = \pm\sqrt{\omega^2\epsilon_x\mu_x - \frac{\mu_x}{\mu_y}\lambda_x^2}$ and when $l \neq 0$, $\lambda_y = \pm\sqrt{\omega^2\epsilon_x\mu_x - \frac{\mu_x}{\mu_y}\lambda_x^2 - \frac{\mu_x}{\mu_y}\left(\frac{l\pi}{d}\right)^2}$

$$-\sum_{l=0}^{\infty}\oint_{\lambda_{yA}}\frac{f(z)}{z-z_0}=-j2\pi\sum_{l=0}^{\infty}\frac{f_1(z_0)}{f_2'(z_0)}$$

$$f(\lambda_y)=\frac{\lambda_y^2}{(\frac{n\pi}{b}-\lambda_y)(\frac{n\pi}{b}+\lambda_y)}\frac{\cos(k_{ZTE}(d))}{k_{ZTE}\sin(k_{ZTE}d)}\frac{(1-e^{-j\lambda_y b}(-1)^n)}{(\lambda_y-\omega\sqrt{\epsilon_x\mu_x})(\lambda_y+\omega\sqrt{\epsilon_x\mu_x})}$$

Evaluating the l=0 part first

$$f_1(\lambda_{yl=0})=\frac{\lambda_y^2}{(\frac{n\pi}{b}-\lambda_y)(\frac{n\pi}{b}+\lambda_y)}\frac{\cos(k_{ZTE}(d))}{1}\frac{(1-e^{-j\lambda_y b}(-1)^n)}{(\lambda_y-\omega\sqrt{\epsilon_x\mu_x})(\lambda_y+\omega\sqrt{\epsilon_x\mu_x})}$$

$$f_2(\lambda_y)=k_{ZTE}\sin(k_{ZTE}d)$$

$$f_2'(\lambda_{yl=0})=\sin(k_{ZTE}d)\frac{1}{2k_{ZTE}}\left(-2\frac{\mu_y}{\mu_x}\lambda_y d\right)+k_{ZTE}\cos(k_{ZTE}d)\frac{1}{2k_{ZTE}}\left(-2\frac{\mu_y}{\mu_x}\lambda_y d\right)$$

$$f_2'(\lambda_{yl=0})=-\sin(k_{ZTE}d)\frac{1}{k_{ZTE}}\left(\frac{\mu_y}{\mu_x}\lambda_y d\right)-cos(k_{ZTE}d)\left(\frac{\mu_y}{\mu_x}\lambda_y d\right)$$

$$f_2'(\lambda_{yl=0})=-\left(\frac{\mu_y}{\mu_x}\lambda_y d\right)\left[\sin(k_{ZTE}d)\frac{1}{k_{ZTE}}+cos(k_{ZTE}d)\right]$$

$$f_2'(\lambda_{yl=0})=-\left(\frac{\mu_y}{\mu_x}\sqrt{\omega^2\epsilon_x\mu_x-\frac{\mu_x}{\mu_y}\lambda_x^2}d\right)[1+1]$$

$$f_2'(\lambda_{yl=0})=-2\left(\frac{\mu_y}{\mu_x}\sqrt{\omega^2\epsilon_x\mu_x-\frac{\mu_x}{\mu_y}\lambda_x^2}d\right)$$

$$f_1(\lambda_{yl=0})=\frac{\lambda_y^2}{(\frac{n\pi}{b}-\lambda_y)(\frac{n\pi}{b}+\lambda_y)}\frac{\cos(k_{ZTE}(d))}{1}\frac{(1-e^{-j\lambda_y b}(-1)^n)}{(\lambda_y-\omega\sqrt{\epsilon_x\mu_x})(\lambda_y+\omega\sqrt{\epsilon_x\mu_x})}$$

$$f_1(\lambda_{yl=0})=\frac{\omega^2\epsilon_x\mu_x-\frac{\mu_x}{\mu_y}\lambda_x^2}{((\frac{n\pi}{b})^2-\omega^2\epsilon_x\mu_x+\frac{\mu_x}{\mu_y}\lambda_x^2)}\frac{(1-e^{-j\sqrt{\omega^2\epsilon_x\mu_x-\frac{\mu_x}{\mu_y}\lambda_x^2}b}(-1)^n)}{-\frac{\mu_x}{\mu_y}\lambda_x^2}$$

$$-j2\pi\frac{f_1(\lambda_{yl=0})}{f_2'(\lambda_{yl=0})}=-j2\pi\frac{\omega^2\epsilon_x\mu_x-\frac{\mu_x}{\mu_y}\lambda_x^2}{((\frac{n\pi}{b})^2-\omega^2\epsilon_x\mu_x+\frac{\mu_x}{\mu_y}\lambda_x^2)}\frac{(e^{-j\sqrt{\omega^2\epsilon_x\mu_x-\frac{\mu_x}{\mu_y}\lambda_x^2}b}(-1)^n-1)}{-\frac{\mu_x}{\mu_y}\lambda_x^2(-2\frac{\mu_y}{\mu_x}\sqrt{\omega^2\epsilon_x\mu_x-\frac{\mu_x}{\mu_y}\lambda_x^2}d)}$$

(D.173)

$$-j2\pi\frac{f_1(\lambda_{yl=0})}{f_2'(\lambda_{yl=0})} = -j2\pi\frac{\sqrt{\omega^2\epsilon_x\mu_x - \frac{\mu_x}{\mu_y}\lambda_x^2}}{((\frac{n\pi}{b})^2 - \omega^2\epsilon_x\mu_x + \frac{\mu_x}{\mu_y}\lambda_x^2)}\frac{(e^{-j\sqrt{\omega^2\epsilon_x\mu_x - \frac{\mu_x}{\mu_y}\lambda_x^2}b}(-1)^n - 1)}{-\lambda_x^2(-2d)} \tag{D.174}$$

$$-\sum_{l=0}^{\infty}\oint_{\lambda_{yB}}\frac{f(z)}{z-z_0} = -j2\pi\sum_{l=0}^{\infty}\frac{f_1(z_0)}{f_2'(z_0)}$$

$$f(\lambda_y) = \frac{\lambda_y^2}{(\frac{n\pi}{b} - \lambda_y)(\frac{v\pi}{b} + \lambda_y)}\frac{\cos(k_{ZTE}(d))}{k_{ZTE}\sin(k_{ZTE}d)}\frac{(1 - e^{-j\lambda_y b}(-1)^n)}{(\lambda_y - \omega\sqrt{\epsilon_x\mu_x})(\lambda_y + \omega\sqrt{\epsilon_x\mu_x})}$$

Evaluating the $l \neq 0$ part second:

$$f_1(\lambda_{yl\neq 0}) = \frac{\lambda_y^2}{(\frac{n\pi}{b} - \lambda_y)(\frac{v\pi}{b} + \lambda_y)}\frac{\cos(k_{ZTE}(d))}{k_{ZTE}}\frac{(1 - e^{-j\lambda_y b}(-1)^n)}{(\lambda_y - \omega\sqrt{\epsilon_x\mu_x})(\lambda_y + \omega\sqrt{\epsilon_x\mu_x})}$$

$$f_2(\lambda_{yl\neq 0}) = \sin(k_{ZTE}d)$$

$$f_2'(\lambda_{yl\neq 0}) = \cos(k_{ZTE}d)\frac{1}{2k_{ZTE}}\left(-2\frac{\mu_y}{\mu_x}\lambda_y d\right) \tag{D.175}$$

$$f_2'(\lambda_{yl\neq 0}) = -cos(k_{ZTE}d)\frac{1}{k_{ZTE}}\left(\frac{\mu_y}{\mu_x}\lambda_y d\right)$$

$$f_2'(\lambda_{yl\neq 0}) = -\frac{(-1)^l}{\pm\frac{l\pi}{d}}\left(\frac{\mu_y}{\mu_x}\sqrt{\omega^2\epsilon_x\mu_x - \frac{\mu_x}{\mu_y}\lambda_x^2 - \frac{\mu_x}{\mu_y}\left(\frac{l\pi}{d}\right)^2}d\right)$$

$$f_1(\lambda_{yl\neq 0}) = \frac{\lambda_y^2}{(\frac{n\pi}{b} - \lambda_y)(\frac{n\pi}{b} + \lambda_y)}\frac{\cos(k_{ZTE}(d))}{k_{ZTE}}\frac{(1 - e^{-j\lambda_y b})(-1)^n}{(\lambda_y - \omega\sqrt{\epsilon_x\mu_x})(\lambda_y + \omega\sqrt{\epsilon_x\mu_x})}$$

$$f_1(\lambda_{yl\neq 0}) = \frac{\omega^2\epsilon_x\mu_x - \frac{\mu_x}{\mu_y}\lambda_x^2 - \frac{\mu_x}{\mu_y}\left(\frac{l\pi}{d}\right)^2}{((\frac{n\pi}{b})^2 - \omega^2\epsilon_x\mu_x + \frac{\mu_x}{\mu_y}\lambda_x^2 + \frac{\mu_x}{\mu_y}\left(\frac{l\pi}{d}\right)^2)}\frac{(-1)^l}{\frac{l\pi}{d}}\frac{(1 - e^{-j\sqrt{\omega^2\epsilon_x\mu_x - \frac{\mu_x}{\mu_y}\lambda_x^2 - \frac{\mu_x}{\mu_y}\left(\frac{l\pi}{d}\right)^2}b}(-1)^n)}{(\omega^2\epsilon_x\mu_x - \frac{\mu_x}{\mu_y}\lambda_x^2 - \frac{\mu_x}{\mu_y}\left(\frac{l\pi}{d}\right)^2 - \omega^2\epsilon_x\mu_x)}$$

$$f_1(\lambda_{yl\neq 0}) = \frac{\omega^2\epsilon_x\mu_x - \frac{\mu_x}{\mu_y}\lambda_x^2 - \frac{\mu_x}{\mu_y}\left(\frac{l\pi}{d}\right)^2}{((\frac{n\pi}{b})^2 - \omega^2\epsilon_x\mu_x + \frac{\mu_x}{\mu_y}\lambda_x^2 + \frac{\mu_x}{\mu_y}\left(\frac{l\pi}{d}\right)^2)} \frac{(-1)^l}{\frac{l\pi}{d}} \frac{(1 - e^{-j\sqrt{\omega^2\epsilon_x\mu_x - \frac{\mu_x}{\mu_y}\lambda_x^2 - \frac{\mu_x}{\mu_y}\left(\frac{l\pi}{d}\right)^2}b}(-1)^n)}{-\frac{\mu_x}{\mu_y}(\lambda_x^2 + \left(\frac{l\pi}{d}\right)^2)} \tag{D.176}$$

$$-j2\pi\frac{f_1(\lambda_{yl\neq 0})}{f_2'(\lambda_{yl\neq 0})} =$$

$$-j2\pi\frac{\omega^2\epsilon_x\mu_x - \frac{\mu_x}{\mu_y}\left(\lambda_x^2 + \left(\frac{l\pi}{d}\right)^2\right)}{((\frac{n\pi}{b})^2 - \omega^2\epsilon_x\mu_x + \frac{\mu_x}{\mu_y}\left(\lambda_x^2 + \left(\frac{l\pi}{d}\right)^2\right))} \frac{(-1)^l}{\frac{l\pi}{d}} \frac{(1 - e^{-j\sqrt{\omega^2\epsilon_x\mu_x - \frac{\mu_x}{\mu_y}\lambda_x^2 - \frac{\mu_x}{\mu_y}\left(\frac{l\pi}{d}\right)^2}b}(-1)^n)}{-\frac{\mu_x}{\mu_y}(\lambda_x^2 + \left(\frac{l\pi}{d}\right)^2)} \cdot \tag{D.177}$$

$$-\frac{\pm\frac{l\pi}{d}}{(-1)^l}\left(\frac{\mu_x}{\mu_y}\frac{1}{\sqrt{\omega^2\epsilon_x\mu_x - \frac{\mu_x}{\mu_y}\lambda_x^2 - \frac{\mu_x}{\mu_y}\left(\frac{l\pi}{d}\right)^2}d}\right)$$

$$= -j2\pi\frac{\sqrt{\omega^2\epsilon_x\mu_x - \frac{\mu_x}{\mu_y}\lambda_x^2 - \frac{\mu_x}{\mu_y}\left(\frac{l\pi}{d}\right)^2}}{((\frac{n\pi}{b})^2 - \omega^2\epsilon_x\mu_x + \frac{\mu_x}{\mu_y}\left(\lambda_x^2 + \left(\frac{l\pi}{d}\right)^2\right))} \frac{(1 - e^{-j\sqrt{\omega^2\epsilon_x\mu_x - \frac{\mu_x}{\mu_y}\lambda_x^2 - \frac{\mu_x}{\mu_y}\left(\frac{l\pi}{d}\right)^2}b}(-1)^n)}{(\lambda_x^2 + \left(\frac{l\pi}{d}\right)^2)d} \tag{D.178}$$

$$= -j2\pi\frac{f_1(\lambda_{yl\neq 0})}{f_2'(\lambda_{yl\neq 0})} =$$

$$-j2\pi\frac{\sqrt{\omega^2\epsilon_x\mu_x - \frac{\mu_x}{\mu_y}\lambda_x^2 - \frac{\mu_x}{\mu_y}\left(\frac{l\pi}{d}\right)^2}}{((\frac{n\pi}{b})^2 - \omega^2\epsilon_x\mu_x + \frac{\mu_x}{\mu_y}\left(\lambda_x^2 + \left(\frac{l\pi}{d}\right)^2\right))} \frac{(1 - e^{-j\sqrt{\omega^2\epsilon_x\mu_x - \frac{\mu_x}{\mu_y}\lambda_x^2 - \frac{\mu_x}{\mu_y}\left(\frac{l\pi}{d}\right)^2}b}(-1)^n)}{(\lambda_x^2 + \left(\frac{l\pi}{d}\right)^2)d} \tag{D.179}$$

Combining: $l \neq 0$ and $l = 0$

$$-j2\pi\frac{f_1(z_0)}{f_2'(z_0)} = \frac{\sqrt{\omega^2\epsilon_x\mu_x - \frac{\mu_x}{\mu_y}\lambda_x^2}}{((\frac{n\pi}{b})^2 - \omega^2\epsilon_x\mu_x + \frac{\mu_x}{\mu_y}\lambda_x^2)} \frac{(1 - e^{-j\sqrt{\omega^2\epsilon_x\mu_x - \frac{\mu_x}{\mu_y}\lambda_x^2}b}(-1)^n)}{-\lambda_x^2} \frac{1}{-2d} \tag{D.180}$$

$$-j2\pi\frac{f_1(\lambda_{yl\neq 0})}{f_2'(\lambda_{yl\neq 0})} =$$

$$-j2\pi\sum_{l=0}^{\infty}\frac{\sqrt{\omega^2\epsilon_x\mu_x-\frac{\mu_x}{\mu_y}\lambda_x^2-\frac{\mu_x}{\mu_y}\left(\frac{l\pi}{d}\right)^2}}{((\frac{n\pi}{b})^2-\omega^2\epsilon_x\mu_x+\frac{\mu_x}{\mu_y}\left(\lambda_x^2+\left(\frac{l\pi}{d}\right)^2\right))}\frac{(1-e^{-j\sqrt{\omega^2\epsilon_x\mu_x-\frac{\mu_x}{\mu_y}\lambda_x^2-\frac{\mu_x}{\mu_y}\left(\frac{l\pi}{d}\right)^2}b}(-1)^n)}{(\lambda_x^2+\left(\frac{l\pi}{d}\right)^2)d} \tag{D.181}$$

$$\boxed{--j2\pi\sum_{l=0}^{\infty}\frac{\sqrt{\omega^2\epsilon_x\mu_x-\frac{\mu_x}{\mu_y}\lambda_x^2-\frac{\mu_x}{\mu_y}\left(\frac{l\pi}{d}\right)^2}}{((\frac{n\pi}{b})^2-\omega^2\epsilon_x\mu_x+\frac{\mu_x}{\mu_y}\left(\lambda_x^2+\left(\frac{l\pi}{d}\right)^2\right))}\frac{(1-e^{-j\sqrt{\omega^2\epsilon_x\mu_x-\frac{\mu_x}{\mu_y}\lambda_x^2-\frac{\mu_x}{\mu_y}\left(\frac{l\pi}{d}\right)^2}b}(-1)^n)}{(\lambda_x^2+\left(\frac{l\pi}{d}\right)^2)d(1+\delta_{l=0})}} \tag{D.182}$$

for LHP Pole λ_{yA}

On to the next pole:

$$-\oint_{\lambda_{yC}}\frac{f(z)}{z-z_0} = -j\pi f(z_0) =$$

$$-j\pi\left.\frac{\lambda_y^2}{(\frac{n\pi}{b}-\lambda_y)}\frac{\cos(k_{ZTE}(d))}{k_{ZTE}\sin(k_{ZTE}d)}\frac{(1-e^{-j\lambda_y b}(-1)^n)}{(\lambda_y+\omega\sqrt{\epsilon_x\mu_x})(\lambda_y-\omega\sqrt{\epsilon_x\mu_x})}\right|_{\lambda_y=-\frac{n\pi}{b}} \tag{D.183}$$

$$(1-e^{j(\frac{n\pi}{b})b}(-1)^n) = (1-e^{j(n\pi)}(-1)^n) = (1-(-1)^n(-1)^n) = (1-(-1)^{2n}) = (1-1) = 0$$

On to the next pole:

$$-\oint_{\lambda_{yD}} \frac{f(z)}{z-z_0} = -j\pi f(z_0) =$$
$$-j\pi \left. \frac{\lambda_y^2}{(\frac{n\pi}{b}+\lambda_y)} \frac{\cos(k_{ZTE}(d))}{k_{ZTE}\sin(k_{ZTE}d)} \frac{(1-e^{-j\lambda_y b}(-1)^n)}{(\lambda_y+\omega\sqrt{\epsilon_x\mu_x})(\lambda_y-\omega\sqrt{\epsilon_x\mu_x})} \right|_{\lambda_y=\frac{n\pi}{b}} \tag{D.184}$$
$$(1-e^{j(\frac{n\pi}{b})b}(-1)^n) = (1-e^{j(n\pi)}(-1)^n) = (1-(-1)^n(-1)^n) = (1-(-1)^{2n}) = (1-1) = 0$$

Combining the UHP and LHP yields the total solution for the Case 3:

$$\Omega_y = \int_{-\infty}^{\infty} \frac{\lambda_y^4}{k_{ZTE}(\lambda_y^2-\omega^2\epsilon_x\mu_x)} \frac{\cos(k_{ZTE}d)}{\sin(k_{ZTE}d)} \frac{(e^{j(b\lambda_y)}(-1)^v-1)}{((\frac{v\pi}{b})^2-\lambda_y^2)} \frac{(e^{-j(b\lambda_y)}(-1)^n-1)}{(k_y^2-\lambda_y^2)} d\lambda_y = \tag{D.185}$$

$$(-1^n+1)\pi\omega\sqrt{\epsilon_x\mu_x} \frac{\cos(j\lambda_x d)}{\lambda_x \sin(j\lambda_x d)} \frac{(1-e^{-j\omega\sqrt{\epsilon_x\mu_x}b}(-1)^n)}{((\frac{n\pi}{b})^2-\omega^2\epsilon_x\mu_x)} +$$
$$(-1^n+1)j2\pi \sum_{l=0}^{\infty} \frac{\sqrt{\omega^2\epsilon_x\mu_x - \frac{\mu_x}{\mu_y}\lambda_x^2 - \frac{\mu_x}{\mu_y}\left(\frac{l\pi}{d}\right)^2}}{((\frac{n\pi}{b})^2-\omega^2\epsilon_x\mu_x+\frac{\mu_x}{\mu_y}\lambda_x^2+\frac{\mu_x}{\mu_y}\left(\frac{l\pi}{d}\right)^2)} \frac{(1-e^{-j\sqrt{\omega^2\epsilon_x\mu_x-\frac{\mu_x}{\mu_y}\lambda_x^2-\frac{\mu_x}{\mu_y}\left(\frac{l\pi}{d}\right)^2}b}(-1)^n)}{(\lambda_x^2+\left(\frac{l\pi}{d}\right)^2)d(1+\delta_{l=0})} \tag{D.186}$$

Case 2 $n = v \neq 0$**.**

$$\Omega_y = \int_{-\infty}^{\infty} \frac{\lambda_y^4}{k_{ZTE}(\lambda_y^2-\omega^2\epsilon_x\mu_x)} \frac{\cos(k_{ZTE}d)}{\sin(k_{ZTE}d)} \frac{(e^{j(b\lambda_y)}(-1)^v-1)}{((\frac{v\pi}{b})^2-\lambda_y^2)} \frac{(e^{-j(b\lambda_y)}(-1)^n-1)}{(k_y^2-\lambda_y^2)} d\lambda_y \tag{D.187}$$

Simplifying Further:

UHP:

$$\Omega_y = (-1)^{n+v} \int_{-\infty}^{\infty} \frac{\lambda_y^4}{k_{ZTE}(\lambda_y^2 - \omega^2\epsilon_x\mu_x)} \frac{\cos(k_{ZTE}d)}{\sin(k_{ZTE}d)} \frac{(1 - e^{jb\lambda_y}(-1)^n)}{((\frac{v\pi}{b})^2 - \lambda_y^2)(k_y^2 - \lambda_y^2)} d\lambda_y + \tag{D.188}$$

LHP:

$$\int_{-\infty}^{\infty} \frac{\lambda_y^4}{k_{ZTE}(\lambda_y^2 - \omega^2\epsilon_x\mu_x)} \frac{\cos(k_{ZTE}d)}{\sin(k_{ZTE}d)} \frac{(1 - e^{-jb\lambda_y}(-1)^n)}{((\frac{v\pi}{b})^2 - \lambda_y^2)(k_y^2 - \lambda_y^2)} d\lambda_y \tag{D.189}$$

Evaluating each part:

UHP:

$$\Omega_y = (-1)^{n+v} \int_{-\infty}^{\infty} \frac{\lambda_y^4}{k_{ZTE}(\lambda_y^2 - \omega^2\epsilon_x\mu_x)} \frac{\cos(k_{ZTE}d)}{\sin(k_{ZTE}d)} \frac{(1 - e^{jb\lambda_y}(-1)^n)}{((\frac{v\pi}{b})^2 - \lambda_y^2)(k_y^2 - \lambda_y^2)} d\lambda_y + \tag{D.190}$$

$$\Omega_y = \int_{-\infty}^{\infty} \frac{\lambda_y^4}{k_{ZTE}(\lambda_y^2 - \omega^2\epsilon_x\mu_x)} \frac{\cos(k_{ZTE}d)}{\sin(k_{ZTE}d)} \frac{(1 - e^{jb\lambda_y}(-1)^n)}{((\frac{n\pi}{b})^2 - \lambda_y^2)(k_y^2 - \lambda_y^2)} d\lambda_y + \tag{D.191}$$

Identification of the poles:

$$\lambda_y = \pm\sqrt{\omega^2\epsilon_x\mu_x - \frac{\mu_x}{\mu_y}\lambda_x^2} \tag{D.192}$$

$$\lambda_y = \pm\sqrt{\omega^2\epsilon_x\mu_x - \frac{\mu_x}{\mu_y}\lambda_x^2 - \frac{\mu_x}{\mu_y}\left(\frac{l\pi}{d}\right)^2} \tag{D.193}$$

$$\pm \sqrt{\omega^2 \epsilon_x \mu_x} = \lambda_y \tag{D.194}$$

$$\pm \frac{n\pi}{b} = \lambda_y \tag{D.195}$$

$$\pm \frac{n\pi}{b} = \lambda_y \tag{D.196}$$

Plotting the poles on the complex plane yields Figure 65. Note that there are double poles at $\pm\frac{n\pi}{b} = \lambda_y$.

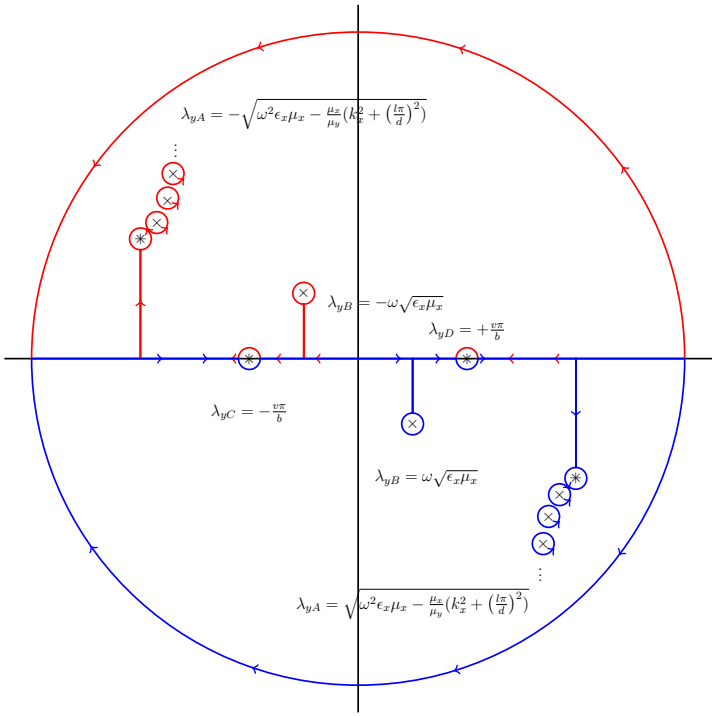

Figure 65. The complex plane showing the poles for the λ_y part of the integral. Note the series of poles induced by the $\sin(k_{ZTE}d)$ part, which represent the modes exhibited in the parallel-plate waveguide structure. A double pole occurs due to $k_{ZTE}\sin(k_{ZTE}d)$ at the $l = 0$ parallel-plate mode. Individual poles are denoted by a $\times$ symbol, while a double pole is denoted by $*$ symbol.

$$\int_{-\infty}^{\infty} + \oint_{\lambda_{yA}} + \oint_{\lambda_{yB}} + \oint_{\lambda_{yC}} + \oint_{\lambda_{yC}} + \oint_{C_R} = 0 \tag{D.197}$$

where C_R is the radius at infinity.

$$\int_{-\infty}^{\infty} + \oint_{\lambda_{yA}} + \oint_{\lambda_{yB}} + \oint_{\lambda_{yC}} + \oint_{\lambda_{yD}} \overset{0}{\oint_{C_R}} = 0 \tag{D.198}$$

$$\int_{-\infty}^{\infty} = -\oint_{\lambda_{yA}} - \oint_{\lambda_{yB}} - \oint_{\lambda_{yC}} - \oint_{\lambda_{yD}} \tag{D.199}$$

$$\int_{-\infty}^{\infty} = \oint_{\lambda_{yA}} + \oint_{\lambda_{yB}} + \oint_{\lambda_{yC}} + \oint_{\lambda_{yD}} \tag{D.200}$$

Utilizing Cauchy's Integral Theorem:

$$\begin{aligned}
\oint_{\lambda_{yB}} \frac{f(z)}{z - z_0} &= j2\pi f(z_0) = \\
j2\pi \, \frac{\lambda_y^4 \cos(k_{ZTE}(d))}{k_{ZTE}\sin(k_{ZTE}d)} \frac{(1 - e^{j\lambda_y b}(-1)^n)}{((\frac{n\pi}{b})^2 - \lambda_y^2)((\frac{n\pi}{b})^2 - \lambda_y^2)(\lambda_y - \omega\sqrt{\epsilon_x\mu_x})}\bigg|_{\lambda_y = -\omega\sqrt{\epsilon_x\mu_x}} &= \\
j2\pi \frac{\left(\omega\sqrt{\epsilon_x\mu_x}\right)^3 \cos(\sqrt{-\lambda_x^2}(d))}{\sqrt{-\lambda_x^2}\sin(\sqrt{-\lambda_x^2}d)} \frac{(1 - e^{-j\left(\omega\sqrt{\epsilon_x\mu_x}\right)b}(-1)^n)}{-2((\frac{n\pi}{b})^2 - \omega^2\epsilon_x\mu_x)((\frac{n\pi}{b})^2 - \omega^2\epsilon_x\mu_x)} &= \\
-j\pi \frac{\left(\omega\sqrt{\epsilon_x\mu_x}\right)^3 \cos(j\lambda_x(d))}{j\lambda_x\sin(j\lambda_x d)} \frac{(1 - e^{-j\left(\omega\sqrt{\epsilon_x\mu_x}\right)b}(-1)^n)}{((\frac{n\pi}{b})^2 - \omega^2\epsilon_x\mu_x)((\frac{n\pi}{b})^2 - \omega^2\epsilon_x\mu_x)} &= \\
-\pi \frac{\left(\omega\sqrt{\epsilon_x\mu_x}\right)^3 \cos(j\lambda_x(d))}{\lambda_x\sin(j\lambda_x d)} \frac{(1 - e^{-j\left(\omega\sqrt{\epsilon_x\mu_x}\right)b}(-1)^n)}{((\frac{n\pi}{b})^2 - \omega^2\epsilon_x\mu_x)((\frac{n\pi}{b})^2 - \omega^2\epsilon_x\mu_x)} &=
\end{aligned} \tag{D.201}$$

$$\boxed{-\pi \frac{\left(\omega\sqrt{\epsilon_x\mu_x}\right)^3 \cos(j\lambda_x d)}{\lambda_x\sin(j\lambda_x d)} \frac{(1 - e^{-j\left(\omega\sqrt{\epsilon_x\mu_x}\right)b}(-1)^n)}{((\frac{n\pi}{b})^2 - \omega^2\epsilon_x\mu_x)((\frac{n\pi}{b})^2 - \omega^2\epsilon_x\mu_x)}} \quad \text{for UHP Pole } \lambda_{yB}. \tag{D.202}$$

$\oint_{\lambda_{yB}}$ contains a double pole and is not a simple pole. Additionally it is constituted by a sum of terms l. When $l = 0$, $\lambda_y = \pm\sqrt{\omega^2\epsilon_x\mu_x - \frac{\mu_x}{\mu_y}\lambda_x^2}$ and when $l \neq 0$, $\lambda_y = \pm\sqrt{\omega^2\epsilon_x\mu_x - \frac{\mu_x}{\mu_y}\lambda_x^2 - \frac{\mu_x}{\mu_y}\left(\frac{l\pi}{d}\right)^2}$

$$\sum_{l=0}^{\infty}\oint_{\lambda_{yA}}\frac{f(z)}{z-z_0} = j2\pi\sum_{l=0}^{\infty}\frac{f_1(z_0)}{f_2'(z_0)}$$

$$f(\lambda_y) = \frac{\lambda_y^4}{((\frac{n\pi}{b})^2-\lambda_y^2)((\frac{n\pi}{b})^2-\lambda_y^2)}\frac{\cos(k_{ZTE}(d))}{k_{ZTE}\sin(k_{ZTE}d)}\frac{(1-e^{j\lambda_y b}(-1)^n)}{(\lambda_y-\omega\sqrt{\epsilon_x\mu_x})(\lambda_y+\omega\sqrt{\epsilon_x\mu_x})}$$

Evaluating the l=0 part first:

$$f_1(\lambda_{yl=0}) = \frac{\lambda_y^4}{((\frac{n\pi}{b})^2-\lambda_y^2)((\frac{n\pi}{b})^2-\lambda_y^2)}\frac{\cos(k_{ZTE}(d))}{1}\frac{(1-e^{j\lambda_y b}(-1)^n)}{(\lambda_y-\omega\sqrt{\epsilon_x\mu_x})(\lambda_y+\omega\sqrt{\epsilon_x\mu_x})} \tag{D.203}$$

$$f_2(\lambda_{yl=0}) = k_{ZTE}\sin(k_{ZTE}d)$$

$$f_2'(\lambda_{yl=0}) = \sin(k_{ZTE}d)\frac{1}{2k_{ZTE}}\left(-2\frac{\mu_y}{\mu_x}\lambda_y d\right) + k_{ZTE}\cos(k_{ZTE}d)\frac{1}{2k_{ZTE}}\left(-2\frac{\mu_y}{\mu_x}k_y d\right)$$

$$f_2'(\lambda_{yl=0}) = -\sin(k_{ZTE}d)\frac{1}{k_{ZTE}}\left(\frac{\mu_y}{\mu_x}\lambda_y d\right) - cos(k_{ZTE}d)\left(\frac{\mu_y}{\mu_x}\lambda_y d\right)$$

$$f_2'(\lambda_{yl=0}) = -\left(\frac{\mu_y}{\mu_x}\lambda_y d\right)\left[\sin(k_{ZTE}d)\frac{1}{k_{ZTE}} + cos(k_{ZTE}d)\right]$$

$$f_2'(\lambda_{yl=0}) = \left(\frac{\mu_y}{\mu_x}\sqrt{\omega^2\epsilon_x\mu_x - \frac{\mu_x}{\mu_y}\lambda_x^2}d\right)[1+1]$$

$$f_2'(\lambda_{yl=0}) = 2\left(\frac{\mu_y}{\mu_x}\sqrt{\omega^2\epsilon_x\mu_x - \frac{\mu_x}{\mu_y}\lambda_x^2}d\right)$$

$$f_1(\lambda_{yl=0}) = \frac{\lambda_y^4}{((\frac{n\pi}{b})^2 - \lambda_y^2)((\frac{n\pi}{b})^2 - \lambda_y^2)}\frac{\cos(k_{ZTE}(d))}{1}\frac{(1-e^{j\lambda_y b}(-1)^n)}{(\lambda_y - \omega\sqrt{\epsilon_x\mu_x})(\lambda_y + \omega\sqrt{\epsilon_x\mu_x})}$$

$$f_1(\lambda_{yl=0}) = \frac{\left(\omega^2\epsilon_x\mu_x - \frac{\mu_x}{\mu_y}\lambda_x^2\right)^2}{((\frac{n\pi}{b})^2 - \omega^2\epsilon_x\mu_x + \frac{\mu_x}{\mu_y}\lambda_x^2)((\frac{n\pi}{b})^2 - \omega^2\epsilon_x\mu_x + \frac{\mu_x}{\mu_y}\lambda_x^2)}\frac{(1-e^{-j\sqrt{\omega^2\epsilon_x\mu_x - \frac{\mu_x}{\mu_y}\lambda_x^2}b}(-1)^n)}{-\frac{\mu_x}{\mu_y}\lambda_x^2} \tag{D.204}$$

$$j2\pi\frac{f_1(\lambda_{yl=0})}{f_2'(\lambda_{yl=0})} = j2\pi\sum_{l=0}^{\infty}\frac{\left(\sqrt{\omega^2\epsilon_x\mu_x - \frac{\mu_x}{\mu_y}\lambda_x^2}\right)^4}{((\frac{n\pi}{b})^2 - \omega^2\epsilon_x\mu_x + \frac{\mu_x}{\mu_y}\lambda_x^2)((\frac{n\pi}{b})^2 - \omega^2\epsilon_x\mu_x + \frac{\mu_x}{\mu_y}\lambda_x^2)}\cdot$$
$$\frac{(1-e^{-j\sqrt{\omega^2\epsilon_x\mu_x - \frac{\mu_x}{\mu_y}\lambda_x^2}b}(-1)^n)}{-\frac{\mu_x}{\mu_y}\lambda_x^2 2\frac{\mu_y}{\mu_x}\sqrt{\omega^2\epsilon_x\mu_x - \frac{\mu_x}{\mu_y}\lambda_x^2}d}$$

$$j2\pi\frac{f_1(z_0)}{f_2'(z_0)} = j2\pi\sum_{l=0}^{\infty}\frac{\left(\sqrt{\omega^2\epsilon_x\mu_x - \frac{\mu_x}{\mu_y}\lambda_x^2}\right)^3}{((\frac{n\pi}{b})^2 - \omega^2\epsilon_x\mu_x + \frac{\mu_x}{\mu_y}\lambda_x^2)((\frac{n\pi}{b})^2 - \omega^2\epsilon_x\mu_x + \frac{\mu_x}{\mu_y}\lambda_x^2)}\cdot \tag{D.205}$$
$$\frac{(1-e^{-j\sqrt{\omega^2\epsilon_x\mu_x - \frac{\mu_x}{\mu_y}\lambda_x^2}b}(-1)^n)}{-\lambda_x^2(2d)}$$

$$\sum_{l=0}^{\infty} \oint_{\lambda_{yA}} \frac{f(z)}{z-z_0} = j2\pi \sum_{l=0}^{\infty} \frac{f_1(z_0)}{f_2'(z_0)}$$

$$f(\lambda_y) = \frac{\lambda_y^4}{((\frac{n\pi}{b})^2-\lambda_y^2)((\frac{n\pi}{b})^2-\lambda_y^2)} \frac{\cos(k_{ZTE}(d))}{k_{ZTE}\sin(k_{ZTE}d)} \frac{(1-e^{j\lambda_y b}(-1)^n)}{(\lambda_y-\omega\sqrt{\epsilon_x\mu_x})(\lambda_y+\omega\sqrt{\epsilon_x\mu_x})}$$

Evaluating the $l \neq 0$ part second

$$f_1(\lambda_{yl\neq 0}) = \frac{\lambda_y^4}{((\frac{n\pi}{b})^2-\lambda_y^2)((\frac{n\pi}{b})^2-\lambda_y^2)} \frac{\cos(k_{ZTE}(d))}{k_{ZTE}} \frac{(1-e^{j\lambda_y b}(-1)^n)}{(\lambda_y-\omega\sqrt{\epsilon_x\mu_x})(\lambda_y+\omega\sqrt{\epsilon_x\mu_x})}$$

$$f_2(\lambda_y) = \sin(k_{ZTE}d)$$

$$f_2'(\lambda_{yl\neq 0}) = \cos(k_{ZTE}d)\frac{1}{2k_{ZTE}}\left(-2\frac{\mu_y}{\mu_x}\lambda_y d\right)$$

$$f_2'(\lambda_{yl\neq 0}) = -cos(k_{ZTE}d)\frac{1}{k_{ZTE}}\left(\frac{\mu_y}{\mu_x}\lambda_y d\right) \tag{D.206}$$

$$f_2'(\lambda_{yl\neq 0}) = \frac{(-1)^l}{\pm\frac{l\pi}{d}}\left(\frac{\mu_y}{\mu_x}\sqrt{\omega^2\epsilon_x\mu_x - \frac{\mu_x}{\mu_y}\lambda_x^2 - \frac{\mu_x}{\mu_y}\left(\frac{l\pi}{d}\right)^2}\, d\right)$$

$$f_1(\lambda_{yl\neq 0}) = \frac{\lambda_y^4}{((\frac{n\pi}{b})^2-\lambda_y^2)((\frac{n\pi}{b})^2-\lambda_y^2)} \frac{\cos(k_{ZTE}(d))}{k_{ZTE}} \frac{(1-e^{j\lambda_y b}(-1)^n)}{(\lambda_y-\omega\sqrt{\epsilon_x\mu_x})(\lambda_y+\omega\sqrt{\epsilon_x\mu_x})}$$

$$f_1(\lambda_{yl\neq 0}) = \frac{\left(\omega^2\epsilon_x\mu_x - \frac{\mu_x}{\mu_y}\lambda_x^2 - \frac{\mu_x}{\mu_y}\left(\frac{l\pi}{d}\right)^2\right)}{((\frac{n\pi}{b})^2 - \omega^2\epsilon_x\mu_x + \frac{\mu_x}{\mu_y}\lambda_x^2 + \frac{\mu_x}{\mu_y}\left(\frac{l\pi}{d}\right)^2)((\frac{n\pi}{b})^2 - \omega^2\epsilon_x\mu_x + \frac{\mu_x}{\mu_y}\lambda_x^2 + \frac{\mu_x}{\mu_y}\left(\frac{l\pi}{d}\right)^2)}.$$

$$\frac{(-1)^l}{\frac{l\pi}{d}} \frac{(1-e^{-j\sqrt{\omega^2\epsilon_x\mu_x - \frac{\mu_x}{\mu_y}\lambda_x^2 - \frac{\mu_x}{\mu_y}\left(\frac{l\pi}{d}\right)^2}b}(-1)^n)}{(\omega^2\epsilon_x\mu_x - \frac{\mu_x}{\mu_y}\lambda_x^2 - \frac{\mu_x}{\mu_y}\left(\frac{l\pi}{d}\right)^2 - \omega^2\epsilon_x\mu_x)}$$

$$j2\pi\frac{f_1(\lambda_{yl\neq 0})}{f_2'(\lambda_{yl\neq 0})} =$$

$$j2\pi\sum_{l=0}^{\infty}\frac{\left(\omega^2\epsilon_x\mu_x-\frac{\mu_x}{\mu_y}\lambda_x^2-\frac{\mu_x}{\mu_y}\left(\frac{l\pi}{d}\right)^2\right)^2}{((\frac{n\pi}{b})^2-\omega^2\epsilon_x\mu_x+\frac{\mu_x}{\mu_y}\lambda_x^2+\frac{\mu_x}{\mu_y}\left(\frac{l\pi}{d}\right)^2)((\frac{n\pi}{b})^2-\omega^2\epsilon_x\mu_x+\frac{\mu_x}{\mu_y}\lambda_x^2+\frac{\mu_x}{\mu_y}\left(\frac{l\pi}{d}\right)^2)}\cdot \tag{D.207}$$

$$\frac{(-1)^l}{\frac{l\pi}{d}}\frac{(1-e^{-j\sqrt{\omega^2\epsilon_x\mu_x-\frac{\mu_x}{\mu_y}\lambda_x^2-\frac{\mu_x}{\mu_y}\left(\frac{l\pi}{d}\right)^2}b}(-1)^n)}{-\frac{\mu_x}{\mu_y}(\lambda_x^2+\left(\frac{l\pi}{d}\right)^2)}\cdot\frac{\pm\frac{l\pi}{d}}{(-1)^l}\left(\frac{\mu_x}{\mu_y}\frac{1}{\sqrt{\omega^2\epsilon_x\mu_x-\frac{\mu_x}{\mu_y}\lambda_x^2-\frac{\mu_x}{\mu_y}\left(\frac{l\pi}{d}\right)^2}d}\right)$$

$$j2\pi\frac{f_1(\lambda_{yl\neq 0})}{f_2'(\lambda_{yl\neq 0})}$$

$$= j2\pi\sum_{l=0}^{\infty}\frac{\left(\sqrt{\omega^2\epsilon_x\mu_x-\frac{\mu_x}{\mu_y}\lambda_x^2-\frac{\mu_x}{\mu_y}\left(\frac{l\pi}{d}\right)^2}\right)^3}{((\frac{n\pi}{b})^2-\omega^2\epsilon_x\mu_x+\frac{\mu_x}{\mu_y}\lambda_x^2+\frac{\mu_x}{\mu_y}\left(\frac{l\pi}{d}\right)^2)((\frac{n\pi}{b})^2-\omega^2\epsilon_x\mu_x+\frac{\mu_x}{\mu_y}\lambda_x^2+\frac{\mu_x}{\mu_y}\left(\frac{l\pi}{d}\right)^2)}\cdot \tag{D.208}$$

$$\frac{(1-e^{-j\sqrt{\omega^2\epsilon_x\mu_x-\frac{\mu_x}{\mu_y}\lambda_x^2-\frac{\mu_x}{\mu_y}\left(\frac{l\pi}{d}\right)^2}b}(-1)^n)}{-(\lambda_x^2+\left(\frac{l\pi}{d}\right)^2d)}$$

Combining: $l\neq 0$ and $l=0$

$$j2\pi\frac{f_1(\lambda_{yl=0})}{f_2'(\lambda_{yl=0})} = \frac{\left(\sqrt{\omega^2\epsilon_x\mu_x-\frac{\mu_x}{\mu_y}\lambda_x^2}\right)}{((\frac{n\pi}{b})^2-\omega^2\epsilon_x\mu_x+\frac{\mu_x}{\mu_y}\lambda_x^2)((\frac{n\pi}{b})^2-\omega^2\epsilon_x\mu_x+\frac{\mu_x}{\mu_y}\lambda_x^2)}\frac{(1-e^{-j\sqrt{\omega^2\epsilon_x\mu_x-\frac{\mu_x}{\mu_y}\lambda_x^2}b}(-1)^n)}{-\lambda_x^2 2d} \tag{D.209}$$

$$= j2\pi \sum_{l=0}^{\infty} \frac{f_1(\lambda_{yl\neq 0})}{f_2'(\lambda_{yl\neq 0})}$$

$$= j2\pi \sum_{l=0}^{\infty} \frac{\left(\sqrt{\omega^2\epsilon_x\mu_x - \frac{\mu_x}{\mu_y}\lambda_x^2 - \frac{\mu_x}{\mu_y}\left(\frac{l\pi}{d}\right)^2}\right)^3}{((\frac{n\pi}{b})^2 - \omega^2\epsilon_x\mu_x + \frac{\mu_x}{\mu_y}\lambda_x^2 + \frac{\mu_x}{\mu_y}\left(\frac{l\pi}{d}\right)^2)((\frac{n\pi}{b})^2 - \omega^2\epsilon_x\mu_x + \frac{\mu_x}{\mu_y}\lambda_x^2 + \frac{\mu_x}{\mu_y}\left(\frac{l\pi}{d}\right)^2)} \cdot \frac{(1 - e^{-j\sqrt{\omega^2\epsilon_x\mu_x - \frac{\mu_x}{\mu_y}\lambda_x^2 - \frac{\mu_x}{\mu_y}\left(\frac{l\pi}{d}\right)^2}b}(-1)^n)}{-(\lambda_x^2 + \left(\frac{l\pi}{d}\right)^2 d)} \tag{D.210}$$

$$\boxed{= -j2\pi \sum_{l=0}^{\infty} \frac{\left(\sqrt{\omega^2\epsilon_x\mu_x - \frac{\mu_x}{\mu_y}\lambda_x^2 - \frac{\mu_x}{\mu_y}\left(\frac{l\pi}{d}\right)^2}\right)}{((\frac{n\pi}{b})^2 - \omega^2\epsilon_x\mu_x + \frac{\mu_x}{\mu_y}\lambda_x^2 + \frac{\mu_x}{\mu_y}\left(\frac{l\pi}{d}\right)^2)^2} \frac{(1 - e^{-j\sqrt{\omega^2\epsilon_x\mu_x - \frac{\mu_x}{\mu_y}\lambda_x^2 - \frac{\mu_x}{\mu_y}\left(\frac{l\pi}{d}\right)^2}b}(-1)^n)}{(\lambda_x^2 + \left(\frac{l\pi}{d}\right)^2)d(1 + \delta_{l=0})}} \tag{D.211}$$

for UHP Pole λ_{yA}.

$$\oint_{\lambda_y C} \frac{f(z)}{(z - z_0)^2} = j\pi \frac{d}{dz} f(z_0) = j\pi \frac{d}{d\lambda_y} \frac{\lambda_y^4 \cos(k_{ZTE}(d))}{k_{ZTE}\sin(k_{ZTE}d)} \frac{(1 - e^{j\lambda_y b}(-1)^n)}{((\frac{n\pi}{b}) - \lambda_y)((\frac{n\pi}{b}) - \lambda_y)(\lambda_y - \omega\sqrt{\epsilon_x\mu_x})(\lambda_y + \omega\sqrt{\epsilon_x\mu_x})}\Bigg|_{\lambda_y = -\frac{n\pi}{b}} = \tag{D.212}$$

Evaluating the double pole case ($\lambda_y = -\frac{n\pi}{b}$). There are values that go to zero because:

$$(1 - e^{j(\frac{n\pi}{b})b}(-1)^n) = (1 - e^{j(n\pi)}(-1)^n) = (1 - (-1)^n(-1)^n) = (1 - (-1)^{2n}) = (1 - 1) = 0 \tag{D.213}$$

The result after evaluating the derivatives yields:

$$\oint_{\lambda_{yC}} \frac{f(z)}{(z-z_0)^2} = j\pi \frac{(-\frac{n\pi}{b})^4 \cos(k_{ZTE}(d))}{k_{ZTE}\sin(k_{ZTE}d)} \cdot \frac{\left[-jbe^{jb(-\frac{n\pi}{b})}(-1)^n\right]}{((\frac{n\pi}{b})-(-\frac{n\pi}{b}))((\frac{n\pi}{b})-(-\frac{n\pi}{b}))((-\frac{n\pi}{b})-\omega\sqrt{\epsilon_x\mu_x})((-\frac{n\pi}{b})+\omega\sqrt{\epsilon_x\mu_x})} \tag{D.214}$$

$$= j\pi \frac{(-\frac{n\pi}{b})^4 \cos(\sqrt{\omega^2\epsilon_x\mu_y - \lambda_x^2 - \frac{\mu_y}{\mu_x}((\frac{n\pi}{b}))^2}(d))}{\sqrt{\omega^2\epsilon_x\mu_y - \lambda_x^2 - \frac{\mu_y}{\mu_x}((\frac{n\pi}{b}))^2}\sin(\sqrt{\omega^2\epsilon_x\mu_y - \lambda_x^2 - \frac{\mu_y}{\mu_x}((\frac{n\pi}{b}))^2}d)} \frac{\left[-jbe^{jb(-\frac{n\pi}{b})}(-1)^n\right]}{(4(\frac{n\pi}{b})^2)((\frac{n\pi}{b})^2-\omega^2\epsilon_x\mu_x)} \tag{D.215}$$

$$= j\pi \frac{(\frac{n\pi}{b})^2 \cos(\sqrt{\omega^2\epsilon_x\mu_y - \lambda_x^2 - \frac{\mu_y}{\mu_x}((\frac{n\pi}{b}))^2}d)}{\sqrt{\omega^2\epsilon_x\mu_y - \lambda_x^2 - \frac{\mu_y}{\mu_x}((\frac{n\pi}{b}))^2}\sin(\sqrt{\omega^2\epsilon_x\mu_y - \lambda_x^2 - \frac{\mu_y}{\mu_x}((\frac{n\pi}{b}))^2}d)} \frac{-jb}{4((\frac{n\pi}{b})^2-\omega^2\epsilon_x\mu_x)} \tag{D.216}$$

$$\boxed{\pi \frac{(\frac{n\pi}{b})^2 \cos(\sqrt{\omega^2\epsilon_x\mu_y - \lambda_x^2 - \frac{\mu_y}{\mu_x}((\frac{n\pi}{b}))^2}d)}{\sqrt{\omega^2\epsilon_x\mu_y - \lambda_x^2 - \frac{\mu_y}{\mu_x}((\frac{n\pi}{b}))^2}\sin(\sqrt{\omega^2\epsilon_x\mu_y - \lambda_x^2 - \frac{\mu_y}{\mu_x}((\frac{n\pi}{b}))^2}d)} \frac{b}{4((\frac{n\pi}{b})^2-\omega^2\epsilon_x\mu_x)}} \tag{D.217}$$

for UHP Pole λ_{yC}.

$$\oint_{\lambda_{yD}} \frac{f(z)}{(z-z_0)^2} = j\pi \frac{d}{dz} f(z_0) = \\ j\pi \frac{d}{dz} \left. \frac{\lambda_y^4 \cos(k_{ZTE}(d))}{k_{ZTE} \sin(k_{ZTE} d)} \frac{(1 - e^{j\lambda_y b}(-1)^n)}{((\frac{n\pi}{b}) - \lambda_y)((\frac{n\pi}{b}) - \lambda_y)(\lambda_y - \omega\sqrt{\epsilon_x \mu_x})(\lambda_y + \omega\sqrt{\epsilon_x \mu_x})} \right|_{\lambda_y = \frac{n\pi}{b}} = \tag{D.218}$$

Apply the pole ($\lambda_y = \frac{n\pi}{b}$): There are values that go to zero because:

$$(1 - e^{j(\frac{n\pi}{b})b}(-1)^n) = (1 - e^{j(n\pi)}(-1)^n) = (1 - (-1)^n(-1)^n) = (1 - (-1)^{2n}) = (1-1) = 0 \tag{D.219}$$

So we are left with:

$$\oint_{\lambda_{yD}} \frac{f(z)}{(z-z_0)^2} \\ = j\pi \frac{(-\frac{n\pi}{b})^4 \cos(\sqrt{\omega^2 \epsilon_x \mu_y - \lambda_x^2 - \frac{\mu_y}{\mu_x}((\frac{n\pi}{b}))^2}(d))}{\sqrt{\omega^2 \epsilon_x \mu_y - \lambda_x^2 - \frac{\mu_y}{\mu_x}((\frac{n\pi}{b}))^2} \sin(\sqrt{\omega^2 \epsilon_x \mu_y - \lambda_x^2 - \frac{\mu_y}{\mu_x}((\frac{n\pi}{b}))^2} d)} \frac{\left[-jbe^{jb(-\frac{n\pi}{b})}(-1)^n\right]}{(4(\frac{n\pi}{b})^2)((\frac{n\pi}{b})^2 - \omega^2 \epsilon_x \mu_x)} \tag{D.220}$$

$$\oint_{\lambda_{yD}} \frac{f(z)}{(z-z_0)^2} \\ = j\pi \frac{(\frac{n\pi}{b})^2 \cos(\sqrt{\omega^2 \epsilon_x \mu_y - \lambda_x^2 - \frac{\mu_y}{\mu_x}((\frac{n\pi}{b}))^2} d)}{\sqrt{\omega^2 \epsilon_x \mu_y - \lambda_x^2 - \frac{\mu_y}{\mu_x}((\frac{n\pi}{b}))^2} \sin(\sqrt{\omega^2 \epsilon_x \mu_y - \lambda_x^2 - \frac{\mu_y}{\mu_x}((\frac{n\pi}{b}))^2} d)} \frac{-jb}{4((\frac{n\pi}{b})^2 - \omega^2 \epsilon_x \mu_x)} \tag{D.221}$$

$$\boxed{\pi \frac{(\frac{n\pi}{b})^2 \cos(\sqrt{\omega^2\epsilon_x\mu_y - \lambda_x^2 - \frac{\mu_y}{\mu_x}((\frac{n\pi}{b}))^2}d)}{\sqrt{\omega^2\epsilon_x\mu_y - \lambda_x^2 - \frac{\mu_y}{\mu_x}((\frac{n\pi}{b}))^2}\sin(\sqrt{\omega^2\epsilon_x\mu_y - \lambda_x^2 - \frac{\mu_y}{\mu_x}((\frac{n\pi}{b}))^2}d)} \frac{b}{4((\frac{n\pi}{b})^2 - \omega^2\epsilon_x\mu_x)}} \tag{D.222}$$

for UHP Pole λ_{yD}.

LHP:

$$\int_{-\infty}^{\infty} \frac{\lambda_y^4}{k_{ZTE}(\lambda_y^2 - \omega^2\epsilon_x\mu_x)} \frac{\cos(k_{ZTE}d)}{\sin(k_{ZTE}d)} \frac{(1 - e^{-jb\lambda_y}(-1)^n)}{((\frac{v\pi}{b})^2 - \lambda_y^2)(k_y^2 - \lambda_y^2)} d\lambda_y \tag{D.223}$$

Identification of the poles:

$$\lambda_y = \pm\sqrt{\omega^2\epsilon_x\mu_x - \frac{\mu_x}{\mu_y}\lambda_x^2} \tag{D.224}$$

$$\lambda_y = \pm\sqrt{\omega^2\epsilon_x\mu_x - \frac{\mu_x}{\mu_y}\lambda_x^2 - \frac{\mu_x}{\mu_y}\left(\frac{l\pi}{d}\right)^2} \tag{D.225}$$

$$\pm\sqrt{\omega^2\epsilon_x\mu_x} = \lambda_y \tag{D.226}$$

$$\pm\frac{n\pi}{b} = \lambda_y \tag{D.227}$$

$$\pm\frac{n\pi}{b} = \lambda_y \tag{D.228}$$

Now doing the lower half plane.

$$\int_{-\infty}^{\infty} + \oint_{\lambda_{yA}} + \oint_{\lambda_{yB}} + \oint_{\lambda_{yC}} + \oint_{\lambda_{yD}} + \oint_{C_R} = 0 \tag{D.229}$$

where C_R is the radius at infinity.

$$\int_{-\infty}^{\infty} + \oint_{\lambda_{yA}} + \oint_{\lambda_{yB}} + \oint_{\lambda_{yC}} + \oint_{\lambda_{yD}} + \cancelto{0}{\oint_{C_R}} = 0 \tag{D.230}$$

$$\int_{-\infty}^{\infty} = -\oint_{\lambda_{yA}} - \oint_{\lambda_{yB}} - \oint_{\lambda_{yC}} - \oint_{\lambda_{yD}} \tag{D.231}$$

Evaluating the λ_{yB} pole.

$$\begin{aligned}
-\oint_{\lambda_{yB}} \frac{f(z)}{z-z_0} = -j2\pi f(z_0) = \\
-j2\pi \left. \frac{\lambda_y^4}{((\frac{n\pi}{b})^2-\lambda_y^2)((\frac{n\pi}{b})^2-\lambda_y^2)} \frac{\cos(k_{ZTE}(d))}{k_{ZTE}\sin(k_{ZTE}d)} \frac{(1-e^{-j\lambda_y b}(-1)^n)}{(\lambda_y+\omega\sqrt{\epsilon_x\mu_x})} \right|_{\lambda_y=\omega\sqrt{\epsilon_x\mu_x}} = \\
-j2\pi \frac{(\omega\sqrt{\epsilon_x\mu_x})^4}{((\frac{n\pi}{b})^2-\omega^2\epsilon_x\mu_x)((\frac{n\pi}{b})^2-\omega^2\epsilon_x\mu_x)} \frac{\cos(\sqrt{-\lambda_x^2}(d))}{\sqrt{-\lambda_x^2}\sin(\sqrt{-\lambda_x^2}d)} \frac{(e^{-j\left(\omega\sqrt{\epsilon_x\mu_x}\right)b}(-1)^n-1)}{2\omega\sqrt{\epsilon_x\mu_x}} = \\
-\pi \frac{(\omega\sqrt{\epsilon_x\mu_x})^3}{((\frac{n\pi}{b})^2-\omega^2\epsilon_x\mu_x)((\frac{n\pi}{b})^2-\omega^2\epsilon_x\mu_x)} \frac{\cos(j\lambda_x d)}{\lambda_x\sin(j\lambda_x d)} \frac{(e^{-j\omega\sqrt{\epsilon_x\mu_x}b}(-1)^n-1)}{1} =
\end{aligned} \tag{D.232}$$

$$\boxed{-\pi \frac{(\omega\sqrt{\epsilon_x\mu_x})^3}{((\frac{n\pi}{b})^2-\omega^2\epsilon_x\mu_x)((\frac{n\pi}{b})^2-\omega^2\epsilon_x\mu_x)} \frac{\cos(j\lambda_x d)}{\lambda_x\sin(j\lambda_x d)} \frac{(e^{-j\omega\sqrt{\epsilon_x\mu_x}b}(-1)^n-1)}{1}} \tag{D.233}$$

for LHP Pole λ_{yB}.

$\oint_{\lambda_{yA}}$ contains a double pole and is not a simple pole. Additionally it is constituted by a sum of terms l. When $l = 0$, $\lambda_y = \pm\sqrt{\omega^2\epsilon_x\mu_x - \frac{\mu_x}{\mu_y}\lambda_x^2}$ and when $l \neq 0$, $\lambda_y = \pm\sqrt{\omega^2\epsilon_x\mu_x - \frac{\mu_x}{\mu_y}\lambda_x^2 - \frac{\mu_x}{\mu_y}\left(\frac{l\pi}{d}\right)^2}$

$$-\sum_{l=0}^{\infty}\oint_{\lambda_{yA}}\frac{f(z)}{z-z_0} = -j2\pi\sum_{l=0}^{\infty}\frac{f_1(z_0)}{f_2'(z_0)}$$

$$f(\lambda_y) = \frac{\lambda_y^4}{((\frac{n\pi}{b})^2-\lambda_y^2)((\frac{n\pi}{b})^2-\lambda_y^2)}\frac{\cos(k_{ZTE}(d))}{k_{ZTE}\sin(k_{ZTE}d)}\frac{(1-e^{-j\lambda_y b}(-1)^n)}{(\lambda_y-\omega\sqrt{\epsilon_x\mu_x})(\lambda_y+\omega\sqrt{\epsilon_x\mu_x})}$$

Evaluating the l=0 part first:

$$f_1(\lambda_{yl=0}) = \frac{\lambda_y^4}{((\frac{n\pi}{b})^2-\lambda_y^2)((\frac{n\pi}{b})^2-\lambda_y^2)}\frac{\cos(k_{ZTE}(d))}{1}\frac{(1-e^{-j\lambda_y b}(-1)^n)}{(\lambda_y-\omega\sqrt{\epsilon_x\mu_x})(\lambda_y+\omega\sqrt{\epsilon_x\mu_x})} \tag{D.234}$$

$$f_2(\lambda_{yl=0}) = k_{ZTE}\sin(k_{ZTE}d)$$

$$f_2'(\lambda_{yl=0}) = \sin(k_{ZTE}d)\frac{1}{2k_{ZTE}}\left(-2\frac{\mu_y}{\mu_x}\lambda_y d\right) + k_{ZTE}\cos(k_{ZTE}d)\frac{1}{2k_{ZTE}}\left(-2\frac{\mu_y}{\mu_x}\lambda_y d\right)$$

$$f_2'(\lambda_{yl=0}) = -\sin(k_{ZTE}d)\frac{1}{k_{ZTE}}\left(\frac{\mu_y}{\mu_x}\lambda_y d\right) - cos(k_{ZTE}d)\left(\frac{\mu_y}{\mu_x}\lambda_y d\right)$$

$$f_2'(\lambda_{yl=0}) = -\left(\frac{\mu_y}{\mu_x}\lambda_y d\right)\left[\sin(k_{ZTE}d)\frac{1}{k_{ZTE}} + cos(k_{ZTE}d)\right]$$

$$f_2'(\lambda_{yl=0}) = -\left(\frac{\mu_y}{\mu_x}\sqrt{\omega^2\epsilon_x\mu_x - \frac{\mu_x}{\mu_y}\lambda_x^2}d\right)[1+1]$$

$$f_2'(\lambda_{yl=0}) = -2\left(\frac{\mu_y}{\mu_x}\sqrt{\omega^2\epsilon_x\mu_x - \frac{\mu_x}{\mu_y}\lambda_x^2}d\right)$$

$$f_1(\lambda_{y=0}) = \frac{\lambda_y^4\cos(k_{ZTE}(d))}{((\frac{n\pi}{b})^2-\lambda_y^2)((\frac{n\pi}{b})^2-\lambda_y^2)}\frac{(1-e^{-j\lambda_y b}(-1)^n)}{(\lambda_y-\omega\sqrt{\epsilon_x\mu_x})(\lambda_y+\omega\sqrt{\epsilon_x\mu_x})}$$

$$f_1(\lambda_{yl=0}) = \frac{\left(\omega^2\epsilon_x\mu_x - \frac{\mu_x}{\mu_y}\lambda_x^2\right)^2}{((\frac{n\pi}{b})^2-\omega^2\epsilon_x\mu_x+\frac{\mu_x}{\mu_y}\lambda_x^2)((\frac{n\pi}{b})^2-\omega^2\epsilon_x\mu_x+\frac{\mu_x}{\mu_y}\lambda_x^2)}\cdot \tag{D.235}$$

$$\frac{(1-e^{-j\sqrt{\omega^2\epsilon_x\mu_x-\frac{\mu_x}{\mu_y}\lambda_x^2}b}(-1)^n)}{-\frac{\mu_x}{\mu_y}\lambda_x^2}$$

$$-j2\pi\frac{f_1(\lambda_{yl=0})}{f_2'(\lambda_{yl=0})} = -j2\pi\frac{\left(\omega^2\epsilon_x\mu_x - \frac{\mu_x}{\mu_y}\lambda_x^2\right)^2}{((\frac{n\pi}{b})^2-\omega^2\epsilon_x\mu_x+\frac{\mu_x}{\mu_y}\lambda_x^2)((\frac{n\pi}{b})^2-\omega^2\epsilon_x\mu_x+\frac{\mu_x}{\mu_y}\lambda_x^2)}\cdot$$

$$\frac{(1-e^{-j\sqrt{\omega^2\epsilon_x\mu_x-\frac{\mu_x}{\mu_y}\lambda_x^2}b}(-1)^n)}{-\frac{\mu_x}{\mu_y}\lambda_x^2(-2\frac{\mu_y}{\mu_x}\sqrt{\omega^2\epsilon_x\mu_x-\frac{\mu_x}{\mu_y}\lambda_x^2}d)}$$

$$= -j2\pi\frac{\left(\sqrt{\omega^2\epsilon_x\mu_x - \frac{\mu_x}{\mu_y}\lambda_x^2}\right)^3}{((\frac{n\pi}{b})^2-\omega^2\epsilon_x\mu_x+\frac{\mu_x}{\mu_y}\lambda_x^2)((\frac{n\pi}{b})^2-\omega^2\epsilon_x\mu_x+\frac{\mu_x}{\mu_y}\lambda_x^2)}\frac{(e^{-j\sqrt{\omega^2\epsilon_x\mu_x-\frac{\mu_x}{\mu_y}\lambda_x^2}b}(-1)^n-1)}{-\lambda_x^2(-2d)} \tag{D.236}$$

$$-\sum_{l=0}^{\infty}\oint_{\lambda_{yB}}\frac{f(z)}{z-z_0}=-j2\pi\sum_{l=0}^{\infty}\frac{f_1(z_0)}{f_2'(z_0)}$$

$$f(\lambda_y)=\frac{\lambda_y^4}{((\frac{n\pi}{b})^2-\lambda_y^2)((\frac{n\pi}{b})^2-\lambda_y^2)}\frac{\cos(k_{ZTE}(d))}{k_{ZTE}\sin(k_{ZTE}d)}\frac{(1-e^{-j\lambda_y b}(-1)^n)}{(\lambda_y-\omega\sqrt{\epsilon_x\mu_x})(\lambda_y+\omega\sqrt{\epsilon_x\mu_x})}$$

Evaluaing the $l\neq 0$ part second:

$$f_1(\lambda_{yl\neq 0})=\frac{\lambda_y^4}{((\frac{n\pi}{b})^2-\lambda_y^2)((\frac{n\pi}{b})^2-\lambda_y^2)}\frac{\cos(k_{ZTE}(d))}{k_{ZTE}}\frac{(1-e^{-j\lambda_y b}(-1)^n)}{(\lambda_y-\omega\sqrt{\epsilon_x\mu_x})(\lambda_y+\omega\sqrt{\epsilon_x\mu_x})}$$

$$f_2(\lambda_{yl\neq 0})=\sin(k_{ZTE}d) \tag{D.237}$$

$$f_2'(\lambda_{yl\neq 0})=\cos(k_{ZTE}d)\frac{1}{2k_{ZTE}}\left(-2\frac{\mu_y}{\mu_x}\lambda_y d\right)$$

$$f_2'(\lambda_{yl\neq 0})=-cos(k_{ZTE}d)\frac{1}{k_{ZTE}}\left(\frac{\mu_y}{\mu_x}\lambda_y d\right)$$

$$f_2'(\lambda_{yl\neq 0})=-\frac{(-1)^l}{\pm\frac{l\pi}{d}}\left(\frac{\mu_y}{\mu_x}\sqrt{\omega^2\epsilon_x\mu_x-\frac{\mu_x}{\mu_y}\lambda_x^2-\frac{\mu_x}{\mu_y}\left(\frac{l\pi}{d}\right)^2}d\right)$$

$$f_1(\lambda_{yl\neq 0})=\frac{\lambda_y^4}{((\frac{n\pi}{b})^2-\lambda_y^2)((\frac{n\pi}{b})^2-\lambda_y^2)}\frac{\cos(k_{ZTE}(d))}{k_{ZTE}}\frac{(1-e^{-j\lambda_y b})(-1)^n}{(\lambda_y-\omega\sqrt{\epsilon_x\mu_x})(\lambda_y+\omega\sqrt{\epsilon_x\mu_x})}$$

Combining the $l\neq 0$ and $l=0$ parts:

$$-j2\pi\frac{\left(\sqrt{\omega^2\epsilon_x\mu_x-\frac{\mu_x}{\mu_y}\lambda_x^2}\right)^3}{((\frac{n\pi}{b})^2-\omega^2\epsilon_x\mu_x+\frac{\mu_x}{\mu_y}\lambda_x^2)((\frac{n\pi}{b})^2-\omega^2\epsilon_x\mu_x+\frac{\mu_x}{\mu_y}\lambda_x^2)}\frac{(1-e^{-j\sqrt{\omega^2\epsilon_x\mu_x-\frac{\mu_x}{\mu_y}\lambda_x^2}b}(-1)^n)}{-\lambda_x^2}\frac{1}{-2d} \tag{D.238}$$

$$-j2\pi\sum_{l=0}^{\infty}\frac{f_1(\lambda_{yl\neq 0})}{f_2'(\lambda_{yl\neq 0})}=$$

$$-j2\pi\sum_{l=0}^{\infty}\frac{\left(\sqrt{\omega^2\epsilon_x\mu_x-\frac{\mu_x}{\mu_y}\lambda_x^2-\frac{\mu_x}{\mu_y}\left(\frac{l\pi}{d}\right)^2}\right)^3}{((\frac{n\pi}{b})^2-\omega^2\epsilon_x\mu_x+\frac{\mu_x}{\mu_y}\left(\lambda_x^2+\left(\frac{l\pi}{d}\right)^2\right))((\frac{n\pi}{b})^2-\omega^2\epsilon_x\mu_x+\frac{\mu_x}{\mu_y}\left(\lambda_x^2+\left(\frac{l\pi}{d}\right)^2\right))}\cdot \tag{D.239}$$

$$\frac{(1-e^{-j\sqrt{\omega^2\epsilon_x\mu_x-\frac{\mu_x}{\mu_y}\lambda_x^2-\frac{\mu_x}{\mu_y}\left(\frac{l\pi}{d}\right)^2}b}(-1)^n)}{(\lambda_x^2+\left(\frac{l\pi}{d}\right)^2)d}$$

$$\boxed{-j2\pi\sum_{l=0}^{\infty}\frac{\left(\sqrt{\omega^2\epsilon_x\mu_x-\frac{\mu_x}{\mu_y}\lambda_x^2-\frac{\mu_x}{\mu_y}\left(\frac{l\pi}{d}\right)^2}\right)^3}{((\frac{n\pi}{b})^2-\omega^2\epsilon_x\mu_x+\frac{\mu_x}{\mu_y}\left(\lambda_x^2+\left(\frac{l\pi}{d}\right)^2\right))^2}\frac{(1-e^{-j\sqrt{\omega^2\epsilon_x\mu_x-\frac{\mu_x}{\mu_y}\lambda_x^2-\frac{\mu_x}{\mu_y}\left(\frac{l\pi}{d}\right)^2}b}(-1)^n)}{(\lambda_x^2+\left(\frac{l\pi}{d}\right)^2)d(1+\delta_{l=0})}} \tag{D.240}$$

for LHP Pole λ_{yA}.

On to the next pole:

$$-\oint_{\lambda_{yC}}\frac{f(z)}{(z-z_0)^2}=-j\pi\frac{d}{dz}f(z_0)=$$

$$-j\pi\frac{d}{dz}\left.\frac{\lambda_y^4\cos(k_{ZTE}(d))}{k_{ZTE}\sin(k_{ZTE}d)}\frac{(1-e^{-j\lambda_y b}(-1)^n)}{((\frac{n\pi}{b})-\lambda_y)((\frac{n\pi}{b})-\lambda_y)(\lambda_y-\omega\sqrt{\epsilon_x\mu_x})(\lambda_y+\omega\sqrt{\epsilon_x\mu_x})}\right|_{\lambda_y=-\frac{n\pi}{b}}= \tag{D.241}$$

Evaluating the derivatives: Apply the pole ($\lambda_y=-\frac{n\pi}{b}$):

There are values that go to zero because:

$$(1-e^{j(\frac{n\pi}{b})b}(-1)^n) = (1-e^{j(n\pi)}(-1)^n) = (1-(-1)^n(-1)^n) = (1-(-1)^{2n}) = (1-1) = 0 \tag{D.242}$$

This results in:

$$\oint_{\lambda_{yC}} \frac{f(z)}{(z-z_0)^2} = \tag{D.243}$$
$$-j\pi \frac{(-\frac{n\pi}{b})^4 \cos(k_{ZTE}(d))}{k_{ZTE}\sin(k_{ZTE}d)} \frac{\left[jbe^{jb(-\frac{n\pi}{b})}(-1)^n\right]}{((\frac{n\pi}{b})-(-\frac{n\pi}{b}))((\frac{n\pi}{b})-(-\frac{n\pi}{b}))((-\frac{n\pi}{b})-\omega\sqrt{\epsilon_x\mu_x})((-\frac{n\pi}{b})+\omega\sqrt{\epsilon_x\mu_x})}$$

$$\oint_{\lambda_{yC}} \frac{f(z)}{(z-z_0)^2} = \tag{D.244}$$
$$-j\pi \frac{(-\frac{n\pi}{b})^4 \cos(\sqrt{\omega^2\epsilon_x\mu_y - \lambda_x^2 - \frac{\mu_y}{\mu_x}((\frac{n\pi}{b}))^2}(d))}{\sqrt{\omega^2\epsilon_x\mu_y - \lambda_x^2 - \frac{\mu_y}{\mu_x}((\frac{n\pi}{b}))^2}\sin(\sqrt{\omega^2\epsilon_x\mu_y - \lambda_x^2 - \frac{\mu_y}{\mu_x}((\frac{n\pi}{b}))^2}d)} \frac{\left[jbe^{-jb(-\frac{n\pi}{b})}(-1)^n\right]}{(4(\frac{n\pi}{b})^2)((\frac{n\pi}{b})^2-\omega^2\epsilon_x\mu_x)}$$

$$-j\pi \frac{(\frac{n\pi}{b})^2 \cos(\sqrt{\omega^2\epsilon_x\mu_y - \lambda_x^2 - \frac{\mu_y}{\mu_x}((\frac{n\pi}{b}))^2}d)}{\sqrt{\omega^2\epsilon_x\mu_y - \lambda_x^2 - \frac{\mu_y}{\mu_x}((\frac{n\pi}{b}))^2}\sin(\sqrt{\omega^2\epsilon_x\mu_y - \lambda_x^2 - \frac{\mu_y}{\mu_x}((\frac{n\pi}{b}))^2}d)} \frac{jb}{4((\frac{n\pi}{b})^2-\omega^2\epsilon_x\mu_x)} \tag{D.245}$$

$$\boxed{\pi \frac{(\frac{n\pi}{b})^2 \cos(\sqrt{\omega^2\epsilon_x\mu_y - \lambda_x^2 - \frac{\mu_y}{\mu_x}((\frac{n\pi}{b}))^2}d)}{\sqrt{\omega^2\epsilon_x\mu_y - \lambda_x^2 - \frac{\mu_y}{\mu_x}((\frac{n\pi}{b}))^2}\sin(\sqrt{\omega^2\epsilon_x\mu_y - \lambda_x^2 - \frac{\mu_y}{\mu_x}((\frac{n\pi}{b}))^2}d)} \frac{b}{4((\frac{n\pi}{b})^2-\omega^2\epsilon_x\mu_x)}} \tag{D.246}$$

Evaluating the next double pole:

$$\oint_{\lambda_{yD}} \frac{f(z)}{(z-z_0)^2} = -j\pi \frac{d}{dz} f(z_0) = \\ j\pi \frac{d}{dz} \left. \frac{\lambda_y^4 \cos(k_{ZTE}(d))}{k_{ZTE}\sin(k_{ZTE}d)} \frac{(1-e^{-j\lambda_y b}(-1)^n)}{((\frac{n\pi}{b})-\lambda_y)((\frac{n\pi}{b})-\lambda_y)(\lambda_y-\omega\sqrt{\epsilon_x\mu_x})(\lambda_y+\omega\sqrt{\epsilon_x\mu_x})} \right|_{\lambda_y=\frac{n\pi}{b}} \tag{D.247}$$

Evaluating the derivatives:

Apply the pole ($\lambda_y = \frac{n\pi}{b}$): There are values that go to zero because:

$$(1-e^{j(\frac{n\pi}{b})b}(-1)^n) = (1-e^{j(n\pi)}(-1)^n) = (1-(-1)^n(-1)^n) = (1-(-1)^{2n}) = (1-1) = 0 \tag{D.248}$$

This results in:

$$\oint_{\lambda_{yD}} \frac{f(z)}{(z-z_0)^2} = \\ -j\pi \frac{(-\frac{n\pi}{b})^4 \cos(\sqrt{\omega^2\epsilon_x\mu_y - \lambda_x^2 - \frac{\mu_y}{\mu_x}((\frac{n\pi}{b}))^2}(d))}{\sqrt{\omega^2\epsilon_x\mu_y - \lambda_x^2 - \frac{\mu_y}{\mu_x}((\frac{n\pi}{b}))^2}\sin(\sqrt{\omega^2\epsilon_x\mu_y - \lambda_x^2 - \frac{\mu_y}{\mu_x}((\frac{n\pi}{b}))^2}d)} \frac{\left[jbe^{-jb(-\frac{n\pi}{b})}(-1)^n\right]}{(4(\frac{n\pi}{b})^2)((\frac{n\pi}{b})^2-\omega^2\epsilon_x\mu_x)} \tag{D.249}$$

$$= -j\pi \frac{(\frac{n\pi}{b})^2 \cos(\sqrt{\omega^2\epsilon_x\mu_y - \lambda_x^2 - \frac{\mu_y}{\mu_x}((\frac{n\pi}{b}))^2}d)}{\sqrt{\omega^2\epsilon_x\mu_y - \lambda_x^2 - \frac{\mu_y}{\mu_x}((\frac{n\pi}{b}))^2}\sin(\sqrt{\omega^2\epsilon_x\mu_y - \lambda_x^2 - \frac{\mu_y}{\mu_x}((\frac{n\pi}{b}))^2}d)} \frac{jb}{4((\frac{n\pi}{b})^2-\omega^2\epsilon_x\mu_x)} \tag{D.250}$$

$$\boxed{\pi \frac{(\frac{n\pi}{b})^2 \cos(\sqrt{\omega^2\epsilon_x\mu_y - \lambda_x^2 - \frac{\mu_y}{\mu_x}((\frac{n\pi}{b}))^2}d)}{\sqrt{\omega^2\epsilon_x\mu_y - \lambda_x^2 - \frac{\mu_y}{\mu_x}((\frac{n\pi}{b}))^2}\sin(\sqrt{\omega^2\epsilon_x\mu_y - \lambda_x^2 - \frac{\mu_y}{\mu_x}((\frac{n\pi}{b}))^2}d)} \frac{b}{4((\frac{n\pi}{b})^2 - \omega^2\epsilon_x\mu_x)}} \tag{D.251}$$

The total solution for Case 2 $n = v \neq 0$:

$$\Omega_y = \int_{-\infty}^{\infty} \frac{\lambda_y^4}{k_{ZTE}(\lambda_y^2 - \omega^2\epsilon_x\mu_x)} \frac{\cos(k_{ZTE}d)}{\sin(k_{ZTE}d)} \frac{(e^{j(b\lambda_y)}(-1)^v - 1)}{((\frac{v\pi}{b})^2 - \lambda_y^2)} \frac{(e^{-j(b\lambda_y)}(-1)^n - 1)}{(k_y^2 - \lambda_y^2)} d\lambda_y = \tag{D.252}$$

$$\begin{aligned} &-2\pi \frac{\left(\omega\sqrt{\epsilon_x\mu_x}\right)^3 \cos(j\lambda_x d)}{\lambda_x \sin(j\lambda_x d)} \frac{(1 - e^{-j\left(\omega\sqrt{\epsilon_x\mu_x}\right)b}(-1)^n)}{((\frac{n\pi}{b})^2 - \omega^2\epsilon_x\mu_x)((\frac{n\pi}{b})^2 - \omega^2\epsilon_x\mu_x)} + \\ &-j4\pi \sum_{l=0}^{\infty} \frac{\left(\sqrt{\omega^2\epsilon_x\mu_x - \frac{\mu_x}{\mu_y}\lambda_x^2 - \frac{\mu_x}{\mu_y}\left(\frac{l\pi}{d}\right)^2}\right)^3}{((\frac{n\pi}{b})^2 - \omega^2\epsilon_x\mu_x + \frac{\mu_x}{\mu_y}\lambda_x^2 + \frac{\mu_x}{\mu_y}\left(\frac{l\pi}{d}\right)^2)^2} \frac{(1 - e^{-j\sqrt{\omega^2\epsilon_x\mu_x - \frac{\mu_x}{\mu_y}\lambda_x^2 - \frac{\mu_x}{\mu_y}\left(\frac{l\pi}{d}\right)^2}b}(-1)^n)}{(\lambda_x^2 + \left(\frac{l\pi}{d}\right)^2)d(1 + \delta_{l=0})} + \\ &\pi \frac{(\frac{n\pi}{b})^2 \cos(\sqrt{\omega^2\epsilon_x\mu_y - \lambda_x^2 - \frac{\mu_y}{\mu_x}((\frac{n\pi}{b}))^2}d)}{\sqrt{\omega^2\epsilon_x\mu_y - \lambda_x^2 - \frac{\mu_y}{\mu_x}((\frac{n\pi}{b}))^2}\sin(\sqrt{\omega^2\epsilon_x\mu_y - \lambda_x^2 - \frac{\mu_y}{\mu_x}((\frac{n\pi}{b}))^2}d)} \frac{b}{((\frac{n\pi}{b})^2 - \omega^2\epsilon_x\mu_x)} \end{aligned} \tag{D.253}$$

Case 1 $n \neq v \neq 0$**.**

$$\Omega_y = \int_{-\infty}^{\infty} \frac{\lambda_y^4}{k_{ZTE}(\lambda_y^2 - \omega^2\epsilon_x\mu_x)} \frac{\cos(k_{ZTE}d)}{\sin(k_{ZTE}d)} \frac{(e^{j(b\lambda_y)}(-1)^v - 1)}{((\frac{v\pi}{b})^2 - \lambda_y^2)} \frac{(e^{-j(b\lambda_y)}(-1)^n - 1)}{(k_y^2 - \lambda_y^2)} d\lambda_y \tag{D.254}$$

Simplifying Further:

UHP:

$$\Omega_y = (-1)^{n+v} \int_{-\infty}^{\infty} \frac{\lambda_y^4}{k_{ZTE}(\lambda_y^2 - \omega^2\epsilon_x\mu_x)} \frac{\cos(k_{ZTE}d)}{\sin(k_{ZTE}d)} \frac{(1 - e^{jb\lambda_y}(-1)^n)}{((\frac{v\pi}{b})^2 - \lambda_y^2)(k_y^2 - \lambda_y^2)} d\lambda_y + \tag{D.255}$$

LHP:

$$\int_{-\infty}^{\infty} \frac{\lambda_y^4}{k_{ZTE}(\lambda_y^2 - \omega^2\epsilon_x\mu_x)} \frac{\cos(k_{ZTE}d)}{\sin(k_{ZTE}d)} \frac{(1 - e^{-jb\lambda_y}(-1)^n)}{((\frac{v\pi}{b})^2 - \lambda_y^2)(k_y^2 - \lambda_y^2)} d\lambda_y \tag{D.256}$$

Evaluating each part:

UHP:

$$\Omega_y = (-1)^{n+v} \int_{-\infty}^{\infty} \frac{\lambda_y^4}{k_{ZTE}(\lambda_y^2 - \omega^2\epsilon_x\mu_x)} \frac{\cos(k_{ZTE}d)}{\sin(k_{ZTE}d)} \frac{(1 - e^{jb\lambda_y}(-1)^n)}{((\frac{v\pi}{b})^2 - \lambda_y^2)(k_y^2 - \lambda_y^2)} d\lambda_y + \tag{D.257}$$

Identification of the poles:

$$\lambda_y = \pm\sqrt{\omega^2\epsilon_x\mu_x - \frac{\mu_x}{\mu_y}\lambda_x^2} \tag{D.258}$$

$$\lambda_y = \pm\sqrt{\omega^2\epsilon_x\mu_x - \frac{\mu_x}{\mu_y}\lambda_x^2 - \frac{\mu_x}{\mu_y}\left(\frac{l\pi}{d}\right)^2} \tag{D.259}$$

$$\pm\sqrt{\omega^2\epsilon_x\mu_x} = \lambda_y \tag{D.260}$$

$$\pm\frac{n\pi}{b} = \lambda_y \tag{D.261}$$

$$\pm \frac{v\pi}{b} = \lambda_y \tag{D.262}$$

Plotting the poles on the complex plane results in Figure 66.

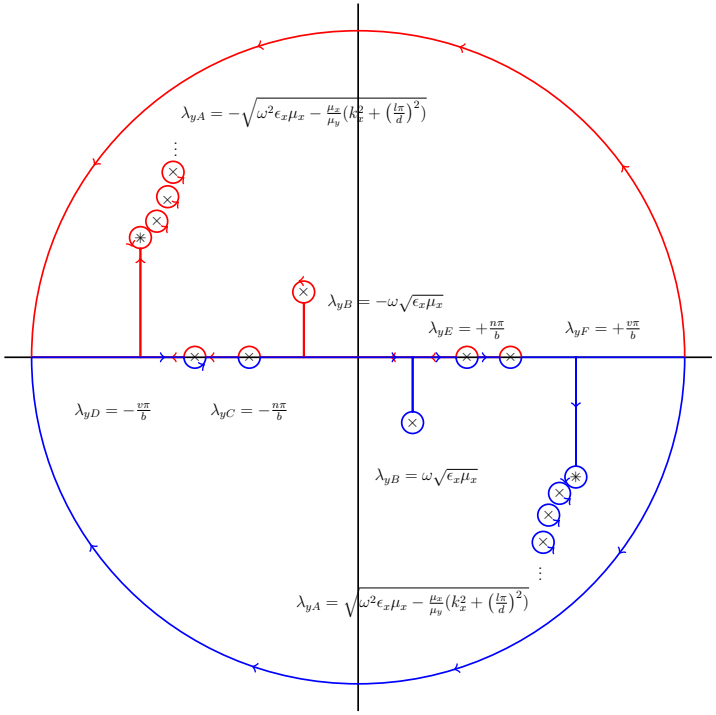

Figure 66. The complex plane showing the poles for the λ_y part of the integral. Note the series of poles induced by the $\sin(k_{ZTE}d)$ part, which represent the modes exhibited in the parallel-plate waveguide structure. A double pole occurs due to $k_{ZTE}\sin(k_{ZTE}d)$ at the $l = 0$ parallel-plate mode. Individual poles are denoted by a $\times$ symbol, while a double pole is denoted by $*$ symbol.

$$\int_{-\infty}^{\infty} + \oint_{\lambda_{yA}} + \oint_{\lambda_{yB}} + \oint_{\lambda_{yC}} + \oint_{\lambda_{yD}} + \oint_{\lambda_{yE}} + \oint_{\lambda_{yF}} + \oint_{C_R} = 0 \tag{D.263}$$

where C_R is the radius at infinity.

$$\int_{-\infty}^{\infty} + \oint_{\lambda_{yA}} + \oint_{\lambda_{yB}} + \oint_{\lambda_{yC}} + \oint_{\lambda_{yD}} + \oint_{\lambda_{yE}} + \oint_{\lambda_{yF}} \cancelto{0}{\oint_{C_R}} = 0 \tag{D.264}$$

$$\int_{-\infty}^{\infty} = -\oint_{\lambda_{yA}} - \oint_{\lambda_{yB}} - \oint_{\lambda_{yC}} - \oint_{\lambda_{yD}} - \oint_{\lambda_{yE}} - \oint_{\lambda_{yF}} \tag{D.265}$$

$$\int_{-\infty}^{\infty} = \oint_{\lambda_{yA}} + \oint_{\lambda_{yB}} + \oint_{\lambda_{yC}} + \oint_{\lambda_{yD}} + \oint_{\lambda_{yE}} + \oint_{\lambda_{yF}} \tag{D.266}$$

Utilizing Cauchy's Integral Theorem:

$$\oint_{\lambda_{yB}} \frac{f(z)}{z-z_0} = j2\pi f(z_0) = j2\pi \frac{\lambda_y^4 \cos(k_{ZTE}(d))}{k_{ZTE}\sin(k_{ZTE}d)}$$

$$\frac{(-1)^{n+v}(1-e^{j\lambda_y b}(-1)^n)}{((\frac{n\pi}{b})-\lambda_y)((\frac{n\pi}{b})+\lambda_y)((\frac{v\pi}{b})-\lambda_y)((\frac{v\pi}{b})+\lambda_y)(\lambda_y-\omega\sqrt{\epsilon_x\mu_x})}\Bigg|_{\lambda_y=-\omega\sqrt{\epsilon_x\mu_x}} = \tag{D.267}$$

$$(-1)^{n+v}j2\pi\frac{\left(\omega\sqrt{\epsilon_x\mu_x}\right)^3\cos(\sqrt{-\lambda_x^2}(d))}{\sqrt{-\lambda_x^2}\sin(\sqrt{-\lambda_x^2}d)}\frac{(1-e^{-j\left(\omega\sqrt{\epsilon_x\mu_x}\right)b}(-1)^n)}{-2((\frac{n\pi}{b})^2-\omega^2\epsilon_x\mu_x)((\frac{v\pi}{b})^2-\omega^2\epsilon_x\mu_x)} =$$

$$-(-1)^{n+v}\pi\frac{\left(\omega\sqrt{\epsilon_x\mu_x}\right)^3\cos(j\lambda_x d)}{\lambda_x\sin(j\lambda_x d)}\frac{(1-e^{-j\omega\sqrt{\epsilon_x\mu_x}b}(-1)^n)}{((\frac{n\pi}{b})^2-\omega^2\epsilon_x\mu_x)((\frac{v\pi}{b})^2-\omega^2\epsilon_x\mu_x)} =$$

$$\boxed{-(-1)^{n+v}\pi\frac{\left(\omega\sqrt{\epsilon_x\mu_x}\right)^3\cos(j\lambda_x d)}{\lambda_x\sin(j\lambda_x d)}\frac{(1-e^{-j\omega\sqrt{\epsilon_x\mu_x}b}(-1)^n)}{((\frac{n\pi}{b})^2-\omega^2\epsilon_x\mu_x)((\frac{v\pi}{b})^2-\omega^2\epsilon_x\mu_x)}} \tag{D.268}$$

for UHP Pole λ_{yB}. $\oint_{\lambda_{yA}}$ contains a double pole and is not a simple pole. Additionally it is constituted by a sum of terms l. When $l=0$, $\lambda_y = \pm\sqrt{\omega^2\epsilon_x\mu_x - \frac{\mu_x}{\mu_y}\lambda_x^2}$ and when $l\neq 0$, $\lambda_y = \pm\sqrt{\omega^2\epsilon_x\mu_x - \frac{\mu_x}{\mu_y}\lambda_x^2 - \frac{\mu_x}{\mu_y}\left(\frac{l\pi}{d}\right)^2}$

$$\sum_{l=0}^{\infty} \oint_{\lambda_{yA}} \frac{f(z)}{z-z_0} = j2\pi \sum_{l=0}^{\infty} \frac{f_1(z_0)}{f_2'(z_0)}$$

$$f(\lambda_y) = \frac{\lambda_y^4}{((\frac{n\pi}{b})-\lambda_y)((\frac{n\pi}{b})+\lambda_y)((\frac{v\pi}{b})-\lambda_y)((\frac{v\pi}{b})+\lambda_y)} \frac{\cos(k_{ZTE}(d))}{k_{ZTE}\sin(k_{ZTE}d)} \cdot \frac{(1-e^{j\lambda_y b}(-1)^n)}{(\lambda_y - \omega\sqrt{\epsilon_x\mu_x})(\lambda_y + \omega\sqrt{\epsilon_x\mu_x})}$$

Evaluating the l=0 part first:

$$f_1(\lambda_{yl=0}) = \frac{\lambda_y^4}{((\frac{n\pi}{b})-\lambda_y)((\frac{n\pi}{b})+\lambda_y)((\frac{v\pi}{b})-\lambda_y)((\frac{v\pi}{b})+\lambda_y)} \frac{\cos(k_{ZTE}(d))}{1} \cdot \frac{(1-e^{j\lambda_y b}(-1)^n)}{(\lambda_y - \omega\sqrt{\epsilon_x\mu_x})(\lambda_y + \omega\sqrt{\epsilon_x\mu_x})} \tag{D.269}$$

$$f_2(\lambda_y) = k_{ZTE}\sin(k_{ZTE}d)$$

$$f_2'(\lambda_{yl=0}) = \sin(k_{ZTE}d)\frac{1}{2k_{ZTE}}\left(-2\frac{\mu_y}{\mu_x}\lambda_y d\right) + k_{ZTE}\cos(k_{ZTE}d)\frac{1}{2k_{ZTE}}\left(-2\frac{\mu_y}{\mu_x}k_y d\right)$$

$$f_2'(\lambda_{yl=0}) = -\sin(k_{ZTE}d)\frac{1}{k_{ZTE}}\left(\frac{\mu_y}{\mu_x}\lambda_y d\right) - cos(k_{ZTE}d)\left(\frac{\mu_y}{\mu_x}\lambda_y d\right)$$

$$
\begin{aligned}
f_2'(\lambda_{yl=0}) &= -\left(\frac{\mu_y}{\mu_x}\lambda_y d\right)\left[\sin(k_{ZTE}d)\frac{1}{k_{ZTE}} + cos(k_{ZTE}d)\right] \\
f_2'(\lambda_{yl=0}) &= \left(\frac{\mu_y}{\mu_x}\sqrt{\omega^2\epsilon_x\mu_x - \frac{\mu_x}{\mu_y}\lambda_x^2}d\right)[1+1] \\
f_2'(\lambda_{yl=0}) &= 2\left(\frac{\mu_y}{\mu_x}\sqrt{\omega^2\epsilon_x\mu_x - \frac{\mu_x}{\mu_y}\lambda_x^2}d\right) \\
f_1(\lambda_y) &= \frac{\lambda_y^4}{((\frac{n\pi}{b}) - \lambda_y)((\frac{n\pi}{b}) + \lambda_y)((\frac{v\pi}{b}) - \lambda_y)((\frac{v\pi}{b}) + \lambda_y)}\frac{\cos(k_{ZTE}(d))}{1}\cdot \\
&\qquad \frac{(1 - e^{j\lambda_y b}(-1)^n)}{(\lambda_y - \omega\sqrt{\epsilon_x\mu_x})(\lambda_y + \omega\sqrt{\epsilon_x\mu_x})}
\end{aligned}
\tag{D.270}
$$

$$
\begin{aligned}
f_1(\lambda_{yl=0}) &= \frac{\omega^2\epsilon_x\mu_x - \frac{\mu_x}{\mu_y}\lambda_x^2}{((\frac{n\pi}{b})^2 - \omega^2\epsilon_x\mu_x + \frac{\mu_x}{\mu_y}\lambda_x^2)}\frac{(1 - e^{-j\sqrt{\omega^2\epsilon_x\mu_x - \frac{\mu_x}{\mu_y}\lambda_x^2}b}(-1)^n)}{(\omega^2\epsilon_x\mu_x - \frac{\mu_x}{\mu_y}\lambda_x^2 - \omega^2\epsilon_x\mu_x)} \\
f_1(\lambda_{yl=0}) &= \frac{\left(\omega^2\epsilon_x\mu_x - \frac{\mu_x}{\mu_y}\lambda_x^2\right)^2}{((\frac{n\pi}{b})^2 - \omega^2\epsilon_x\mu_x + \frac{\mu_x}{\mu_y}\lambda_x^2)((\frac{v\pi}{b})^2 - \omega^2\epsilon_x\mu_x + \frac{\mu_x}{\mu_y}\lambda_x^2)}\frac{(1 - e^{-j\sqrt{\omega^2\epsilon_x\mu_x - \frac{\mu_x}{\mu_y}\lambda_x^2}b}(-1)^n)}{-\frac{\mu_x}{\mu_y}\lambda_x^2} \\
j2\pi\frac{f_1(\lambda_{yl=0})}{f_2'(\lambda_{yl=0})} &= \frac{\left(\omega^2\epsilon_x\mu_x - \frac{\mu_x}{\mu_y}\lambda_x^2\right)^2}{((\frac{n\pi}{b})^2 - \omega^2\epsilon_x\mu_x + \frac{\mu_x}{\mu_y}\lambda_x^2)((\frac{v\pi}{b})^2 - \omega^2\epsilon_x\mu_x + \frac{\mu_x}{\mu_y}\lambda_x^2)}\frac{(1 - e^{-j\sqrt{\omega^2\epsilon_x\mu_x - \frac{\mu_x}{\mu_y}\lambda_x^2}b}(-1)^n)}{-\frac{\mu_x}{\mu_y}\lambda_x^2}\cdot \\
&\qquad \frac{1}{2\frac{\mu_y}{\mu_x}\sqrt{\omega^2\epsilon_x\mu_x - \frac{\mu_x}{\mu_y}\lambda_x^2}d}
\end{aligned}
\tag{D.271}
$$

$$j2\pi\frac{f_1(\lambda_{yl=0})}{f_2'(\lambda_{yl=0})}=\frac{\left(\sqrt{\omega^2\epsilon_x\mu_x-\frac{\mu_x}{\mu_y}\lambda_x^2}\right)^3}{((\frac{n\pi}{b})^2-\omega^2\epsilon_x\mu_x+\frac{\mu_x}{\mu_y}\lambda_x^2)((\frac{v\pi}{b})^2-\omega^2\epsilon_x\mu_x+\frac{\mu_x}{\mu_y}\lambda_x^2)}\frac{(1-e^{-j\sqrt{\omega^2\epsilon_x\mu_x-\frac{\mu_x}{\mu_y}\lambda_x^2}b}(-1)^n)}{-\lambda_x^2 2d} \tag{D.272}$$

$$\sum_{l=0}^{\infty}\oint_{\lambda_{yA}}\frac{f(z)}{z-z_0}=j2\pi\sum_{l=0}^{\infty}\frac{f_1(z_0)}{f_2'(z_0)}$$

$$f(\lambda_y)=\frac{\lambda_y^4}{((\frac{n\pi}{b})-\lambda_y)((\frac{n\pi}{b})+\lambda_y)((\frac{v\pi}{b})-\lambda_y)((\frac{v\pi}{b})+\lambda_y)}\frac{\cos(k_{ZTE}(d))}{k_{ZTE}\sin(k_{ZTE}d)}\cdot$$
$$\frac{(1-e^{j\lambda_y b}(-1)^n)}{(\lambda_y-\omega\sqrt{\epsilon_x\mu_x})(\lambda_y+\omega\sqrt{\epsilon_x\mu_x})}$$

Evaluating the $l\neq 0$ part second:

$$f_1(\lambda_{yl\neq 0})=\frac{\lambda_y^4}{((\frac{n\pi}{b})-\lambda_y)((\frac{n\pi}{b})+\lambda_y)((\frac{v\pi}{b})-\lambda_y)((\frac{v\pi}{b})+\lambda_y)}\frac{\cos(k_{ZTE}(d))}{k_{ZTE}}\cdot \tag{D.273}$$
$$\frac{(1-e^{j\lambda_y b}(-1)^n)}{(\lambda_y-\omega\sqrt{\epsilon_x\mu_x})(\lambda_y+\omega\sqrt{\epsilon_x\mu_x})}$$

$$f_2(\lambda_{yl\neq 0})=\sin(k_{ZTE}d)$$

$$f_2'(\lambda_{yl\neq 0})=\cos(k_{ZTE}d)\frac{1}{2k_{ZTE}}\left(-2\frac{\mu_y}{\mu_x}\lambda_y d\right)$$

$$f_2'(\lambda_{yl\neq 0})=-cos(k_{ZTE}d)\frac{1}{k_{ZTE}}\left(\frac{\mu_y}{\mu_x}\lambda_y d\right)$$

$$f_2'(\lambda_{yl\neq 0}) = \frac{(-1)^l}{\pm\frac{l\pi}{d}}\left(\frac{\mu_y}{\mu_x}\sqrt{\omega^2\epsilon_x\mu_x - \frac{\mu_x}{\mu_y}\lambda_x^2 - \frac{\mu_x}{\mu_y}\left(\frac{l\pi}{d}\right)^2}d\right)$$

$$f_1(\lambda_{yl\neq 0}) = \frac{\lambda_y^4}{((\frac{n\pi}{b})-\lambda_y)((\frac{n\pi}{b})+\lambda_y)((\frac{v\pi}{b})-\lambda_y)((\frac{v\pi}{b})+\lambda_y)}\frac{\cos(k_{ZTE}(d))}{k_{ZTE}}\cdot \frac{(1-e^{j\lambda_y b}(-1)^n)}{(\lambda_y-\omega\sqrt{\epsilon_x\mu_x})(\lambda_y+\omega\sqrt{\epsilon_x\mu_x})} \tag{D.274}$$

$$f_1(\lambda_{yl\neq 0}) = \frac{\left(\omega^2\epsilon_x\mu_x - \frac{\mu_x}{\mu_y}\lambda_x^2 - \frac{\mu_x}{\mu_y}\left(\frac{l\pi}{d}\right)^2\right)^2}{((\frac{n\pi}{b})^2 - \omega^2\epsilon_x\mu_x + \frac{\mu_x}{\mu_y}\lambda_x^2 + \frac{\mu_x}{\mu_y}\left(\frac{l\pi}{d}\right)^2)((\frac{v\pi}{b})^2 - \omega^2\epsilon_x\mu_x + \frac{\mu_x}{\mu_y}\lambda_x^2 + \frac{\mu_x}{\mu_y}\left(\frac{l\pi}{d}\right)^2)}\cdot \frac{(-1)^l}{\frac{l\pi}{d}}\frac{(1-e^{-j\sqrt{\omega^2\epsilon_x\mu_x - \frac{\mu_x}{\mu_y}\lambda_x^2 - \frac{\mu_x}{\mu_y}\left(\frac{l\pi}{d}\right)^2}b}(-1)^n)}{(\omega^2\epsilon_x\mu_x - \frac{\mu_x}{\mu_y}\lambda_x^2 - \frac{\mu_x}{\mu_y}\left(\frac{l\pi}{d}\right)^2 - \omega^2\epsilon_x\mu_x)}$$

$$f_1(\lambda_{yl\neq 0}) = \frac{\left(\omega^2\epsilon_x\mu_x - \frac{\mu_x}{\mu_y}\lambda_x^2 - \frac{\mu_x}{\mu_y}\left(\frac{l\pi}{d}\right)^2\right)^2}{((\frac{n\pi}{b})^2 - \omega^2\epsilon_x\mu_x + \frac{\mu_x}{\mu_y}\lambda_x^2 + \frac{\mu_x}{\mu_y}\left(\frac{l\pi}{d}\right)^2)((\frac{v\pi}{b})^2 - \omega^2\epsilon_x\mu_x + \frac{\mu_x}{\mu_y}\lambda_x^2 + \frac{\mu_x}{\mu_y}\left(\frac{l\pi}{d}\right)^2)}\cdot \frac{(-1)^l}{\frac{l\pi}{d}}\frac{(1-e^{-j\sqrt{\omega^2\epsilon_x\mu_x - \frac{\mu_x}{\mu_y}\lambda_x^2 - \frac{\mu_x}{\mu_y}\left(\frac{l\pi}{d}\right)^2}b}(-1)^n)}{-\frac{\mu_x}{\mu_y}(\lambda_x^2 + \left(\frac{l\pi}{d}\right)^2)} \tag{D.275}$$

$$= j2\pi \sum_{l=0}^{\infty} \frac{f_1(\lambda_{yl\neq 0})}{f_2'(\lambda_{yl\neq 0})}$$

$$= j2\pi \sum_{l=0}^{\infty} \frac{\left(\omega^2\epsilon_x\mu_x - \frac{\mu_x}{\mu_y}\lambda_x^2 - \frac{\mu_x}{\mu_y}\left(\frac{l\pi}{d}\right)^2\right)^2}{((\frac{n\pi}{b})^2 - \omega^2\epsilon_x\mu_x + \frac{\mu_x}{\mu_y}\lambda_x^2 + \frac{\mu_x}{\mu_y}\left(\frac{l\pi}{d}\right)^2)((\frac{v\pi}{b})^2 - \omega^2\epsilon_x\mu_x + \frac{\mu_x}{\mu_y}\lambda_x^2 + \frac{\mu_x}{\mu_y}\left(\frac{l\pi}{d}\right)^2)} \cdot \frac{(-1)^l}{\frac{l\pi}{d}} \frac{(1 - e^{-j\sqrt{\omega^2\epsilon_x\mu_x - \frac{\mu_x}{\mu_y}\lambda_x^2 - \frac{\mu_x}{\mu_y}\left(\frac{l\pi}{d}\right)^2}b}(-1)^n)}{-\frac{\mu_x}{\mu_y}(\lambda_x^2 + \left(\frac{l\pi}{d}\right)^2)} \cdot \frac{\pm\frac{l\pi}{d}}{(-1)^l}\left(\frac{\mu_x}{\mu_y}\frac{1}{\sqrt{\omega^2\epsilon_x\mu_x - \frac{\mu_x}{\mu_y}\lambda_x^2 - \frac{\mu_x}{\mu_y}\left(\frac{l\pi}{d}\right)^2}d}\right) \tag{D.276}$$

$$= j2\pi \sum_{l=0}^{\infty} \frac{f_1(\lambda_{yl\neq 0})}{f_2'(\lambda_{yl\neq 0})}$$

$$= j2\pi \sum_{l=0}^{\infty} \frac{\left(\omega^2\epsilon_x\mu_x - \frac{\mu_x}{\mu_y}\lambda_x^2 - \frac{\mu_x}{\mu_y}\left(\frac{l\pi}{d}\right)^2\right)^2}{((\frac{n\pi}{b})^2 - \omega^2\epsilon_x\mu_x + \frac{\mu_x}{\mu_y}\lambda_x^2 + \frac{\mu_x}{\mu_y}\left(\frac{l\pi}{d}\right)^2)((\frac{v\pi}{b})^2 - \omega^2\epsilon_x\mu_x + \frac{\mu_x}{\mu_y}\lambda_x^2 + \frac{\mu_x}{\mu_y}\left(\frac{l\pi}{d}\right)^2)} \cdot \frac{(1 - e^{-j\sqrt{\omega^2\epsilon_x\mu_x - \frac{\mu_x}{\mu_y}\lambda_x^2 - \frac{\mu_x}{\mu_y}\left(\frac{l\pi}{d}\right)^2}b}(-1)^n)}{-(\lambda_x^2 + \left(\frac{l\pi}{d}\right)^2)} \cdot \left(\frac{1}{\sqrt{\omega^2\epsilon_x\mu_x - \frac{\mu_x}{\mu_y}\lambda_x^2 - \frac{\mu_x}{\mu_y}\left(\frac{l\pi}{d}\right)^2}d}\right) \tag{D.277}$$

$$= j2\pi \sum_{l=0}^{\infty} \frac{f_1(\lambda_{yl\neq 0})}{f_2'(\lambda_{yl\neq 0})} =$$

$$j2\pi \sum_{l=0}^{\infty} \frac{\left(\sqrt{\omega^2\epsilon_x\mu_x - \frac{\mu_x}{\mu_y}\lambda_x^2 - \frac{\mu_x}{\mu_y}\left(\frac{l\pi}{d}\right)^2}\right)^3}{((\frac{n\pi}{b})^2 - \omega^2\epsilon_x\mu_x + \frac{\mu_x}{\mu_y}\lambda_x^2 + \frac{\mu_x}{\mu_y}\left(\frac{l\pi}{d}\right)^2)((\frac{v\pi}{b})^2 - \omega^2\epsilon_x\mu_x + \frac{\mu_x}{\mu_y}\lambda_x^2 + \frac{\mu_x}{\mu_y}\left(\frac{l\pi}{d}\right)^2)} \cdot \frac{(1 - e^{-j\sqrt{\omega^2\epsilon_x\mu_x - \frac{\mu_x}{\mu_y}\lambda_x^2 - \frac{\mu_x}{\mu_y}\left(\frac{l\pi}{d}\right)^2}b}(-1)^n)}{-(\lambda_x^2 + \left(\frac{l\pi}{d}\right)^2)d} \tag{D.278}$$

Combining $l \neq 0$ and $l = 0$ parts:

$$j2\pi \sum_{l=0}^{\infty} \frac{f_1(\lambda_{yl=0})}{f_2'(\lambda_{yl=0})}$$

$$= j2\pi \frac{\left(\sqrt{\omega^2\epsilon_x\mu_x - \frac{\mu_x}{\mu_y}\lambda_x^2}\right)^3}{((\frac{n\pi}{b})^2 - \omega^2\epsilon_x\mu_x + \frac{\mu_x}{\mu_y}\lambda_x^2)((\frac{v\pi}{b})^2 - \omega^2\epsilon_x\mu_x + \frac{\mu_x}{\mu_y}\lambda_x^2)} \cdot \frac{(1 - e^{-j\sqrt{\omega^2\epsilon_x\mu_x - \frac{\mu_x}{\mu_y}\lambda_x^2}b}(-1)^n)}{-\lambda_x^2} \frac{1}{2d} \tag{D.279}$$

$$= j2\pi \sum_{l=0}^{\infty} \frac{f_1(\lambda_{yl\neq 0})}{f_2'(\lambda_{yl\neq 0})}$$

$$= j2\pi \sum_{l=0}^{\infty} \frac{\left(\sqrt{\omega^2\epsilon_x\mu_x - \frac{\mu_x}{\mu_y}\lambda_x^2 - \frac{\mu_x}{\mu_y}\left(\frac{l\pi}{d}\right)^2}\right)^3}{((\frac{n\pi}{b})^2 - \omega^2\epsilon_x\mu_x + \frac{\mu_x}{\mu_y}\lambda_x^2 + \frac{\mu_x}{\mu_y}\left(\frac{l\pi}{d}\right)^2)((\frac{v\pi}{b})^2 - \omega^2\epsilon_x\mu_x + \frac{\mu_x}{\mu_y}\lambda_x^2 + \frac{\mu_x}{\mu_y}\left(\frac{l\pi}{d}\right)^2)} \cdot \frac{(1 - e^{-j\sqrt{\omega^2\epsilon_x\mu_x - \frac{\mu_x}{\mu_y}\lambda_x^2 - \frac{\mu_x}{\mu_y}\left(\frac{l\pi}{d}\right)^2}b}(-1)^n)}{-(\lambda_x^2 + \left(\frac{l\pi}{d}\right)^2)d} \tag{D.280}$$

$$= j2\pi \sum_{l=0}^{\infty} \frac{f_1(\lambda_{yl\neq 0})}{f_2'(\lambda_{yl\neq 0})}$$

$$= -j2\pi \sum_{l=0}^{\infty} \frac{\left(\sqrt{\omega^2\epsilon_x\mu_x - \frac{\mu_x}{\mu_y}\lambda_x^2 - \frac{\mu_x}{\mu_y}\left(\frac{l\pi}{d}\right)^2}\right)^3}{((\frac{n\pi}{b})^2 - \omega^2\epsilon_x\mu_x + \frac{\mu_x}{\mu_y}\lambda_x^2 + \frac{\mu_x}{\mu_y}\left(\frac{l\pi}{d}\right)^2)((\frac{v\pi}{b})^2 - \omega^2\epsilon_x\mu_x + \frac{\mu_x}{\mu_y}\lambda_x^2 + \frac{\mu_x}{\mu_y}\left(\frac{l\pi}{d}\right)^2)} \cdot \frac{(1 - e^{-j\sqrt{\omega^2\epsilon_x\mu_x - \frac{\mu_x}{\mu_y}\lambda_x^2 - \frac{\mu_x}{\mu_y}\left(\frac{l\pi}{d}\right)^2}b}(-1)^n)}{(\lambda_x^2 + \left(\frac{l\pi}{d}\right)^2)d(1 + \delta_{l=0})} \tag{D.281}$$

$$= j2\pi \sum_{l=0}^{\infty} \frac{f_1(\lambda_{yl\neq 0})}{f_2'(\lambda_{yl\neq 0})}$$

$$= -j2\pi \sum_{l=0}^{\infty} \frac{\left(\sqrt{\omega^2\epsilon_x\mu_x - \frac{\mu_x}{\mu_y}\lambda_x^2 - \frac{\mu_x}{\mu_y}\left(\frac{l\pi}{d}\right)^2}\right)^3}{((\frac{n\pi}{b})^2 - \omega^2\epsilon_x\mu_x + \frac{\mu_x}{\mu_y}\lambda_x^2 + \frac{\mu_x}{\mu_y}\left(\frac{l\pi}{d}\right)^2)((\frac{v\pi}{b})^2 - \omega^2\epsilon_x\mu_x + \frac{\mu_x}{\mu_y}\lambda_x^2 + \frac{\mu_x}{\mu_y}\left(\frac{l\pi}{d}\right)^2)} \cdot \frac{(1 - e^{-j\sqrt{\omega^2\epsilon_x\mu_x - \frac{\mu_x}{\mu_y}\lambda_x^2 - \frac{\mu_x}{\mu_y}\left(\frac{l\pi}{d}\right)^2}b}(-1)^n)}{(\lambda_x^2 + \left(\frac{l\pi}{d}\right)^2)d(1 + \delta_{l=0})} \tag{D.282}$$

$$= j2\pi \sum_{l=0}^{\infty} \frac{f_1(\lambda_{yl\neq 0})}{f_2'(\lambda_{yl\neq 0})}$$

$$= -(-1)^{n+v} j2\pi \sum_{l=0}^{\infty} \frac{\left(\sqrt{\omega^2\epsilon_x\mu_x - \frac{\mu_x}{\mu_y}\lambda_x^2 - \frac{\mu_x}{\mu_y}\left(\frac{l\pi}{d}\right)^2}\right)^3}{((\frac{n\pi}{b})^2 - \omega^2\epsilon_x\mu_x + \frac{\mu_x}{\mu_y}\lambda_x^2 + \frac{\mu_x}{\mu_y}\left(\frac{l\pi}{d}\right)^2)((\frac{v\pi}{b})^2 - \omega^2\epsilon_x\mu_x + \frac{\mu_x}{\mu_y}\lambda_x^2 + \frac{\mu_x}{\mu_y}\left(\frac{l\pi}{d}\right)^2)} \cdot \frac{(1 - e^{-j\sqrt{\omega^2\epsilon_x\mu_x - \frac{\mu_x}{\mu_y}\lambda_x^2 - \frac{\mu_x}{\mu_y}\left(\frac{l\pi}{d}\right)^2}b}(-1)^n)}{(\lambda_x^2 + \left(\frac{l\pi}{d}\right)^2)d(1+\delta_{l=0})} \tag{D.283}$$

for UHP Pole λ_{yA}.

$$\oint_{\lambda_{yC}} \frac{f(z)}{z - z_0} = j\pi f(z_0) =$$

$$(-1)^{n+v} j\pi \frac{\lambda_y^4 \cos(k_{ZTE}(d))}{k_{ZTE}\sin(k_{ZTE}d)} \cdot$$

$$\frac{(1 - e^{j\lambda_y b}(-1)^n)}{((\frac{n\pi}{b}) - \lambda_y)((\frac{v\pi}{b}) - \lambda_y)((\frac{v\pi}{b}) + \lambda_y)(\lambda_y - \omega\sqrt{\epsilon_x\mu_x})(\lambda_y + \omega\sqrt{\epsilon_x\mu_x})}\Bigg|_{\lambda_y = -\frac{n\pi}{b}} \tag{D.284}$$

$$(1 - e^{j(-\frac{n\pi}{b})b}(-1)^n) = (1 - (-1)^n(-1)^n) = (1 - (-1)^{2n}) = (1 - 1) = 0$$

$$\boxed{0} \qquad \text{for UHP Pole } \lambda_{yC}.$$

$$\oint_{\lambda_{yD}} \frac{f(z)}{z - z_0} = j\pi f(z_0) =$$

$$(-1)^{n+v} j\pi \frac{\lambda_y^4 \cos(k_{ZTE}(d))}{k_{ZTE} \sin(k_{ZTE} d)} \cdot$$

$$\frac{(1 - e^{j\lambda_y b}(-1)^n)}{((\frac{n\pi}{b}) + \lambda_y)((\frac{v\pi}{b}) - \lambda_y)((\frac{v\pi}{b}) + \lambda_y)(\lambda_y - \omega\sqrt{\epsilon_x \mu_x})(\lambda_y + \omega\sqrt{\epsilon_x \mu_x})}\Bigg|_{\lambda_y = \frac{n\pi}{b}} \tag{D.285}$$

$$(1 - e^{j(\frac{n\pi}{b})b}(-1)^n) = (1 - (-1)^n(-1)^n) = (1 - (-1)^{2n}) = (1 - 1) = 0$$

$$= \boxed{0} \qquad \text{for UHP Pole } \lambda_{yD}.$$

$$\oint_{\lambda_{yC}} \frac{f(z)}{z-z_0} = j\pi f(z_0) =$$

$$(-1)^{n+v} j\pi \frac{\lambda_y^4 \cos(k_{ZTE}(d))}{k_{ZTE}\sin(k_{ZTE}d)} \cdot$$

$$\frac{(1-e^{j\lambda_y b}(-1)^n)}{((\frac{v\pi}{b})-\lambda_y)((\frac{n\pi}{b})-\lambda_y)((\frac{n\pi}{b})+\lambda_y)(\lambda_y-\omega\sqrt{\epsilon_x\mu_x})(\lambda_y+\omega\sqrt{\epsilon_x\mu_x})}\Bigg|_{\lambda_y=-\frac{v\pi}{b}} =$$

$$= (-1)^{n+v} j\pi \frac{(\frac{v\pi}{b})^3 \cos(\sqrt{\omega^2\epsilon_x\mu_y - \lambda_x^2 - \frac{\mu_y}{\mu_x}(\frac{v\pi}{b})^2}(d))}{\sqrt{\omega^2\epsilon_x\mu_y - \lambda_x^2 - \frac{\mu_y}{\mu_x}(\frac{v\pi}{b})^2}\sin(\sqrt{\omega^2\epsilon_x\mu_y - \lambda_x^2 - \frac{\mu_y}{\mu_x}(\frac{v\pi}{b})^2}d)} \cdot \tag{D.286}$$

$$\frac{(1-(-1)^v(-1)^n)}{2((\frac{n\pi}{b})^2-(\frac{v\pi}{b})^2)((\frac{v\pi}{b})^2-\omega^2\epsilon_x\mu_x)} =$$

$$= (-1)^{n+v} j\pi \frac{(\frac{v\pi}{b})^3 \cos(\sqrt{\omega^2\epsilon_x\mu_y - \lambda_x^2 - \frac{\mu_y}{\mu_x}(\frac{v\pi}{b})^2}(d))}{\sqrt{\omega^2\epsilon_x\mu_y - \lambda_x^2 - \frac{\mu_y}{\mu_x}(\frac{v\pi}{b})^2}\sin(\sqrt{\omega^2\epsilon_x\mu_y - \lambda_x^2 - \frac{\mu_y}{\mu_x}(\frac{v\pi}{b})^2}d)} \cdot$$

$$\frac{(1-(-1)^v(-1)^n)}{2((\frac{n\pi}{b})^2-(\frac{v\pi}{b})^2)((\frac{v\pi}{b})^2-\omega^2\epsilon_x\mu_x)} =$$

$$\boxed{(-1)^{n+v} j\pi \frac{(\frac{v\pi}{b})^3 \cos(\sqrt{\omega^2\epsilon_x\mu_y - \lambda_x^2 - \frac{\mu_y}{\mu_x}(\frac{v\pi}{b})^2}(d))}{\sqrt{\omega^2\epsilon_x\mu_y - \lambda_x^2 - \frac{\mu_y}{\mu_x}(\frac{v\pi}{b})^2}\sin(\sqrt{\omega^2\epsilon_x\mu_y - \lambda_x^2 - \frac{\mu_y}{\mu_x}(\frac{v\pi}{b})^2}d)} \cdot \frac{(1-(-1)^v(-1)^n)}{2((\frac{n\pi}{b})^2-(\frac{v\pi}{b})^2)((\frac{v\pi}{b})^2-\omega^2\epsilon_x\mu_x)}} \tag{D.287}$$

for UHP Pole λ_{yE}.

$$\oint_{\lambda_{yD}} \frac{f(z)}{z-z_0} = j\pi f(z_0) = (-1)^{n+v} j\pi \frac{\lambda_y^4 \cos(k_{ZTE}(d))}{k_{ZTE}\sin(k_{ZTE}d)} \cdot \left. \frac{(1-e^{j\lambda_y b}(-1)^n)}{((\frac{v\pi}{b})-\lambda_y)((\frac{n\pi}{b})-\lambda_y)((\frac{n\pi}{b})+\lambda_y)(\lambda_y-\omega\sqrt{\epsilon_x\mu_x})(\lambda_y+\omega\sqrt{\epsilon_x\mu_x})} \right|_{\lambda_y=\frac{v\pi}{b}} = \tag{D.288}$$

$$(-1)^{n+v} j\pi \frac{(\frac{v\pi}{b})^3 \cos(\sqrt{\omega^2\epsilon_x\mu_y - \lambda_x^2 - \frac{\mu_y}{\mu_x}(\frac{v\pi}{b})^2}(d))}{\sqrt{\omega^2\epsilon_x\mu_y - \lambda_x^2 - \frac{\mu_y}{\mu_x}(\frac{v\pi}{b})^2}\sin(\sqrt{\omega^2\epsilon_x\mu_y - \lambda_x^2 - \frac{\mu_y}{\mu_x}(\frac{v\pi}{b})^2}d)} \cdot \frac{(1-(-1)^v(-1)^n)}{2((\frac{n\pi}{b})^2-(\frac{v\pi}{b})^2)((\frac{v\pi}{b})^2-\omega^2\epsilon_x\mu_x)} =$$

$$\boxed{(-1)^{n+v} j\pi \frac{(\frac{v\pi}{b})^3 \cos(\sqrt{\omega^2\epsilon_x\mu_y - \lambda_x^2 - \frac{\mu_y}{\mu_x}(\frac{v\pi}{b})^2}(d))}{\sqrt{\omega^2\epsilon_x\mu_y - \lambda_x^2 - \frac{\mu_y}{\mu_x}(\frac{v\pi}{b})^2}\sin(\sqrt{\omega^2\epsilon_x\mu_y - \lambda_x^2 - \frac{\mu_y}{\mu_x}(\frac{v\pi}{b})^2}d)} \cdot \frac{(1-(-1)^v(-1)^n)}{2((\frac{n\pi}{b})^2-(\frac{v\pi}{b})^2)((\frac{v\pi}{b})^2-\omega^2\epsilon_x\mu_x)}} \tag{D.289}$$

for UHP Pole λ_{yF}.

LHP:

$$\int_{-\infty}^{\infty} \frac{\lambda_y^4}{k_{ZTE}(\lambda_y^2-\omega^2\epsilon_x\mu_x)} \frac{\cos(k_{ZTE}d)}{\sin(k_{ZTE}d)} \frac{(1-e^{-jb\lambda_y}(-1)^n)}{((\frac{v\pi}{b})^2-\lambda_y^2)(k_y^2-\lambda_y^2)} d\lambda_y \tag{D.290}$$

Identification of the poles:

$$\lambda_y = \pm\sqrt{\omega^2\epsilon_x\mu_x - \frac{\mu_x}{\mu_y}\lambda_x^2} \tag{D.291}$$

$$\lambda_y = \pm\sqrt{\omega^2\epsilon_x\mu_x - \frac{\mu_x}{\mu_y}\lambda_x^2 - \frac{\mu_x}{\mu_y}\left(\frac{l\pi}{d}\right)^2} \tag{D.292}$$

$$\pm\sqrt{\omega^2\epsilon_x\mu_x} = \lambda_y \tag{D.293}$$

$$\pm\frac{n\pi}{b} = \lambda_y \tag{D.294}$$

Now doing the lower half plane.

$$\int_{-\infty}^{\infty} + \oint_{\lambda_{yA}} + \oint_{\lambda_{yB}} + \oint_{\lambda_{yC}} + \oint_{\lambda_{yD}} + \oint_{\lambda_{yE}} + \oint_{\lambda_{yF}} + \oint_{C_R} = 0 \tag{D.295}$$

where C_R is the radius at infinity.

$$\int_{-\infty}^{\infty} + \oint_{\lambda_{yA}} + \oint_{\lambda_{yB}} + \oint_{\lambda_{yC}} + \oint_{\lambda_{yD}} + \oint_{\lambda_{yE}} + \oint_{\lambda_{yF}} + \overset{0}{\oint_{C_R}} = 0 \tag{D.296}$$

$$\int_{-\infty}^{\infty} = -\oint_{\lambda_{yA}} - \oint_{\lambda_{yB}} - \oint_{\lambda_{yC}} - \oint_{\lambda_{yD}} - \oint_{\lambda_{yE}} - \oint_{\lambda_{yF}} \tag{D.297}$$

Watch the signs!

$$
\begin{aligned}
-\oint_{\lambda_{yB}} \frac{f(z)}{z-z_0} = -j2\pi f(z_0) = \\
-j2\pi \left. \frac{\lambda_y^4}{(\frac{n\pi}{b}-\lambda_y)(\frac{n\pi}{b}+\lambda_y)(\frac{v\pi}{b}-\lambda_y)(\frac{v\pi}{b}+\lambda_y)} \frac{\cos(k_{ZTE}(d))}{k_{ZTE}\sin(k_{ZTE}d)} \frac{(1-e^{-j\lambda_y b}(-1)^n)}{(\lambda_y+\omega\sqrt{\epsilon_x\mu_x})} \right|_{\lambda_y=\omega\sqrt{\epsilon_x\mu_x}} = \\
-j2\pi \frac{\left(\omega\sqrt{\epsilon_x\mu_x}\right)^3}{((\frac{n\pi}{b})^2-\omega^2\epsilon_x\mu_x)((\frac{v\pi}{b})^2-\omega^2\epsilon_x\mu_x)} \frac{\cos(j\lambda_x(d))}{j\lambda_x\sin(j\lambda_x d)} \frac{(e^{-j\omega\sqrt{\epsilon_x\mu_x}b}(-1)^n-1)}{2} = \\
-\pi \frac{\left(\omega\sqrt{\epsilon_x\mu_x}\right)^3}{((\frac{n\pi}{b})^2-\omega^2\epsilon_x\mu_x)((\frac{v\pi}{b})^2-\omega^2\epsilon_x\mu_x)} \frac{\cos(j\lambda_x d)}{\lambda_x\sin(j\lambda_x d)} \frac{(e^{-j\omega\sqrt{\epsilon_x\mu_x}b}(-1)^n-1)}{1} =
\end{aligned}
\tag{D.298}
$$

$$
\boxed{-\pi \frac{\left(\omega\sqrt{\epsilon_x\mu_x}\right)^3}{((\frac{n\pi}{b})^2-\omega^2\epsilon_x\mu_x)((\frac{v\pi}{b})^2-\omega^2\epsilon_x\mu_x)} \frac{\cos(j\lambda_x d)}{\lambda_x\sin(j\lambda_x d)} \frac{(e^{-j\omega\sqrt{\epsilon_x\mu_x}b}(-1)^n-1)}{1}} \quad \text{for LHP Pole } \lambda_{yB}. \tag{D.299}
$$

$\oint_{\lambda_{yA}}$ contains a double pole and is not a simple pole. Additionally it is constituted by a sum of terms l. When $l=0$, $\lambda_y = \pm\sqrt{\omega^2\epsilon_x\mu_x - \frac{\mu_x}{\mu_y}\lambda_x^2}$ and when $l \neq 0$, $\lambda_y = \pm\sqrt{\omega^2\epsilon_x\mu_x - \frac{\mu_x}{\mu_y}\lambda_x^2 - \frac{\mu_x}{\mu_y}\left(\frac{l\pi}{d}\right)^2}$

$$-\sum_{l=0}^{\infty}\oint_{\lambda_{yA}}\frac{f(z)}{z-z_0}=-j2\pi\sum_{l=0}^{\infty}\frac{f_1(z_0)}{f_2'(z_0)}$$

$$f(\lambda_y)=\frac{\lambda_y^4}{(\frac{n\pi}{b}-\lambda_y)(\frac{n\pi}{b}+\lambda_y)(\frac{v\pi}{b}-\lambda_y)(\frac{v\pi}{b}+\lambda_y)}\cdot$$
$$\frac{\cos(k_{ZTE}(d))}{k_{ZTE}\sin(k_{ZTE}d)}\frac{(1-e^{-j\lambda_y b}(-1)^n)}{(\lambda_y-\omega\sqrt{\epsilon_x\mu_x})(\lambda_y+\omega\sqrt{\epsilon_x\mu_x})}$$

Evaluate the l=0 part first:

$$f_1(\lambda_{yl=0})=\frac{\lambda_y^4}{(\frac{n\pi}{b}-\lambda_y)(\frac{n\pi}{b}+\lambda_y)(\frac{v\pi}{b}-\lambda_y)(\frac{v\pi}{b}+\lambda_y)}\cdot$$
$$\frac{\cos(k_{ZTE}(d))}{1}\frac{(1-e^{-j\lambda_y b}(-1)^n)}{(\lambda_y-\omega\sqrt{\epsilon_x\mu_x})(\lambda_y+\omega\sqrt{\epsilon_x\mu_x})} \tag{D.300}$$

$$f_2(\lambda_{yl=0})=k_{ZTE}\sin(k_{ZTE}d)$$

$$f_2'(\lambda_{yl=0})=\sin(k_{ZTE}d)\frac{1}{2k_{ZTE}}\left(-2\frac{\mu_y}{\mu_x}\lambda_y d\right)\cdot$$
$$+k_{ZTE}\cos(k_{ZTE}d)\frac{1}{2k_{ZTE}}\left(-2\frac{\mu_y}{\mu_x}\lambda_y d\right)$$

$$f_2'(\lambda_{yl=0})=-\sin(k_{ZTE}d)\frac{1}{k_{ZTE}}\left(\frac{\mu_y}{\mu_x}\lambda_y d\right)-cos(k_{ZTE}d)\left(\frac{\mu_y}{\mu_x}\lambda_y d\right)$$

$$f_2'(\lambda_{yl=0})=-\left(\frac{\mu_y}{\mu_x}\lambda_y d\right)\left[\sin(k_{ZTE}d)\frac{1}{k_{ZTE}}+cos(k_{ZTE}d)\right]$$

$$f_2'(\lambda_{yl=0})=-\left(\frac{\mu_y}{\mu_x}\sqrt{\omega^2\epsilon_x\mu_x-\frac{\mu_x}{\mu_y}\lambda_x^2}d\right)[1+1]$$

$$f_2'(\lambda_{yl=0}) = -2\left(\frac{\mu_y}{\mu_x}\sqrt{\omega^2\epsilon_x\mu_x - \frac{\mu_x}{\mu_y}\lambda_x^2}d\right)$$

$$f_1(\lambda_{yl=0}) = \frac{\lambda_y^4}{(\frac{n\pi}{b}-\lambda_y)(\frac{n\pi}{b}+\lambda_y)(\frac{v\pi}{b}-\lambda_y)(\frac{v\pi}{b}+\lambda_y)}\frac{\cos(k_{ZTE}(d))}{1}\cdot \frac{(1-e^{-j\lambda_y b}(-1)^n)}{(\lambda_y-\omega\sqrt{\epsilon_x\mu_x})(\lambda_y+\omega\sqrt{\epsilon_x\mu_x})} \tag{D.301}$$

$$f_1(\lambda_{yl=0}) = \frac{\left(\omega^2\epsilon_x\mu_x - \frac{\mu_x}{\mu_y}\lambda_x^2\right)^2}{((\frac{n\pi}{b})^2-\omega^2\epsilon_x\mu_x+\frac{\mu_x}{\mu_y}\lambda_x^2)((\frac{v\pi}{b})^2-\omega^2\epsilon_x\mu_x+\frac{\mu_x}{\mu_y}\lambda_x^2)}\cdot \frac{(1-e^{-j\sqrt{\omega^2\epsilon_x\mu_x-\frac{\mu_x}{\mu_y}\lambda_x^2}b}(-1)^n)}{-\frac{\mu_x}{\mu_y}\lambda_x^2}$$

$$-j2\pi\sum_{l=0}^{\infty}\frac{f_1(\lambda_{yl=0})}{f_2'(\lambda_{yl=0})} = -j2\pi\frac{\left(\omega^2\epsilon_x\mu_x - \frac{\mu_x}{\mu_y}\lambda_x^2\right)^2}{((\frac{n\pi}{b})^2-\omega^2\epsilon_x\mu_x+\frac{\mu_x}{\mu_y}\lambda_x^2)((\frac{v\pi}{b})^2-\omega^2\epsilon_x\mu_x+\frac{\mu_x}{\mu_y}\lambda_x^2)}\cdot \frac{(1-e^{-j\sqrt{\omega^2\epsilon_x\mu_x-\frac{\mu_x}{\mu_y}\lambda_x^2}b}(-1)^n)}{-\frac{\mu_x}{\mu_y}\lambda_x^2}\frac{1}{-2\frac{\mu_y}{\mu_x}\sqrt{\omega^2\epsilon_x\mu_x-\frac{\mu_x}{\mu_y}\lambda_x^2}d} \tag{D.302}$$

$$-j2\pi\sum_{l=0}^{\infty}\frac{f_1(\lambda_{yl=0})}{f_2'(\lambda_{yl=0})} = -j2\pi\frac{\left(\sqrt{\omega^2\epsilon_x\mu_x - \frac{\mu_x}{\mu_y}\lambda_x^2}\right)^3}{((\frac{n\pi}{b})^2-\omega^2\epsilon_x\mu_x+\frac{\mu_x}{\mu_y}\lambda_x^2)((\frac{v\pi}{b})^2-\omega^2\epsilon_x\mu_x+\frac{\mu_x}{\mu_y}\lambda_x^2)}\cdot \frac{(1-e^{-j\sqrt{\omega^2\epsilon_x\mu_x-\frac{\mu_x}{\mu_y}\lambda_x^2}b}(-1)^n)}{-\lambda_x^2(-2d)} \tag{D.303}$$

$$-\sum_{l=0}^{\infty}\oint_{\lambda_{yB}}\frac{f(z)}{z-z_0}=-j2\pi\sum_{l=0}^{\infty}\frac{f_1(z_0)}{f_2'(z_0)}$$

$$f(\lambda_y)=\frac{\lambda_y^4}{(\frac{n\pi}{b}-\lambda_y)(\frac{n\pi}{b}+\lambda_y)(\frac{v\pi}{b}-\lambda_y)(\frac{v\pi}{b}+\lambda_y)}\frac{\cos(k_{ZTE}(d))}{k_{ZTE}\sin(k_{ZTE}d)}\frac{(1-e^{-j\lambda_y b}(-1)^n)}{(\lambda_y-\omega\sqrt{\epsilon_x\mu_x})(\lambda_y+\omega\sqrt{\epsilon_x\mu_x})}$$

Evaluating the $l\neq 0$ part second:

$$f_1(\lambda_y)=\frac{\lambda_y^4}{(\frac{n\pi}{b}-\lambda_y)(\frac{n\pi}{b}+\lambda_y)(\frac{v\pi}{b}-\lambda_y)(\frac{v\pi}{b}+\lambda_y)}\frac{\cos(k_{ZTE}(d))}{k_{ZTE}}\frac{(1-e^{-j\lambda_y b}(-1)^n)}{(\lambda_y-\omega\sqrt{\epsilon_x\mu_x})(\lambda_y+\omega\sqrt{\epsilon_x\mu_x})}$$

$$f_2(\lambda_{yl\neq 0})=\sin(k_{ZTE}d)$$

$$f_2'(\lambda_{yl\neq 0})=\cos(k_{ZTE}d)\frac{1}{2k_{ZTE}}\left(-2\frac{\mu_y}{\mu_x}\lambda_y d\right)$$

$$f_2'(\lambda_{yl\neq 0})=-cos(k_{ZTE}d)\frac{1}{k_{ZTE}}\left(\frac{\mu_y}{\mu_x}\lambda_y d\right)$$

$$f_2'(\lambda_{yl\neq 0})=-\frac{(-1)^l}{\pm\frac{l\pi}{d}}\left(\frac{\mu_y}{\mu_x}\sqrt{\omega^2\epsilon_x\mu_x-\frac{\mu_x}{\mu_y}\lambda_x^2-\frac{\mu_x}{\mu_y}\left(\frac{l\pi}{d}\right)^2}\,d\right)$$

$$f_1(\lambda_{yl\neq 0})=\frac{\lambda_y^4}{(\frac{n\pi}{b}-\lambda_y)(\frac{n\pi}{b}+\lambda_y)(\frac{v\pi}{b}-\lambda_y)(\frac{v\pi}{b}+\lambda_y)}\cdot$$
$$\frac{\cos(k_{ZTE}(d))}{k_{ZTE}}\frac{(1-e^{-j\lambda_y b})(-1)^n}{(\lambda_y-\omega\sqrt{\epsilon_x\mu_x})(\lambda_y+\omega\sqrt{\epsilon_x\mu_x})}$$

$$f_1(\lambda_{yl\neq 0})=\frac{\left(\omega^2\epsilon_x\mu_x-\frac{\mu_x}{\mu_y}\lambda_x^2-\frac{\mu_x}{\mu_y}\left(\frac{l\pi}{d}\right)^2\right)^2}{((\frac{n\pi}{b})^2-\omega^2\epsilon_x\mu_x+\frac{\mu_x}{\mu_y}\lambda_x^2+\frac{\mu_x}{\mu_y}\left(\frac{l\pi}{d}\right)^2)((\frac{v\pi}{b})^2-\omega^2\epsilon_x\mu_x+\frac{\mu_x}{\mu_y}\lambda_x^2+\frac{\mu_x}{\mu_y}\left(\frac{l\pi}{d}\right)^2)}\cdot$$
$$\frac{(-1)^l}{\frac{l\pi}{d}}\frac{(1-e^{-j\sqrt{\omega^2\epsilon_x\mu_x-\frac{\mu_x}{\mu_y}\lambda_x^2-\frac{\mu_x}{\mu_y}\left(\frac{l\pi}{d}\right)^2}b}(-1)^n)}{(\omega^2\epsilon_x\mu_x-\frac{\mu_x}{\mu_y}\lambda_x^2-\frac{\mu_x}{\mu_y}\left(\frac{l\pi}{d}\right)^2-\omega^2\epsilon_x\mu_x)}$$

(D.304)

$$f_1(\lambda_{yl\neq 0}) = \frac{\left(\omega^2\epsilon_x\mu_x - \frac{\mu_x}{\mu_y}\lambda_x^2 - \frac{\mu_x}{\mu_y}\left(\frac{l\pi}{d}\right)^2\right)^2}{((\frac{n\pi}{b})^2 - \omega^2\epsilon_x\mu_x + \frac{\mu_x}{\mu_y}\lambda_x^2 + \frac{\mu_x}{\mu_y}\left(\frac{l\pi}{d}\right)^2)((\frac{v\pi}{b})^2 - \omega^2\epsilon_x\mu_x + \frac{\mu_x}{\mu_y}\lambda_x^2 + \frac{\mu_x}{\mu_y}\left(\frac{l\pi}{d}\right)^2)} \cdot \frac{(-1)^l}{\frac{l\pi}{d}} \frac{(1 - e^{-j\sqrt{\omega^2\epsilon_x\mu_x - \frac{\mu_x}{\mu_y}\lambda_x^2 - \frac{\mu_x}{\mu_y}\left(\frac{l\pi}{d}\right)^2}b}(-1)^n)}{-\frac{\mu_x}{\mu_y}(\lambda_x^2 + \left(\frac{l\pi}{d}\right)^2)} \tag{D.305}$$

$$= -j2\pi \sum_{l=0}^{\infty} \frac{f_1(\lambda_{yl\neq 0})}{f_2'(\lambda_{yl\neq 0})}$$

$$= -j2\pi \sum_{l=0}^{\infty} \frac{\left(\omega^2\epsilon_x\mu_x - \frac{\mu_x}{\mu_y}\lambda_x^2 - \frac{\mu_x}{\mu_y}\left(\frac{l\pi}{d}\right)^2\right)^2}{((\frac{n\pi}{b})^2 - \omega^2\epsilon_x\mu_x + \frac{\mu_x}{\mu_y}\lambda_x^2 + \frac{\mu_x}{\mu_y}\left(\frac{l\pi}{d}\right)^2)((\frac{v\pi}{b})^2 - \omega^2\epsilon_x\mu_x + \frac{\mu_x}{\mu_y}\lambda_x^2 + \frac{\mu_x}{\mu_y}\left(\frac{l\pi}{d}\right)^2)} \cdot \tag{D.306}$$

$$\frac{(-1)^l}{\frac{l\pi}{d}} \frac{(1 - e^{-j\sqrt{\omega^2\epsilon_x\mu_x - \frac{\mu_x}{\mu_y}\lambda_x^2 - \frac{\mu_x}{\mu_y}\left(\frac{l\pi}{d}\right)^2}b}(-1)^n)}{-\frac{\mu_x}{\mu_y}(\lambda_x^2 + \left(\frac{l\pi}{d}\right)^2)} \cdot -\frac{\pm\frac{l\pi}{d}}{(-1)^l} \left(\frac{\mu_x}{\mu_y} \frac{1}{\sqrt{\omega^2\epsilon_x\mu_x - \frac{\mu_x}{\mu_y}\lambda_x^2 - \frac{\mu_x}{\mu_y}\left(\frac{l\pi}{d}\right)^2}d}\right)$$

$$= -j2\pi \sum_{l=0}^{\infty} \frac{f_1(\lambda_{yl\neq 0})}{f_2'(\lambda_{yl\neq 0})}$$

$$= -j2\pi \sum_{l=0}^{\infty} \frac{\left(\sqrt{\omega^2\epsilon_x\mu_x - \frac{\mu_x}{\mu_y}\lambda_x^2 - \frac{\mu_x}{\mu_y}\left(\frac{l\pi}{d}\right)^2}\right)^3}{((\frac{n\pi}{b})^2 - \omega^2\epsilon_x\mu_x + \frac{\mu_x}{\mu_y}\left(\lambda_x^2 + \left(\frac{l\pi}{d}\right)^2\right))((\frac{v\pi}{b})^2 - \omega^2\epsilon_x\mu_x + \frac{\mu_x}{\mu_y}\left(\lambda_x^2 + \left(\frac{l\pi}{d}\right)^2\right))} \cdot \tag{D.307}$$

$$\frac{(1 - e^{-j\sqrt{\omega^2\epsilon_x\mu_x - \frac{\mu_x}{\mu_y}\lambda_x^2 - \frac{\mu_x}{\mu_y}\left(\frac{l\pi}{d}\right)^2}b}(-1)^n)}{(\lambda_x^2 + \left(\frac{l\pi}{d}\right)^2)} \left(\frac{1}{d}\right)$$

$$= -j2\pi \sum_{l=0}^{\infty} \frac{f_1(\lambda_{yl\neq 0})}{f_2'(\lambda_{yl\neq 0})}$$

$$= -j2\pi \sum_{l=0}^{\infty} \frac{\left(\sqrt{\omega^2\epsilon_x\mu_x - \frac{\mu_x}{\mu_y}\lambda_x^2 - \frac{\mu_x}{\mu_y}\left(\frac{l\pi}{d}\right)^2}\right)^3}{((\frac{n\pi}{b})^2 - \omega^2\epsilon_x\mu_x + \frac{\mu_x}{\mu_y}\left(\lambda_x^2 + \left(\frac{l\pi}{d}\right)^2\right))((\frac{v\pi}{b})^2 - \omega^2\epsilon_x\mu_x + \frac{\mu_x}{\mu_y}\left(\lambda_x^2 + \left(\frac{l\pi}{d}\right)^2\right))} \cdot \frac{(1 - e^{-j\sqrt{\omega^2\epsilon_x\mu_x - \frac{\mu_x}{\mu_y}\lambda_x^2 - \frac{\mu_x}{\mu_y}\left(\frac{l\pi}{d}\right)^2}b}(-1)^n)}{(\lambda_x^2 + \left(\frac{l\pi}{d}\right)^2)d} \tag{D.308}$$

Combining: $l \neq 0$ and $l = 0$

$$-j2\pi \sum_{l=0}^{\infty} \frac{f_1(z_0)}{f_2'(z_0)}$$

$$= \frac{\left(\sqrt{\omega^2\epsilon_x\mu_x - \frac{\mu_x}{\mu_y}\lambda_x^2}\right)^3}{((\frac{n\pi}{b})^2 - \omega^2\epsilon_x\mu_x + \frac{\mu_x}{\mu_y}\lambda_x^2)((\frac{v\pi}{b})^2 - \omega^2\epsilon_x\mu_x + \frac{\mu_x}{\mu_y}\lambda_x^2)} \cdot \frac{(1 - e^{-j\sqrt{\omega^2\epsilon_x\mu_x - \frac{\mu_x}{\mu_y}\lambda_x^2}b}(-1)^n)}{-\lambda_x^2(-2d)} \tag{D.309}$$

$$= -j2\pi \sum_{l=0}^{\infty} \frac{f_1(\lambda_{yl\neq 0})}{f_2'(\lambda_{yl\neq 0})}$$

$$= -j2\pi \sum_{l=0}^{\infty} \frac{\left(\sqrt{\omega^2\epsilon_x\mu_x - \frac{\mu_x}{\mu_y}\lambda_x^2 - \frac{\mu_x}{\mu_y}\left(\frac{l\pi}{d}\right)^2}\right)^3}{((\frac{n\pi}{b})^2 - \omega^2\epsilon_x\mu_x + \frac{\mu_x}{\mu_y}\left(\lambda_x^2 + \left(\frac{l\pi}{d}\right)^2\right))((\frac{v\pi}{b})^2 - \omega^2\epsilon_x\mu_x + \frac{\mu_x}{\mu_y}\left(\lambda_x^2 + \left(\frac{l\pi}{d}\right)^2\right))} \cdot \frac{(1 - e^{-j\sqrt{\omega^2\epsilon_x\mu_x - \frac{\mu_x}{\mu_y}\lambda_x^2 - \frac{\mu_x}{\mu_y}\left(\frac{l\pi}{d}\right)^2}b}(-1)^n)}{(\lambda_x^2 + \left(\frac{l\pi}{d}\right)^2)d} \tag{D.310}$$

$$\boxed{\begin{aligned} &-j2\pi\frac{f_1(\lambda_{yl\neq 0})}{f_2'(\lambda_{yl\neq 0})} \\ &= -j2\pi\frac{\left(\sqrt{\omega^2\epsilon_x\mu_x - \frac{\mu_x}{\mu_y}\lambda_x^2 - \frac{\mu_x}{\mu_y}\left(\frac{l\pi}{d}\right)^2}\right)^3}{((\frac{n\pi}{b})^2 - \omega^2\epsilon_x\mu_x + \frac{\mu_x}{\mu_y}\left(\lambda_x^2 + \left(\frac{l\pi}{d}\right)^2\right))((\frac{v\pi}{b})^2 - \omega^2\epsilon_x\mu_x + \frac{\mu_x}{\mu_y}\left(\lambda_x^2 + \left(\frac{l\pi}{d}\right)^2\right))}\cdot \\ &\qquad\qquad \frac{(1 - e^{-j\sqrt{\omega^2\epsilon_x\mu_x - \frac{\mu_x}{\mu_y}\lambda_x^2 - \frac{\mu_x}{\mu_y}\left(\frac{l\pi}{d}\right)^2}b}(-1)^n)}{(\lambda_x^2 + \left(\frac{l\pi}{d}\right)^2)d(1+\delta_{l=0})} \end{aligned}} \tag{D.311}$$

for LHP Pole $\lambda_y A$.

On to the next pole:

$$-\oint_{\lambda_{yC}} \frac{f(z)}{z - z_0} = -j\pi f(z_0) =$$

$$-j\pi\ \frac{\lambda_y^2}{(\frac{n\pi}{b} - \lambda_y)}\frac{\cos(k_{ZTE}(d))}{k_{ZTE}\sin(k_{ZTE}d)}\frac{(1 - e^{-j\lambda_y b}(-1)^n)}{(\lambda_y + \omega\sqrt{\epsilon_x\mu_x})(\lambda_y - \omega\sqrt{\epsilon_x\mu_x})}\Bigg|_{\lambda_y = -\frac{n\pi}{b}} \tag{D.312}$$

$$(1 - e^{j(\frac{n\pi}{b})b}(-1)^n) = (1 - e^{j(n\pi)}(-1)^n) = (1 - (-1)^n(-1)^n) = (1 - (-1)^{2n}) = (1-1) = 0$$

$\boxed{0}$ for UHP Pole λ_{yC}.

On to the next pole:

$$-\oint_{\lambda_{yD}} \frac{f(z)}{z-z_0} = -j\pi f(z_0) =$$

$$-j\pi \left. \frac{\lambda_y^2}{(\frac{n\pi}{b}+\lambda_y)} \frac{\cos(k_{ZTE}(d))}{k_{ZTE}\sin(k_{ZTE}d)} \frac{(1-e^{-j\lambda_y b}(-1)^n)}{(\lambda_y+\omega\sqrt{\epsilon_x\mu_x})(\lambda_y-\omega\sqrt{\epsilon_x\mu_x})} \right|_{\lambda_y=\frac{n\pi}{b}} \tag{D.313}$$

$$(1-e^{j(\frac{n\pi}{b})b}(-1)^n) = (1-e^{j(n\pi)}(-1)^n) = (1-(-1)^n(-1)^n) = (1-(-1)^{2n}) = (1-1) = 0$$

$$\boxed{0} \qquad \text{for UHP Pole } \lambda_{yD}.$$

$$-\oint_{\lambda_{yE}} \frac{f(z)}{z-z_0} = -j\pi f(z_0) =$$

$$-j\pi \left. \frac{\lambda_y^4 \cos(k_{ZTE}(d))}{k_{ZTE}\sin(k_{ZTE}d)} \frac{(1-e^{-j\lambda_y b}(-1)^n)}{((\frac{v\pi}{b})-\lambda_y)((\frac{n\pi}{b})-\lambda_y)((\frac{n\pi}{b})+\lambda_y)(\lambda_y-\omega\sqrt{\epsilon_x\mu_x})(\lambda_y+\omega\sqrt{\epsilon_x\mu_x})} \right|_{\lambda_y=-\frac{v\pi}{b}}$$

$$-j\pi \frac{(\frac{v\pi}{b})^3 \cos(\sqrt{\omega^2\epsilon_x\mu_y - \lambda_x^2 - \frac{\mu_y}{\mu_x}(\frac{v\pi}{b})^2}(d))}{\sqrt{\omega^2\epsilon_x\mu_y - \lambda_x^2 - \frac{\mu_y}{\mu_x}(\frac{v\pi}{b})^2}\sin(\sqrt{\omega^2\epsilon_x\mu_y - \lambda_x^2 - \frac{\mu_y}{\mu_x}(\frac{v\pi}{b})^2}d)} \cdot \tag{D.314}$$

$$\frac{(1-(-1)^v(-1)^n)}{2((\frac{n\pi}{b})^2-(\frac{v\pi}{b})^2)((\frac{v\pi}{b})^2-\omega^2\epsilon_x\mu_x)} =$$

$$\boxed{-j\pi \frac{(\frac{v\pi}{b})^3 \cos(\sqrt{\omega^2\epsilon_x\mu_y - \lambda_x^2 - \frac{\mu_y}{\mu_x}(\frac{v\pi}{b})^2}(d))}{\sqrt{\omega^2\epsilon_x\mu_y - \lambda_x^2 - \frac{\mu_y}{\mu_x}(\frac{v\pi}{b})^2}\sin(\sqrt{\omega^2\epsilon_x\mu_y - \lambda_x^2 - \frac{\mu_y}{\mu_x}(\frac{v\pi}{b})^2}d)} \cdot \frac{(1-(-1)^v(-1)^n)}{2((\frac{n\pi}{b})^2-(\frac{v\pi}{b})^2)((\frac{v\pi}{b})^2-\omega^2\epsilon_x\mu_x)}} \qquad \text{for UHP Pole } \lambda_{yE}. \tag{D.315}$$

$$-\oint_{\lambda_{yF}} \frac{f(z)}{z-z_0} = -j\pi f(z_0) =$$

$$-j\pi \left. \frac{\lambda_y^4 \cos(k_{ZTE}(d))}{k_{ZTE}\sin(k_{ZTE}d)} \frac{(1-e^{j\lambda_y b}(-1)^n)}{((\frac{v\pi}{b})-\lambda_y)((\frac{n\pi}{b})-\lambda_y)((\frac{n\pi}{b})+\lambda_y)(\lambda_y-\omega\sqrt{\epsilon_x\mu_x})(\lambda_y+\omega\sqrt{\epsilon_x\mu_x})} \right|_{\lambda_y=\frac{v\pi}{b}} = \tag{D.316}$$

$$-j\pi \frac{(\frac{v\pi}{b})^3 \cos(\sqrt{\omega^2\epsilon_x\mu_y - \lambda_x^2 - \frac{\mu_y}{\mu_x}(\frac{v\pi}{b})^2}(d))}{\sqrt{\omega^2\epsilon_x\mu_y - \lambda_x^2 - \frac{\mu_y}{\mu_x}(\frac{v\pi}{b})^2}\sin(\sqrt{\omega^2\epsilon_x\mu_y - \lambda_x^2 - \frac{\mu_y}{\mu_x}(\frac{v\pi}{b})^2}d)} \frac{(1-(-1)^v(-1)^n)}{2((\frac{n\pi}{b})^2-(\frac{v\pi}{b})^2)((\frac{v\pi}{b})^2-\omega^2\epsilon_x\mu_x)} =$$

$$\boxed{-j\pi \frac{(\frac{v\pi}{b})^3 \cos(\sqrt{\omega^2\epsilon_x\mu_y - \lambda_x^2 - \frac{\mu_y}{\mu_x}(\frac{v\pi}{b})^2}(d))}{\sqrt{\omega^2\epsilon_x\mu_y - \lambda_x^2 - \frac{\mu_y}{\mu_x}(\frac{v\pi}{b})^2}\sin(\sqrt{\omega^2\epsilon_x\mu_y - \lambda_x^2 - \frac{\mu_y}{\mu_x}(\frac{v\pi}{b})^2}d)} \cdot \frac{(1-(-1)^v(-1)^n)}{2((\frac{n\pi}{b})^2-(\frac{v\pi}{b})^2)((\frac{v\pi}{b})^2-\omega^2\epsilon_x\mu_x)}} \quad \text{for UHP Pole } \lambda_{yF}. \tag{D.317}$$

Combining the UHP and LHP parts results in the total solution for the Case 1 $n \neq v \neq 0$:

$$\Omega_y = \int_{-\infty}^{\infty} \frac{\lambda_y^4}{k_{ZTE}(\lambda_y^2-\omega^2\epsilon_x\mu_x)} \frac{\cos(k_{ZTE}d)}{\sin(k_{ZTE}d)} \frac{(e^{j(b\lambda_y)}(-1)^v-1)}{((\frac{v\pi}{b})^2-\lambda_y^2)} \frac{(e^{-j(b\lambda_y)}(-1)^n-1)}{(k_y^2-\lambda_y^2)} d\lambda_y = \tag{D.318}$$

$$
\begin{aligned}
&-((-1)^{n+v}+1)\pi\frac{\left(\omega\sqrt{\epsilon_x\mu_x}\right)^3\cos(j\lambda_x d)}{\lambda_x\sin(j\lambda_x d)}\frac{(1-e^{-j\omega\sqrt{\epsilon_x\mu_x}b}(-1)^n)}{((\frac{n\pi}{b})^2-\omega^2\epsilon_x\mu_x)((\frac{v\pi}{b})^2-\omega^2\epsilon_x\mu_x)}\\
&-((-1)^{n+v}+1)j2\pi\cdot\\
&\sum_{l=0}^{\infty}\left(\frac{\left(\sqrt{\omega^2\epsilon_x\mu_x-\frac{\mu_x}{\mu_y}\lambda_x^2-\frac{\mu_x}{\mu_y}\left(\frac{l\pi}{d}\right)^2}\right)^3}{((\frac{n\pi}{b})^2-\omega^2\epsilon_x\mu_x+\frac{\mu_x}{\mu_y}\lambda_x^2+\frac{\mu_x}{\mu_y}\left(\frac{l\pi}{d}\right)^2)((\frac{v\pi}{b})^2-\omega^2\epsilon_x\mu_x+\frac{\mu_x}{\mu_y}\lambda_x^2+\frac{\mu_x}{\mu_y}\left(\frac{l\pi}{d}\right)^2)}\cdot\right.\\
&\left.\frac{(1-e^{-j\sqrt{\omega^2\epsilon_x\mu_x-\frac{\mu_x}{\mu_y}\lambda_x^2-\frac{\mu_x}{\mu_y}\left(\frac{l\pi}{d}\right)^2}b}(-1)^n)}{(\lambda_x^2+\left(\frac{l\pi}{d}\right)^2)d(1+\delta_{l=0})}\right)+\\
&((-1)^{n+v}-1)j\pi\frac{(\frac{v\pi}{b})^3\cos(\sqrt{\omega^2\epsilon_x\mu_y-\lambda_x^2-\frac{\mu_y}{\mu_x}(\frac{v\pi}{b})^2}(d))}{\sqrt{\omega^2\epsilon_x\mu_y-\lambda_x^2-\frac{\mu_y}{\mu_x}(\frac{v\pi}{b})^2}\sin(\sqrt{\omega^2\epsilon_x\mu_y-\lambda_x^2-\frac{\mu_y}{\mu_x}(\frac{v\pi}{b})^2}d)}\cdot\\
&\frac{(1-(-1)^v(-1)^n)}{((\frac{n\pi}{b})^2-(\frac{v\pi}{b})^2)((\frac{v\pi}{b})^2-\omega^2\epsilon_x\mu_x)}
\end{aligned}
\tag{D.319}
$$

Appendix E. Rotated Uniaxial Moment Method Details

E.1 Solution Summary

Orientation 1.

$$
\begin{aligned}
2\left(\frac{(\frac{\pi}{a})^2}{Z_{10}^{TE*}Z_{10}^{TE}}\right)\frac{ab}{2}\delta_{uv10}^{TE} = \sum_{m=0}^{\infty}\sum_{n=0}^{\infty}\Bigg[\overline{\Gamma}_{mn}^{TE}\Bigg(\left(\left(\frac{m\pi}{a}\right)^2+\left(\frac{n\pi}{b}\right)^2\right)\frac{ab(1+\delta_{uvm0}^{TE})}{4Z_{mn}^{TE*}Z_{mn}^{TE}}\delta_{uvmn}^{TE} \\
-\frac{1}{(2\pi)^2}\int_{-\infty}^{\infty}\frac{(e^{j(a\lambda_x)}(-1)^u-1)}{((\frac{u\pi}{a})^2-\lambda_x^2)}\frac{(e^{-j(a\lambda_x)}(-1)^m-1)}{(k_x^2-\lambda_x^2)}\left(\Omega_{yTE}+\Phi_{yTE}+\Upsilon_{yTE}+X_{yTE}\right)d\lambda_x\Bigg)\Bigg] \\
+\sum_{m=0}^{\infty}\sum_{n=0}^{\infty}\Bigg[\Gamma_{mn}^{TM}\Bigg(\left(\left(\frac{m\pi}{a}\right)^2+\left(\frac{n\pi}{b}\right)^2\right)\frac{ab(1+\delta_{uvm0}^{TM})}{4Z_{mn}^{TM*}Z_{mn}^{TM}}\delta_{uvmn}^{TM} \\
-\frac{k_xk_y}{(2\pi)^2}\int_{-\infty}^{\infty}\frac{(e^{j(a\lambda_x)}(-1)^u-1)}{((\frac{u\pi}{a})^2-\lambda_x^2)}\frac{(e^{-j(a\lambda_x)}(-1)^m-1)}{(k_x^2-\lambda_x^2)}\left(\Omega_{yTM}+\Phi_{yTM}+\Upsilon_{yTM}+X_{yTM}\right)d\lambda_x\Bigg)\Bigg].
\end{aligned}
\tag{E.1}
$$

The terms C_x and C_y are:

$$
C_x = \begin{cases} \frac{-j(\frac{u\pi}{a})^{2\,*}}{Z_{uv}^{TE}}, & h_{uvx}^* \implies h_{uvx}^{*\ TE} \\ \frac{j\frac{u\pi}{a}\frac{v\pi}{b}^{*}}{Z_{uv}^{TM}}, & h_{uvx}^* \implies h_{uvx}^{*\ TM} \end{cases} \tag{E.2}
$$

$$
C_y = \begin{cases} \frac{-j(\frac{v\pi}{b})^{2\,*}}{Z_{uv}^{TE}}, & h_{uvy}^* \implies h_{uvy}^{*\ TE} \\ \frac{-j\frac{u\pi}{a}\frac{v\pi}{b}^{*}}{Z_{uv}^{TM}}, & h_{uvy}^* \implies h_{uvy}^{*\ TM} \end{cases} \tag{E.3}
$$

depending on which component is being tested, i.e. TE test, TE expand; TM test, TE expand; TE test, TM expand; or TM test, TM expand.

Each case describe which values are implicated. If the term is not explicitly stated, then it not implicated and is consider to be '0'.

Case 5 $n = v = 0$**.**

$$\Omega_{yTE} = -j4\pi \frac{C_x k_x^2}{\mu_x \omega} \sum_{l=0}^{\infty} \frac{\lambda_x^2 (1 - e^{-j\lambda_{yTE} b})}{(\lambda_x^2 + \left(\frac{l\pi}{d}\right)^2) \lambda_{yTE} d (1 + \delta_{l=0})} \tag{E.4}$$

$$X_{yTE} = -2\pi C_x k_x^2 \omega \epsilon_x \frac{\lambda_{zTM}^n \cos(\lambda_{zTM}^n (d)) b}{(\omega^2 \epsilon_x \mu_x) (\sin(\lambda_{zTM}^n d))} - j4\pi C_x k_x^2 \omega \epsilon_x \sum_{l=0}^{\infty} \frac{\left(\frac{l\pi}{d}\right)^2}{(\lambda_x^2 + \left(\frac{l\pi}{d}\right)^2)} \frac{(1 - e^{-j\lambda_{yTM} b})}{(\lambda_{yTM})^3 d} \tag{E.5}$$

Case 4 $n = 0$ **and** $v \neq 0$**.**

$$\Omega_{yTE} = j4\pi \frac{C_x k_x^2}{\mu_x \omega} \sum_{l=0}^{\infty} \frac{\lambda_x^2 \lambda_{yTE}}{((\frac{v\pi}{b})^2 - \lambda_{yTE}^2)} \frac{(1 - e^{-j\lambda_{yTE} b})}{(\lambda_x^2 + \left(\frac{l\pi}{d}\right)^2) d (1 + \delta_{l=0})} \tag{E.6}$$

$$\Phi_{yTE} = -j4\pi \frac{(C_y k_x^2)}{\mu_x \omega} \sum_{l=0}^{\infty} \frac{\lambda_x^2 (1 - e^{-j\lambda_{yTE} b})}{((\frac{v\pi}{b})^2 - \lambda_{yTE}^2} \frac{1}{\frac{\mu_y}{\mu_x} \lambda_{yTE} d (1 + \delta_{l=0})} \tag{E.7}$$

$$X_{yTE} = -j4\pi C_x k_x^2 \omega \epsilon_x \sum_{l=0}^{\infty} \frac{\left(\frac{l\pi}{d}\right)^2}{(-\lambda_x^2 - \left(\frac{l\pi}{d}\right)^2)} \frac{(1 - e^{-j\lambda_{yTM} b})}{\left((\frac{v\pi}{b})^2 - \lambda_{yTM}^2\right)} \frac{1}{\lambda_{yTM} d} \tag{E.8}$$

Case 3 $n \neq 0$ **and** $v = 0$**.**

$$\Omega_{yTE} = j4\pi \frac{C_x k_x^2}{\mu_x \omega} \sum_{l=0}^{\infty} \frac{\lambda_x^2 \lambda_{yTE}}{((\frac{n\pi}{b})^2 - \lambda_{yTE}^2)} \frac{(1 - e^{-j\lambda_{yTE} b} (-1)^n)}{(\lambda_x^2 + \left(\frac{l\pi}{d}\right)^2) d (1 + \delta_{l=0})} \tag{E.9}$$

$$\Phi_{yTE} = -j4\pi \frac{(C_x k_y^2)}{\mu_x \omega} \sum_{l=0}^{\infty} \frac{\lambda_x^2 (1 - e^{-j\lambda_{yTE} b} (-1)^n)}{(\frac{n\pi}{b})^2 - \lambda_{yTE}^2} \frac{1}{\frac{\mu_y}{\mu_x} \lambda_{yTE} d (1 + \delta_{l=0})} \tag{E.10}$$

$$X_{yTE} = -j4\pi C_x k_x^2 \omega \epsilon_x \sum_{l=0}^{\infty} \frac{\left(\frac{l\pi}{d}\right)^2}{(-\lambda_x^2 - \left(\frac{l\pi}{d}\right)^2)} \frac{(1 - (-1)^n e^{-j\lambda_{yTM} b})}{\left((\frac{n\pi}{b})^2 - \lambda_{yTM}^2\right)} \frac{1}{\lambda_{yTM} d} \tag{E.11}$$

$$\Omega_{yTM} = -j4\pi \left(\frac{C_x}{\mu_x \omega}\right) \sum_{l=0}^{\infty} \frac{\lambda_x^2 \lambda_{yTE}}{((\frac{n\pi}{b})^2 - \lambda_{yTE}^2)} \frac{(1 - e^{-j\lambda_{yTE} b} (-1)^n)}{(\lambda_x^2 + \left(\frac{l\pi}{d}\right)^2) d (1 + \delta_{l=0})} \tag{E.12}$$

$$\Phi_{yTM} = -j4\pi\frac{(C_x)}{\mu_x\omega}\sum_{l=0}^{\infty}\frac{\lambda_x^2(1-e^{-j\lambda_{yTE}b}(-1)^n)}{((\frac{n\pi}{b})^2-\lambda_{yTE}^2}\frac{1}{\frac{\mu_y}{\mu_x}\lambda_{yTE}d(1+\delta_{l=0})} \tag{E.13}$$

$$X_{yTM} = j4\pi\left(C_x\omega\epsilon_x\right)\sum_{l=0}^{\infty}\frac{\left(\frac{l\pi}{d}\right)^2}{(-\lambda_x^2-\left(\frac{l\pi}{d}\right)^2)}\frac{(1-(-1)^n e^{-j\lambda_{yTM}b})}{\left((\frac{n\pi}{b})^2-\lambda_{yTM}^2\right)}\frac{1}{\lambda_{yTM}d} \tag{E.14}$$

Case 2 $n = v \neq 0$**.**

$$\Omega_{yTE} = -j4\pi\frac{C_xk_x^2}{\mu_x\omega}\sum_{l=0}^{\infty}\left(\frac{\lambda_x^2\left(\lambda_{yTE}\right)^3}{((\frac{n\pi}{b})^2-\lambda_{yTE}^2)((\frac{n\pi}{b})^2-\lambda_{yTE}^2)}\frac{(1-e^{-j\lambda_{yTE}b}(-1)^n)}{(\lambda_x^2+\left(\frac{l\pi}{d}\right)^2)d(1+\delta_{l=0})}\right)+ \pi\frac{C_xk_x^2}{\mu_x\omega}\frac{\lambda_x^2(\frac{n\pi}{b})^2\cos(\lambda_{zTE}^n d)}{\lambda_{zTE}^n\sin(\lambda_{zTE}^n d)}\frac{b}{((\frac{n\pi}{b})^2-\omega^2\epsilon_x\mu_x)} \tag{E.15}$$

$$\Phi_{yTE} = j4\pi\frac{(C_xk_y^2+C_yk_x^2)}{\mu_x\omega}\sum_{l=0}^{\infty}\left(\frac{\lambda_x^2\left(\lambda_{yTE}\right)}{((\frac{n\pi}{b})^2-\lambda_{yTE}^2)((\frac{n\pi}{b})^2-\lambda_{yTE}^2)}\frac{(1-e^{-j\lambda_{yTE}b}(-1)^n)}{\frac{\mu_y}{\mu_x}d(1+\delta_{l=0})}\right)+ \pi\frac{(C_xk_y^2+C_yk_x^2)}{\mu_x\omega}\frac{\lambda_x^2\cos(\lambda_{zTE}^n d)}{\lambda_{zTE}^n\sin(\lambda_{zTE}^n d)}b \tag{E.16}$$

$$\Upsilon_{yTE} = j4\pi\frac{C_yk_y^2}{\mu_x\omega}\sum_{l=0}^{\infty}\left(\frac{\lambda_x^2\frac{\mu_x}{\mu_y}\left(-\frac{\mu_x}{\mu_y}\lambda_x^2-\frac{\mu_x}{\mu_y}\left(\frac{l\pi}{d}\right)^2\right)}{((\frac{n\pi}{b})^2-\lambda_{yTE}^2)((\frac{n\pi}{b})^2-\lambda_{yTE}^2)}\frac{(1-e^{-j\lambda_{yTE}b}(-1)^n)}{\lambda_{yTE}d(1+\delta_{l=0})}\right) + \pi\frac{C_yk_y^2}{\mu_x\omega}\frac{\lambda_x^2\left((\frac{n\pi}{b})^2-\omega^2\epsilon_x\mu_x\right)\cos(\lambda_{zTE}^n(d))}{\lambda_{zTE}^n\sin(\lambda_{zTE}^n d)}\frac{b}{((\frac{n\pi}{b})^2)} \tag{E.17}$$

$$X_{yTE} = \pi C_xk_x^2\omega\epsilon_x\frac{(\frac{n\pi}{b})\lambda_{zTM}^n\cos(\lambda_{zTM}^n(d))b(-1)^n}{((\frac{n\pi}{b})^2-\omega^2\epsilon_x\mu_x)\left(\sin(\lambda_{zTM}^n d)\right)} + j4\pi C_xk_x^2\omega\epsilon_x\sum_{l=0}^{\infty}\left(\frac{\left(\frac{l\pi}{d}\right)^2\left(\lambda_{yTM}\right)}{(-\lambda_x^2-\left(\frac{l\pi}{d}\right)^2)}\frac{(1-(-1)^n e^{-j\lambda_{yTM}b})}{\left((\frac{n\pi}{b})^2-\lambda_{yTM}^2\right)\left((\frac{n\pi}{b})^2-\lambda_{yTM}^2\right)}\frac{1}{d}\right) \tag{E.18}$$

$$\Omega_{yTM} = j4\pi\left(\frac{C_x}{\mu_x\omega}\right)\sum_{l=0}^{\infty}\left(\frac{\lambda_x^2\left(\lambda_{yTE}\right)^3}{((\frac{n\pi}{b})^2-\lambda_{yTE}^2)((\frac{n\pi}{b})^2-\lambda_{yTE}^2)}\frac{(1-e^{-j\lambda_{yTE}b}(-1)^n)}{(\lambda_x^2+\left(\frac{l\pi}{d}\right)^2)d(1+\delta_{l=0})}\right)+ \\ -\pi\left(\frac{C_x}{\mu_x\omega}\right)\frac{\lambda_x^2(\frac{n\pi}{b})^2\cos(\lambda_{zTE}^n d)}{\lambda_{zTE}^n\sin(\lambda_{zTE}^n d)}\frac{b}{((\frac{n\pi}{b})^2-\omega^2\epsilon_x\mu_x)} \tag{E.19}$$

$$\Phi_{yTM} = j4\pi\frac{(C_x-C_y)}{\mu_x\omega}\sum_{l=0}^{\infty}\left(\frac{\lambda_x^2\left(\lambda_{yTE}\right)}{((\frac{n\pi}{b})^2-\lambda_{yTE}^2)((\frac{n\pi}{b})^2-\lambda_{yTE}^2)}\frac{(1-e^{-j\lambda_{yTE}b}(-1)^n)}{\frac{\mu_y}{\mu_x}d(1+\delta_{l=0})}\right)+ \\ \pi\frac{(C_x-C_y)}{\mu_x\omega}\frac{\lambda_x^2\cos(\lambda_{zTE}^n d)}{\lambda_{zTE}^n\sin(\lambda_{zTE}^n d)}b \tag{E.20}$$

$$\Upsilon_{yTM} = j4\pi\frac{C_y}{\mu_x\omega}\sum_{l=0}^{\infty}\left(\frac{\lambda_x^2\frac{\mu_x}{\mu_y}\left(-\frac{\mu_x}{\mu_y}\lambda_x^2-\frac{\mu_x}{\mu_y}\left(\frac{l\pi}{d}\right)^2\right)}{((\frac{n\pi}{b})^2-\lambda_{yTE}^2)((\frac{n\pi}{b})^2-\lambda_{yTE}^2)}\frac{(1-e^{-j\lambda_{yTE}b}(-1)^n)}{\lambda_{yTE}d(1+\delta_{l=0})}\right) \\ +\pi\frac{C_y}{\mu_x\omega}\frac{\lambda_x^2\left((\frac{n\pi}{b})^2-\omega^2\epsilon_x\mu_x\right)\cos(\lambda_{zTE}^n(d))}{\lambda_{zTE}^n\sin(\lambda_{zTE}^n d)}\frac{b}{((\frac{n\pi}{b})^2)} \tag{E.21}$$

$$X_{yTM} = -\pi C_x\omega\epsilon_x\frac{(\frac{n\pi}{b})\lambda_{zTM}^n\cos(\lambda_{zTM}^n(d))b(-1)^n}{((\frac{n\pi}{b})^2-\omega^2\epsilon_x\mu_x)\left(\sin(\lambda_{zTM}^n d)\right)} \\ -j4\pi C_x\omega\epsilon_x\sum_{l=0}^{\infty}\left(\frac{\left(\frac{l\pi}{d}\right)^2\left(\lambda_{yTM}\right)}{(-\lambda_x^2-\left(\frac{l\pi}{d}\right)^2)}\frac{(1-(-1)^n e^{-j\lambda_{yTM}b})}{\left((\frac{n\pi}{b})^2-\lambda_{yTM}^2\right)\left((\frac{n\pi}{b})^2-\lambda_{yTM}^2\right)}\frac{1}{d}\right) \tag{E.22}$$

Case 1 $n \neq v \neq 0$**.**

$$\Omega_{yTE} = -j4\pi\frac{C_x k_x^2}{\mu_x\omega}\sum_{l=0}^{\infty}\frac{\lambda_x^2\left(\lambda_{yTE}\right)^3}{((\frac{n\pi}{b})^2-\lambda_{yTE}^2)((\frac{v\pi}{b})^2-\lambda_{yTE}^2)}\frac{(1-e^{-j\lambda_{yTE}b})}{(\lambda_x^2+\left(\frac{l\pi}{d}\right)^2)d(1+\delta_{l=0})} \tag{E.23}$$

$$\Phi_{yTE} = j4\pi\frac{(C_x k_y^2+C_y k_x^2)}{\mu_x\omega}\sum_{l=0}^{\infty}\frac{\lambda_x^2\left(\lambda_{yTE}\right)}{((\frac{n\pi}{b})^2-\lambda_{yTE}^2)((\frac{v\pi}{b})^2-\lambda_{yTE}^2)}\frac{(1-e^{-j\lambda_{yTE}b})}{\frac{\mu_y}{\mu_x}d(1+\delta_{l=0})} \tag{E.24}$$

$$\Upsilon_{yTE} = j4\pi\frac{C_y k_y^2}{\mu_x\omega}\sum_{l=0}^{\infty}\frac{\lambda_x^2\left(-\frac{\mu_x}{\mu_y}\lambda_x^2-\frac{\mu_x}{\mu_y}\left(\frac{l\pi}{d}\right)^2\right)}{((\frac{n\pi}{b})^2-\lambda_{yTE}^2)((\frac{v\pi}{b})^2-\lambda_{yTE}^2)}\frac{(1-e^{-j\lambda_{yTE}b})}{\frac{\mu_y}{\mu_x}\lambda_{yTE}d(1+\delta_{l=0})} \tag{E.25}$$

$$X_{yTE} = j4\pi C_x k_x^2\omega\epsilon_x\sum_{l=0}^{\infty}\frac{\left(\frac{l\pi}{d}\right)^2\left(\lambda_{yTM}\right)}{(-\lambda_x^2-\left(\frac{l\pi}{d}\right)^2)}\frac{(1-e^{-j\lambda_{yTM}b})}{\left((\frac{n\pi}{b})^2-\lambda_{yTM}^2\right)\left((\frac{v\pi}{b})^2-\lambda_{yTM}^2\right)}\frac{1}{d} \tag{E.26}$$

$$\Omega_{yTM} = j4\pi(\frac{C_x}{\mu_x\omega})\sum_{l=0}^{\infty}\frac{\lambda_x^2\left(\lambda_{yTE}\right)^3}{((\frac{n\pi}{b})^2-\lambda_{yTE}^2)((\frac{v\pi}{b})^2-\lambda_{yTE}^2)}\frac{(1-e^{-j\lambda_{yTE}b})}{(\lambda_x^2+\left(\frac{l\pi}{d}\right)^2)d(1+\delta_{l=0})} \tag{E.27}$$

$$\Phi_{yTM} = j4\pi\frac{(C_x-C_y)}{\mu_x\omega}\sum_{l=0}^{\infty}\frac{\lambda_x^2\left(\lambda_{yTE}\right)}{((\frac{n\pi}{b})^2-\lambda_{yTE}^2)((\frac{v\pi}{b})^2-\lambda_{yTE}^2)}\frac{(1-e^{-j\lambda_{yTE}b})}{\frac{\mu_y}{\mu_x}d(1+\delta_{l=0})} \tag{E.28}$$

$$\Upsilon_{yTM} = j4\pi\frac{C_y}{\mu_x\omega}\sum_{l=0}^{\infty}\frac{\lambda_x^2\left(-\frac{\mu_x}{\mu_y}\lambda_x^2-\frac{\mu_x}{\mu_y}\left(\frac{l\pi}{d}\right)^2\right)}{((\frac{n\pi}{b})^2-\lambda_{yTE}^2)((\frac{v\pi}{b})^2-\lambda_{yTE}^2)}\frac{(1-e^{-j\lambda_{yTE}b})}{\frac{\mu_y}{\mu_x}\lambda_{yTE}d(1+\delta_{l=0})} \tag{E.29}$$

$$X_{yTM} = j4\pi(-C_x\omega\epsilon_x)\sum_{l=0}^{\infty}\frac{\left(\frac{l\pi}{d}\right)^2\left(\lambda_{yTM}\right)}{(-\lambda_x^2-\left(\frac{l\pi}{d}\right)^2)}\frac{(1-e^{-j\lambda_{yTM}b})}{\left((\frac{n\pi}{b})^2-\lambda_{yTM}^2\right)\left((\frac{v\pi}{b})^2-\lambda_{yTM}^2\right)}\frac{1}{d} \tag{E.30}$$

Orientation 2.

$$\begin{aligned}
2\left(\frac{(\frac{\pi}{a})^2}{Z_{10}^{TE*}Z_{10}^{TE}}\right)\frac{ab}{2}\delta_{uv10}^{TE} = \sum_{m=0}^{\infty}\sum_{n=0}^{\infty}\Bigg[\overline{\Gamma}_{mn}^{TE}\Bigg(\left(\left(\frac{m\pi}{a}\right)^2+\left(\frac{n\pi}{b}\right)^2\right)\frac{ab(1+\delta_{uvm0}^{TE})}{4Z_{mn}^{TE*}Z_{mn}^{TE}}\delta_{uvmn}^{TE} \\
-\frac{1}{(2\pi)^2}\int_{-\infty}^{\infty}\frac{(e^{j(b\lambda_x)}(-1)^v-1)}{((\frac{v\pi}{b})^2-\lambda_x^2)}\frac{(e^{-j(b\lambda_x)}(-1)^n-1)}{(k_y^2-\lambda_x^2)}\left(\Omega_{yTE}+\Phi_{yTE}+\Upsilon_{yTE}+X_{yTE}\right)d\lambda_x\Bigg)\Bigg] \\
+\sum_{m=0}^{\infty}\sum_{n=0}^{\infty}\Bigg[\Gamma_{mn}^{TM}\Bigg(\left(\left(\frac{m\pi}{a}\right)^2+\left(\frac{n\pi}{b}\right)^2\right)\frac{ab(1+\delta_{uvm0}^{TM})}{4Z_{mn}^{TM*}Z_{mn}^{TM}}\delta_{uvmn}^{TM} \\
-\frac{k_xk_y}{(2\pi)^2}\int_{-\infty}^{\infty}\frac{(e^{j(b\lambda_x)}(-1)^v-1)}{((\frac{v\pi}{b})^2-\lambda_x^2)}\frac{(e^{-j(b\lambda_x)}(-1)^n-1)}{(k_y^2-\lambda_x^2)}\left(\Omega_{yTM}+\Phi_{yTM}+\Upsilon_{yTM}+X_{yTM}\right)d\lambda_x\Bigg)\Bigg].
\end{aligned} \tag{E.31}$$

As before:

$$C_x = \begin{cases} \frac{-j(\frac{v\pi}{b})^{2\,*}}{Z_{uv}^{TE}}, & h_{uvx}^* \implies h_{uvx}^{*\ TE} \\ -\frac{j\frac{u\pi}{a}\frac{v\pi}{b}^*}{Z_{uv}^{TM}}, & h_{uvx}^* \implies h_{uvx}^{*\ TM} \end{cases} \tag{E.32}$$

$$C_y = \begin{cases} \frac{-j(\frac{u\pi}{b})^{2\,*}}{Z_{uv}^{TE}}, & h_{uvy}^* \implies h_{uvy}^{*\ TE} \\ \frac{j\frac{u\pi}{a}\frac{v\pi}{b}^*}{Z_{uv}^{TM}}, & h_{uvy}^* \implies h_{uvy}^{*\ TM} \end{cases} \tag{E.33}$$

Each case describe which values are implicated. If the term is not explicitly stated, then it not implicated and is consider to be '0'.

Case 2 $m = u \neq 0$**.**

$$\Omega_{yTE} = -j4\pi \frac{C_x k_y^2}{\mu_x \omega} \sum_{l=0}^{\infty} \left(\frac{\lambda_x^2 \left(\lambda_{yTE}\right)^3}{((\frac{m\pi}{a})^2 - \lambda_{yTE}^2)((\frac{m\pi}{a})^2 - \lambda_{yTE}^2)} \frac{(1 - e^{-j\lambda_{yTE}a}(-1)^m)}{(\lambda_x^2 + \left(\frac{l\pi}{d}\right)^2) d(1 + \delta_{l=0})} \right) + \pi \frac{C_x k_y^2}{\mu_x \omega} \frac{\lambda_x^2 (\frac{m\pi}{a})^2 \cos(\lambda_{zTE}^{n\,rot} d)}{\lambda_{zTE}^{n\,rot} \sin(\lambda_{zTE}^{n\,rot} d)} \frac{a}{((\frac{m\pi}{a})^2 - \omega^2 \epsilon_x \mu_x)} \tag{E.34}$$

$$\Phi_{yTE} = j4\pi \frac{(C_y k_y^2 + C_x k_x^2)}{\mu_x \omega} \sum_{l=0}^{\infty} \left(\frac{\lambda_x^2 \left(\lambda_{yTE}\right)}{((\frac{m\pi}{a})^2 - \lambda_{yTE}^2)((\frac{m\pi}{a})^2 - \lambda_{yTE}^2)} \frac{(1 - e^{-j\lambda_{yTE}a}(-1)^m)}{\frac{\mu_y}{\mu_x} d(1 + \delta_{l=0})} \right) + \pi \frac{(C_y k_y^2 + C_x k_x^2)}{\mu_x \omega} \frac{\lambda_x^2 \cos(\lambda_{zTE}^{n\,rot} d)}{\lambda_{zTE}^{n\,rot} \sin(\lambda_{zTE}^{n\,rot} d)} a \tag{E.35}$$

$$\Upsilon_{yTE} = j4\pi \frac{C_y k_x^2}{\mu_x \omega} \sum_{l=0}^{\infty} \left(\frac{\lambda_x^2 \frac{\mu_x}{\mu_y} \left(-\frac{\mu_x}{\mu_y} \lambda_x^2 - \frac{\mu_x}{\mu_y} \left(\frac{l\pi}{d}\right)^2 \right)}{((\frac{m\pi}{a})^2 - \lambda_{yTE}^2)((\frac{m\pi}{a})^2 - \lambda_{yTE}^2)} \frac{(1 - e^{-j\lambda_{yTE}a}(-1)^m)}{\lambda_{yTE} d(1 + \delta_{l=0})} \right) + \pi \frac{C_y k_x^2}{\mu_x \omega} \frac{\lambda_x^2 \left((\frac{m\pi}{a})^2 - \omega^2 \epsilon_x \mu_x \right) \cos(\lambda_{zTE}^{n\,rot}(d))}{\lambda_{zTE}^{n\,rot} \sin(\lambda_{zTE}^{n\,rot} d)} \frac{a}{((\frac{m\pi}{a})^2)} \tag{E.36}$$

$$\begin{aligned} X_{yTE} &= +\pi \frac{C_x k_y^2 \omega \epsilon_x}{1} \frac{(\frac{m\pi}{a}) \lambda_{zTM}^{n\,rot} \cos(\lambda_{zTM}^{n\,rot}(d)) a (-1)^m}{((\frac{m\pi}{a})^2 - \omega^2 \epsilon_x \mu_x) \left(\sin(\lambda_{zTM}^{n\,rot} d)\right)} \\ &+ j4\pi \frac{C_x k_y^2 \omega \epsilon_x}{1} \sum_{l=0}^{\infty} \left(\frac{\left(\frac{l\pi}{d}\right)^2 \left(\lambda_{yTM}\right)}{(-\lambda_x^2 - \left(\frac{l\pi}{d}\right)^2)} \frac{(1 - (-1)^m e^{-j\lambda_{yTM}a})}{\left((\frac{m\pi}{a})^2 - \lambda_{yTM}^2\right) \left((\frac{m\pi}{a})^2 - \lambda_{yTM}^2\right)} \frac{1}{d} \right) \end{aligned} \tag{E.37}$$

$$\Omega_{yTM} = -j4\pi \frac{C_x}{\mu_x \omega} \sum_{l=0}^{\infty} \left(\frac{\lambda_x^2 \left(\lambda_{yTE}\right)^3}{((\frac{m\pi}{a})^2 - \lambda_{yTE}^2)((\frac{m\pi}{a})^2 - \lambda_{yTE}^2)} \frac{(1 - e^{-j\lambda_{yTE}a}(-1)^m)}{(\lambda_x^2 + \left(\frac{l\pi}{d}\right)^2) d(1 + \delta_{l=0})} \right) + \pi \frac{C_x}{\mu_x \omega} \frac{\lambda_x^2 (\frac{m\pi}{a})^2 \cos(\lambda_{zTE}^{n\,rot} d)}{\lambda_{zTE}^{n\,rot} \sin(\lambda_{zTE}^{n\,rot} d)} \frac{a}{((\frac{m\pi}{a})^2 - \omega^2 \epsilon_x \mu_x)} \tag{E.38}$$

$$\Phi_{yTM} = j4\pi\frac{(C_y - C_x)}{\mu_x\omega}\sum_{l=0}^{\infty}\left(\frac{\lambda_x^2\left(\lambda_{yTE}\right)}{((\frac{m\pi}{a})^2-\lambda_{yTE}^2)((\frac{m\pi}{a})^2-\lambda_{yTE}^2)}\frac{(1-e^{-j\lambda_{yTE}a}(-1)^m)}{\frac{\mu_y}{\mu_x}d(1+\delta_{l=0})}\right)+ \pi\frac{(C_y - C_x)}{\mu_x\omega}\frac{\lambda_x^2\cos(\lambda_{zTE}^{n\,rot}d)}{\lambda_{zTE}^{n\,rot}\sin(\lambda_{zTE}^{n\,rot}d)}a \tag{E.39}$$

$$\Upsilon_{yTM} = j4\pi - \frac{C_y}{\mu_x\omega}\sum_{l=0}^{\infty}\left(\frac{\lambda_x^2\frac{\mu_x}{\mu_y}\left(-\frac{\mu_x}{\mu_y}\lambda_x^2-\frac{\mu_x}{\mu_y}\left(\frac{l\pi}{d}\right)^2\right)}{((\frac{m\pi}{a})^2-\lambda_{yTE}^2)((\frac{m\pi}{a})^2-\lambda_{yTE}^2)}\frac{(1-e^{-j\lambda_{yTE}a}(-1)^m)}{\lambda_{yTE}d(1+\delta_{l=0})}\right) -\pi\frac{C_y}{\mu_x\omega}\frac{\lambda_x^2\left((\frac{m\pi}{a})^2-\omega^2\epsilon_x\mu_x\right)\cos(\lambda_{zTE}^{n\,rot}(d))}{\lambda_{zTE}^{n\,rot}\sin(\lambda_{zTE}^{n\,rot}d)}\frac{a}{((\frac{m\pi}{a})^2)} \tag{E.40}$$

$$\begin{aligned} X_{yTM} &= +\pi\frac{(\frac{m\pi}{a})\lambda_{zTM}^{n\,rot}\cos(\lambda_{zTM}^{n\,rot}(d))a(-1)^m}{((\frac{m\pi}{a})^2-\omega^2\epsilon_x\mu_x)\left(\sin(\lambda_{zTM}^{n\,rot}d)\right)} \\ &+j4\pi\frac{C_x\omega\epsilon_x}{1}\sum_{l=0}^{\infty}\left(\frac{\left(\frac{l\pi}{d}\right)^2\left(\lambda_{yTM}\right)}{\left(-\lambda_x^2-\left(\frac{l\pi}{d}\right)^2\right)}\frac{(1-(-1)^m e^{-j\lambda_{yTM}a})}{\left((\frac{m\pi}{a})^2-\lambda_{yTM}^2\right)\left((\frac{m\pi}{a})^2-\lambda_{yTM}^2\right)}\frac{1}{d}\right) \end{aligned} \tag{E.41}$$

Case 1 $m \neq u \neq 0$**.**

$$\Omega_{yTE} = -j4\pi\lambda_x^2\frac{C_x k_y^2}{\mu_x\omega}\sum_{l=0}^{\infty}\left(\frac{\left(\lambda_{yTE}\right)^3}{((\frac{m\pi}{a})^2-\lambda_{yTE}^2)((\frac{u\pi}{a})^2-\lambda_{yTE}^2)}\frac{(1-e^{-j\lambda_{yTE}a}(-1)^m)}{(\lambda_x^2+\left(\frac{l\pi}{d}\right)^2)d(1+\delta_{l=0})}\right) \tag{E.42}$$

$$\Phi_{yTE} = j4\pi\lambda_x^2\frac{(C_y k_y^2 + C_x k_x^2)}{\mu_x\omega}\sum_{l=0}^{\infty}\left(\frac{\left(\lambda_{yTE}\right)}{((\frac{m\pi}{a})^2-\lambda_{yTE}^2)((\frac{u\pi}{a})^2-\lambda_{yTE}^2)}\frac{(1-e^{-j\lambda_{yTE}a}(-1)^m)}{\frac{\mu_y}{\mu_x}d(1+\delta_{l=0})}\right) \tag{E.43}$$

$$\Upsilon_{yTE} = j4\pi\lambda_x^2\frac{C_y k_x^2}{\mu_x\omega}\sum_{l=0}^{\infty}\left(\frac{\left(-\frac{\mu_x}{\mu_y}\lambda_x^2-\frac{\mu_x}{\mu_y}\left(\frac{l\pi}{d}\right)^2\right)}{((\frac{m\pi}{a})^2-\lambda_{yTE}^2)((\frac{u\pi}{a})^2-\lambda_{yTE}^2)}\frac{(1-e^{-j\lambda_{yTE}a}(-1)^m)}{\frac{\mu_y}{\mu_x}\lambda_{yTE}d(1+\delta_{l=0})}\right) \tag{E.44}$$

$$X_{yTE} = j4\pi \frac{C_x k_y^2 \omega \epsilon_x}{1} \sum_{l=0}^{\infty} \left(\frac{\left(\frac{l\pi}{d}\right)^2 (\lambda_{yTM})}{(-\lambda_x^2 - \left(\frac{l\pi}{d}\right)^2)} \frac{(1-(-1)^m e^{-j\lambda_{yTM}a})}{\left((\frac{m\pi}{a})^2 - \lambda_{yTM}^2\right)\left((\frac{v\pi}{b})^2 - \lambda_{yTM}^2\right)} \frac{1}{d} \right) \tag{E.45}$$

$$\Omega_{yTM} = -j4\pi\lambda_x^2 \frac{C_x}{\mu_x \omega} \sum_{l=0}^{\infty} \left(\frac{(\lambda_{yTE})^3}{((\frac{m\pi}{a})^2 - \lambda_{yTE}^2)((\frac{u\pi}{a})^2 - \lambda_{yTE}^2)} \frac{(1-e^{-j\lambda_{yTE}a}(-1)^m)}{(\lambda_x^2 + \left(\frac{l\pi}{d}\right)^2) d(1+\delta_{l=0})} \right) \tag{E.46}$$

$$\Phi_{yTM} = j4\pi\lambda_x^2 \frac{(C_y - C_x)}{\mu_x \omega} \sum_{l=0}^{\infty} \left(\frac{(\lambda_{yTE})}{((\frac{m\pi}{a})^2 - \lambda_{yTE}^2)((\frac{u\pi}{a})^2 - \lambda_{yTE}^2)} \frac{(1-e^{-j\lambda_{yTE}a}(-1)^m)}{\frac{\mu_y}{\mu_x} d(1+\delta_{l=0})} \right) \tag{E.47}$$

$$\Upsilon_{yTM} = j4\pi\lambda_x^2 (-\frac{C_y}{\mu_x \omega}) \sum_{l=0}^{\infty} \left(\frac{\left(-\frac{\mu_x}{\mu_y}\lambda_x^2 - \frac{\mu_x}{\mu_y}\left(\frac{l\pi}{d}\right)^2\right)}{((\frac{m\pi}{a})^2 - \lambda_{yTE}^2)((\frac{u\pi}{a})^2 - \lambda_{yTE}^2)} \frac{(1-e^{-j\lambda_{yTE}a}(-1)^m)}{\frac{\mu_y}{\mu_x}\lambda_{yTE} d(1+\delta_{l=0})} \right) \tag{E.48}$$

$$X_{yTM} = j4\pi \frac{C_x \omega \epsilon_x}{1} \sum_{l=0}^{\infty} \left(\frac{\left(\frac{l\pi}{d}\right)^2 (\lambda_{yTM})}{(-\lambda_x^2 - \left(\frac{l\pi}{d}\right)^2)} \frac{(1-(-1)^m e^{-j\lambda_{yTM}a})}{\left((\frac{m\pi}{a})^2 - \lambda_{yTM}^2\right)\left((\frac{u\pi}{a})^2 - \lambda_{yTM}^2\right)} \frac{1}{d} \right) \tag{E.49}$$

For all cases described above, the parallel plate and waveguide modes describe propagation constraints in the parallel plate region:

$$\lambda_{yTE} = k_t \sqrt{1 - \left(\frac{\lambda_x}{k_{tz}}\right)^2 - \left(\frac{l\pi}{k_{tz}d}\right)^2} \quad \lambda_{yTM} = k_t \sqrt{1 - \left(\frac{\lambda_x}{k_{zt}}\right)^2 - \left(\frac{l\pi}{k_{zt}d}\right)^2} \tag{E.50}$$

$$\lambda_{zTE}^n = k_{tz} \sqrt{1 - \left(\frac{\lambda_x}{k_{tz}}\right)^2 - \left(\frac{\frac{\pm n\pi}{b}}{k_t}\right)^2} \quad \lambda_{zTM}^n = k_{zt} \sqrt{1 - \left(\frac{\lambda_x}{k_{zt}}\right)^2 - \left(\frac{\frac{\pm n\pi}{b}}{k_t}\right)^2} \tag{E.51}$$

$$\lambda_{zTE}^{n\ rot} = k_{tz} \sqrt{1 - \left(\frac{\lambda_x}{k_{tz}}\right)^2 - \left(\frac{\frac{\pm m\pi}{a}}{k_t}\right)^2} \quad \lambda_{zTM}^{n\ rot} = k_{zt} \sqrt{1 - \left(\frac{\lambda_x}{k_{zt}}\right)^2 - \left(\frac{\frac{\pm m\pi}{a}}{k_t}\right)^2} \tag{E.52}$$

where

$$k_t^2 = \omega^2 \epsilon_x \mu_x \quad k_{zt}^2 = \omega^2 \epsilon_y \mu_x \quad k_{tz}^2 = \omega^2 \epsilon_x \mu_y \tag{E.53}$$

Bibliography

1. V. Dmitriev, "Tables of the second rank constitutive tensors for linear homogeneous media described by the point magnetic groups of symmetry," *Progress In Electromagnetics Research*, vol. 28, pp. 43–95, 2000.

2. R. Collin, "A simple artificial anisotropic dielectric medium," *IRE Transactions on Microwave Theory and Techniques*, vol. 6, no. 2, pp. 206–209, 1958.

3. A. Knisely, "Biaxial anisotropic material development and characterization using rectangular to square waveguide," M.S. thesis, Air Force Institute of Technology., Hobson Way, WPAFB, OH, USA 2015.

4. J. W. Stewart and M. J. Havrilla, "Electromagnetic characterization of a magnetic material using an open-ended waveguide probe and a rigorous full-wave multimode model," *Journal of Electromagnetic Waves and Applications*, vol. 20, no. 14, pp. 2037–2052, 2006. [Online]. Available: http://dx.doi.org/10.1163/156939306779322693

5. G. D. Dester, E. J. Rothwell, M. J. Havrilla, and M. W. Hyde, "Error analysis of a two-layer method for the electromagnetic characterization of conductor-backed absorbing material using an open-ended waveguide probe," *PIER B*, vol. 26, pp. 1–21, 2010.

6. M. W. Hyde, M. J. Havrilla, A. E. Bogle, E. J. Rothwell, and G. D. Dester, "An Improved Two-Layer Method for Nondestructively Characterizing Magnetic Sheet Materials Using a Single Rectangular Waveguide Probe," *Electromagnetics*, vol. 32, no. 7, pp. 411–425, 2012.

7. M. W. Hyde, A. E. Bogle, and M. J. Havrilla, "Nondestructive characterization of pec-backed materials using the combined measurements of a rectangular waveguide and coaxial probe," *IEEE Microwave and Wireless Components Letters*, vol. 24, no. 11, pp. 808–810, Nov 2014.

8. M. W. Hyde, J. W. Stewart, M. J. Havrilla, W. P. Baker, E. J. Rothwell, and D. P. Nyquist, "Nondestructive electromagnetic material characterization using a dual waveguide probe: A full wave solution," *Radio Science*, vol. 44, no. 3, pp. n/a–n/a, 2009, rS3013. [Online]. Available: http://dx.doi.org/10.1029/2008RS003937

9. N. Rogers, "Nondestructive electromagnetic characterization of uniaxial materials," PhD Dissertation, Air Force Institute of Technology., Hobson Way, WPAFB, OH, USA 2014.

10. M. W. H. IV, M. J. Havrilla, and A. E. Bogle, "Nondestructive determination of the permittivity tensor of a uniaxial material using a two-port clamped coaxial probe," *IEEE Transactions on Microwave Theory and Techniques*, vol. 64, no. 1, pp. 239–246, Jan 2016.

11. C.-W. Chang, K.-M. Chen, and J. Qian, "Nondestructive measurements of complex tensor permittivity of anisotropic materials using a waveguide probe system," *IEEE Transactions on Microwave Theory and Techniques*, vol. 44, no. 7, pp. 1081–1090, Jul 1996.

12. A. G. Knisely, M. W. Hyde, M. J. Havrilla, and P. J. Collins, "Uniaxial anisotropic material measurement using a single port waveguide probe," in *AMTA 2016 Proceedings*, Oct 2016, pp. 1–6.

13. A. Peterson, S. Ray, R. Mittra, I. Antennas, and P. Society, *Computational Methods for Electromagnetics*, ser. IEEE Press Series on Electromagnetic Wave Theory. Wiley, 1998.

14. M. J. Havrilla, "Uniaxial parallel-plate waveguide green's functions using a scalar potential formulation," in *Radio Science Meeting (Joint with AP-S Symposium), 2014 USNC-URSI*, July 2014, pp. 92–92.

15. G. Arfken and H. Weber, *Mathematical methods for physicists*. Elsevier Acad. Press, 2008.

16. A. Nicolson and G. F. Ross, "Measurement of the intrinsic properties of materials by time-domain techniques," *IEEE Transactions on Instrumentation and Measurement*, vol. 19, no. 4, pp. 377–382, 1970.

17. W. B. Weir, "Automatic measurement of complex dielectric constant and permeability at microwave frequencies," *Proceedings of the IEEE*, vol. 62, no. 1, pp. 33–36, 1974.

18. A. Knisely and M. J. Havrilla, "Material characterization de-embedding for rectangular to square waveguide," in *The 9th European Conference on Antennas and Propagation (EuCAP 2015) (EuCAP 2015)*, Lisbon, Portugal, Apr. 2015.

19. M. W. Hyde and M. J. Havrilla, "Reducing the measurement footprint in the characterization of low-loss materials using the flanged-waveguide measurement geometry," in *Electromagnetics in Advanced Applications (ICEAA), 2010 International Conference on*, Sept 2010, pp. 43–46.

20. A. Knisely, M. Havrilla, and P. Collins, "Biaxial anisotropic sample design and rectangular to square waveguide material characterization system," in *Advanced Electromagnetic Materials in Microwaves and Optics (Metamaterials), 2015 9th International Congress on*, Sept 2015, pp. 346–348.

21. J. Baker-Jarvis, E. Vanzura, and W. Kissick, "Improved technique for determining complex permittivity with the transmission/reflection method," *IEEE Transactions on Microwave Theory and Techniques*, vol. 38, no. 8, pp. 1096–1103, 1990.

22. "Cuming microwave c-ram hc," *Cuming Microwave Technical Bulletin 360-1*. [Online]. Available: http://www.cumingmicrowave.com/pdf/360-Honeycomb%20&%20High%20Power/360-1%20C-RAM%20HC.pdf

23. T. Blakney and W. Weir, "Comments on "automatic measurement of complex dielectric constant and permeability at microwave frequencies"," *Proceedings of the IEEE*, vol. 63, no. 1, pp. 203–205, Jan 1975.

24. G. D. Dester, E. J. Rothwell, and M. J. Havrilla, "An extrapolation method for improving waveguide probe material characterization accuracy," *IEEE Microwave and Wireless Components Letters*, vol. 20, no. 5, pp. 298–300, May 2010.

25. A. G. Knisely, M. W. Hyde, M. J. Havrilla, and P. J. Collins, "Rotated uniaxial anisotropic material characterization - theory," in *AMTA 2017 Proceedings*, Oct 2017, pp. 361–365.

26. I. Stakgold and M. Holst, *Green's Functions and Boundary Value Problems*, ser. Pure and Applied Mathematics: A Wiley Series of Texts, Monographs and Tracts. Wiley, 2011.

27. M. Havrilla, "Electric and magnetic field dyadic green's functions and depolarizing dyad for a magnetic current immersed in a uniaxial dielectric-filled parallel plate waveguide," in *2011 XXXth URSI General Assembly and Scientific Symposium*, Aug 2011, pp. 1–4.

28. A. G. Knisely, M. W. Hyde, M. J. Havrilla, and P. J. Collins, "Rotated uniaxial anisotropic material characterization - experiment," in *AMTA 2017 Proceedings*, Oct 2017, pp. 366–371.

29. "Downloadable vector network analyzer uncertainty calculator," *Keysight Technologies Software*. [Online]. Available: http://www.keysight.com/main/home.jspx?cc=US&lc=eng

REPORT DOCUMENTATION PAGE

Form Approved
OMB No. 0704–0188

1. REPORT DATE *(DD–MM–YYYY)*	2. REPORT TYPE	3. DATES COVERED *(From — To)*
13–09–2018	PhD Dissertation	Sept 2015 — Sept 2018

4. TITLE AND SUBTITLE

Non-Destructive Characterization
of
Rotated Uniaxial Anisotropic Materials

5a. CONTRACT NUMBER

5b. GRANT NUMBER

5c. PROGRAM ELEMENT NUMBER

6. AUTHOR(S)

Knisely, Alexander G., Mr., Civ.

5d. PROJECT NUMBER

5e. TASK NUMBER

5f. WORK UNIT NUMBER

7. PERFORMING ORGANIZATION NAME(S) AND ADDRESS(ES)

Air Force Institute of Technology
Graduate School of Engineering and Management (AFIT/EN)
2950 Hobson Way
WPAFB OH 45433-7765

8. PERFORMING ORGANIZATION REPORT NUMBER

AFIT-ENG-DS-18-S-013

9. SPONSORING / MONITORING AGENCY NAME(S) AND ADDRESS(ES)

Air Force Research Laboratory, Sensors Directorate
Attn: Garrett J. Stenholm
2591 K Street, Bldg 254
WPAFB OH 45433-7602
COMM 937-656-4690
Email: Garrett.Stenholm@us.af.mil

10. SPONSOR/MONITOR'S ACRONYM(S)

AFRL

11. SPONSOR/MONITOR'S REPORT NUMBER(S)

12. DISTRIBUTION / AVAILABILITY STATEMENT

DISTRIBUTION STATEMENT A:
APPROVED FOR PUBLIC RELEASE; DISTRIBUTION UNLIMITED.

13. SUPPLEMENTARY NOTES

This material is declared a work of the U.S. Government and is not subject to copytight protection in the United States.

14. ABSTRACT

Electromagnetic material characterization of anisotropic media requires measurement diversity, minimal measurement uncertainty and insight into sample symmetry. Additionally, non-destructive characterization techniques are valued over legacy measurement techniques because a destructive approach requires sample preparation to execute a measurement. A Single Port Waveguide Probe (SPWP) non-destructive material characterization technique is proposed to accommodate measuring a metal backed, known thickness, rotated uniaxial anisotropic material. A rotated uniaxial sample possesses unique transverse constitutive components and a longitudinal constitutive component which is the same as one of the transverse values. The SPWP consists of a rectangular waveguide aperture cut in the center of a square flange. The flange is place upon a metal-backed material surface, which forms a parallel plate region. Two orthogonal transverse plane measurements aligned with the sample's transverse constitutive parameter components offers measurement diversity. A rotated uniaxial anisotropic parallel plate Green's function is developed and employed in a moment method forward model and is then used to extract the material constitutive parameters. Measured and simulated results are utilized to demonstrate the analytical approach and uncertainty is evaluated demonstrating system accuracy of the non-destructive rotated uniaxial anisotropic measurement technique.

15. SUBJECT TERMS

RF Material Characterization, Anisotropic, Uniaxial, Electromagnetics, Non-Destructive, Metamaterials

16. SECURITY CLASSIFICATION OF:			17. LIMITATION OF ABSTRACT	18. NUMBER OF PAGES	19a. NAME OF RESPONSIBLE PERSON
a. REPORT	b. ABSTRACT	c. THIS PAGE			Dr. Michael J. Havrilla, AFIT/ENG
U	U	U	UU	263	19b. TELEPHONE NUMBER *(include area code)* (937) 255-3636, x4582 michael.havrilla@afit.edu